

CORRECTIONS

Page 14	Paragraph 1	Line 4	"has been" should read "have been"
Page 15	"	5	" 3 "attachig" should read "attaching"
Page 17	"	3	" 5 insert "rotor" after "generator"
Page 22	"	2	" 5 delete "is" after "this"
Page 24	"	3	" 4 delete "by" after "combining"
Page 27	"	2	" 6 "constitutive" should read "constitutive"
Page 34	"	1	" 5 "turning" should read "turn"
Page 34	"	1	" 6 "flowing" should read "flow"
Page 35	"	3	" 9 " $(N_W)^T$ " should read " $(N_W/)$ "
Page 35	Equation (2.24)		" $(N_W)^T$ " should read " $(N_W/)$ "
Page 37	Paragraph 6	Line 5	"calculaed" should read "calculated"
Page 38	"	1	" 1 "resuls" should read "results"
Page 56	References [50,51]		should read [5,50]
Page 64	Table 4.2 for "conductivities"		should read "resistivities"
Page 91	Section 5.4	Line 1	"transfromer" should read "transformer"
Page 97		Line 1	delete "at" after "required"
Page 144	Paragraph 2	Line 2	"concequat" should read "consequent"
Page 147	"	1	" 5 "compilcated" should read "complicated".
Page 147	"	1	" 6 "provides and" should read "provides an"
Page 151	Figure 6.1	Labels V_b and V_c	should be interchanged
Page 200	Paragraph 6.8.4	Line 3	"then" should read "when"
Page 232	Paragraph 4	Line 2	"have have" should read "which have"
Page 249	Reference 45		"Vogh" should read "Voght"

UNIVERSITY OF LONDON
IMPERIAL COLLEGE OF SCIENCE AND TECHNOLOGY
DEPARTMENT OF ELECTRICAL ENGINEERING

**FINITE ELEMENT ELECTROMAGNETIC
ANALYSIS OF GENERATOR
TRANSIENT PERFORMANCE**

by

Jonathan Peter Sturgess

Thesis submitted for the degree of
Doctor of Philosophy and the Diploma of
Imperial College in the Faculty of Engineering

October 1987

ABSTRACT

The transient behaviour of a turbine-generator is analysed using first order, two-dimensional finite elements in a magnetic vector potential formulation. The Newton-Raphson method is used to solve the non-linear problem arising from magnetic saturation of iron materials. Eddy currents are calculated step by step during the transient using conductivity matrices to allow for the effects of induced voltages and currents in the solid rotor body, stator and field windings.

The behaviour of an initially loaded generator when subjected to a three-phase short circuit followed by fault clearance and reconnection to the grid is calculated, incorporating changes in rotor speed and angle. Full account is taken of losses arising from eddy currents in the rotor, of changes in energy storage in magnetic fields within the machine and of power exported to the infinite busbar. Although the model is essentially two-dimensional, allowance is made for effects within the machine length, such as inertia equalising slits and the contribution of the endbell to eddy current distribution and losses. Machine governor and exciter models are also included in the calculation.

Two methods of representation of the stator winding are compared. In the first, d and q axis winding distributions are used, and the stator transformer voltages are ignored. In the second, the phase bands are modelled directly, requiring that relative motion between rotor and stator be included.

Flux and eddy current plots are presented, enabling the progress of the transient to be more easily visualised and the machine behaviour explained.

The calculated rotor movement, currents and voltages are compared with experimental results obtained by the C.E.G.B. during tests on a 120 MW turbine generator.

ACKNOWLEDGEMENTS

This thesis presents work carried out under the supervision of D. C. Macdonald Ph.D., B.Sc., ACGI, FIEE, Lecturer in the Electrical Engineering Department, Imperial College. I would like to thank Dr Macdonald for his constant advice and encouragement and for the great interest that he has shown throughout the project.

I would also like to thank Mr A.B.J.Reece and Dr T.Preston of GEC Engineering Research, Stafford Laboratory and Dr P.Turner of GEC Turbine Generators who collaborated with the research and who provided programs and computing facilities, details of the generator and much helpful advice and comment.

I am grateful to the Science and Engineering Research Council for supporting this work under a CASE award studentship.

Thanks must also go to Dr R.McGee and Dr P.Henser of the C.E.G.B. System Technical Branch for making available the test results and data; and to my colleagues in GEC and the Energy and Power Systems Group at Imperial College who assisted in many ways and made for a lively and friendly working environment. Finally, I would like to thank Alison Wilson for proof reading the whole work, any remaining errors, however, are entirely my own responsibility.

I would like to dedicate this thesis to my parents, who have provided much quiet support and encouragement over the last three years.

TABLE OF CONTENTS

List of symbols and abbreviations.	10
Chapter one : Introduction.	
1.1 Turbine generator design and development.	14
1.2 Machine modelling.	16
1.2.1 Circuit analysis	17
1.2.2 Electromagnetic analysis.	19
1.3 Objectives of the research.	21
1.4 Outline of the thesis.	22
1.4.1 Contribution of the thesis.	23
Chapter two : The finite element method.	
2.1 Introduction.	26
2.2 Governing equations.	27
2.3 Formulation.	28
2.3.1 The nodal method.	28
2.3.2 Periodicity.	30
2.3.3 Discretisation.	30
2.3.4 Magnetic non-linearity.	31
2.4 Voltages and currents in machine windings and solid iron.	32
2.4.1 Winding currents.	32
2.4.2 Winding voltages.	33
2.4.3 Eddy currents.	34

	5
3.6 Conclusions.	58

Chapter four : The pole slipping tests at Uskmouth B Power Station.

4.1 Introduction.	60
4.2 Generator set details.	61
4.3 Generator transformer.	64
4.3.1 Transformer details.	64
4.3.2 Transformer modelling.	67
4.4 The transmission line network.	67
4.4.1 Transmission line details.	67
4.4.2 Transmission line modelling.	68
4.4.3 Calculation of infinite busbar voltage from the initial condition.	70
4.5 The C.E.G.B. transient tests.	73
4.5.1 Fault condition.	73
4.5.2 Fault throwing.	73
4.5.3 Generator terminal measurements.	73
4.5.4 Data filtering.	75
4.5.5 Rotor angle measurement.	75
4.6 The automatic voltage regulator and exciter.	76
4.7 The machine governor and steam turbine.	77
4.8 Conclusions.	78

5.10 Conclusions.	144
-------------------	-----

Chapter six : The phase band stator model.

6.1 Introduction.	147
6.2 Stator winding representation.	148
6.3 Stator winding vectors.	149
6.4 Terminal voltage and current.	151
6.5 Initial condition.	152
6.6 Transient initiation.	153
6.7 Time step length.	153
6.8 Comparison of simulated and measured results, C.E.G.B. Test B.	154
6.8.1 Initial condition.	154
6.8.2 Transient behaviour : time series data.	157
6.8.3 Transient behaviour : flux and eddy current plots.	164
6.8.4 The effect of discretisation.	200
6.8.5 Performance of the program.	201
6.8.6 Comparison of Maxwell Stress and Power Balance methods.	201
6.9 Comparison of two-axis and phase band models, C.E.G.B. Test B.	203
6.10 Comparison of calculated and measured results, C.E.G.B. Test C1.	205
6.11 Discussion of discrepancies between calculated and measured results.	208
6.12 Conclusions.	212

**Chapter seven : Obtaining equivalent circuit parameters
from the finite element model.**

7.1 Introduction.	216
7.2 The equivalent circuit model.	217
7.3 Obtaining two-axis parameters from the phase band model.	219
7.3.1 Base values.	219
7.3.2 Main axis reactances.	220
7.3.3 Damper circuit impedance.	220
7.4 Computation of damper circuit impedances.	222
7.4.1 Resistance.	222
7.4.2 Reactance.	224
7.5 Equivalent circuit solution.	224
7.5.1 Comparison of finite element and equivalent circuit results.	226
7.6 Conclusions.	229

Chapter eight : Conclusions and recommendations for further work.

8.1 Conclusions.	231
8.1.1 Problem formulation.	232
8.1.2 Transient modelling.	233
8.1.2 Equivalent circuit parameters.	237
8.2 Further work.	238
8.2.1 Unresolving modelling problems.	238
8.2.2 Improvements to the existing method.	239
8.2.3 Developments of the method.	240
8.2.4 Machine parameters.	241

**Appendix : Efficient solution of the asymmetric matrix resulting from
the two-axis stator winding conductivity matrices. 242**

References. 245

LIST OF SYMBOLS AND ABBREVIATIONS USED

a	controller response, Laplace transform output
b	Laplace transform input
d	differential operator
e	electromotive force
f	Lorentz force
i	current, integer
j	$\sqrt{-1}$
n	number of stator parallel paths
p	number of machine poles, differential operator $\frac{d}{dt}$
s	Laplacian operator
t	time
u	per unit voltage
x	reactance, controller response rate
A	magnetic vector potential, number of turns
B	flux density
E	electric field strength, stored energy
G	conductance
H	magnetic field strength, inertia constant
I	current
J	current density, rotational inertia
K	gain
L	inductance, length
P	real power
Q	reactive power
R	resistance

S	volt-amperes
T	torque, time constant, Maxwell stress tensor
U	controller set point
V	voltage, valve position
X	reactance
α	angular measure
δ	small increment, partial differential operator
Δ	increment, area
θ	angular measure
λ	circumferential length
ν	reluctivity
σ	conductivity
τ	time constant
ϕ	potential function, angular measure, flux
ψ	flux linkage
ω	angular frequency
(E)	error vector
(N_w)	winding vector
$[P]$	Hessian matrix
$[S]$	system (stiffness) matrix
∇	vector differential operator
$[\Delta\sigma]$	conductivity matrix

Superscripts

a	actual (i.e. in amps, volts etc.)
T	transpose
u	unsaturated
$'$	transient
$"$	subtransient
\bar{O}	average

Subscripts

a, b, c)
r, y, b) phase values
$1, 2, 3$)
a	armature
b	infinite busbar
d	direct axis
e	element
eff	effective
ex	exciter
f, fd	field
i, j	nodes
k	damper
m	mutual linkage
o	open circuit, at air gap
q	quadrature axis
r	rotor
s	source
sc	short circuit

t	transformer, at time t
w	winding
0	initial
2	2-phase
\underline{Q}	vector quantity

Abbreviations

a.c.	alternating current
AVR	automatic voltage regulator
C.E.G.B.	Central Electricity Generating Board
d.c.	direct current
emf	electromotive force
mmf	magnetomotive force
p.u.	per unit
rms	root mean square

CHAPTER ONE

INTRODUCTION

1.1 TURBINE GENERATOR DESIGN AND DEVELOPMENT.

The economic pressure to produce turbine generators of ever higher ratings has led to a steady increase in unit size and current loading. At the same time, reductions in weight and manufacturing cost and an increase in efficiency has been required. These aims have been met by optimisation of design and by improvements in cooling methods, manufacturing techniques and materials both for their strength and magnetic and insulating properties.

Improved methods of heat removal have made the greatest contribution to the increase in unit size and efficiency. Most modern large turbine generators feature hydrogen cooled rotors, where the gas is fed in at the base of the rotor slots and escapes through ducts in the winding and wedges; and water cooled stators, where the small size of the individual conductors, imposed by the need to transpose parallel conductors on the Roebel method, would require too high a gas pressure to achieve the necessary flow.

The rotor is normally a steel forging, machined to take the winding, and fitted at each end with a retaining ring, or endbell, to support the endwinding. The endbell is usually made of non-magnetic steel and must be able to withstand the large forces imposed under fault conditions and carry the eddy currents that flow into it from the rotor body and wedges, without reduction in strength.

To reduce vibration, it is necessary to compensate for the non-uniform flexibility of the rotor caused by the distribution of the rotor slots. This is done

by cutting flexibility, or inertia equalising, slits in the pole faces. Two common methods are either to cut additional axial slots, which may be plugged with steel bars to reduce magnetic saturation if deep, or left unfilled or plugged with conductive wedges if shallow; or to cut deep, semi-circular transverse gashes in the pole face, which are sometimes bridged with axial wedges.

The increase in current loadings and flux density levels has led to many design problems. Vibratory forces on conductors, at twice operating frequency, are proportional to the square of the current; and this leads to fatigue cracking of the winding and fretting of the insulation. Higher loadings require thicker teeth to withstand the higher forces and carry the higher flux levels, but this leaves less area available for the windings, despite the higher currents that they have to carry. Unfortunately, the rotor diameter is limited by centripetal forces, and increased ratings are generally achieved by an increase in machine length.

The stator has a laminated structure to reduce eddy current losses, but leakage fields at the ends of the machine enter the laminations axially, and give rise to core-end heating. One solution to this problem has been to introduce conductive screens of aluminium or copper, which may be water cooled.

Future developments in turbine generator design may occur in a number of different areas; the most evident is a continual refinement of existing designs with improved cooling and reduced losses.

A full slotless generator has been proposed [1] in which both rotor and stator windings are placed entirely in the airgap, so permitting the airgap flux density to be increased. Special methods of attaching the winding must be provided to enable them to transmit transient torques several times the full load value, without damage. Modern developments in carbon fibres, epoxy resins and plastics materials are likely to be utilised. A 280kW d.c. motor has already been built with a slotless rotor.

Turbine generators with superconducting rotor windings are another possible development. The excitation loss is thereby reduced to the power required to run the refrigeration plant, and the very high current densities can produce fields of up to 5 T without the need for iron in the rotor. This allows a substantial reduction in size and weight, but gives rise to problems of greater winding forces, eddy current losses, reduced machine damping and a very small machine inertia. Design problems to be overcome include providing for the integrity of the machine should the superconducting properties be lost for any reason, and assuring machine stability with a very light rotor. Recent discoveries of materials which become superconducting much closer to room temperature than any previously known, may renew interest in the superconducting generator.

1.2 MACHINE MODELLING

The ability to model the steady state and transient behaviour of electrical machines is required so that they may be reliably operated within their capability, and that that capability may be established.

The machine designer would like to know that the design specification will be achieved, and be able to locate the areas of high mechanical electrical and thermal stress, to ensure adequate strength in design, and sufficient cooling.

The designer of machine control systems needs to know the steady state, dynamic and transient behaviour of the machine in order that the control systems may be designed to extract the optimum performance from the unit.

Power systems analysers are also interested in machine performance, to enable the accurate design, location and specification of protection systems to be determined; and the effect of the machine dynamics on the power system to which it is connected to be assessed. The response of the machine to sudden load

changes, system faults and disturbances is also required so that system stability limits may be set, maximum power transfer capability calculated and the siting of power system stabilisers and optimal controllers determined.

1.2.1 Circuit analysis.

The most commonly used type of machine model is the machine equivalent circuit based on the general two-axis equations developed by Park [2] and Kron [3]. More recent applications to synchronous machines have been made by Canay [4], Adkins and Harley [5] and Shackshaft [6]. A useful summary of different models in current use was made by Dandeno et al. [7].

The advantage of the generalised theory is the small number of parameters required for the model and the speed of solution. However, the theory is only approximate, and makes fundamental simplifying assumptions such as neglecting harmonics and saturation, and representing the machine as a small number of interlinked electric and magnetic circuits. Usually the turbine generator is modelled by two circuits on the d-axis, one of which represents the field winding, and one circuit on the q-axis. These few circuits are required to model the complex transient behaviour of the rotor body, wedges and poles as eddy currents are induced in them during a fault. Tests by the C.E.G.B. at Northfleet have shown the inadequacies of such models, [8].

A further, and fundamental, problem with equivalent circuit models arises in providing the required data. Some of these may be estimated from the machine design, but this is very difficult to do accurately for the damper circuit parameters.

In the past, accurate determination of machine parameters has only been made using practical test methods [6,8,9,10]. Tests in the manufacturer's

works are usually limited to the open circuit and sustained short circuit characteristics and the sudden short circuit test at reduced terminal voltage. These tests only give d-axis parameters. Standstill frequency response tests have also been used, which can be performed to obtain data on any machine axis. The stationary machine is excited from the stator over a wide range of frequencies, the stator input impedance measured and the results are fitted to a transfer function derived from the machine model required. Since the machine is not operating at normal speed, temperature or saturation level, the frequency response method has been criticised for producing unrepresentative parameters [11].

Decrement tests are made with the machine operating under near normal conditions. The machine is run at rated speed under stator or rotor excitation, with the unexcited winding either open or short circuited. The excitation is then removed, and the rate of decay of voltage or current used to determine the equivalent circuit parameters [6]. Both d- and q-axis parameters may be found this way.

Each method of determining machine parameters will yield a different set of values according to the different initial conditions and levels of saturation in the test. The choice of the most appropriate set for any particular simulation is a matter for engineering skill and judgement.

More recently, numerical methods of simulating these different tests have been developed, which enable the parameters to be determined before the machine is built, but the basic criticism of the inadequacy of the equivalent circuit method of modelling machines remains.

1.2.2 Electromagnetic analysis.

Simple methods of analysing electromagnetic problems reduce the complexity of the solution either by making the assumption that only that part of the magnetic circuit which is in air contributes to the reluctance of the flux path, or by simplifying the machine geometry. These methods are still unable to model local saturation effects.

A more detailed treatment of the magnetic circuits of a machine consists of lumped reluctances assigned to each flux path to represent stator and rotor teeth, flux leakage paths and the air gap reluctance. These magnetic circuits link the electric circuit provided by currents in the slots, and can be used to produce a set of simultaneous equations describing the machine. The method was used by Binns et al.[12,13] to calculate turbine generator steady state load performance, and more recently by Haydock [14] to model flux decay tests. Haydock's work is also interesting in that he has shown exactly the assumptions required to progressively simplify such a model until any of the familiar equivalent circuit ones are reached. These lumped circuit models are reasonably fast and simple to solve, but require that the general form of the field distribution is known.

The field within a turbine generator is described by Maxwell's equations, and a solution of these throughout the machine would completely specify its electromagnetic behaviour. Finite element and finite difference methods attempt to produce a numerical solution that is a close approximation to the Maxwell equations at a number of discrete points throughout the machine. The finite difference method was used by Demerdash [15] in an analysis of steady state load operation of turbine generators, but has now declined in popularity at the expense of the finite element method.

The finite element method was pioneered for many engineering applications by Zienkiewicz [16], and for electromagnetic and electrostatic problems by

Silvester [17,18]. The technique involves dividing the region into a finite number of triangular elements over which the field is assumed to vary in a known manner. The problem is then solved at points throughout the region defined by the apexes of the elements, and if the discretisation of the region is fine enough, the calculated field variation within the element is a close approximation to the real solution. There have been a very large number of machine problems solved using the finite element method in both two and three dimensions. Two useful reviews of methods and applications have been made by Chari et al., [19,20].

Three basic types of field solution can be identified, magnetostatic, steady state but sinusoidally excited and transient. Magnetostatic solutions can be used for the calculation of the steady state performance of rotating machines by adopting a rotor frame of reference, in which the field is stationary. Sinusoidally excited steady state problems, such as occur in static frequency response tests, may be solved using a complex-variable form of the magnetic vector potential to enable phase differences to be modelled. In both these types of solution, a single calculation only is required to completely describe the field, although it may be necessary to iterate to the solution because of magnetic non-linearity. A full transient analysis, on the other hand, requires the field to be calculated at successive instants in time, allowing for changes in iron permeabilities at each. A large number of calculations may thus be required to specify a full transient field solution.

The finite element method is a differential one. The Maxwell equations may also be solved using an integral formulation [21], in which the field is calculated only at the points at which it is required. Integral methods are particularly useful for problems with open boundaries, and where the field must be computed to a high degree of accuracy. Because the problem is only solved at the points of interest, the solution is economic to compute, although the matrix formulation is densely packed. Unfortunately, errors tend to arise where the field is mostly

contained within non-linear iron regions; and where the solution is required at a large number of points, such as across a winding, the solution becomes uneconomic. Simkin has made a useful comparison of the finite element and integral methods [22]. Hybrid methods, using both methods where appropriate, are being developed [16,23,24] and show promise for problems which feature non-linear iron regions surrounded by air. For most rotating machine studies, though, the region outside the core-back may be ignored.

There are thus a variety of different techniques available, of varying degrees of complexity and precision, for the modelling of turbine generators. The more commonly used were summarised at a recent IEEE symposium [25].

1.3 OBJECTIVES OF THE RESEARCH.

The objective of this work has been to develop a finite element based method for simulating the widest possible range of turbine generator transient behaviour. In particular, to analyse the electromagnetic and mechanical response of a machine, under load, to a transient such as a transmission line fault sequence consisting of fault imposition, clearance and reconnection to the system, and possibly subsequent tripping of the set. The method should be capable of including the actions of the machine controls, and of predicting pole-slipping behaviour.

Such a technique would enable the machine transient performance to be directly investigated at the design stage. (At present the nearest approach to this is to use the finite element method to simulate works' tests, from which parameters are obtained for equivalent circuit simulations of the transient response.) It would also enable design optimisation of details such as machine damping characteristics, and provide a first step towards incorporating a thermal analysis. A complete machine model could be used as an accurate test bed for the design of excitation

and governor control systems, and the development of power system stabilisers and optimal controllers.

The provision of an accurate machine model would also enable a detailed study of the performance of equivalent circuit methods to be undertaken. This would allow investigation of the applicability of using one set of machine parameters for modelling a wide range of system transients under different operating conditions and, arising from this, is how one set of parameters might be modified in a simple way, in the course of a simulation, to more closely model the actual machine behaviour. This requires the development of novel ways of deriving the necessary parameters.

1.4 OUTLINE OF THE THESIS.

The thesis describes a continuation of the work of Turner and Macdonald [26,27,28]. Using the nodal method, and the concept of conductivity matrices, the transient finite element numerical equations are formulated in an efficient manner that permits the iterative solution of problems containing magnetically non-linear iron materials.

Two methods of modelling the stator windings are presented in detail. The two-axis method is more familiar, but neglects the stator transformer effect component of the transient response in order that the time step length may be gradually increased and the total time in computation may be thereby reduced. The phase band model provides a full solution, but requires substantially more computational time, due to the need to accurately model supply frequency waveforms.

In order that the two methods may be validated, simulations are performed of two actual system transient tests, undertaken by the C.E.G.B. at

Uskmouth in 1979. One of the tests to be simulated demonstrated pole-slipping behaviour. The results obtained are discussed at length.

The behaviour of the machine is studied with reference to flux and eddy current plots, winding currents and voltages, rotor angle changes, power dissipation in rotor eddy current heating and power flow into magnetic circuit energy storage. These combine to give a detailed picture of the machine transient performance.

Parameters for an equivalent circuit machine model are calculated directly from the finite element solution, for both axes of the generator. The damper circuit parameters are particularly concentrated upon, being found at intervals throughout the transient period. Previous methods, based on curve fitting, have assumed them invariant. With this method, their variation over time may be studied.

1.4.1 Contribution of the thesis.

A brief description of the contents and contribution of each chapter is given below.

Chapter 2. An introduction to the finite element method is made and the numerical equations are established using the nodal method. The calculation of currents and voltages within the machine is developed in a general formulation, the concept of the conductivity matrix is introduced, numerical allowances for effects within the machine length are described and the A-average technique is presented. A recently published method for accelerating the solution is applied to the transient problem. This is believed to be new.

Chapter 3. Two well established methods for calculating rotor torque, Maxwell's stress tensor and the virtual work principal, are outlined and rejected

in favour of an entirely new method based upon performing a power balance within the machine. This proves simple to compute and provides a deeper and more useful insight into the transient process. Methods of efficiently incorporating Laplace-transform-based governor and automatic voltage regulator models into the finite element calculation are described. The work of this chapter is the first known attempt at introducing into the finite element method the mechanical behaviour of a rotating machine under transient conditions.

Chapter 4. Details of the generator, its controls, the generator transformer and the transmission line used by the C.E.G.B. in transient stability tests at Uskmouth are presented. Methods of modelling them, and the two particular tests to be simulated, are described and discussed.

Chapter 5. The general formulation of Chapter 2 is applied to a turbine generator model where the stator winding is represented in a two-axis formulation. The solution of the resulting asymmetric matrix, in an entirely new and highly efficient manner by combining the A-average technique with a modified Gaussian elimination scheme, is described. The analysis deliberately neglects the stator transformer component of the transient response in order to obtain a more rapid solution of the problem. Methods of increasing the computational time step length are discussed, and a further reduction of the stator model to a current sheet is described. Specific problems associated with the incorporation of an infinite busbar representation into the method are dealt with and the results of a simulated transient compared with those measured in the C.E.G.B. tests. This computation of the transient behaviour of a generator on load, where the flux axis is not aligned with a machine axis, is entirely new.

Chapter 6. To perform a full solution of the machine transient, a phase band stator model is adopted. The problem of allowing for relative motion between rotor and stator is overcome by backwards rotation of the stator phase bands within a fixed mesh. Methods of rapidly calculating the initial condition with the machine under load are described, and the results of simulating two of the C.E.G.B. tests, one involving pole-slipping, are presented. The outcome is, unfortunately, not good, as an overprediction of stator voltage on clearance of the fault leads to substantial errors in the calculation of rotor angle. Possible reasons for this are discussed at length. The new power balance calculation of rotor torque is compared favourably with the well known Maxwell stress method, and an example design study shows the benefits of changing the specification of the rotor slot wedges. This method of analysis of a machine transient from a loaded initial condition is also new.

Chapter 7. A new method for calculating equivalent circuit parameters directly from the transient finite element solution is presented. The basic machine reactances are computed using an established method, but the damper circuit values are calculated at intervals throughout the transient by equating the power dissipative terms in the equivalent circuit and finite element models. The variation of resistance values obtained proves interesting, but the calculation of inductance unfortunately gives non-physical values. To attempt to understand why this is, the axis values derived from the finite element solution are compared with those given by a standard solution of the equivalent circuit model.

Chapter 8. A summary of the main results and conclusions described in the previous chapters is made, and an outline of future work is described.

CHAPTER TWO

THE FINITE ELEMENT METHOD

2.1 INTRODUCTION.

The finite element method is now an established technique for solving electromagnetic field problems. Originally applied to linear, two-dimensional magnetostatic cases, these restrictions have been gradually removed, although not all the problems have by any means been resolved. Incorporation of the external circuits coupled to a machine has proved difficult to achieve in an efficient manner, particularly where the orientation of the main flux axis within the machine is unknown.

This chapter describes the application of the finite element method to a two-dimensional computation of the transient, non-linear, electromagnetic field variation within a turbine generator. The machine is considered to be initially on load and is subjected to a fault on the high voltage side of the generator transformer, followed by clearance of the fault and reconnection of the machine to the grid through the transmission line. The nodal method is used for formulating the governing equations and the Newton-Raphson technique for iteratively solving them at each time step.

The calculation of induced voltages and currents within the machine during both steady state and transient operation is described, and the concept of a conductivity matrix is introduced to represent current terms in the problem formulation. Methods explicitly allowing for field and material variations within the machine length are discussed.

Time stepped solutions inevitably involve long computational times, and the chapter presents several ways of reducing these, such as the A-average technique and methods designed to minimise the number of matrix inversions required at each time step.

2.2 GOVERNING EQUATIONS.

A region of space containing current sources may be described by Maxwell's equations in terms of the magnetic field strength \underline{H} by

$$\nabla \wedge \underline{H} = \underline{J} \quad (2.1)$$

where \underline{J} is a vector of current density.

Displacement currents are assumed to be insignificant. Equation 2.1 is used in conjunction with two constitutive equations :

$$\underline{H} = \nu \underline{B} \quad (2.2)$$

and

$$\underline{J} = \sigma \underline{E} \quad (2.3)$$

where \underline{B} is the magnetic flux density

\underline{E} is the electric field strength

ν is the material reluctivity (1/permeability)

and σ is the material conductivity

There are many possible solution functions for 2.1. For two- dimensional problems the magnetic vector potential function \underline{A} is most often used, since it has only a z-directed component, and points of equal potential are on a common flux line. Thus the difference in the value of \underline{A} between two points is equal to the flux per metre between them.

\underline{A} is defined by :

$$\underline{B} = \nabla \wedge \underline{A} \quad (2.4)$$

and \underline{E} of equation 2.3 may be written as:

$$\underline{E} = -\nabla\phi - \dot{\underline{A}} \quad (2.5)$$

where ϕ is a potential function representing impressed voltage sources.

Combining equations 2.1 - 2.5 gives

$$\nabla \wedge (\nu \nabla \wedge \underline{A}) = -\sigma \nabla\phi - \sigma \dot{\underline{A}} \quad (2.6a)$$

or

$$\nabla \wedge (\nu \nabla \wedge \underline{A}) = \underline{J}_s - \sigma \dot{\underline{A}} \quad (2.6b)$$

where \underline{J}_s is a vector of source currents.

2.3 FORMULATION.

2.3.1 The nodal method

A technique is now required for converting the continuous equation 2.6 into a form suitable for solution at discrete points. Two methods are widely used, Galerkin weighted residuals [16,29,30]; and energy functionals [31,32]. However the one adopted here, the nodal method of Hanalla and Macdonald, [33], has particular advantages in ease of formulation and application to transient studies. It uses the integral form of equation 2.1, which is Ampere's Law.

$$\oint_c \underline{H} \cdot d\underline{l} = \underline{I} \quad (2.7)$$

where \underline{I} is a vector of currents applied at a finite number of points, or nodes, throughout the region.

These nodes are arranged to form the vertices of triangular elements over which the potential solution (A) is approximated by a known function. In this work, first order elements are used, which assume a linear variation of A , and thus constant values of B , ν and J , throughout the element. Material boundaries must therefore be co-incident with element boundaries - implying that the physical outline of the problem must be approximated by straight lines. The use of higher order elements relaxes some of these constraints, but is not considered to be of benefit in solving this specific type of problem.

The formulation of a discrete version of 2.6 is described in references [26] and [34], and yields an equation of the form :

$$[S](A) = (I) - [\Delta\sigma_1](A) - [\Delta\sigma_2]\left(\frac{\delta A}{\delta t}\right) \quad (2.8)$$

where $[S]$ is the system matrix, a square, symmetric and sparse matrix formed from the element geometries and reluctivities

$[\Delta\sigma_1]$) are conductivity matrices relating the induced
 $[\Delta\sigma_2]$) voltage at a node to the resulting current

and (I) is a vector of impressed currents flowing at nodes

The solution of 2.8 as a set of simultaneous equations requires A to be specified at at least one node. In rotating machines this is usually done by setting a Dirichlet boundary condition of $A = 0$ at the node at the centre of the machine cross section.

Since it can be assumed that the amount of flux escaping from the stator core back is very small, the core back may be specified as being coincident with a flux line, all the points thereon being specified as having $A = 0$. This reduces the order of the matrices in equation 2.8.

2.3.2 Periodicity.

A further reduction in problem size may be achieved by recognising that a turbogenerator has a symmetrical cross-section which results in points one pole-pitch apart having equal but opposite potential. Thus it is only necessary to solve for one pole pitch of the machine if a 'periodicity' condition is used to enforce this. The method of incorporating this boundary condition into the finite element equations via the [S] matrix is described by Chari and Silvester, [35] and Turner, [27].

2.3.3 Discretisation.

If the nodal method is applied in the machine cross section, and the machine is assumed axially uniform (ie. end effects are negligible), then the solution of equation 2.8 will give an approximation to equation 2.6 whose accuracy depends upon the fineness of division of the cross section into elements ie the discretisation. The technique piecewise linearises (A), so it will be necessary to use a fine discretisation where (A) changes rapidly in space to accurately model this variation. This is particularly important where sudden changes of flux occur, as the radial discretisation at the rotor surface must be sufficiently fine to properly model the skin effect during the early stages of a transient. In practice, this means a nodal separation of less than half a skin depth. However, as the solution time of equation 2.8 varies approximately as the square of the number of nodes, it is of benefit to coarsen the discretisation in areas where (A) changes slowly, such as the rotor core and stator core back regions.

2.3.4 Magnetic non-linearity.

If the problem to be solved contains iron materials carrying more than a small flux density, the non-linear dependance of B on H makes equation 2.8 non-linear in that $[S]$ is a function of (A) due to its dependance on ν . It will thus be necessary to iterate to a solution which contains a consistant set of (A) and ν . The Newton-Raphson method was adopted in which quadratic convergence is achieved using the derivative of equation 2.8 operating on an error vector.

$$(A)_{j+1} = (A)_j - [P]^{-1}(E) \quad (2.9)$$

where

$$(E) = [S](A) - (I) + [\Delta\sigma_1](A) + [\Delta\sigma_2]\left(\frac{\delta A}{\delta t}\right) \quad (2.10)$$

and

$$[P] = \frac{\delta(E)}{\delta(A)} \quad (2.11)$$

is termed the Hessian matrix.

For accurate modelling of the machine, the B/H curves of the various materials must be incorporated, and an efficient method used to find ν and $\frac{\delta\nu}{\delta B^2}$, since both are required in the construction of $[S]$ and $[P]$ element by element. The B/H curves of most electrical machines may be modelled by analytical approximations [36]. For turbine generators, these are usually of the form:

$$\nu = C_1 + C_2(B^2)^{C_3} \quad (2.12a)$$

$$\frac{\delta\nu}{\delta B^2} = \frac{C_2 C_3 (B^2)^{C_3}}{B^2} \quad \text{with} \quad \left. \frac{\delta\nu}{\delta B^2} \right|_{B=0} = 0 \quad (2.12b)$$

unless $B^2 > C_4$ when

$$\nu = 1 - \frac{C_5}{B} \quad (2.12c)$$

and

$$\frac{\delta\nu}{\delta B^2} = \frac{C_5}{2B^2} \quad (2.12d)$$

the curve is stored as a set of 5 coefficients C_{1-5} , for each material.

2.4 VOLTAGES AND CURRENTS IN MACHINE WINDINGS AND SOLID IRON.

2.4.1 Winding currents.

To model a machine winding carrying a current i_w , it is necessary to assign a proportion of this current to each node of the winding so that the correct ampere turns are achieved. This is performed with a winding vector (N_w) defined so that

$$(I_w) = i_w (N_w) \quad (2.13)$$

(N_w) will reflect the number of parallel paths, turns and conductors per turn in the winding, and the proportion of the area of each winding that is attributed to each node. There are several possible ways of calculating this proportion; for this work, where windings are of rectangular shape and thus may be discretised by right-angled triangles, the weighting used is as in figure 2.1a. For other areas the weighting of figure 2.1b is used.

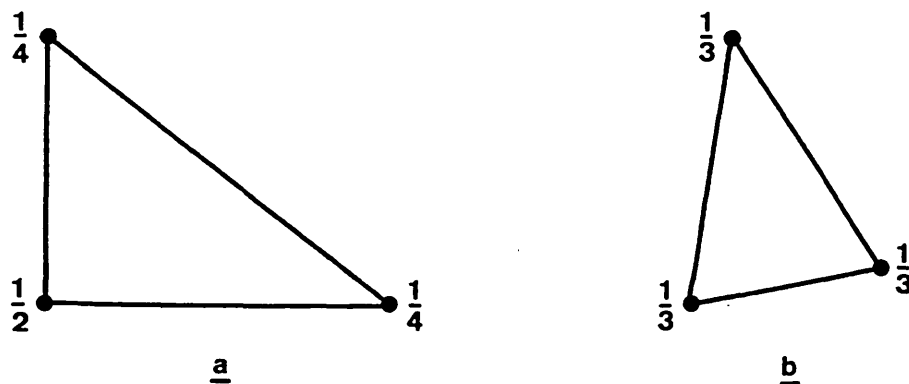


Figure 2.1 Assignment of currents to nodes.

2.4.2 Winding voltages.

Winding voltages are found from the flux linking the nodes that define them. Two nodes i, j one pole pitch apart will be linked by an amount of flux :

$$\psi_{i,j} = (A_i - A_j) \text{ per metre} \quad (2.14)$$

Chari et al. [37,38] show that the total flux linking the winding is simply

$$\psi_w = \sum (A_i - A_j) \frac{p}{2} k \text{ per metre} \quad (2.15)$$

where p is the number of machine poles

and k is a constant relating to the winding arrangement

the summation being over all the winding nodes in one pole pitch.

However, the periodicity condition gives $A_i = -A_j$ so :

$$\psi_w = \sum A_i p k \quad (2.16a)$$

or

$$\psi_w = p (N'_w)^T (A) \quad (2.16b)$$

where (N'_w) is another winding vector.

From the flux linkage, the emf may be found :

$$e_w = \frac{d\psi_w}{dt} = \frac{-d}{dt} ((N'_w)^T (A)) p \quad (2.17)$$

If the winding is connected in a circuit, the resulting current i_w may be found from e_w distributed to the winding nodes using the current winding vector.

2.4.3 Eddy currents.

Turbogenerator stators are laminated to minimise eddy current circulation, and are assumed to carry negligible eddy currents. However, the rotor is constructed from a solid steel forging, and carries further conducting materials in the form of slot wedges and damper bars. When subject to a change in flux levels, voltages will be induced and currents will flow down the machine length, turning in the endbell, and flowing back up the machine at a point one pole pitch away. The induced voltage in a circuit formed by nodes i and j is :

$$e_{ij} = \left(\frac{\delta A}{\delta t} \right)_i - \left(\frac{\delta A}{\delta t} \right)_j \quad \text{per metre} \quad (2.18a)$$

but

$$\left(\frac{\delta A}{\delta t} \right)_i = - \left(\frac{\delta A}{\delta t} \right)_j \quad (2.18b)$$

so

$$e_{ij} = e_i = 2 \left(\frac{\delta A}{\delta t} \right)_i \quad (2.18c)$$

Each node is assumed to carry a current that is the sum of the currents flowing in the 1/3 of each element that has the node as a vertex. The corresponding current is :

$$i_i = 2G_i \left(\frac{\delta A}{\delta t} \right)_i L_{eff} \quad (2.19)$$

where G_i is the conductance associated with node i

and L_{eff} is the machine effective length (allowing for stator overhang)

G_i is found from the sum of the conductances of each element associated with i :

$$G_i = \sum_e \frac{\frac{1}{3} \Delta_e \sigma_e}{2L_{eff}} \quad (2.20)$$

where Δ_e is the element area

σ_e is the element conductivity

the factor of 2 allows for the return path one pole pitch away. The endbell is assumed to have negligible resistance at this stage.

so

$$\mathbf{i}_i = \frac{1}{3} \sum_e \Delta_e \sigma_e \left(\frac{\delta A}{\delta t} \right)_i \quad (2.21)$$

2.4.4 Conductivity matrices.

Equation 2.21 may be used to form an eddy current vector :

$$(\mathbf{I}) = [\Delta\sigma] \left(\frac{\delta A}{\delta t} \right) \quad (2.22)$$

where $[\Delta\sigma]$ has only leading diagonal terms and is known as a conductivity matrix after Hanalla and Macdonald [39]. If the winding current vectors could be similarly separated into a conductivity matrix term independent of (A) multiplying an (A) -related vector leaving only a vector of constant, impressed currents then the formulation of the Hessian matrix in equation 2.11 would be simplified :

$$[P] = \frac{\delta(E)}{\delta(A)} = \frac{\delta[S](A)}{\delta(A)} + [\Delta\sigma_1] + [\Delta\sigma_2] \frac{\delta\left(\frac{\delta A}{\delta t}\right)}{\delta(A)} \quad (2.23)$$

A method is sought for describing winding induced currents in terms of conductivity matrices.

For a winding with time invariant winding vectors (N_w) and $(N_w)^T$ and no inductance $e + iR = 0$. Using equation 2.17 :

$$\mathbf{i}_w R_w = -L_{eff} p (N_w)^T \left(\frac{\delta A}{\delta t} \right) \quad (2.24)$$

and

$$(\mathbf{I}_w) = \mathbf{i}_w (N_w) \quad (2.25a)$$

so

$$(\mathbf{I}_w) = -L_{eff} p \frac{(N_w)(N_w')^T}{R_w} \left(\frac{\delta A}{\delta t} \right) \quad (2.25b)$$

or

$$(\mathbf{I}_w) = [\Delta\sigma'] \left(\frac{\delta A}{\delta t} \right) \quad (2.25c)$$

where

$$[\Delta\sigma'] = \frac{-L_{eff} p}{R} (N_w)(N_w')^T \quad (2.25d)$$

This basic idea may be extended to allow for circuit inductance and direct currents.

If di/dt is approximated by :

$$\frac{di}{dt} \approx \frac{i - i_{-1}}{\delta t} \quad (2.26)$$

$$N \frac{d\psi}{dt} + L \frac{di}{dt} + (i + i_{dc})R = 0 \quad (2.27)$$

then

$$L_{eff} P \frac{(N'_w)^T}{R} \left(\frac{\delta A}{\delta t} \right) + i \left(\frac{L}{R\delta t} + 1 \right) - \frac{L}{R\delta t} i_{-1} + i_{dc} = 0 \quad (2.28)$$

or

$$i = \frac{R\delta t}{L + R\delta t} \left(-L_{eff} P \frac{(N'_w)^T}{R} \left(\frac{\delta A}{\delta t} \right) + \frac{L}{R\delta t} i_{-1} - i_{dc} \right) \quad (2.29)$$

so

$$(I_w) = \left(1 - \frac{L}{L + R\delta t} \right) \left(-L_{eff} P (N_w) \frac{(N'_w)^T}{R} \left(\frac{\delta A}{\delta t} \right) + (N_w) \frac{L}{R\delta t} i_{-1} - (N_w) i_{dc} \right) \quad (2.30)$$

The formulation is seen to be similar to that of equation 2.25b, with a term $(1 - L/L + R\delta t)$ multiplying it; the direct current term and that relating to the current at the last time step will drop out when the Hessian matrix is formed.

2.5. ALLOWANCE FOR EFFECTS WITHIN THE MACHINE LENGTH.

The two-dimensional finite element method assumes an axially uniform machine. Although this is a good approximation for a turbine generator, improvements may be made:

Stator overhang. The effect of rotor fringing fields is modelled by specifying a machine effective length equal to the rotor length plus one air gap length.

Stator endwinding leakage reactance. The leakage fields of the stator winding in the end region are incorporated as a constant inductance in the stator winding circuit.

Laminated stator with cooling ducts. The presence of interlamination insulation and cooling ducts reduces the amount of iron present by an amount termed the stacking factor. The iron is assumed to carry all the flux, however, and the flux density in the iron is thus increased by the inverse of the stacking factor.

Ventilation ducts in rotor wedges. The wedge is modelled in the finite element cross section without the ducts, and assigned a lower conductivity such that the wedge resistance deduced from the modelled cross section is equal to the actual wedge resistance.

Discontinuous damper strips. Some machine designs feature a copper strip fitted under the low conductivity slot wedges to improve machine damping. Where the wedges carry ventilation ducts in the central section, the copper strip is placed at the ends of the machine only. The total resistance of the wedge and damper strip combined is calculated, and the damper included in the machine cross-section to be modelled. Conductivities are assigned to the wedge and damper such that their total resistance deduced from the machine cross section is equal to the actual total, and distributed between them so that their resistances are in the same ratio as actually occurs.

Inertial equalising gashes. The presence of field widening slots results in lower mechanical stiffness in these areas than in the pole region, with attendant vibration problems. To compensate, the pole face is often slotted, either axially or circumferentially. In the latter case, the gashes interrupt the axial flow of eddy currents, which are forced to flow down the edge of the slit and back up, so increasing the resistance of the eddy current path. This effect is modelled by reducing the rotor pole conductivity in two increments in the slitted region to reflect this increased path length, as shown in figure 2.2.

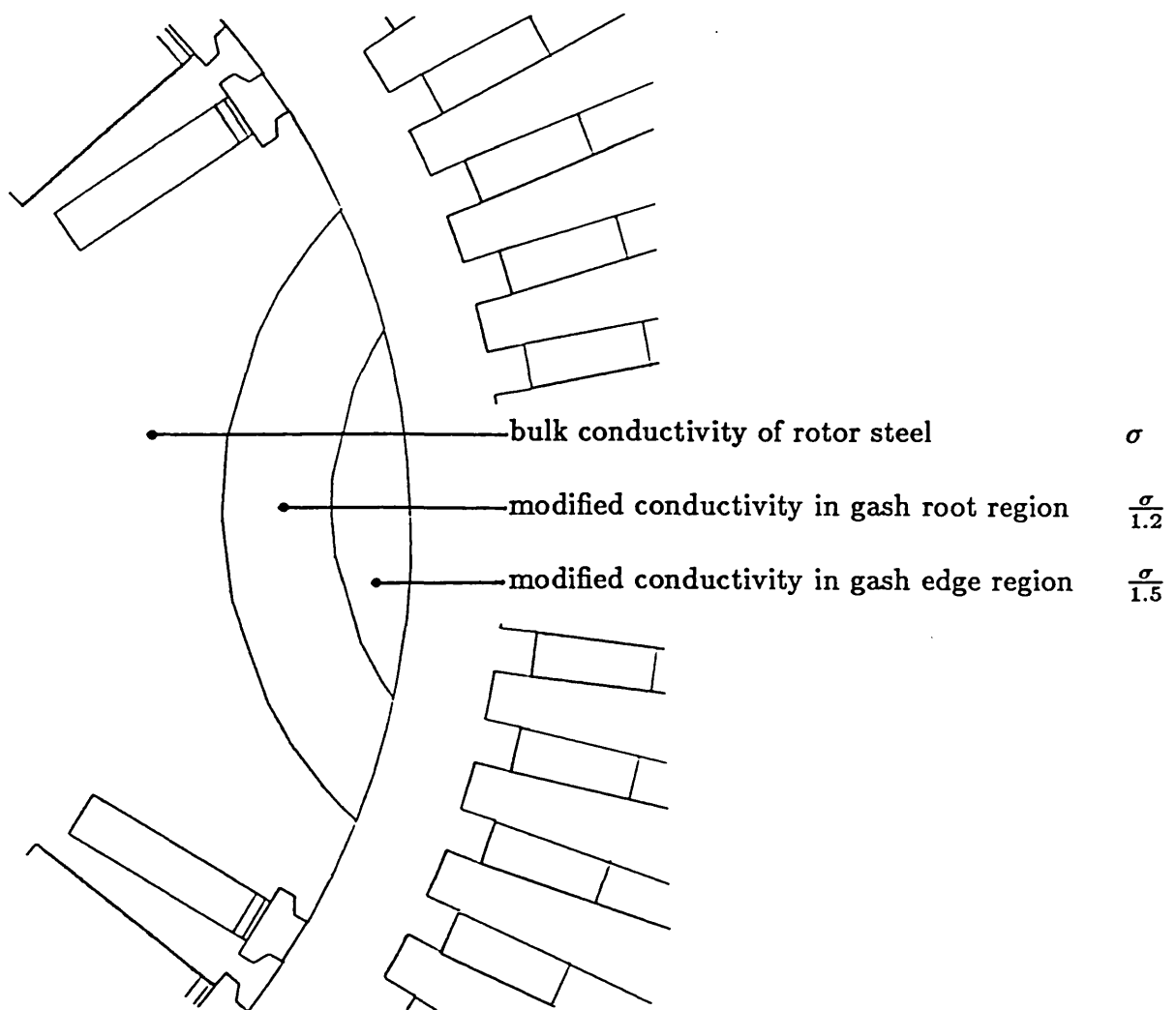


Figure 2.2 Modelling of inertia gashes.

Machine endbell. The rotor endbell is often made of non-magnetic material, such as stainless steel, which has an appreciable resistivity (≈ 3 times that of the rotor steel) Eddy currents flowing down the machine length thus encounter an additional resistance as they turn in the endbell. Two methods have been used to calculate an 'endbell factor' by which the resistivity of materials in the finite element cross section is altered to reflect this effect.

1) Fixed factor. The total axial resistance of those areas of the rotor that feed eddy currents into the endbell is calculated as R_r . The resistance of the endbell, R_b , is found by considering the currents to flow round one pole pitch.

then the endbell factor :

$$ebf = \frac{R_r + R_b}{R_r} \quad (2.31a)$$

$$\sigma' = \frac{\sigma}{ebf} \quad (2.31b)$$

2) Variable factor. The magnitude of the endbell current, and hence the endbell loss, will vary throughout the transient. Different parts of the rotor body will also carry different proportions of the loss at different times. A more accurate calculation of the endbell factor would be

$$ebf = \frac{\text{loss in rotor body} + \text{loss in endbell}}{\text{loss in rotor body}} \quad (2.32)$$

At the start of the transient, skin effect will limit conduction in the rotor and endbell to a shallow surface layer. An endbell factor, as in 1), based on the resistance of one skin depth is more appropriate until such time as the value based on losses exceeds it.

2.6 SOLUTION TECHNIQUES.

2.6.1 Matrix inversion.

By far the heaviest computational burden in the finite element method is the inversion of the Hessian matrix. The techniques most often used, are conjugate gradient methods [40,41], and Gaussian elimination [31,34]. Where the matrix is sparse and symmetric, the latter is faster for problems of less than approximately 2000 nodes. A very efficient Gaussian elimination scheme devised by Jennings [42] is used, which allows storage of the [S] matrix in a linear array containing only data values from the first non-zero in each row up to the leading diagonal. Two integer pointer arrays are used to recover the information. Not only does this reduce the amount of store required, but it also speeds the calculation. In order to take advantage of this, the mesh node numbers are re-ordered to band the non-zeros as close to the leading diagonal as possible [27]

2.6.2 A-Average technique.

Unfortunately, winding conductivity matrices of the form $(N_w)(N_w)^T$ interrupt this sparse form, since every node on the winding is connected to every other node, increasing solution times substantially. The 'A-average' technique restores the sparse nature of the [S] matrix, at the expense of adding a row and column to the matrix for each winding. Suppose only winding w is active, then :

$$[S](A) = -[\Delta\sigma_w] \left(\frac{\delta A}{\delta t} \right) \quad (2.33)$$

where

$$[\Delta\sigma_w] = k(N_w)(N_w)^T \quad (2.34)$$

so that the error vector is :

$$(E) = [S](A) + k(N_w)(N_w)^T \left(\frac{\delta A}{\delta t} \right) \quad (2.35)$$

If an average vector potential over the winding is defined as :

$$\overline{W} = (N_w)^T (A) \quad (2.36)$$

then

$$(E) = [S](A) + k(N_w) \left(\frac{\delta \overline{W}}{\delta t} \right) \quad (2.37)$$

this may be written as :

$$(E) = \begin{bmatrix} [S] & : & 0 \\ \cdots & : & \cdots \\ 0 & : & 0 \end{bmatrix} \begin{pmatrix} (A) \\ \cdots \\ 0 \end{pmatrix} + \begin{bmatrix} 0 & : & k(N_w) \\ \cdots & : & \cdots \\ k(N_w)^T & : & -k \end{bmatrix} \begin{pmatrix} \left(\frac{\delta A}{\delta t} \right) \\ \cdots \\ \left(\frac{\delta \overline{W}}{\delta t} \right) \end{pmatrix} \quad (2.38a)$$

ie. the additional column calculates the conductivity matrix term, while the additional row, added to maintain matrix symmetry, calculates:

$$k(N_w)^T \left(\frac{\delta A}{\delta t} \right) - k \frac{\delta \overline{W}}{\delta t} = 0 \quad (2.38b)$$

then if

$$\frac{\delta}{\delta (A)} ([S](A)) = [H] \quad (2.39a)$$

and

$$\frac{\delta}{\delta (A)} \left(\frac{\delta A}{\delta t} \right) = \frac{1}{\delta t} \quad (2.39b)$$

$$[P] = \begin{bmatrix} [H] & : & \frac{k}{\delta t} (N_w) \\ \cdots & : & \cdots \\ \frac{k}{\delta t} (N_w)^T & : & \frac{-k}{\delta t} \end{bmatrix} \quad (2.40)$$

[H] has the same sparsity pattern as [S] and [P] preserves this except for the bottom row, which is densely packed. The matrix symmetry is preserved. A similar procedure may be followed for the other windings, adding one row and column for each.

This analysis assumes that the winding vectors (N_w) and (N'_w) are equal. Chapter 5 demonstrates how problems arising where this is not so may be minimised.

2.6.3 Time stepping.

At the first iteration of each time step, a new set of potentials may be found from :

$$(A)_{t+\delta t} = (A)_t + \left(\frac{\delta A}{\delta t}\right) \delta t \quad (2.41)$$

Equation 2.8 is then re-solved with the new value of (A) and the old value of $(\delta A/\delta t)$ to give an improved estimate of (A) from which a new value of $(\delta A/\delta t)$ may be estimated using an implicit forward difference method.

$$\left(\frac{\delta A}{\delta t}\right)_{t+\delta t} = \frac{(A)_{t+\delta t} - (A)_t}{\delta t} \quad (2.42)$$

Alternatively, a second order Crank-Nicholson predictor may be used :

$$\left(\frac{\delta A}{\delta t}\right)_{t+\delta t} = 2 \left(\frac{(A)_{t+\delta t} + (A)_t}{\delta t} \right) - \left(\frac{\delta A}{\delta t}\right)_t \quad (2.43)$$

The first order method is required for the first time step and the first iteration of subsequent time steps. The move to a second order approximation has been found to have an advantage in certain cases.

2.6.4 Convergence.

A number of iterations are required at each time step to solve the non-linear equations arising from the saturable magnetic behaviour. Different methods of assessing convergence to a solution have been proposed, the one adopted is based on the rms change in the solution at the last iteration being less than a preset level.

$$rms\ error = \sqrt{\frac{\sum_{i=1}^n \delta A_i^2}{\sum_{i=1}^n A_i^2}} \quad (2.44)$$

where the summation is over nodes and δA_i is the change in A_i from the previous iteration.

A sufficient degree of accuracy is required so that, at the next time step, corrections to the previous solution do not produce spurious eddy currents from the resulting $\delta(A)/\delta t$. On the other hand, a more accurate solution requires more computing time, and is limited by computer numerical accuracy. It has been found that an rms error of $\leq 10^{-5}$ is a satisfactory indication of convergence (considerably higher accuracy than required for terminal values to stabilise).

2.6.5 Solution acceleration.

Once changes in (A) are small, the values of elemental reluctivities are sensibly constant. Further iterations merely producing a more accurate numerical solution with an unchanged set of reluctivities. Demerdash et al. [43] have proposed that after a certain point in an iterative calculation, the reluctivities may be considered fixed. The Hessian matrix and its inverse are also constant, so the task of solving the equations becomes simply that of reforming the right hand side terms and backsubstituting. To allow for slight re-alignment of flux within the machine, the [S] matrix is updated each time for calculation of the error vector. The paper reports substantial computational savings for steady state load point calculations in a 2-axis machine model.

In applying the idea to a transient calculation, comparison was made with a transient solution obtained by inversion at each iteration. The criterion for improvement was a saving in time without loss of accuracy (greatest error in terminal parameters $\leq 0.1\%$) or stability of convergence. Two schemes were tried:

- 1) perform the full inversion for iterations 1 to n and then at each subsequent m th iteration.
- 2) only invert the matrix if the rms error is greater than a preset value.

Neither method proved completely acceptable. 1) either showed no saving in time or proved unstable, the error growing at each iteration. With a preset error level of 10^{-3} method 2) proved stable and accurate, although periodically the solution at a time step refused to converge to below 10^{-5} , while settling below 10^{-4} . Limiting the total number of iterations became necessary, but no effect on accuracy or convergence rates was found. The net savings in time over several hundred time steps proved to be 10 – 15%.

These savings are small compared with those reported by Demerdash. This may partly be due to the use of a more efficiently banded matrix, giving less time difference between full inversion and backsubstitution; and partly to the greater accuracy required.

2.7 CONCLUSIONS.

The chapter has described how the finite element method is applied to the computation of turbine generator transient electromagnetic behaviour. A simple method of formulating the non-linear field problem using Ampere's Law (the Nodal method) was presented, which was combined with the Newton-Raphson technique to allow rapid convergence to a solution at each time step. The accuracy of convergence and level of discretisation required for a satisfactory solution were discussed, and a periodicity condition introduced to halve the problem size. Also described were the calculation of induced currents and voltages using winding vectors and conductivity matrices, allowances for three-dimensional effects within the machine length, and an efficient method for modelling the non-linear magnetic characteristics of the machine. All these techniques were applied in a manner consistent with the underlying formulation of the problem.

Two recent developments in solution methods were introduced and incorporated into the program.

- 1) The A-average technique restores the banded, sparse pattern of the system matrix by incorporating the conductivity matrix terms as additional rows and columns. This reduces the storage requirements and the time taken to invert the matrix.
- 2) After the first few iterations of each time step, the material permeabilities are considered to be invariant and the lengthy process of matrix inversion is thus no longer required. This method has previously only been applied to steady state calculations, and the adaptation required for a transient model was discussed at the end of the chapter. Care was found to be necessary in devising a reliable algorithm for selecting the point at which the full inversion is no longer to be performed.

CHAPTER THREE

THE MECHANICAL EQUATIONS OF MOTION AND MACHINE CONTROLS

3.1 INTRODUCTION.

Previous solutions of machine transient behaviour using the finite element method have assumed conditions of constant speed, ie. the mechanical behaviour of the rotor during the fault has been ignored.

A knowledge of the rotor angle variation is important when assessing machine stability and the contribution made to it by the machine governor and automatic voltage regulator. The rotor dynamics also affect the electromagnetic solution through changes in the instantaneous load angle.

In this chapter, the motion of the machine rotor relative to a synchronous frame of reference is calculated. Different techniques for determining the torque applied to the rotor are compared, and a new method proposed which is based on a balance of power flows. From the torque calculation the rotor speed and angle are found by integration.

In the second half of the chapter, the influence of the turbine dynamics, the speed governor and the automatic voltage regulator on the transient performance are discussed. Simple examples are used to illustrate how existing Laplace-transform-based models may be directly incorporated in a finite element formulation, and various computational problems that arise are discussed. The effect of the exciter circuit on the electromagnetic calculation is included at the end of the chapter.

3.2 ROTOR MECHANICAL BEHAVIOUR DURING A FAULT.

In the steady state operation of a turbine generator the steam-turbine power input is balanced by the sum of the electrical power output and the machine losses, that is the stator copper and iron loss, windage, friction, end region effects and the exciter requirement if the exciter is directly coupled.

When subjected to a transient disturbance, the losses and the electrical power output alter, but the steam turbine continues to give the pre-transient mechanical power, until the speed governor starts to act. As a result, the power balance is disturbed, and the rotor accelerates. In the case of a three phase short circuit, the electrical power falls to nearly zero, and the rotor speeds up, moving forward with respect to a synchronously rotating reference frame. If the fault is cleared sufficiently quickly, and the connection to the electrical supply grid system is re-established, the machine will settle down to its original load angle after a number of lightly damped oscillations. If not, the rotor angle will reach 180 degrees, after which it is more energetically favourable for it to continue on than swing back. The machine is then running at supersynchronous speed and is then said to be pole slipping.

At the instant of the fault, eddy currents are induced in the solid rotor, wedges and dampers. These currents produce heating, and so dissipate energy, which must be supplied from the rotor inertial energy, and a braking effect is thereby produced. The amount of energy stored in the electromagnetic fields within the machine will also change, giving rise to further power flow from the rotor. For a short period, these effects may produce a braking torque greater than the turbine input and initially cause the rotor angle to fall, a phenomenon known as rotor backswing.

3.3 CALCULATION OF ROTOR ACCELERATION.

The rotor acceleration is calculated from the net torque :

$$\bar{\theta} = \frac{T}{J} \quad (3.1)$$

(3.1) where J is the rotor inertia.

Here the shaft carrying the generator rotor and steam turbine is taken to be rigid ie. to exhibit only the coherent mode of oscillation. J is then the inertia of the whole system of rotor, exciter and turbine stages. There is no major problem in extending the analysis to multiple modes of oscillation, except provision of the necessary data. It is further assumed that mechanical damping is negligible. Torque is usually calculated either from the Maxwell stress equations or by the method of virtual work.

3.3.1 Maxwell stress.

The calculation of forces on a body using the Maxwell stress equations is described in [44] and [45]. In outline, the procedure uses a force density vector \underline{f} defined from the Lorentz equation as :

$$\underline{f} = \underline{J} \wedge \underline{B} \quad (3.2a)$$

which can be written as a two-dimensional problem in terms of a contour integral :

$$\underline{f} = \nu \oint_c \underline{T} \cdot d\underline{l} \quad (3.2b)$$

where \underline{T} is the second Maxwell stress tensor given by :

$$\underline{T} = \begin{vmatrix} B_x^2 - \frac{1}{2}|B|^2 & B_x B_y \\ B_y B_x & B_y^2 - \frac{1}{2}|B|^2 \end{vmatrix} \quad (3.2c)$$

If a contour is taken through the air gap, enclosing the rotor, the integral will give the force on the rotor. The accurate calculation of the tangential, torque-producing, component requires the summation of the difference of the squares of two similar numbers round the contour, a numerically difficult procedure on account of rounding errors. Values of \underline{B} are found by differentiating the potential solution, a process that tends to magnify errors. Different values of torque will result depending upon the location of the contour of integration. Where the airgap discretisation is not fine, the calculation may thus give significant errors.

3.3.2 Virtual work.

The method of virtual work uses the energy functional formulation of the finite element problem (see Chapter 2.3) to establish a system co-energy. The torque is then the partial derivative of the co-energy function with respect to the angular measure of virtual motion [46,47]. The integral equations that result are identical to those of the Maxwell stress approach in the limit, but are claimed to be numerically more exact in computation.

3.3.3 Power balance.

For a steady state calculation, careful use of Maxwell stress or virtual work has been shown to give good results, but this is not certain in the transient case. A simpler and easier method may be adopted for the transient that gives greater insight into the machine behaviour. It is first assumed that windage, friction, hysteresis loss and exciter power requirements change little during a transient, and then a power balance is applied between the turbine input and the other much larger power flows occurring within the machine. The components of the balance are :

- 1) Steam turbine input power, as modified by any governor action.
- 2) Electrical power generated. This is calculated from the instantaneous current and rate of change of flux linkage (ie. the 'airgap' voltage behind the stator resistance and overhang leakage reactance)

$$P = e_1 i_1 + e_2 i_2 + e_3 i_3 \quad (3.3)$$

This calculation includes the effects of power losses in the stator winding and external circuit resistance, changes in energy stored in external circuit inductances and power and Var transfer to the infinite busbar, if connected.

- 3) Field circuit power requirement, small, but given by :

$$P = v_f i_f \quad (3.4)$$

- 4) Eddy current power loss in the rotor. The voltage induced at node i due to changes in flux linkages is :

$$e_i = 2L_{eff} \left(\frac{\delta A}{\delta t} \right)_i \quad (3.5)$$

where L_{eff} is the machine effective length.

The conductance associated with this node is G_i :

$$G_i = \frac{1}{3} \sum_e \frac{\Delta_e \sigma_e}{2L_{eff}} \quad (3.6)$$

where σ_e is the element conductivity

and Δ_e is the element area

(See Chapter 2 for derivation of these equations.)

The power dissipated as heat at the node is then :

$$P_i = e_i^2 G_i \quad (3.7)$$

This is for an eddy current circuit covering one pole pitch. The total eddy current power loss in the rotor is then :

$$P = \frac{1}{2} p L_{eff} \sum_{i=1}^n G_i \left(\frac{\delta A}{\delta t} \right)_i^2 \quad (3.8)$$

where the summation is over all the nodes in the mesh and p is the number of machine poles.

Implicit in this analysis is the assumption that the heating effect of the eddy currents is not great enough to alter the material conductivities significantly. Although power dissipation may be high at the start of the transient, the eddy currents are relatively short lived, so the energy input to the conducting materials is not large.

5) Energy storage in magnetic fields within the machine. This is given by :

$$E = \frac{1}{2} B H \text{ per unit volume} \quad (3.9)$$

Within the machine length, the calculation is made element by element in terms of B^2 , which is obtained directly from A. The energy stored in an element is then:

$$E_e = \frac{1}{2} \nu_e B_e^2 (\Delta_e L_{eff}) \quad (3.10)$$

where ν_e is the element reluctivity.

so the total energy stored in the machine, assuming a one pole pitch mesh, is :

$$E = L_{eff} p \sum_e \nu_e B_e^2 \Delta_e \quad (3.11)$$

where the summation is over all the mesh elements

If this energy changes over a small time interval Δt , power ΔP must be supplied or absorbed. A reasonable approximation for ΔP is :

$$\Delta P = \frac{\Delta E}{\Delta t} \quad (3.12)$$

These equations use the machine effective length for both rotor and stator. Although not exact, this is regarded as a reasonable simplifying assumption. Similarly, the use of a modified flux density in the stator region to allow for stacking factor effects is adopted as giving a good approximation to the energy storage division between laminated iron and the inter-lamination air.

Calculation of stored energy changes in end region fields is only approximate, and based on circuit equations. Thus the power flow due to the field circuit end winding inductance L_f is :

$$\Delta P = \frac{1}{2} i_f L_f \frac{di_f}{dt} \quad (3.13)$$

A similar calculation to allow for the stator overhang leakage reactance is already included in equation 3.3 via the circuit equations used to calculate stator currents.

3.4 CALCULATION OF ROTOR SPEED AND ANGLE.

Section 3.3 gives the net power available to accelerate the rotor. From this the torque may be found directly, if speed (and hence frequency) are considered constant over the integration step, using

$$T = \frac{\Delta P}{\omega} = J \ddot{\theta} \quad (3.14a)$$

Alternatively, the differential equation may be recast in terms of speed squared by recognising that $\omega = \dot{\theta}$:

$$\Delta P = \omega J \dot{\omega} = \frac{1}{2} J (\dot{\omega}^2) \quad (3.14b)$$

The machine is assumed to be initially rotating at synchronous speed.

From either procedure, a further integration will give rotor angle. The procedure of 3.14b was adopted as likely to be more accurate, although this does involve finding the difference of two squares, with possible rounding error problems.

The initial rotor angle is taken as the machine load angle calculated from the initial condition ie. the angle of the axis of flux within the machine from the pole axis.

3.5 MACHINE CONTROLS.

Three external factors will influence the machine behaviour; the speed governor, the turbine dynamics and the automatic voltage regulator. The governor and turbine response are normally combined and regarded as one system. There are many models of machine control systems available, a simple, generalised one is shown in figure 3.1.

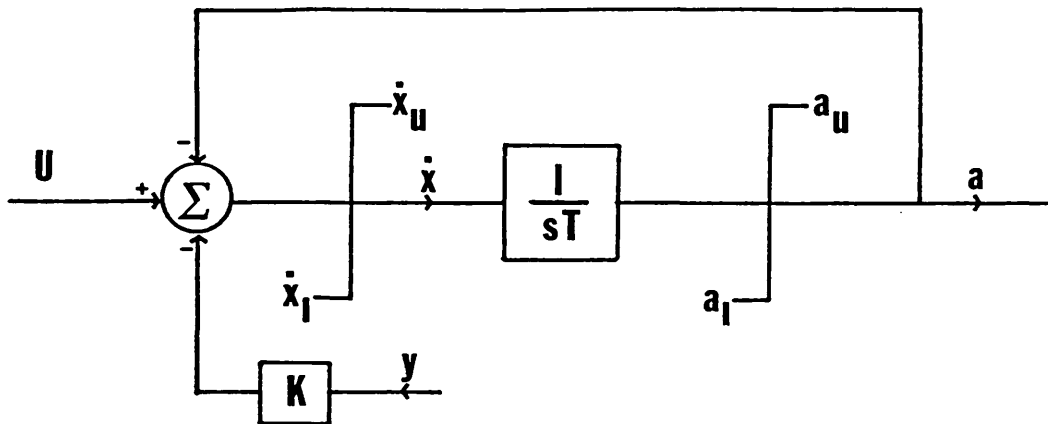
3.5.1 Governor.

A speed governor has two main functions; to control the machine power output in the steady state, and the machine speed during disturbances. It performs these tasks by accepting a no load turbine speed signal and a rotor speed feedback signal, and uses these to control the steam valves on the turbine set. Auxiliary signals from power system stabilisers and optimal controllers could also be added.

The mechanical equations couple directly with the governor inputs and output, so the governor model may be included as a 'black box', performing its calculation separately from the finite element solution.

Governor and turbine performance is conventionally characterised by gains, time constants and rate limits stated in terms of Laplace transforms [48], using a per unit system of base power = rated VA and base speed = 1 rad/s.

The finite element calculation outputs speed at discrete time intervals. It would be possible to transform the Laplace transform governor model to a discrete-time z transform, but calculation of the response in the time domain is



K = controller gain

T = controller time constant

U = controller set point

\dot{x}_u = maximum response rate going positive

\dot{x}_l = maximum response rate going negative

a_u = maximum positive response

a_l = maximum negative response

the response is defined by:

$$\dot{x} = U - ky - a \quad (3.15a)$$

$$\dot{x}_l \leq \dot{x} \leq \dot{x}_u \quad (3.15b)$$

$$\frac{da}{dt} = \frac{\dot{x}}{T} \quad (3.15c)$$

Figure 3.1 Generalised machine control system model.

straightforward, and may be found by superposition of the effects of step inputs at each time step. This allows a simple implementation of rate and position limits. If the time step length is small, the error in the time at which the system reaches a limit is minimal.

Valving rates are usually much slower than the electromagnetic time constants, and it can prove necessary only to update the valve positions periodically, after a fixed number of time steps, to avoid numerical rounding errors.

3.5.1.1 Time lags.

Steam valves are commonly some distance from the turbine blading. There is thus a time lag between valve operation and turbine response due to the intervening entrained steam. Modelling this as a further time constant is not very satisfactory, and a better procedure is to store the valve response at each step, and 'look back' to find the turbine behaviour. If P is the turbine power and V the valve position, then :

$$P|_t \propto V|_{t-t_{lag}} \quad \text{for } t \geq t_{lag} \quad (3.16a)$$

$$P|_t \propto V|_{t=0} \quad \text{for } t \leq t_{lag} \quad (3.16b)$$

The proportionality may be a constant or may allow for non-linearity in the valve fluid dynamics.

3.5.2 Automatic voltage regulator and exciter.

The automatic voltage regulator (AVR) controls machine reactive power output in the steady state, and acts to maintain the machine terminal voltage during a transient. It achieves this by control of the machine excitation. There are many different excitation systems in use, ranging from a fixed d.c. source with rheostat to a.c. sources with thyristor controlled bridge rectifiers [49,50].

The AVR inputs are a set point reactive power and the machine terminal voltage. Terminal voltage is usually derived from a step down transformer, rectifier and smoothing circuit. The circuit may include lags, not all phases may be sampled, and the transformer may be star or delta connected to the terminals.

These different methods will give different feedback signals under unbalanced fault conditions and accurate modelling of the response will require a knowledge of which method has been used in practice.

As with the governor, the AVR model may be added separately to the finite element model, although some approximation may be necessary when finding the terminal voltage feedback signal.

AVR and exciter performance is characterised by Laplace transforms with limits and with rotating exciters, simple saturation characteristics may also be built in. Several different per-unit systems for specifying field quantities are in common use [50,51]. These affect the relation between the exciter output voltage and the field circuit applied voltage; normally an additional scaling factor is required to link the two. This becomes particularly important when transferring the per unit values from the exciter model to the 'actual' values used in the electromagnetic solution.

Many AVR models have feedback terms of the form :

$$\frac{a}{b}(s) = \frac{1}{1 + sT} \quad (3.17)$$

The finite element output, being at discrete intervals, can be represented as a series of step function inputs :

$$b(s) = \frac{\Delta b_i}{s} \quad (3.18)$$

combining 3.17 and 3.18 and transforming to the time domain gives :

$$a_i(t) = \Delta b_i \left(1 - \exp^{-\frac{t}{T}} \right) \quad (3.19)$$

in this form, the present response is the sum of the responses to all the past inputs steps Δb_i , which would require recalculation and summation at each time step. This may be avoided by rewriting 3.19 at time $(t + \delta t)$ as :

$$a_i(t + \delta t) = \Delta b_i \left(1 - \exp^{-\frac{t}{T}} \exp^{-\frac{\delta t}{T}} \right) \quad (3.20a)$$

rearranging equation 3.19 and substituting for $\exp \frac{-t}{T}$ in 3.20b :

$$a_i(t + \delta t) = \Delta b_i (1 - \exp \frac{-\delta t}{T}) + a_i(t) \exp \frac{-\delta t}{T} \quad (3.20b)$$

Now the only information required is a_i at the previous time step. The response to a series of step inputs Δb_i is then simply :

$$a(t + \delta t) = \sum_i a_i(t + \delta t) = (1 - \exp \frac{-\delta t}{T}) \sum_i \Delta b_i + \exp \frac{-\delta t}{T} \sum_i a_i(t) \quad (3.21a)$$

or

$$a(t + \delta t) = (1 - \exp \frac{-\delta t}{T}) (b(t + \delta t) - b(0)) + a(t) \exp \frac{-\delta t}{T} \quad (3.21b)$$

3.5.2.1 Exciter circuit - the effect on the electromagnetic calculation.

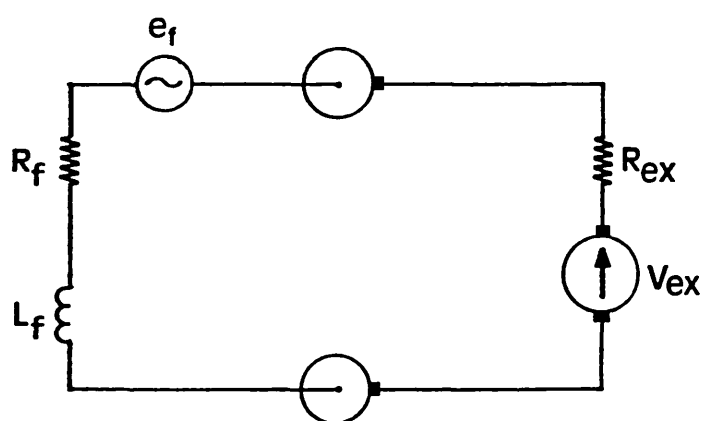
The character of the exciter supply to the field circuit may affect the finite element calculation. If the supply is via a bridge rectifier circuit, then the field current cannot become negative, since the diodes will reverse bias and effectively open circuit the field winding. This effect has not been included, but may be allowed for by adding the field circuit conductivity matrix to the Hessian matrix only where the diodes are forward biased.

Older designs of excitation system utilise a d.c. machine to supply the field voltage through slip rings and control the field voltage by adjusting the exciter field voltage.

The machine field circuit thus contains the exciter and brush contact resistance, as well as the field winding resistance, as in figure 3.2

Brush contact tends to exhibit a constant voltage drop. This may be approximated by an equivalent resistance, R_b , calculated at the nominal current. The field circuit current is then found from :

$$R_f i_f + L_f \frac{di_f}{dt} + e_f + 2R_b i_f + R_{cx} i_f + V_{cx} = 0 \quad (3.22)$$



e_f is the transient induced voltage in the field winding

V_{ex} is the exciter internal voltage

R_{ex} is the exciter internal resistance.

Figure 3.2 Field winding circuit.

Field voltage is normally measured at the sliprings, and is then found from :

$$V_f = e_f + R_f i_f + L_f \frac{di_f}{dt} \quad (3.23a)$$

although it may sometimes be measured across the exciter

$$V'_f = V_e + i_f R_f \quad (3.23b)$$

3.6 CONCLUSIONS.

Three methods of calculating rotor torque have been discussed in this chapter. The Maxwell stress and virtual work approaches present numerical problems and were discarded in favour of a new, and much simpler, method based on a balance of power flows within the model. This proved easier to calculate and provided a deeper physical insight into the transient behaviour of the machine.

It is clearly an advantage to be able to include the widely used Laplace-transform-based machine control models in the calculation without major adaptation and in a manner such that the machine/control interaction may be obtained and compared with test measurements. This was shown to be possible, and a simple means of incorporating governor valve time delays was described. Feedback terms in automatic voltage regulators present a potential problem and an efficient method was outlined for handling them, without recourse either to z-transforms or substantial programme storage.

The behaviour of the excitation system will alter the electromagnetic characteristics of the field circuit. An allowance for this effect has been incorporated in the model and was presented at the end of the chapter.

Although in this chapter the machine has been considered to behave as a single inertia; a multimode response could be calculated, using the method described, by replacing equation 3.14 with the full set of differential equations specifying the rotor dynamic behaviour.

CHAPTER FOUR

THE POLE SLIPPING TESTS AT USKMOUTH B POWER STATION

4.1 INTRODUCTION.

In October 1979 the C.E.G.B. performed a number of system transient tests on the Uskmouth B Unit 14 generator, an initial series of tests having previously been undertaken on this machine to determine its electrical parameters and saturation characteristics. The principal feature of the more recent tests was the inducement of pole slipping by a reduction in the generator excitation and by the application of symmetric and asymmetric faults on the high voltage side of the generator transformer.

The ultimate object of the tests was to assess the performance of protection relays designed to operate under pole slipping conditions, and their discrimination between fault types. Subsidiary objectives were to obtain test results against which existing generator models could be assessed for their representation of pole slipping conditions, and the determination of shaft torques caused by slowly cleared system faults. A considerable quantity of data was collected during the course of the tests, which permits validation of the finite element method [51,52].

This chapter presents detailed information about the pole slipping tests undertaken at the Uskmouth B power station. Data is provided for the generator transformer, transmission line network and the detailed design of the generator set, and the methods used to model them are described.

Specific information is given regarding the transient tests for which simulations are to be undertaken, and some aspects of the presentation of the

data are discussed. The chapter is concluded with details of the governor/turbine and automatic voltage regulator/exciter models to be used.

4.2 GENERATOR SET DETAILS.

The principal features of the machine are given in table 4.1.

Machine inertias are usually given in terms of a normalised inertia constant H , which enables machines of widely different sizes to be compared. H and J are related by :

$$H = \frac{\omega_0^2 J}{2P_b} \quad (4.1)$$

where P_b is the machine rated VA.

The generator cross section is shown in figure 4.1. The centre of the rotor forging is hollow and the machine poles carry 13 inertia equalising gashes distributed along their length. The rotor slot wedges are of stainless steel and are perforated by 16 ventilation ducts in the central region. Under the wedges at each end of the rotor there is a small hard drawn copper damper strip. The construction is illustrated in figure 4.2

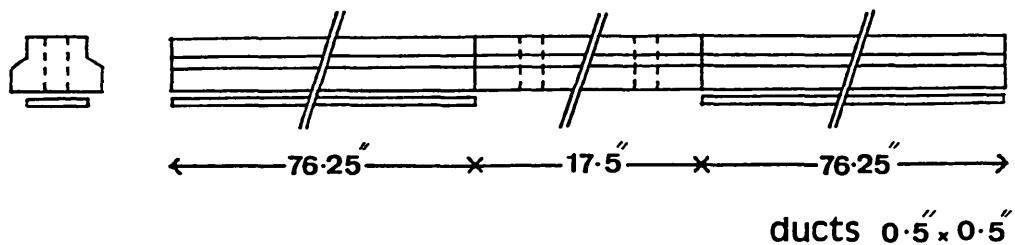


Figure 4.2 Arrangement of slot wedge and damper bar showing ventilation ducts.

TABLE 4.1 USKMOUTH B UNIT 14 GENERATOR

Rating

150 MVA

120 MW

13.8 kV

2 pole

3000 rpm

Stator construction.

number of slots	60
conductors per slot	2
turns per phase	10
coil pitch	$1-26 = \frac{5}{6}th$
total length	170"
stacking factor	0.9

Rotor construction.

cooling	hydrogen
number of slots	32
slot pitch	7.65 deg
turns per pole	79
diameter	40"
inertia constant, H	3.64 kWs/kVA
endbell peripheral cross section	$22" \times 2\frac{3}{4}"$
Airgap	$2\frac{3}{8}"$

The rotor endbell is constructed of non-magnetic steel. Table 4.2 shows further

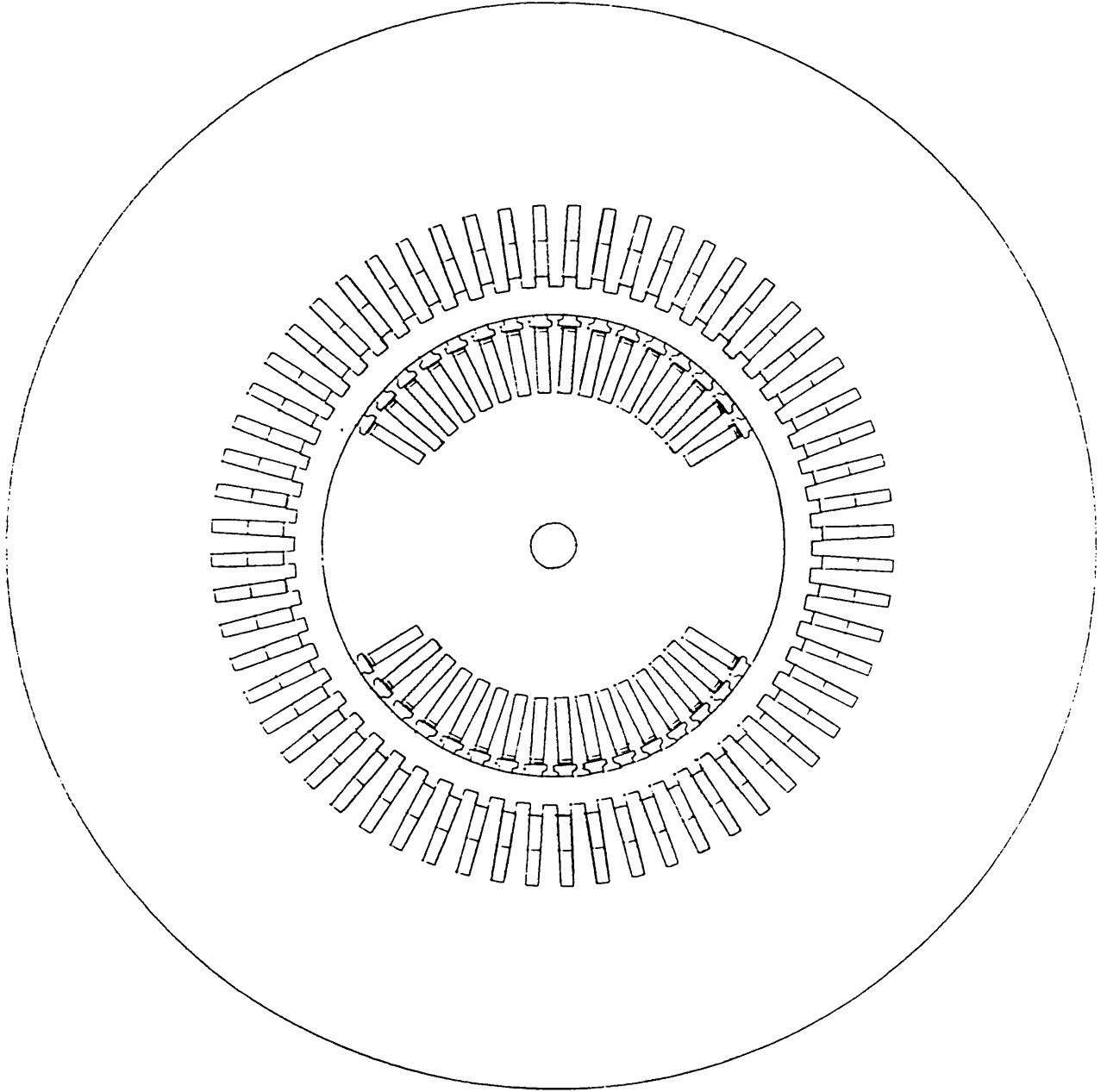


Figure 4.1 Machine cross section.

TABLE 4.2 GENERATOR DETAILS

stator overhang leakage reactance	0.000173	henries/phase
rotor endwinding inductance	0.005	henries
field winding resistance at 50 deg C	0.1559	ohms
exciter resistance	0.00334	ohms
material conductivities at 20 deg C		
rotor body forging	24×10^{-8}	
rotor wedge	71×10^{-8}	
damper strip	1.77×10^{-8}	
endbell	80×10^{-8}	

details of the machine construction.

The generator excitation characteristics are shown in figure 4.3, taken from manufacturer's data. Table 4.3 gives the machine equivalent circuit parameters as determined by the C.E.G.B. tests.

4.3 GENERATOR TRANSFORMER.

4.3.1 Transformer details.

The Uskmouth generator transformer is of the usual delta-star connection. Throughout the tests it was set to its minimum tapping to minimise the stress imposed on the tapping gear and restrict the initial fault current to ≈ 3 p.u.. The required terminal voltage was obtained by control of the system voltage via the supergrid transformer tapplings. The generator transformer parameters are shown in table 4.4.

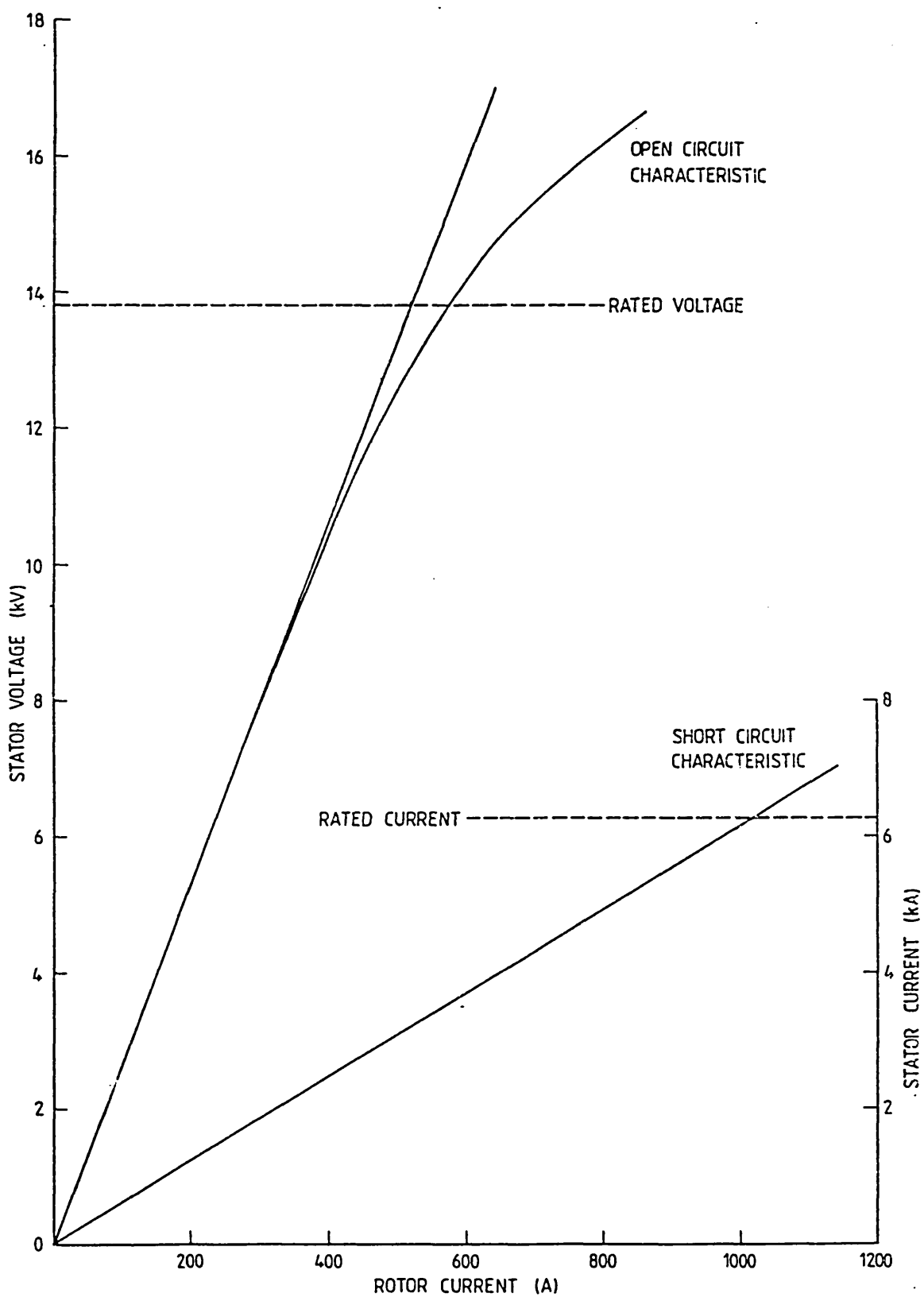


Figure 4.3 Uskmouth excitation characteristics.

TABLE 4.3 GENERATOR PARAMETERS

All parameters are expressed on generator rating base (150MVA)

Direct axis synchronous reactance	$X_d = 1.94$ p.u.
Direct axis transient reactance	$X'_d = 0.219$ p.u.
Direct axis subtransient reactance	$X''_d = 0.149$ p.u.
Quadrature axis synchronous reactance	$X_q = 1.64$ p.u.
Quadrature axis transient reactance	$X'_q = 0.3$ p.u.
Quadrature axis subtransient reactance	$X''_q = 0.208$ p.u.
Zero sequence reactance	$X_o = 0.85$ p.u.
Armature leakage reactance	$X_a = 0.125$ p.u.
Armature resistance	$R_a = 0.0015$ p.u.
Direct axis transient time constant	$T'_d = 0.602$ sec.
Direct axis subtransient time constant	$T''_d = 0.0222$ sec.
Quadrature axis transient time constant	$T'_q = 0.2$ sec.
Quadrature axis subtransient time constant	$T''_q = 0.222$ sec.

TABLE 4.4 GENERATOR TRANSFORMER PARAMETERS

Voltage ratio (p.u. on 13.8/132 kV basis)	= 1 : 0.989
Reactance (p.u. on 144 MVA base)	= 0.169
Resistance (p.u. on 144 MVA base)	= 0.0043

4.3.2 Transformer modelling.

The transformer was modelled as a series R,L as given above. The effect of the delta-star connection was allowed for by modelling a three phase to earth fault on the star side as an isolated three phase-to-phase fault (without earth) at the machine terminals. The problem of the unknown phase shifts in the generator and transmission line transformers is avoided by calculating the initial condition with the transformer, transmission line and infinite busbar referred to the stator terminals (see section 4.4.3) For the simulation of unbalanced faults and circuit breaker scatter a more complete model of the transformer is needed. The method described in [53] could be adapted, although this would then require further data.

The model is a steady state one, except in that it allows for frequency changes by using an $L\frac{di}{dt}$ formulation rather than XI . It may be necessary to model the transient, non-linear, behaviour of the transformer for a more accurate representation of the fault. This could be done in finite element terms, either directly via a linked, time stepped transient model of the transformer, or indirectly via previous saturation studies and a look-up table of parameters. A solution of intermediate complexity might be obtained by incorporating a magnetic circuit approach, such as those of Carpenter [54], Haydock [55] and Turowski [56], into the finite element solution at each time step.

4.4 THE TRANSMISSION LINE NETWORK.

4.4.1 Transmission line details.

For the purposes of the transient tests, the local transmission line network was configured to give an 80km dedicated connection between the Uskmouth

unit 14 generator transformer and the 400 kV busbar at Melksham. The Melksham connection can be considered to be an infinite busbar behind an impedance equivalent to a three phase short circuit infeed of approximately 20,000 MVA. The largest voltage disturbance, measured during the tests, at Melksham was 2.5%. The test system comprised of :

- i) Uskmouth B Unit 14
- ii) Generator 14 transformer
- iii) Uskmouth supergrid transformer, SGT3 - Whitson - Tremorfa circuit (132/275kV)
- iv) Whitson - Iron Acton No.2 circuit (including quadrature booster)
- v) Iron Acton - Melksham No.1 circuit
- vi) Iron Acton - SGT1 and SGT (off load)
- vii) Melksham supergrid transformer, SGT5 (275/400kV)

and is shown in simplified form in figure 4.4. The section parameters are summarised in table 4.5.

4.4.2 Transmission line modelling.

To incorporate the transmission line circuit into the finite element calculation, each section was first reduced to an equivalent π network, converting from per unit to real values at the same time, as in figure 4.5a. The impedances were then referred back to the generator terminals, allowing for the transformer settings, to give figure 4.5b. A Thevenin reduction was then applied to give the final series R,L circuit of figure 4.5c.

The system voltage was recorded during the tests using a chart recorder at a nearby busbar. This chart recorder was not specifically calibrated for the tests, but should have given a reasonably accurate measurement of the voltage at the Melksham busbar.

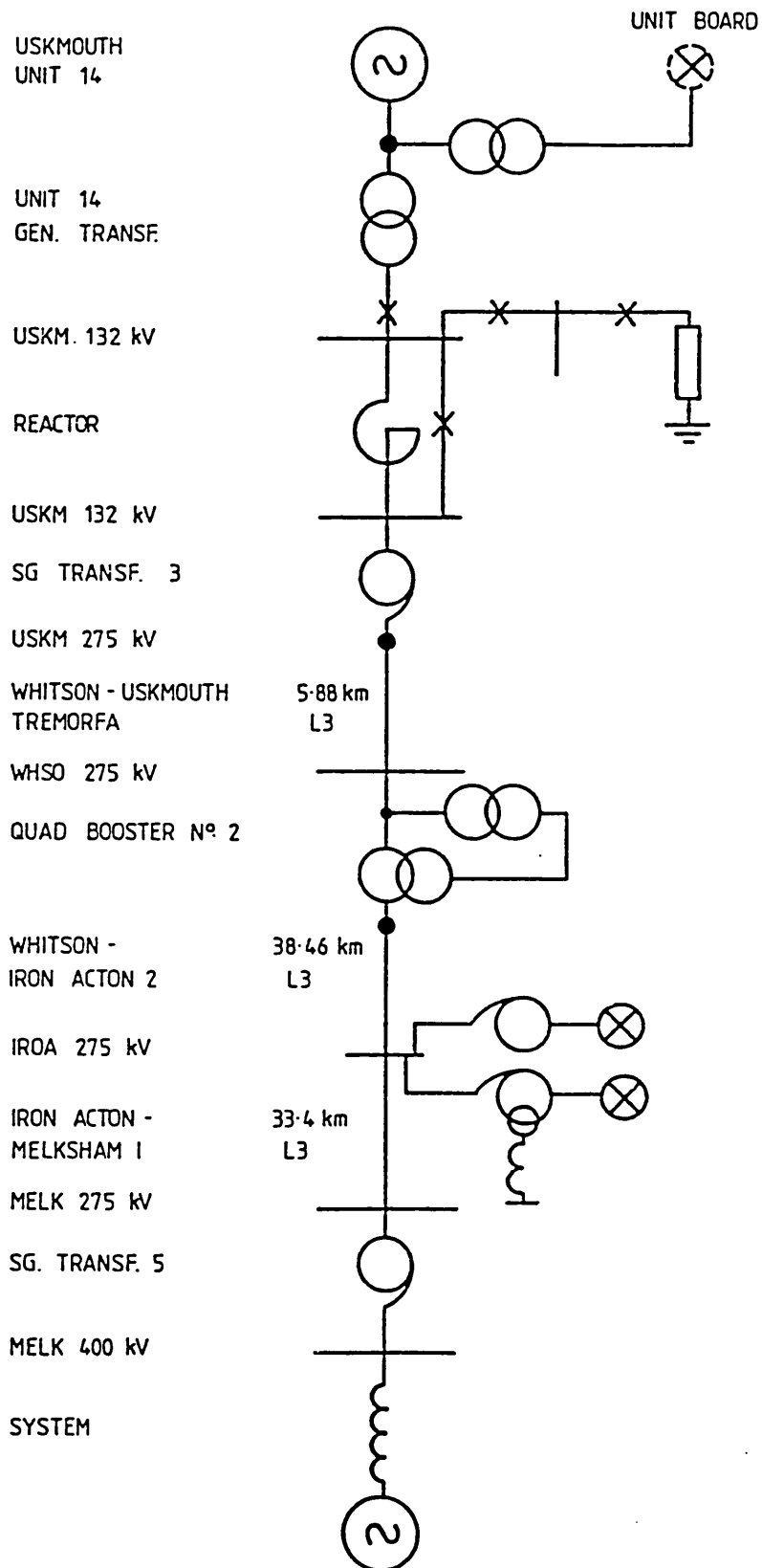


Figure 4.4 Simplified diagram of test system

TABLE 4.5 TRANSMISSION LINE DATA

Supergrid transformer SGT 3

Voltage ratio (p.u. on 132/275 kV basis) = 1 : 1.15

Reactance (p.u. on 120 MVA base) = 0.1455

Resistance (p.u. on 120 MVA base) = 0.0039

	Resistance	Reactance	Susceptance
SGT3 - WHSO2	0.065	0.23	1.5
WHSO2 quad. booster	0.0	0.46	0.0
WHSO2 - IROA2	0.405	1.416	9.57
Iron Acton - neutral	0.0	0.0	-60.0
IROA2 - SGT5	0.398	1.4	13.9
SGT5	0.018	1.6	0.0
SGT5 - Infinite busbar	0.0	0.5	0.0

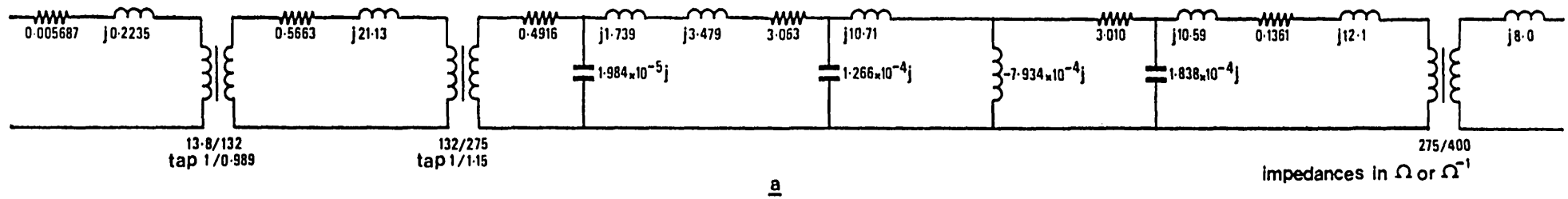
All the above parameters are in percent on 100 MVA base.

4.4.3 Calculation of infinite busbar voltage from the initial condition.

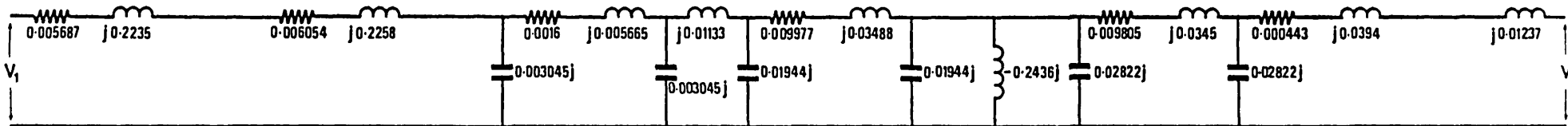
The grid connection is to be modelled as an infinite busbar behind a characteristic infeed impedance. In order to calculate the infinite busbar voltage required, two assumptions are made.

- 1) That the infinite busbar is balanced ie. $\sum i = 0$ and $\sum V = 0$
- 2) That the delta-star transformer balances the machine phase voltages by removing harmonic terms.

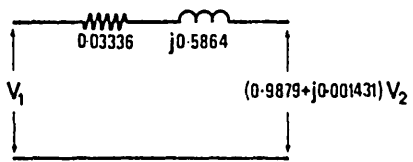
The latter assumption is required to allow that, while the phase voltages at the generator terminals are unbalanced, ie. $e_1 + e_2 + e_3 \neq 0$ where e_i is the phase



a



b



c

Figure 4.5 Progressive reduction of test system to Thevenin equivalent circuit.

i voltage (due particularly to the third harmonic) requirement 1) can still be achieved.

In the infinite busbar voltage calculation, the terminal voltages are balanced as in equation 4.2.

$$e'_i = e_i - \frac{1}{3}(e_1 + e_2 + e_3) \quad (4.2)$$

This is equivalent to removing the third harmonic term, which is the property of a delta connected winding.

The voltages e'_i are applied to the transmission line to find a set of infinite busbar voltages V_i . These three voltages are most conveniently characterised by a magnitude V_b and the angle of one of the phase voltages from its zero crossing going positive at that instant, ϕ . The infinite busbar phase i voltage at a subsequent time t is then :

$$V_i(t) = V_b \sin(\omega_0 t + \phi + (i - 1)\frac{2}{3}\pi) \quad (4.3)$$

The problem of the unknown phase shifts in the delta-star transformer and other parts of the circuit are avoided by this method.

The accuracy of the initial condition was checked by comparing the infinite busbar voltage so calculated with that measured by the C.E.G.B.

At the instant before fault clearance the currents in the transmission line are flowing from the infinite busbar into the fault. Following fault clearance and reconnection of the generator to the transmission line the direction of current flow is reversed. An additional approximation is made that the transmission line pre-fault current has negligible effect and that the value of $\frac{di}{dt}$ derived for the generator side of the fault may be used for the whole of the transmission line. To correctly model this current reversal necessitates modelling of the circuit breaker arcing characteristics in order that a sudden step change in current is not imposed on the system. This requires modelling as an asymmetrical fault condition, which

is not possible with the present generator transformer model. It is not thought that the errors involved are great.

The transmission line model used is essentially steady state, although frequency changes are allowed for by using an $L \frac{di}{dt}$ formulation instead of $X I$, and it may prove necessary to incorporate the transient behaviour of the transmission line for greater accuracy.

4.5 THE C.E.G.B. TRANSIENT TESTS.

4.5.1 Fault condition.

Two of the transient tests undertaken by the C.E.G.B. were selected for simulation, B and C1. Both were simultaneous three phase to earth short circuits followed by removal of the fault and reconnection to the transmission line. The results are summarised in table 4.6.

4.5.2 Fault throwing.

The faults were applied and cleared at the 132kV busbar of the generator transformer using an air blast circuit breaker and the connection from the busbar to the transmission line was not interrupted. Considerable scatter occurred in the operation of the circuit breaker, as table 4.6 shows.

4.5.3 Generator terminal measurements.

Terminal quantities were deduced from phase measurements as :

$$P = V_1 I_1 + V_2 I_2 + V_3 I_3 \quad (4.4a)$$

TABLE 4.6 TEST CONDITIONS

	B	C1
Initial condition		
Terminal power (MW)	111.1	101.6
Terminal reactive power (MVA _r)	-35.2 *	-33.5 *
Terminal voltage (kV)	13.80	14.03
Terminal current (kA)	4.88	4.40
Rotor angle to terminal (deg)	61.5	56.0
Field voltage (V)	120	112
Field current (A)	827	774
Melksham 400kV voltage (kV)	405	407
* leading power factor		
Transient conditions		
Fault on red phase (ms)	14.4	6.4
Fault on yellow phase (ms)	0.8	8.0
Fault on blue phase (ms)	0.0	0.0
Fault off red phase (ms)	148.0	287.2
Fault off yellow phase (ms)	142.4	283.2
Fault off blue phase (ms)	140.8	280.0
Average fault duration (ms)	138.7	278.7
Maximum rotor angle (deg)	101.1	unstable
Rotor angle swing (deg)	39.6	-
Time to maximum rotor angle (s)	0.36	-
Frequency of rotor oscillation (Hz)	1.25	-

In test C1, the unit was automatically tripped after 1.2 seconds, the generator having slipped two poles.

$$V = \sqrt{\frac{V_1^2 + V_2^2 + V_3^2}{3}} \quad (4.4b)$$

$$I = \sqrt{\frac{I_1^2 + I_2^2 + I_3^2}{3}} \quad (4.4c)$$

Only two line-line voltages were measured at the machine terminals, and used to derive the three corresponding phase voltages for use in equation 4.4 above. During unbalanced operation, these will thus be in error.

4.5.4 Data filtering.

The C.E.G.B. recorded test data at 0.8ms intervals and then subjected them to a moving average digital filter to remove the substantial noise present. Stator terminal quantities were filtered over 25 data points ie one a.c. cycle, which caused some distortion during the fault period. It was intended to filter the field quantities over half a cycle to remove any 100Hz component, however this is not possible with a 0.8ms sampling time, so the filter was applied over 13 samples, resulting in a reduction of the 50Hz component to about 60% of the unfiltered amplitude, and a phase advance of around 90 deg. Figure 4.6 illustrates the effect of such filtering when a pure sine wave is suddenly switched on.

4.5.5 Rotor angle measurement.

The machine rotor angle was measured using a fixed detector and a marker on the rotor shaft. The resulting signal was used to reset a ramp generator, so producing a saw-toothed wave. This wave was then sampled at 0.8 ms intervals and the crossover point of the ramp with a pre-set datum compared with the negative going positive crossing of a reference signal varying at system frequency. The rotor angle was found directly from this and, in consequence, was recorded

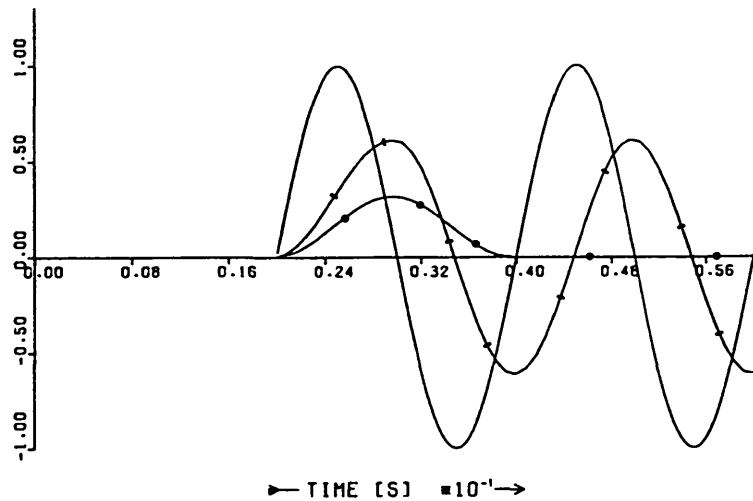


Figure 4.6 Sudden application of a sine wave.

unfiltered ——— full wave filter —●— $\frac{13}{25}$ wave filter —▲—

at only 20ms intervals. The rotor speed was obtained from analysis of the rotor angle ramp waveform.

4.6 THE AUTOMATIC VOLTAGE REGULATOR AND EXCITER.

The Uskmouth generator excitation is supplied by a d.c. machine, control of the generator field voltage being obtained by adjustment of the exciter field. Such a system has a relatively slow response, low ceiling voltage and a non-linear characteristic due to magnetic saturation of the exciter. The exciter commutator presents additional resistance to the circuit, which may be modelled as described in Chapter 3.5.2.1.

The only data available for the Uskmouth AVR and exciter was that given in the test report, [51], intended specifically for use with the C.E.G.B. equivalent circuit based multi-machine transient stability program 'RASM05' [57,58].

The model is shown in figure 4.7. This very simple representation of the excitation system dynamics has the advantage of keeping to a minimum the number of machine states to be solved in the equivalent circuit formulation, but cannot be expected to accurately represent the real system response. On the other hand, with slow response and low ceiling, it is unlikely that the generator excitation control will make a significant contribution to the machine stability.

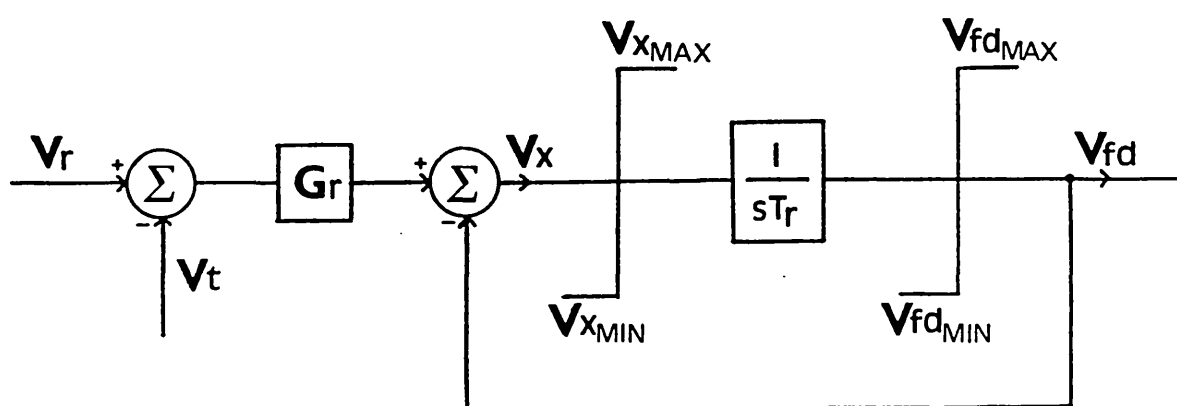


Figure 4.7 Excitation system model.

The model constants, given in table 4.7, are derived from the machine parameters of table 4.3, with an allowance for generator saturation.

4.7 THE MACHINE GOVERNOR AND STEAM TURBINE.

As with the exciter, the governor data and model used was that intended for the RASM05 program. The model is comprehensive and includes the turbine response. It allows for separate governor and interceptor valve motion (the latter only occurring above a preset degree of overspeed), time lags in both valves, time delays in the reheater, pressure drops in piping and the power balance

TABLE 4.7 EXCITATION SYSTEM PARAMETERS

Regulator gain, G_r	=	0.01259
Regulator time constant, T_r	=	1.224s
$V_{fd_{rated}}^*$	=	0.000966 p.u.
$V_{fd_{max}}$	=	0.002136 p.u.
$V_{fd_{min}}$	=	-0.000737 p.u.
$V_{x_{max}}^+$	=	0.00164 p.u.
$V_{x_{min}}$	=	-0.00469 p.u.

The derivation includes a system damping factor of 0.28

* field voltage required to give rated output at rated terminal voltage and rated, lagging power factor (in p.u. on rated MVA)

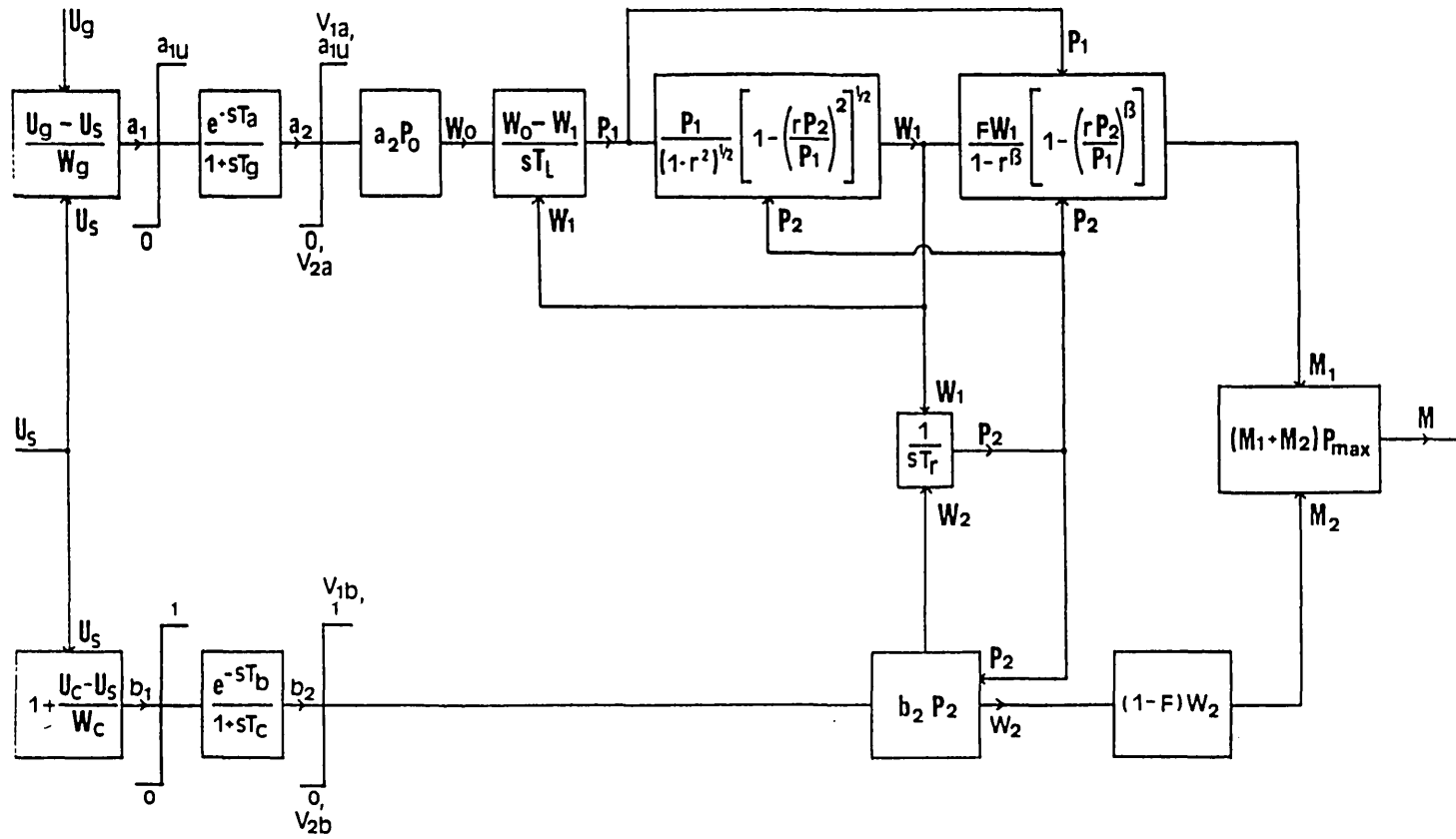
† (maximum rate of change of V_{fd}) $\times T_r$

between the high pressure and other stages. The model is shown in figure 4.8, and the model constants used as given in table 4.8.

4.8 CONCLUSIONS.

The detailed information required for simulation of two of the transient tests performed by the C.E.G.B. has been presented in this chapter, with a summary of how it was incorporated in the finite element calculation.

The transmission line was of considerable complexity and required reduction to a suitable combination of Thevenin equivalent circuit and infinite busbar, which was described. The delta-star transformer representation used was very simple and unable to handle unbalanced faults. Nevertheless, it provided a workable model requiring the minimum of data, although this gave rise to problems



$$\beta = \frac{\gamma - 1}{\gamma}$$

$$U_g = \text{speeder gear setting, } U_s = 1 - \frac{\omega}{\omega_0}$$

Figure 4.8 Governor and turbine system model.

TABLE 4.8 GOVERNOR PARAMETERS

Regulation of speed governor loop	$W_g = 0.04$ p.u.
Time constant of H.P. throttle valve	$T_g = 0.117$ sec
Transport lag in H.P. valves	$T_a = 0.2$ sec
Upper valve position limit	$a_{1u} = 1.1$ p.u.
Upper rate limit on H.P. valves	$V_{1a} = 0.175$ /sec
Lower rate limit on H.P. valves	$V_{2a} = -5.96$ /sec
Regulation of interceptor loop	$W_c = 0.04$ p.u.
Speed at which interceptor starts to close	$U_c = 1.03$ p.u.
Time constant of interceptor valve	$T_c = 0.1$ sec
Transport lag in interceptor valves	$T_b = 0.2$ sec
Upper rate limit on interceptor valves	$V_{1b} = 0.33$ /sec
Lower rate limit on interceptor valves	$V_{2b} = -5.19$ /sec
Loop time constant for H.P. steam flow	$T_l = 0.1$ sec
Reheater time constant	$T_r = 5.1$ sec
Ratio of actual reheater to H.P. inlet pressures at full load	$r = 0.266$
Constant relating output of H.P. and other stages	$F = 0.292$
Isentropic expansion index for steam	$\gamma = 1.3$

in the calculation of the infinite busbar voltage and reference angle. The solution of these difficulties was described and possible improvements to the models were discussed.

The techniques used by the C.E.G.B. for measuring and presenting test data were then discussed, to enable an accurate comparison to be made with the results of the simulations.

Finally, data for the governor and turbine and automatic voltage regulator models were presented, and the adequacy of the models discussed.

CHAPTER FIVE

THE TWO-AXIS STATOR MODEL

5.1 INTRODUCTION.

A significant problem which arises when using the finite element method to model rotating machines occurs in the representation of the relative motion between rotor and stator. The solution used almost exclusively since the earliest application of the finite element method to this type of problem has been to employ the Park transform [2] to produce a two-axis model of the machine.

In this chapter, the analysis of Chapter 2 is simplified by adopting the two-axis transformation of the stator windings. The problems arising from the densely packed, asymmetric matrix that results are minimised by the application of the A-average technique and a new adaptation of Jennings's Gaussian elimination scheme. A further reduction of the stator model to a current sheet is described.

The two-axis approach has been in use for a number of years for solving machine transient problems where the flux is aligned with an axis of symmetry in the machine. It has also been extensively used for modelling steady state conditions where the flux adopts an unknown angle within the machine. This chapter is thought to present the first two-axis finite element analysis of transient conditions where the load angle is unknown, and varying.

By considering rotational and transformer voltages separately, an approximate solution is obtained that enables the computational time step length

to be increased as the transient proceeds. The consequences of this approximation are discussed, and an analytical method for allowing for one of the discarded components is presented.

The incorporation of the infinite busbar into the formulation is described and the further approximations required to permit the Newton-Raphson method to be applied in this situation are discussed.

The chapter concludes by comparing the performance of the two-axis model with the test results. The effects of mesh discretisation, and the use of a current sheet stator are also examined. Flux and eddy current plots are presented to illustrate the progress of the transient.

5.2 STATOR WINDING REPRESENTATION.

5.2.1 Three to two phase transformation.

In a turbine generator, the stator conductors are distributed in phase bands in the stator slots. The effect of the Park transform is to replace the phase bands by two orthogonal windings carrying sinusoidally distributed currents. If the two windings rotate synchronously and carry direct currents equal to the peak value of the three phase alternating current, then the transformed machine will have the same peak fundamental airgap mmf as the three phase machine. This arrangement is different from the one usually adopted for equivalent circuit models, where it is assumed that the two-phase windings have the same number of turns as the turns per pole in each phase of the three phase winding. This latter case allows that the air gap flux will give the same voltage in a two-phase coil as it will in a three phase coil, for the same condition. The choice between the two is, to a large extent, arbitrary; but the equal-current formulation adopted here was utilised because it reduces the number of multiplying constants in the equations.

The two-phase windings are normally centred on the polar and interpolar axes of the machine, when they are known as the direct (d) and quadrature (q) axis windings.

5.2.2 Winding vectors and terminal voltage calculation.

Fractional numbers of conductors are attributed to winding node i as :

$$(N_d)_i = \frac{6}{\pi} N_{eff} \frac{\Delta_i \sin \theta_i}{\sum_{j=1}^n |\Delta_j \sin \theta_j|} \quad (5.1a)$$

$$(N_q)_i = \frac{6}{\pi} N_{eff} \frac{\Delta_i \cos \theta_i}{\sum_{j=1}^n |\Delta_j \cos \theta_j|} \quad (5.1b)$$

where Δ_i is the area of winding attributed to node i

θ_i is the angle that node i makes with the d-axis

and N_{eff} is the effective turns/phase/pole (allowing for winding factors)

The flux linkage, ψ , with a single turn spanning 180 electrical degrees varies sinusoidally as :

$$\psi = \phi \sin(\omega t) \quad (5.2)$$

so the voltage per turn is :

$$V_t = \phi \omega \cos(\omega t) \quad (5.3)$$

Turns at an angle θ from the coil axis contribute voltages at an angle $(90 - \theta)$ from the net voltage. Integrating up the voltages from the individual turns gives the winding voltage V_2 as :

$$V_2 = \frac{6}{\pi} N_{eff} [\phi \omega \cos(\omega t)] \int_0^\pi \sin \theta \cos(90 - \theta) d\theta \quad (5.4a)$$

so

$$V_2 = 3N_{eff} [\phi \omega \cos(\omega t)] \text{ volts/pole pair} \quad (5.4b)$$

The multiplying factor in equation 5.1 assumes that the two and three phase currents are equal. In order that the same power is dissipated in the three and two phase windings, the three phase voltage corresponding to V_2 is $\frac{2}{3}V_2$.

d- and q-axis voltages may be defined by :

$$e_d = \omega \psi_q \frac{p}{2} \quad (5.5a)$$

$$e_q = -\omega \psi_d \frac{p}{2} \quad (5.5b)$$

where p is the number of machine poles

Equation 2.16 shows that the flux linking a winding may be written in terms of a winding vector and the potential solution. This leads to :

$$e_d = p \omega L_{eff} (N_q)^T (A) \quad (5.6a)$$

$$e_q = -p \omega L_{eff} (N_d)^T (A) \quad (5.6b)$$

(A detailed consideration of the sinusoidally distributed winding and the correctness of the resulting winding vectors is given in references [37] and [38].)

Equation 2.6 will then reduce to :

$$[S](A) = (I) - [\Delta\sigma](A) \quad (5.7)$$

The steady state problem has thus been reduced to a magnetostatic one, at the expense of only modelling the fundamental component of the air gap flux.

In the absence of stator currents, the terminal line voltage is then :

$$V_t = \sqrt{3} \sqrt{\frac{2}{3}(e_d^2 + e_q^2)} \quad (5.8)$$

5.2.3 Finding the initial condition.

Any desired open circuit condition may be achieved simply by varying the field current until the correct stator voltage is reached.

When the stator winding carries current, a different procedure must be adopted to arrive at the correct terminal conditions. It is assumed that the terminal voltage and the real and reactive power are known (or equivalently the voltage, current and power factor). A parallel resistance and reactance is added to each of the two axis windings, as in figure 5.1, of such a value that, when the terminal voltage is correct, the required real and reactive powers are present in the external circuits.

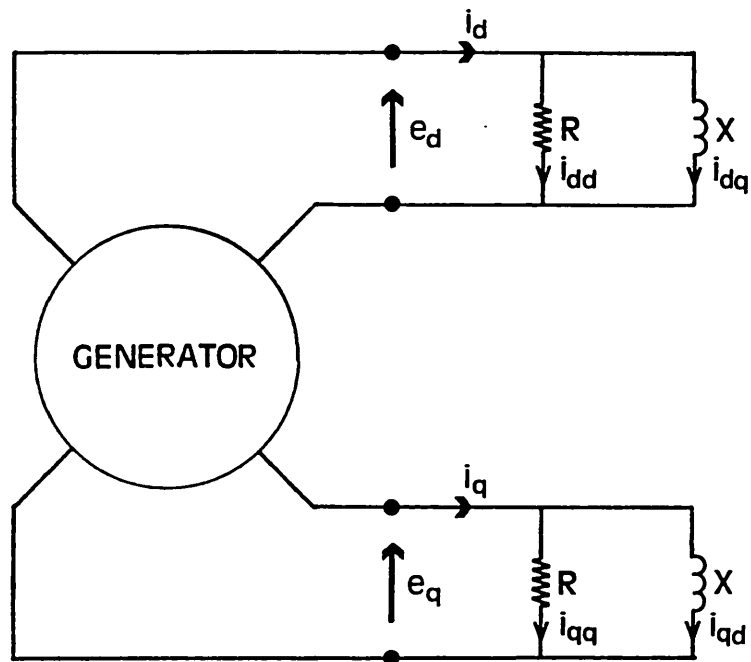


Figure 5.1 Stator circuit representation.

$$I^2 R = \frac{1}{2} \frac{S^2}{P} \quad (5.9a)$$

$$I^2 X = \frac{1}{2} \frac{S^2}{Q} \quad (5.9b)$$

where I is the line current required

S is the total VA) Including winding resistive

P is the total real power) and overhang leakage

Q is the total reactive power) reactive drops

Adopting a parallel circuit separates the phase currents into d- and q-axis components as in figure 5.2, which allows the use of the flux linkage winding vectors to redistribute the phase currents to nodes.

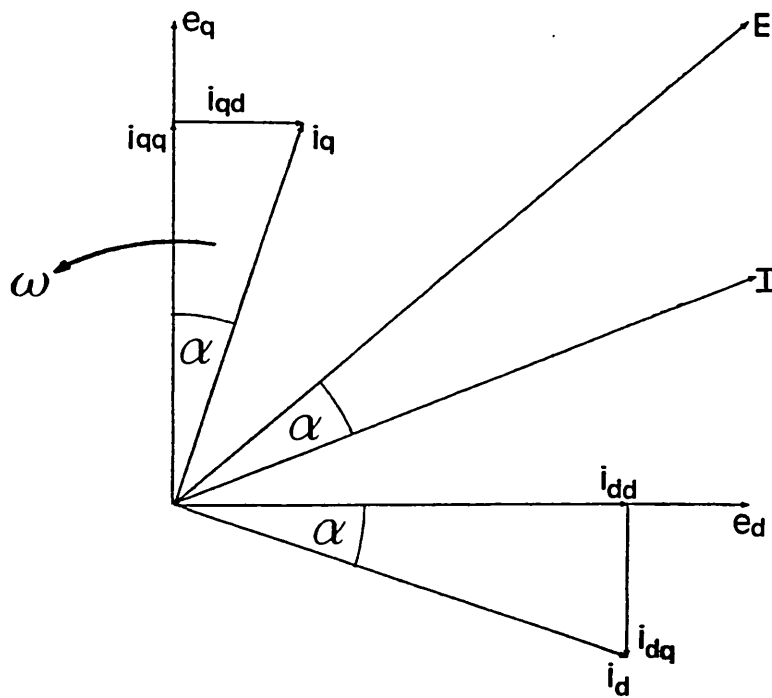


Figure 5.2 Stator current components

$$\begin{aligned}
i_{dd} &= \frac{e_d}{R} \\
i_{dq} &= \frac{e_d}{X} \quad (\text{note : negative direction}) \\
i_{qq} &= \frac{e_q}{R} \\
i_{qd} &= \frac{e_q}{X}
\end{aligned} \tag{5.10}$$

combining these with equation 5.6 :

$$\begin{aligned}
(I_{dd}) &= i_{dd}(N_d) = \frac{p\omega L_{eff}}{R} (N_d)(N_q)^T (A) \\
(I_{dq}) &= -i_{dq}(N_q) = -\frac{p\omega L_{eff}}{X} (N_q)(N_q)^T (A) \\
(I_{qq}) &= i_{qq}(N_q) = -\frac{p\omega L_{eff}}{R} (N_q)(N_d)^T (A) \\
(I_{qd}) &= i_{qd}(N_d) = -\frac{p\omega L_{eff}}{X} (N_d)(N_d)^T (A)
\end{aligned} \tag{5.11}$$

It can be seen that the conductivity matrices that will arise from differentiating equations 5.11 with respect to (A), besides being densely packed, are not symmetric in the i_{dd} and i_{qq} terms. This loss of symmetry significantly increases the time required to invert the matrix. A modification to the A-average technique of chapter 2 reduces the asymmetry to just two terms in the bottom right hand corner of the matrix, which may be efficiently handled by a modification to the Jennings method. Details are given in the Appendix.

5.2.4 Current sheet stator models.

The mmf drop in a turbine generator stator is only a small proportion of the drop in the complete magnetic circuit, yet a finite element machine model uses up a significant number of nodes (and hence computational time) in representing the stator on account of the large number of slots. If the stator could be ignored, substantial savings in solution time would result.

The two-axis approach incorporates many of the phase band features algebraically by distributing the winding currents to the stator slots sinusoidally.

A logical extension of this process is to 'smear out' the sinusoidal winding into a current sheet and discard the stator iron altogether, with a Neuman boundary condition applied to the nodes of the current sheet to force flux to exit normal to the sheet. If desired, the position of the current sheet may be adjusted, using Carter's coefficients, to allow for stator tooth fringing effects and the stator mmf drop now not modelled. The slot leakage component lost in the process is replaced by an equivalent reactance added to the stator overhang leakage reactance.

Stator currents are distributed according to a one-dimensional version of equation 5.1 :

$$(N_d)_i = \frac{6}{\pi} N_{eff} \frac{\lambda_i \sin \theta_i}{\sum_{j=1}^n |\lambda_j \sin \theta_j|} \quad (5.12a)$$

$$(N_q)_i = \frac{6}{\pi} N_{eff} \frac{\lambda_i \cos \theta_i}{\sum_{j=1}^n |\lambda_j \cos \theta_j|} \quad (5.12b)$$

where λ is the length of the current sheet attributed to node i

5.3 ROTATIONAL AND TRANSFORMER VOLTAGES.

Previous work by Hanalla, Macdonald and Turner, [27,59], has identified two components of stator voltage :

1. A 'rotational' voltage, produced by the motion of a constant, direct flux as it cuts a circuit, inducing a voltage proportional to $\omega(A)$. Rotationally induced voltages are alternating but, in a rotor frame of reference, they appear as direct voltages in the d- and q-axis coils.
2. A 'transformer' voltage, produced by a change in the magnitude of the flux linking a circuit inducing a voltage proportional to $(\delta A/\delta t)$. Transformer voltages are direct but, in a rotor frame of reference, they appear as alternating voltages in the d- and q-axis coils.

These definitions relate primarily to the different types of conductivity matrix used in the finite element formulation, and differ slightly from those used with equivalent circuit machine models. In a two-axis representation of the machine steady state, there are no transformer voltages.

For some types of machine transient, it is possible to categorise the source of the stator voltage as being purely transformer eg a field decrement test with the stator open circuited, or a stator decrement test (neglecting the 'second order' effect of flux produced by rotor eddy currents). In others, such as the field decrement test with a short circuited stator, the rotational voltages dominate and transformer voltages are neglected.

A sudden three-phase short circuit features both rotational and transformer voltages of comparable magnitude. These appear in a two-axis model as direct and alternating voltages respectively; and since the alternating voltage may be viewed as a modulation of the direct voltage, and in many cases it is the form of the time response rather than the detail that is required (eg for decay curve fitting), the alternating component is often discarded by incorporating only the stator rotational conductivity matrix in the formulation, [59]. Provided that the alternating component does not drive parts of the machine severely into saturation, the d.c.-only curve will be a close fit to the mean of the envelopes of the full response. With the alternating component missing, it is no longer necessary to limit the time step to capture the oscillations, and (once the sub-transient period is over) the time step length may be increased substantially.

The resulting transient equation is :

$$[S](A) - (I_f) + [\Delta\sigma_r](A) + [\Delta\sigma_t]\left(\frac{\delta A}{\delta t}\right) + [\Delta\sigma_f]\left(\frac{\delta A}{\delta t}\right) = 0 \quad (5.13)$$

where $[\Delta\sigma_r]$ is the stator rotational conductivity matrix

$[\Delta\sigma_t]$ is the solid rotor transformer conductivity matrix

$[\Delta\sigma_f]$ is the rotor winding transformer conductivity matrix
and (I_f) is the field current

5.4 THE EFFECT OF IGNORING STATOR TRANSFORMER TERMS ON THE MECHANICAL BEHAVIOUR.

Discarding the stator transformer conductivity matrix is analogous to ignoring the $p\psi$ terms in the equivalent circuit solution method. Shackshaft, [60], has shown that these $p\psi$ terms give rise to an oscillatory torque as energy flows into and out of magnetic field storage, which occurs as a result of the interaction of the stationary flux pattern frozen in the air gap at the start of the transient with the moving rotor flux pattern. These fluxes alternately reinforce and cancel and give rise to alternating currents in windings and the solid rotor circuits, as described by Say [61].

The net effect of the oscillatory torque is not zero, as Shackshaft demonstrates, but may be considered as equivalent to a step change in rotor speed. In the absence of resistance, and with second order terms ignored, the electrical torque is given by :

$$T_e = T_s \sin(\omega_0 t) \quad (5.14a)$$

$$T_s = \frac{V}{x_d''} \text{ per unit} \quad (5.14b)$$

where V is the per unit pre-fault terminal voltage

and x_d'' is the generator d-axis subtransient reactance,

including the generator transformer reactance.

The resulting average speed change is :

$$\frac{d\theta}{dt} = \frac{T_s}{2H} \text{ rad s}^{-1} \quad (5.15)$$

Alternatively, the effect of the transient torque can be viewed as a torque impulse, T_i , applied over a short time period, t_i , and given by :

$$T_i t_i = \frac{T_s}{\omega_0} \quad (5.16)$$

The two-axis model used does not include the oscillating torque term, so a second set of simulations were performed in which the direct calculation of magnetic stored energy was discarded; and a torque impulse calculated as above and applied over the initial time step, was substituted.

The weakness of this method is that the simulation is now dependent upon a knowledge of the machine parameters, which requires either that the machine has been already built and tested, or that additional calculations have been made to determine x_d'' .

5.5 TRANSIENT INITIATION.

The transient is initiated by changing the parallel R and X at the terminals from the value required by the initial condition to the short circuit values. The potentials are assumed, initially, to be unchanged, and $(\delta A/\delta t) = 0$. The new value of the conductivity matrix, however, will give a revised estimate of the potential solution at time δt , and this allows a first estimate of $(\delta A/\delta t)$:

1st iteration :

$$(A_1)_1 = (A)_0 \quad \left(\frac{\delta A}{\delta t}\right) = 0 \quad (5.17a)$$

$$\text{find new } (A) : (A_2)_1 = (A_1)_1 - [P]^{-1}(E) \quad (5.17b)$$

$$\text{find new } \left(\frac{\delta A}{\delta t}\right) : \left(\frac{\delta A}{\delta t}\right) = \frac{(A_2)_1 - (A)_0}{\delta t} \quad (5.17c)$$

Improved estimates of (A) and $(\delta A/\delta t)$ are then made as described in chapter 2. A convergence limit is set at an rms error of 10^{-5} and the calculation continued to the next time step by estimating a new set of potentials as :

$$(A_1)_2 = (A)_1 + \left(\frac{\delta A}{\delta t}\right)_1 \delta t \quad (5.17d)$$

The second order, Crank-Nicholson predictor for $(\delta A/\delta t)$ was used from the third time step (see chapter 2), but cannot satisfactorily be used for the second step because the very large values of $(\delta A/\delta t)$ at the first time step would thereby be carried through to predict erroneous values of (A) at subsequent steps.

5.6 TIME STEP LENGTHENING.

For an accurate solution, the time step length used must be small enough to give a good forward prediction of the potential at the next time step. As the transient proceeds, the magnitude of $(\delta A/\delta t)$ falls and the time step length may be correspondingly increased, without loss of accuracy, giving very substantial savings in solution time. Turner, [26,27], has discussed factors influencing the optimum time step length with reference to transients involving a slow decay of the stator voltage, such as the flux decay test. When applied to a general machine transient, it was found that no one algorithm for determining the appropriate time step length was completely reliable. The number of iterations required with a fixed step length varies considerably from one step to the next, possibly as the changing axis of saturation within the machine brings different material types into prominence. Thus any method based on the number of iterations or first iteration error level is likely to give indifferent results.

The basis of the method adopted here is the minimum nodal time constant τ

$$\tau = \min \left(\frac{|(A)_i|}{\left| \left(\frac{\delta A}{\delta t}\right)_i \right|} \right) \quad (5.18)$$

When τ exceeds a predetermined fraction of the existing time step length, the step length is doubled. Spuriously short time constants can occur as the result of numerical rounding errors where $(A) \approx 0$, so these values are ignored. This procedure is sensitive to the controlling fraction, too large a value and the process can 'run away', with the time step length doubling at each step, giving significant errors. On the other hand, too low a value, and the time step length is never altered. In some calculations the time step length has been observed to increase smoothly during the subtransient period, but then to remain unchanged during the transient, when it could be expected to continue to be automatically increased.

The first time step of the transient represents a period when currents in windings are allowed to change instantaneously. A very short initial time step length is used to capture this behaviour, which is then rapidly increased. The maximum time step length is effectively limited by the minimum time constant of the machine governor and exciter.

5.7 INCORPORATION OF THE INFINITE BUSBAR AFTER RECLOSURE.

On fault clearance, the machine is reconnected to the grid system via the transmission line, but, unlike the steady state condition, this cannot be modelled purely as a fixed load impedance in parallel with the machine terminals. A method similar to that used for the steady and short circuit conditions was adopted, but which allows for the change in the angle between the rotor axis and the infinite busbar. As before, real and reactive power in the series circuit is equated with that in a parallel one, but the presence of the infinite busbar voltage in the former complicates the analysis. For the circuit of figure 5.3a

$$(e_0 - e_b \cos \alpha)^2 + (e_b \sin \alpha)^2 = I_2^2 (R_2^2 + X_2^2) \quad (5.19a)$$

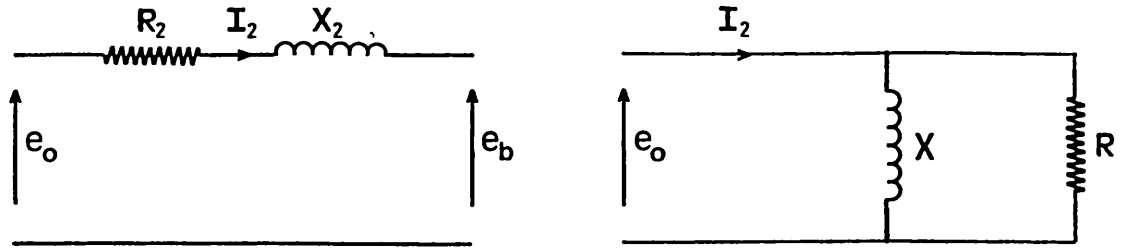


Figure 5.3 Incorporation of the infinite busbar into the stator circuit.

where e_0 is the machine 'air gap' voltage

e_b is the voltage at the infinite busbar

and α is the angle between e_0 and e_b calculated as :

$$\alpha = (\angle e_{b0} + \theta) - \arctan \frac{e_d}{e_q} \quad (5.19b)$$

$\angle e_{b0}$ is the angle of the infinite busbar voltage from the machine quadrature axis at the start of the transient

θ is the change in the rotor angle since the start of the transient

$$P_2 = I_2^2 R_2 + I_2 e_b \cos \phi_b \quad (5.20a)$$

$$Q_2 = I_2^2 X_2 + I_2 e_b \sin \phi_b \quad (5.20b)$$

$$\phi_b = \arctan \frac{i_{da}}{i_{qa}} - (\angle e_{b0} + \theta) \quad (5.20c)$$

where i_{da} , i_{qa} are the components of currents referred to the d- and q-axes, (not i_d and i_q).

$$i_{da} = i_{dd} + i_{qd} \quad (5.20d)$$

$$i_{qa} = i_{qq} + i_{dq}$$

The equivalent parallel circuit of figure 5.3b gives :

$$P_2 = \frac{e_0^2}{R} \quad (5.20e)$$

$$Q_2 = \frac{e_0^2}{X}$$

Equating P_2 and Q_2 enables an expression for R and X to be found.

$$R = \frac{(R_2^2 + X_2^2) e_0^2}{R_2[(e_0 - V_b \cos \alpha)^2 + (V_b \sin \alpha)^2] + \sqrt{R_2^2 + X_2^2} \sqrt{(e_0 - V_b \cos \alpha)^2 + (V_b \sin \alpha)^2} V_b \cos \theta} \quad \Omega \quad (5.21a)$$

$$X = \frac{(R_2^2 + X_2^2) e_0^2}{X_2[(e_0 - V_b \cos \alpha)^2 + (V_b \sin \alpha)^2] + \sqrt{R_2^2 + X_2^2} \sqrt{(e_0 - V_b \cos \alpha)^2 + (V_b \sin \alpha)^2} V_b \sin \theta} \quad j \Omega \quad (5.21b)$$

As a result of the complication of the infinite busbar, R and X are now dependent upon the components of the terminal voltage and current. Thus the derivative of the current vector, when expressed in conductivity matrix terms, is no longer independent of (A); and, strictly, the formulation of the Hessian matrix, [P], is not valid (see Chapter 2.3.4). If the values of R and X do not change rapidly with time, then an acceptable approximation which preserves the conductivity matrix formulation is to fix the values of R and X at the start of each time step and regard them as independent of (A). The penalty to be paid is the increased number of iterations required to cope with the change in R and X from one time step to the next, and the reduction in scope for time step lengthening.

For the first time step of the reclosure period, an estimate must be made of the required values for the calculation of R and X , based on the machine state immediately before the reclosure, but with the new terminal conditions imposed. The values so arrived at will not be correct, but over the subsequent few time steps the correct ones will be approached. In the interim, there will be some fluctuation in the terminal values and spurious eddy currents will have been generated, affecting the loss and storage terms. If the time step length at the point of reclosure is suitably short these will not be very marked.

The Crank-Nicholson second order predictor was tried during the reclosure period, but gave a bad initial estimate of the potentials at the start of each

time step. As a result, a large number of iterations were required at to achieve convergence, which effectively prevented the time step length from being increased. Accordingly, the simple first order predictor was used.

Terminal power is calculated from $P = \sqrt{3} V_l I_l \cos \phi$, the power factor angle being obtained from the current and voltage solution.

$$\phi_b = \arctan \frac{i_{da}}{i_{qa}} - \arctan \frac{e_d}{e_q} \quad (5.22)$$

5.8 COMPARISON OF SIMULATED AND MEASURED RESULTS, C.E.G.B. TEST B.

5.8.1 Meshes.

Two levels of discretisation have been used for the simulations, a relatively crude mesh, UM3, and a more detailed representation, UM9. The meshes are shown in figures 5.4 to 5.10. The detailed mesh has two layers of elements at the rotor surface each with a thickness of 5mm, the order of the skin depth in the rotor steel. The cruder mesh has a rotor surface element thickness of 10mm in the tooth area, and 27mm in the pole area. Two current sheet stator models, designated UM3C and UM9C, were derived from these. The discretisation of each is identical with the mesh it is based upon, the current sheet being defined by the nodes used to model the stator tooth tips. Details of all four meshes are given in Table 5.1.

5.8.2 Initial conditions.

Using the method of section 5.2.3, the initial condition for Test B was established for each mesh, the resulting rotor angle and field current are given in table 5.2. When applied to the transmission line, the initial terminal conditions

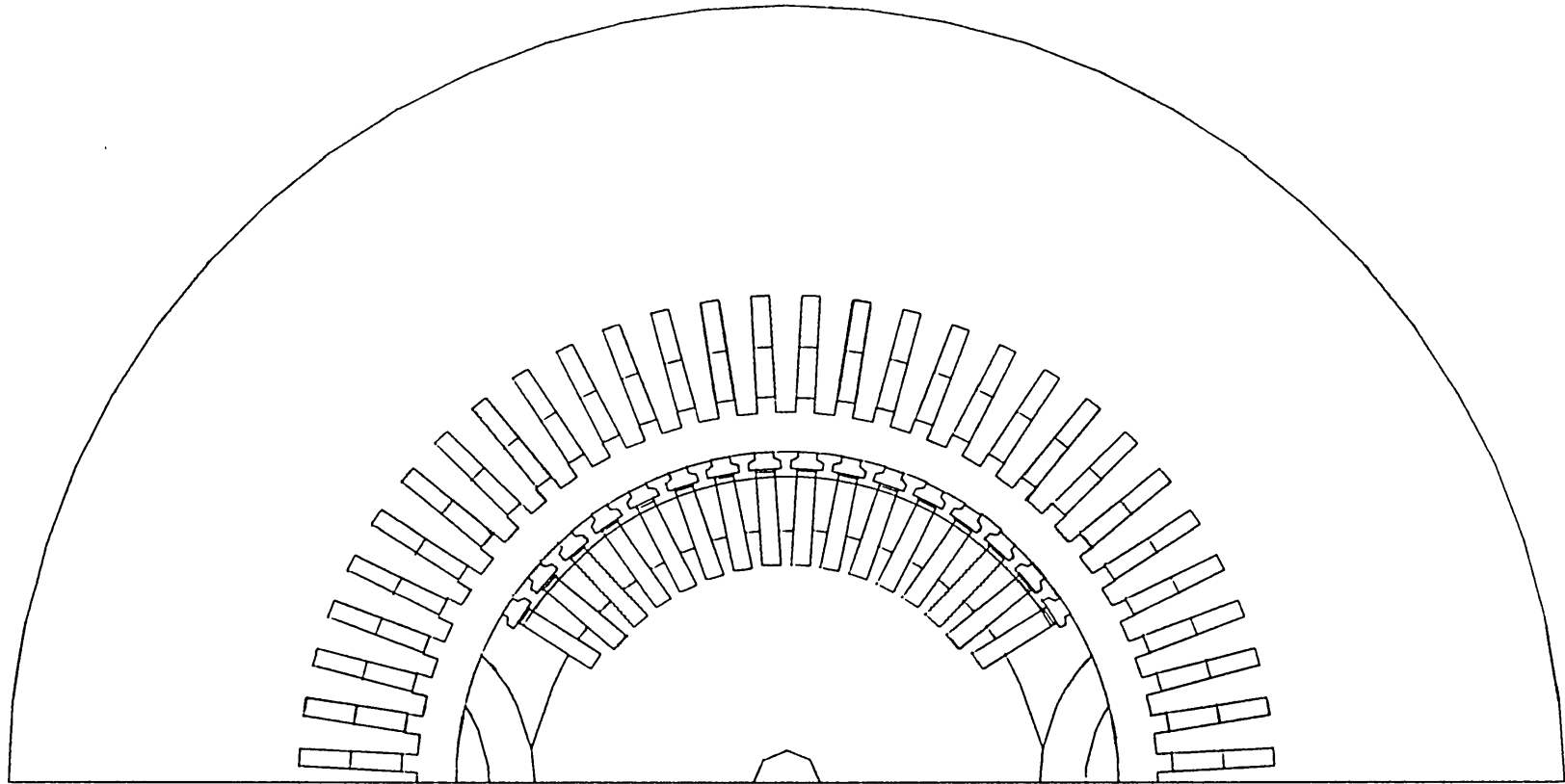


Figure 5.4 Machine outline.

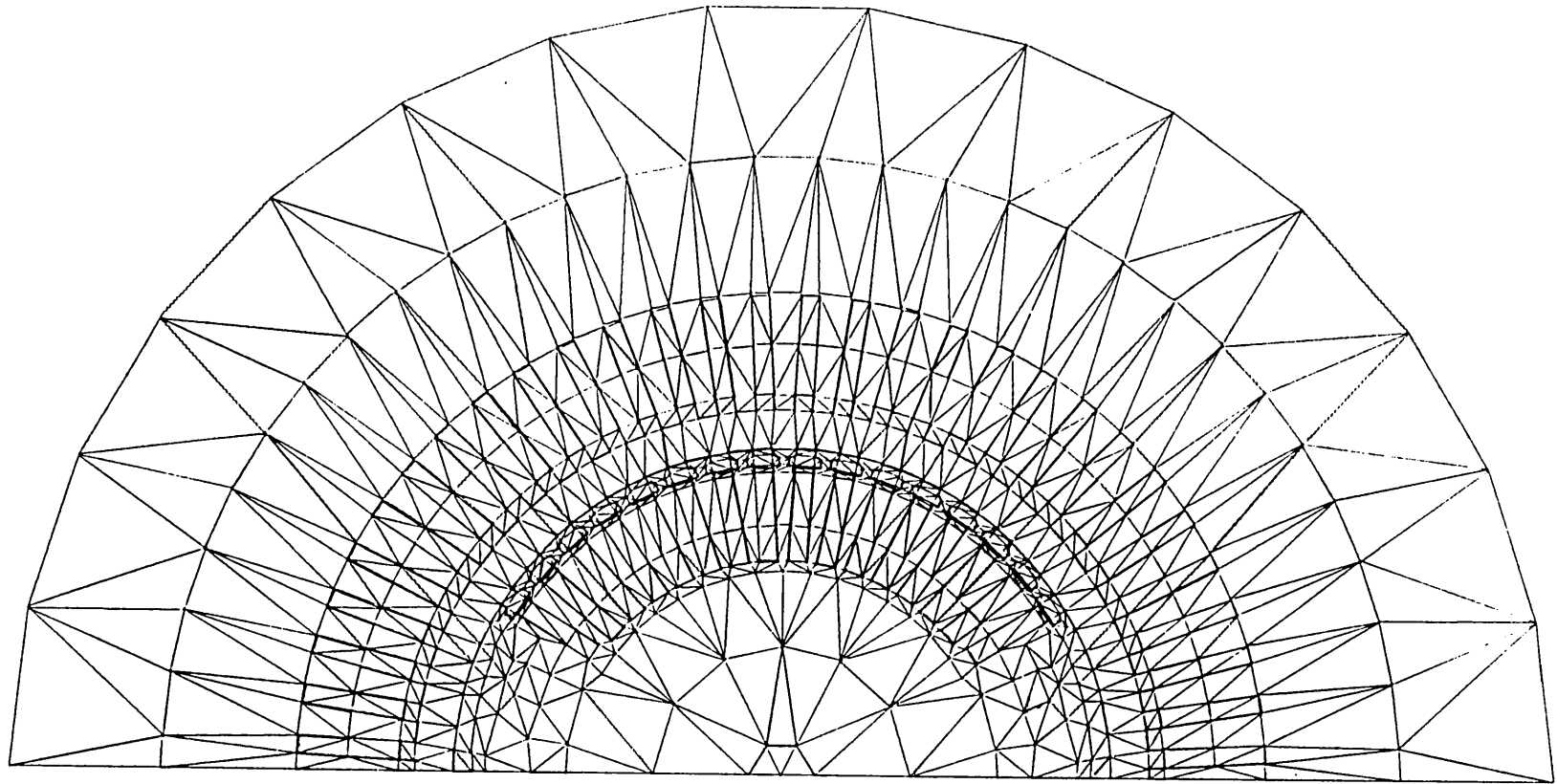


Figure 5.5 Crude mesh UM3. 677 nodes 1313 elements.

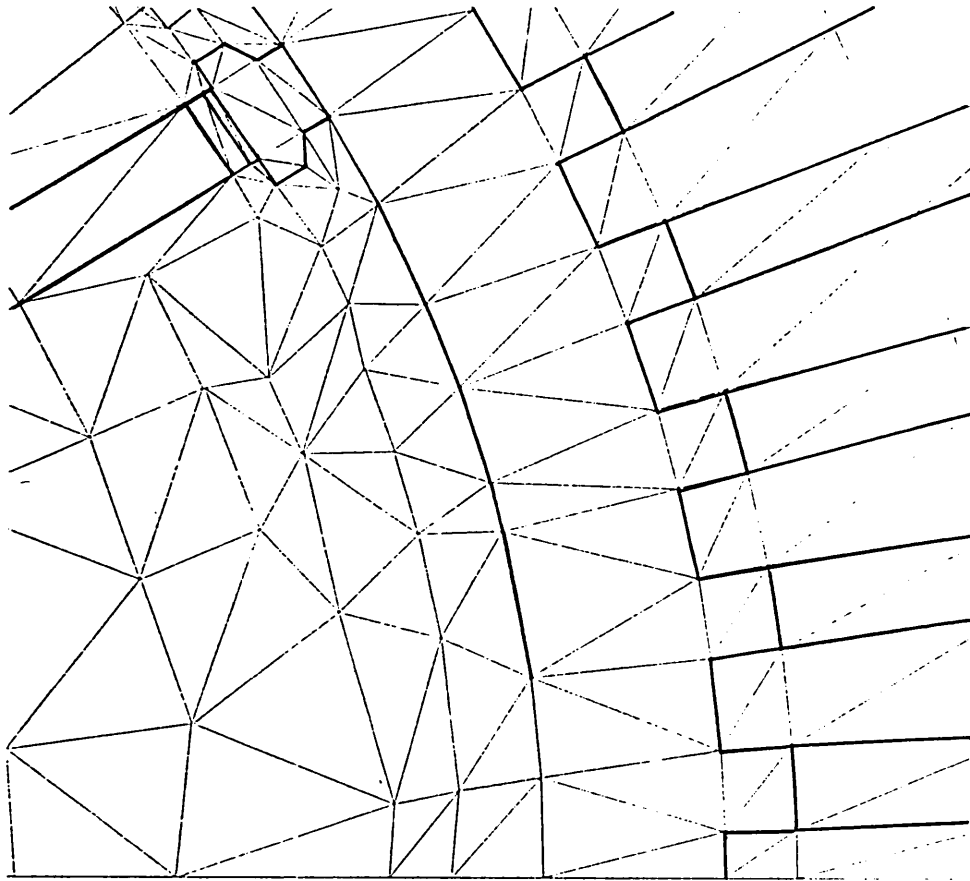


Figure 5.6 Crude mesh UM3 - detail of pole region.

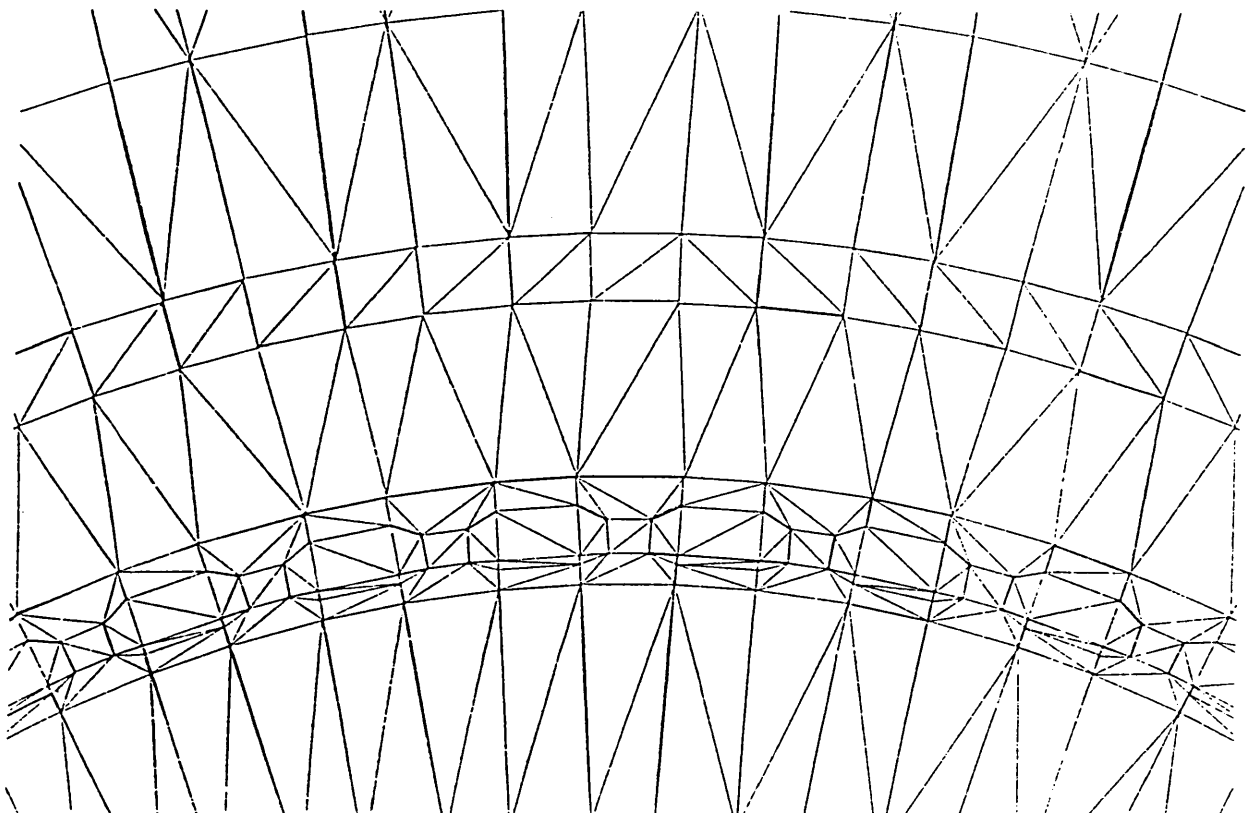


Figure 5.7 Crude mesh UM3 - detail of field winding, wedges and dampers.

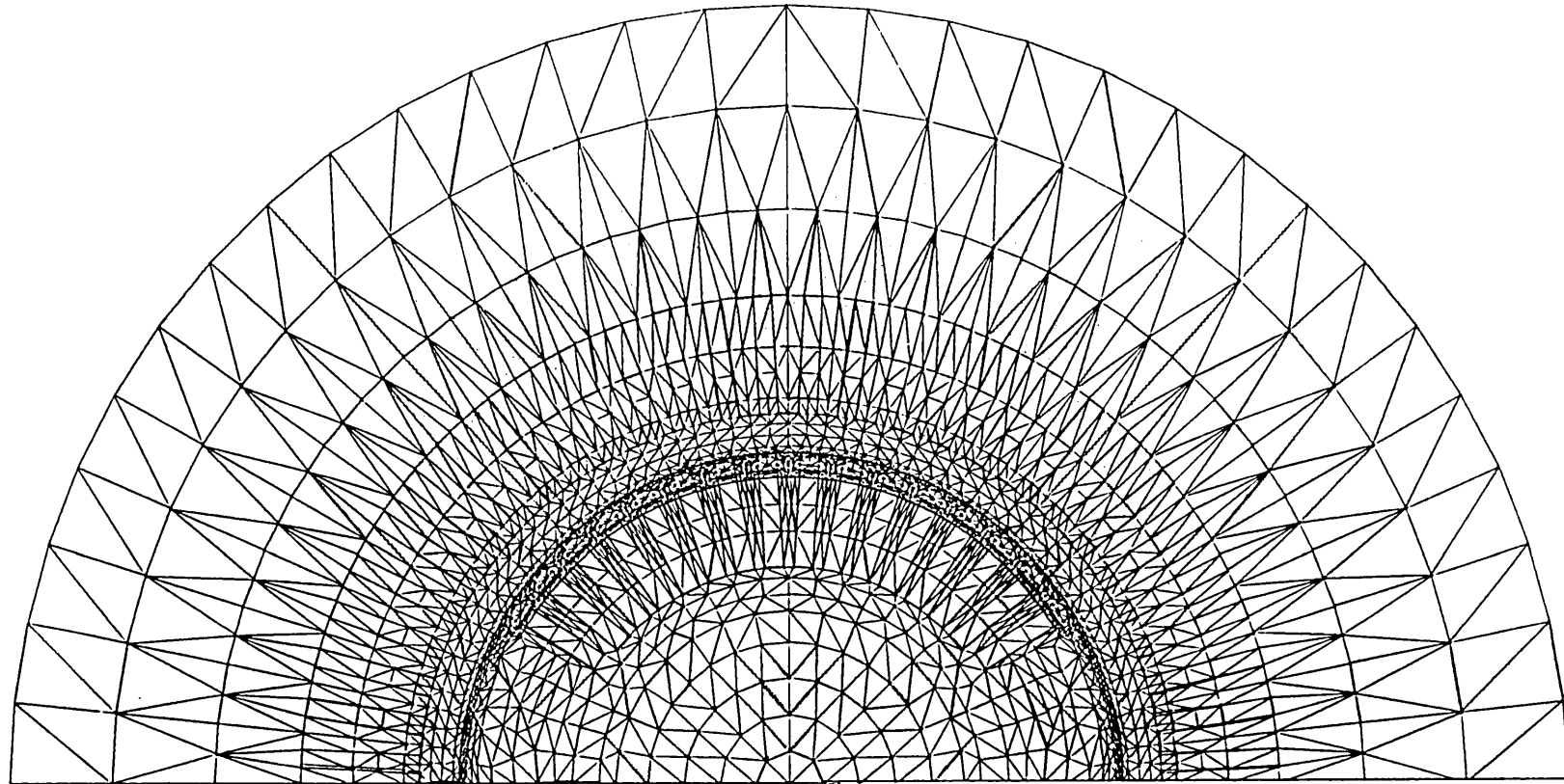


Figure 5.8 Detailed mesh UM9. 1951 nodes 3818 elements.

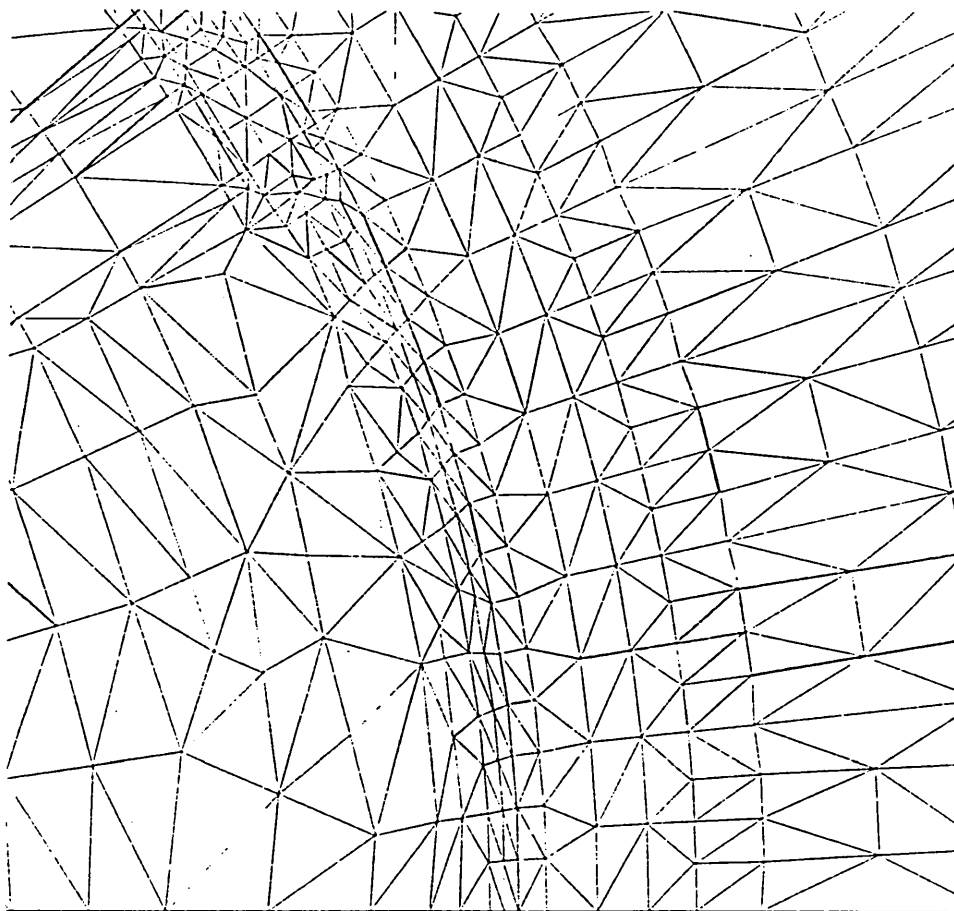


Figure 5.9 Detailed mesh UM9 - detail of pole region.

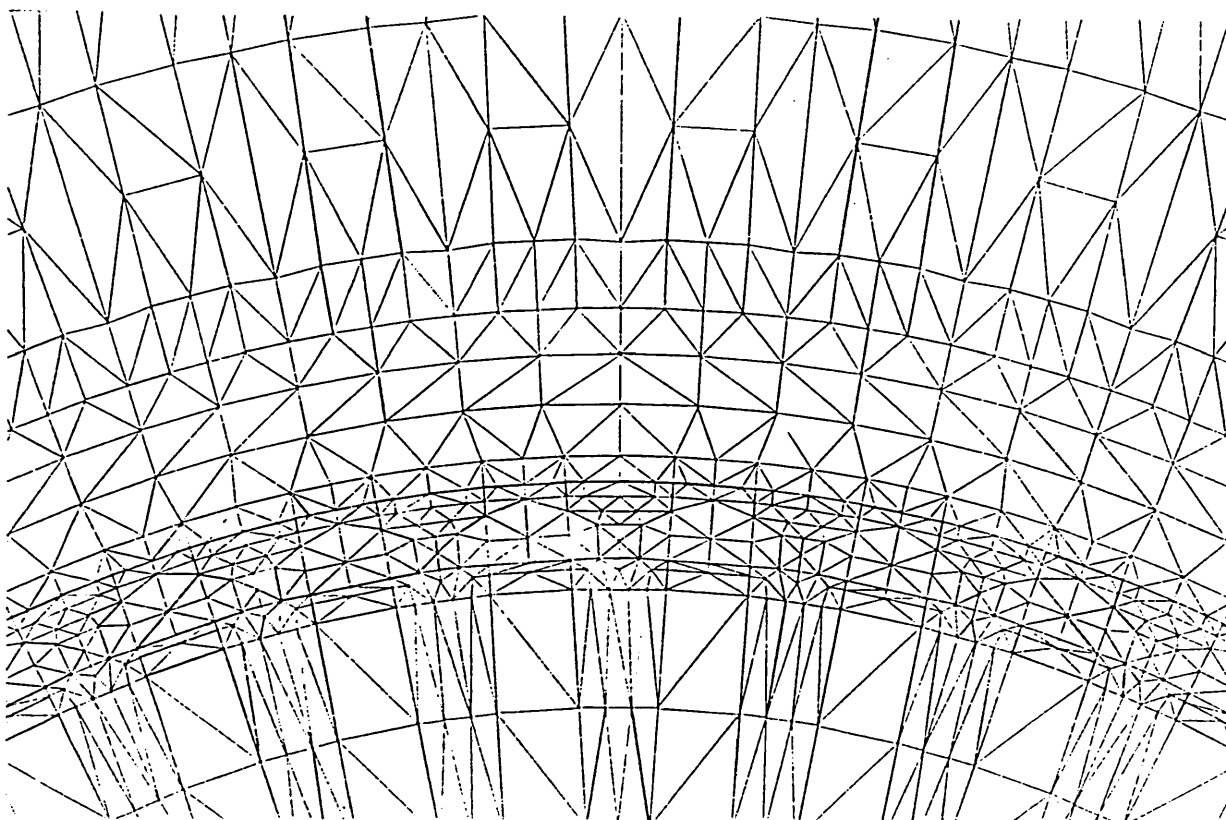


Figure 5.10 Detailed mesh UM9 - detail of field winding, wedges and dampers.

TABLE 5.1 FINITE ELEMENT MESHES

	Nodes	Elements
UM3 - full stator model	677	1313
UM3C - current sheet stator model	445	811
UM9 - full stator model	1951	3818
UM9C - current sheet stator model	1465	2768

TABLE 5.2 TEST B INITIAL CONDITIONS.

Mesh	Field current	Load Angle
UM3	845 A	56.9 deg
UM3C	806 A	60.2 deg
UM9	836 A	59.4 deg
UM9C	821 A	61.5 deg
CEGB Test	827 A	61.5 deg

gave a Melksham busbar voltage of 406kV, which compares very well with the measured value of 405kV.

The current sheet stator models are seen to underpredict the field current, as would be expected from a model where the stator mmf drop does not have to be provided. All the two-axis solutions were performed with a constant endbell resistivity factor (see also section 5.8.4). An initial time step length of 0.02 ms was used, both for the start of the transient calculation, and immediately after reclosure.

5.8.3 Results.

The accuracy of the simulations was established by comparison with results taken from the C.E.G.B. test report [51]. Graphs of the measured machine response were read off at 25ms intervals; but, due to the small size of the plots, some error was incurred, which is shown in the slight unevenness of the traces produced.

For ease of comparison of swing predictions, the differences in the initial rotor angles are removed by adding a constant factor to each set of data in order to bring the initial rotor angle up to 61.5 deg. This compensation is applied only to the mechanical equations, not the electromagnetic calculation.

Chapter 4.5.3 described how the measured values of field quantities were subjected to a near-half-wave moving average digital filter, which, however, did not completely remove the 50Hz oscillations from the data. The details of the field current and voltage traces for Test B given in the report are too fine for accurate digitisation, so the mean of the envelopes of the oscillations were taken. This is not equivalent to applying a full wave filter to the data, because of the 90 deg phase shift introduced by the filter and this difference should be born in mind when comparing calculated and measured results.

The results of the various simulations are summarised in the following figures, listed in Table 5.3 for ease of reference.

The sharp spike seen in the plots of line current and electrical power at the point of fault clearance and reclosure onto the system, occur as a result of the approximation required in order to incorporate the infinite busbar into the stator circuit (see section 5.7)

TABLE 5.3 INDEX OF FIGURES

RESULTS GROUP	FIGURES	SHOWING
1	5.11 - 5.13	Crude mesh UM3. Comparison of the direct calculation of power flow into magnetic field storage with the Shackshaft approximation and test results.
2	5.14	Crude meshes UM3 and UM3C. Comparison of the full and current sheet stator models with test results.
3	5.15	Comparison of the crude mesh UM3 and detailed meshes UM9 and UM9C with test results.
4	5.16 - 5.42	Flux ¹ and eddy current ² plots full and current sheet stator models - Detailed meshes UM9 and UM9C.

¹ Flux plots are contours of constant magnetic vector potential.

² Eddy current plots are contours of constant $(\delta A/\delta t)$ - ie of eddy current density.

5.8.4 Discussion of results in Group 1 : stored energy calculation.

The calculated terminal quantities are seen to be not greatly in error, although all display less damping than the test values. The Shackshaft approximation for the stored energy term gives a more poorly damped result than the direct calculation, and a phase shift between calculated and test results is apparent. This arises from the discrepancy in the rotor angle prediction discussed in the next paragraph.

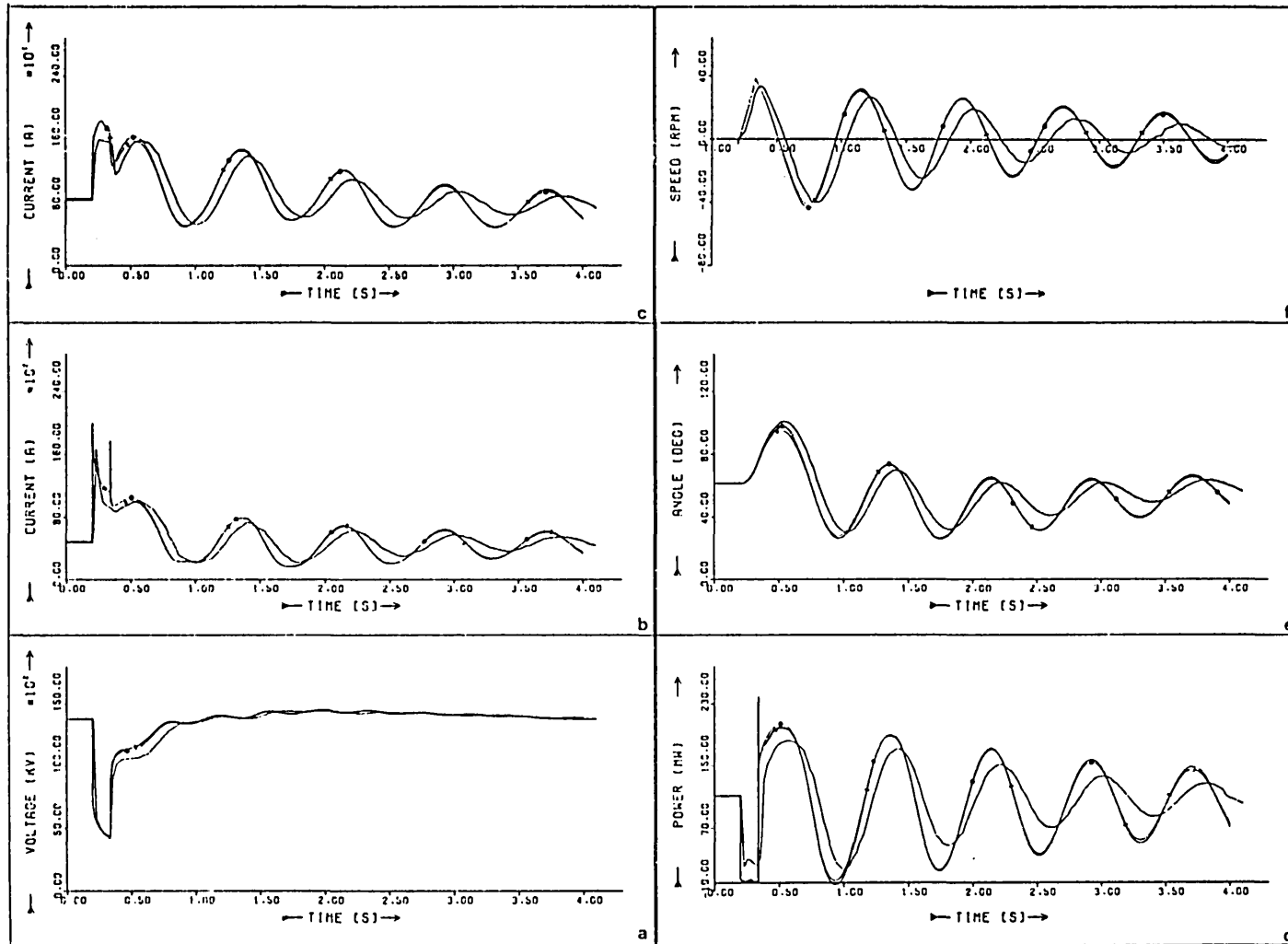


Figure 5.11 Machine response Test B.

— Test results.

—○— Finite element - direct calculation of magnetic storage terms.

—□— Finite element - Shackshaft approximation for magnetic storage terms.

a) line voltage b) line current c) field current

d) electrical power e) speed deviation f) rotor angle

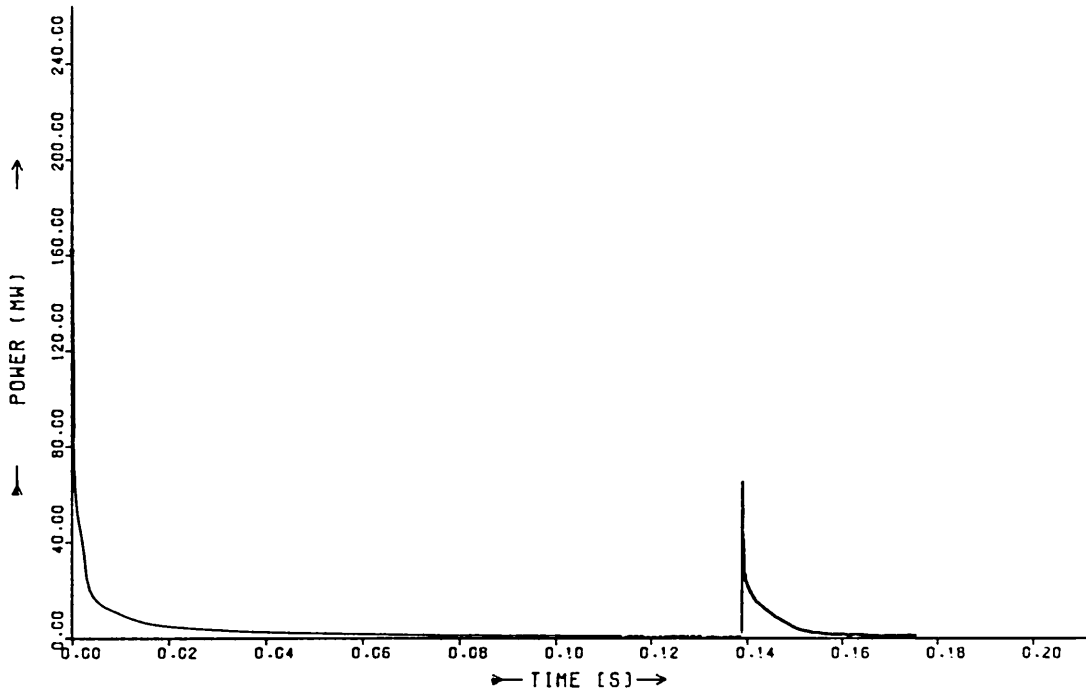


Figure 5.12 Machine response Test B - eddy current power loss.

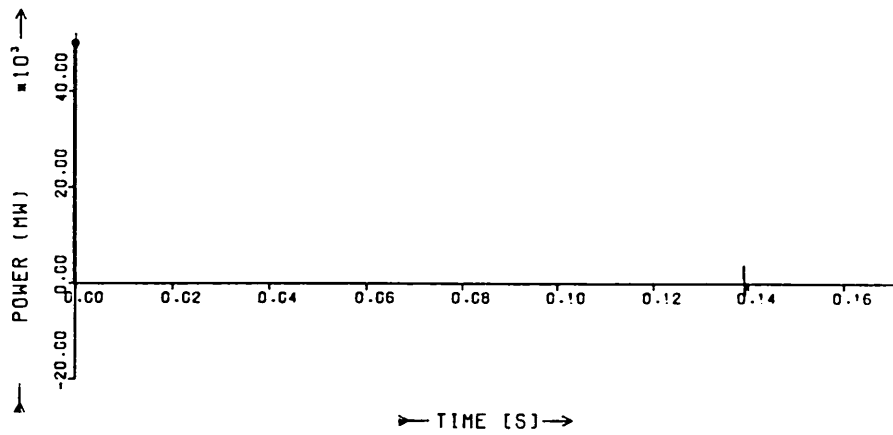


Figure 5.13a Machine response Test B - power flow to magnetic storage.

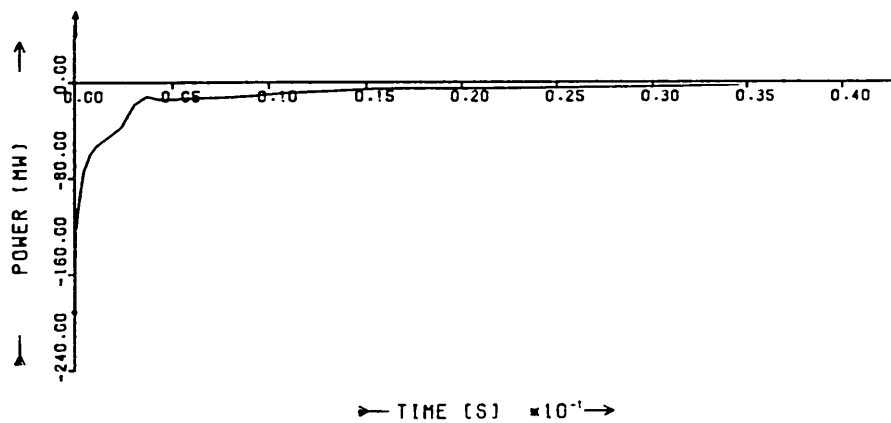


Figure 5.13b Machine response Test B - detail of figure 5.13a.

On clearance of the fault and reconnection of the machine to the transmission line, the terminal voltage rises abruptly, is constant for a short period of time, and then climbs further to oscillate close to the initial value. The level to which the voltage initially 'recovers' on fault clearance is some 500V lower than the simulations predict; and, accordingly, the electrical power generated is lower in the same period. Since the rotor acceleration is determined by the difference between the mechanical and electrical powers (and losses), this small error in generated power can have a large effect on the rotor acceleration. The rotor angle, being the second integral of this quantity, magnifies this difference.

The Shackshaft approximation gives a slightly higher recovery voltage, as a result of the lower rotor angle achieved at the point of reclosure, which increases the rotor retardation and decreases the first swing prediction.

The test results show a larger amount of mechanical damping, attributable partly to the fact that no mechanical damping factor was introduced into the rotor mechanical equations. The swing frequency calculated is the same as that measured, 1.25 Hz, which reflects accurate modelling of the machine inertia and transmission line.

The eddy current power loss decays sharply, falling to less than 1% of its initial value after only 60ms, and a smaller, secondary, peak is seen upon reclosure. Studies using the phase band model of chapter 6, which includes the stator transformer terms, showed that predictions of the eddy current power loss made with the two-axis model are substantially in error. For this reason, the variable endbell factor, calculated from the ratio of eddy current losses in rotor and endbell, was discarded, and the fixed endbell factor used instead. No difference in the eddy current calculation is seen with the Shackshaft approximation.

The direct calculation of magnetic storage shows a sudden, very large, power flow into storage at the first time step, effectively a torque impulse, followed immediately by a much smaller, and rapidly decreasing, release of power as currents decay. The peak power value is very similar to the value used by the Shackshaft approximation over the same time period, although the latter does not subsequently slowly restore energy to the rotor. A much smaller impulse is also observed on reclosure.

5.8.5 Discussion of results in Group 2 : full and current sheet stator models.

The current sheet stator models generally gave a higher first swing prediction and showed less damping than the full stator models. The eddy current and magnetic storage calculations are almost unaffected by the absence of the stator, showing that the stator contributes little to the magnetic behaviour of the machine. The current sheet stator gives rise to a lower induced current in the field circuit during the short circuit, and a slightly greater drop in the stator current on reclosure. Although the instantaneous recovery voltage is the same in both cases, there is a greater delay with the current sheet calculation before it begins to rise further. As a result, less power is generated during this period, and a higher rotor angle is achieved. The time step was observed to lengthen more rapidly with the current sheet stator approximation.

5.8.6 Discussion of results in Group 3 : the effect of discretisation.

The graphs of Group 3 show a much smaller difference between the calculated results for the different discretisations than between the full and current sheet stator models with the same discretisation, except in the field current during the short circuit period. This field current discrepancy is to be expected, since

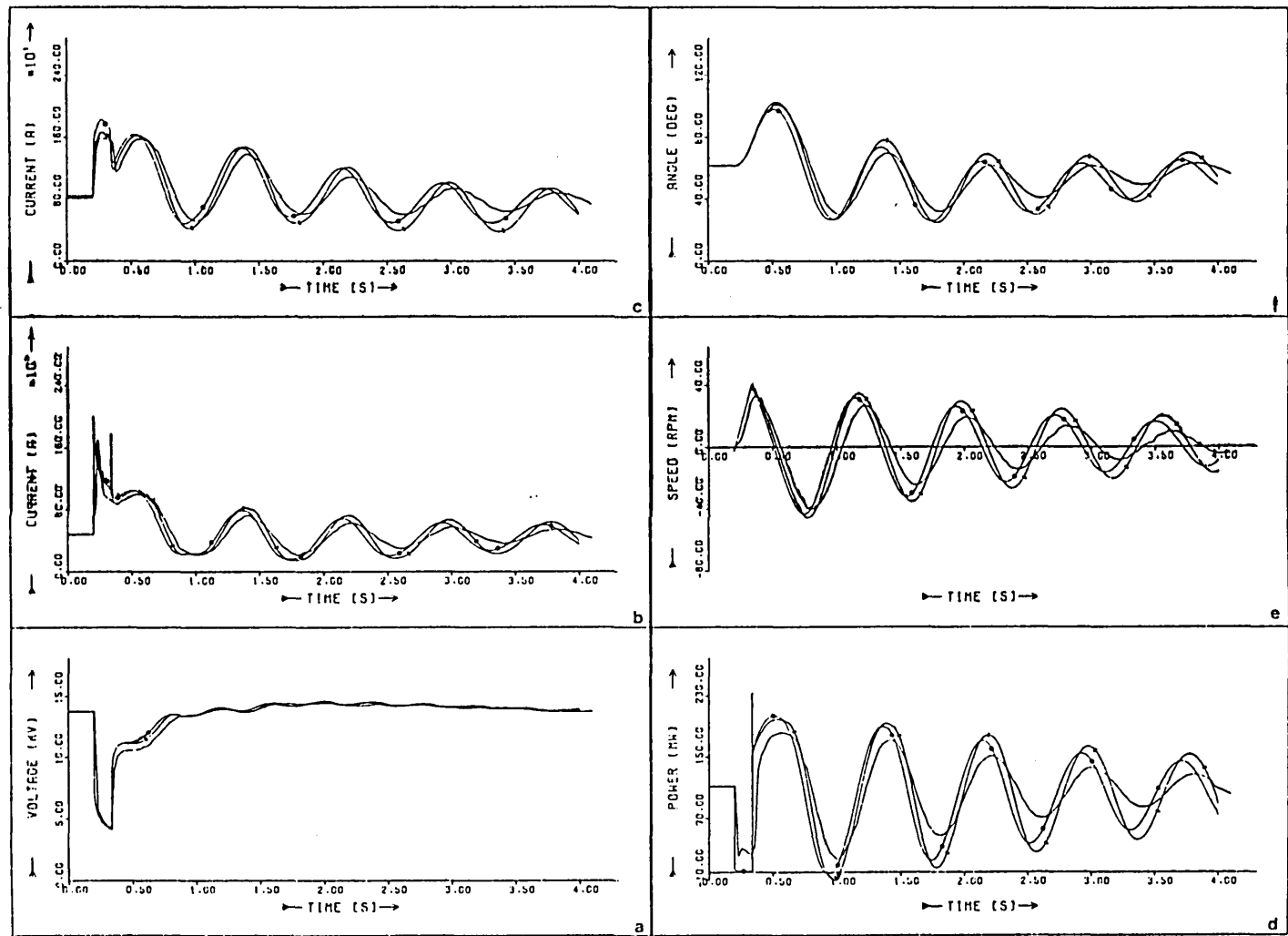


Figure 5.14 Machine response Test B.

— Test results

--- Finite element - full stator model

- - - Finite element - current sheet stator model

a) line voltage b) line current c) field current

d) electrical power e) speed deviation f) rotor angle

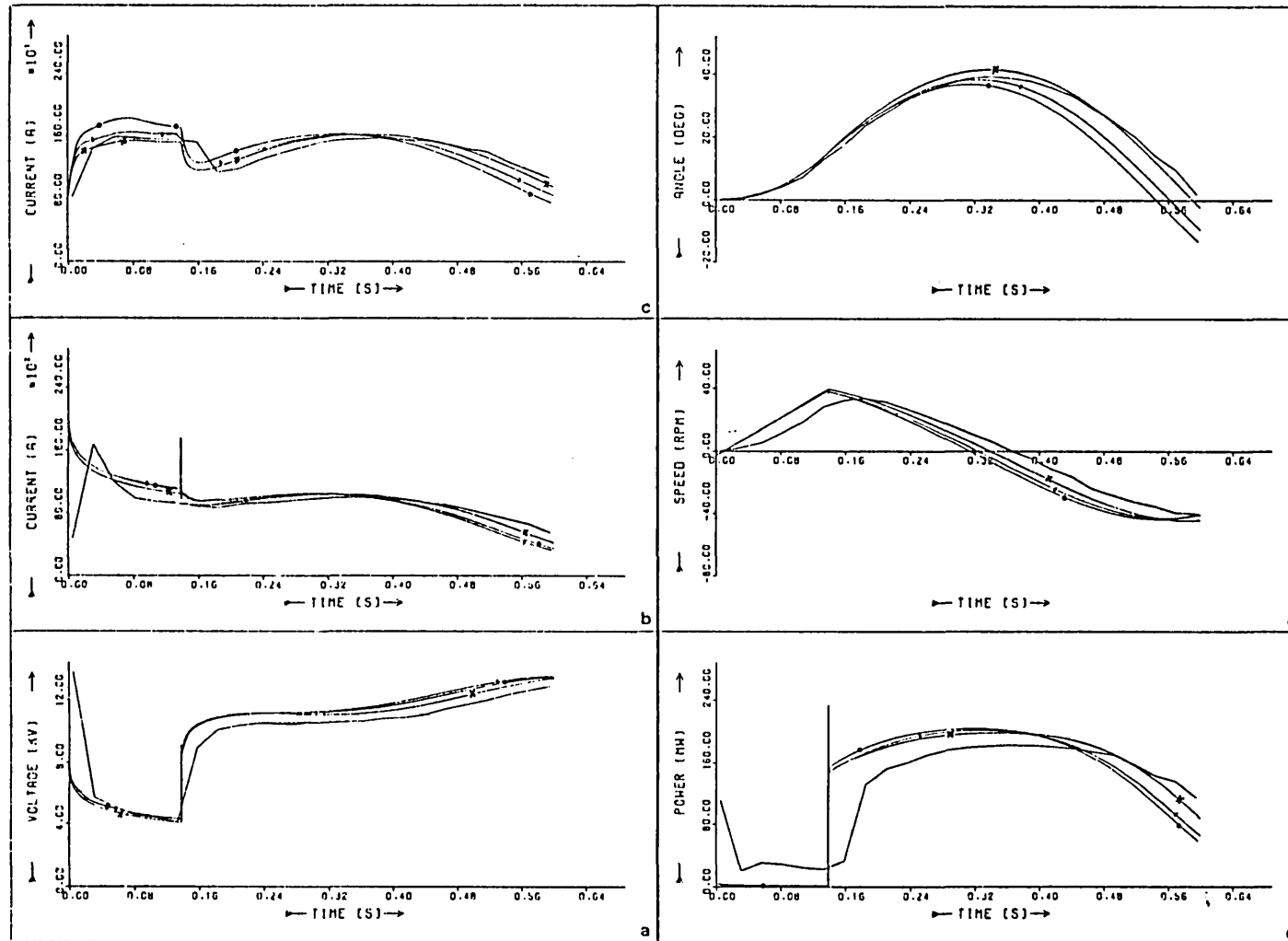


Figure 5.15 Machine response Test B.

- Test results
 - Finite element - crude mesh UM3 full stator model
 - Finite element - detailed mesh UM9 full stator model
 - ×— Finite element - detailed mesh UM9C current sheet stator model
- a) line voltage b) line current c) field current
d) electrical power e) speed deviation f) rotor angle change

it is in the rotor tooth region that much of the increase in discretisation was concentrated. In fact, the detailed current sheet stator mesh underpredicts the field current during the short circuit and overpredicts the rotor swing, and again shows lower damping.

Using a finer mesh increases the amount of magnetic circuit energy fed back into the rotor after the initial impulse, which in turn increases the first swing prediction. Thus the current sheet stator model can overpredict the rotor swing, while also overpredicting the electrical power output.

The differences between the prediction of meshes UM3 and UM9 become minimal once the transient period is over and the machine is swinging against the infinite busbar. This is to be expected, since by this time the calculation is essentially one of a series of load studies at different load angles and levels of excitation. The differences that would be expected are then of the same order as the differences in the initial conditions, a few per cent.

Table 5.4 compares the first swing predictions of each of the methods and meshes used.

5.8.7 Discussion of results in Group 4 : flux and eddy current plots.

All the flux plots are drawn at 5% contour intervals based on 0.4812 Wb m^{-1} or 0.4786 Wb m^{-1} (the maximum value of A in the steady state for the full stator and current sheet stator models respectively) as appropriate.

The eddy current density plots are drawn at 2% and 5% contour intervals using as a reference the maximum eddy current density at each time step. Closely spaced contour lines represent rapidly changing eddy current density, not high eddy current density, ie. closely spaced contour lines designate the boundary between regions of high and low eddy current activity. It will be noticed that

TABLE 5.4 COMPARISON OF CALCULATIONS

MESH	CALCULATION	MAXIMUM ROTOR ANGLE CHANGE
Crude mesh UM3	direct calculation of stored energy, full stator model	36.9 deg.
Crude mesh UM3	Shackshaft approximation, full stator model	33.9 deg.
Crude mesh UM3C	direct calculation of stored energy, current sheet stator	40.8 deg.
Detailed mesh UM9	direct calculation of stored energy, full stator model	38.4 deg.
Detailed mesh UM9C	direct calculation of stored energy, current sheet stator	41.7 deg.
	C.E.G.B. Test	39.6 deg.

some eddy current contours are not continuous, but terminate abruptly, especially in the pole region. This is due to the element-by-element method of calculating the eddy current density. Where a change in conductivity occurs, such as in the pole face region where allowance has been made for the effect of stiffness equalisation gashes (see Chapter 2.5); the eddy current density in the model may change abruptly from one region to the other, although this does not occur in reality.

5.8.7.1 Fully modelled stator.

The flux plots of figures 5.16 to 5.30 show the development of the flux and eddy current distributions within the machine as the transient proceeds.

Immediately the fault is applied, eddy currents are induced in the rotor surface and damper strips, indicated by the sharp change in direction of the flux

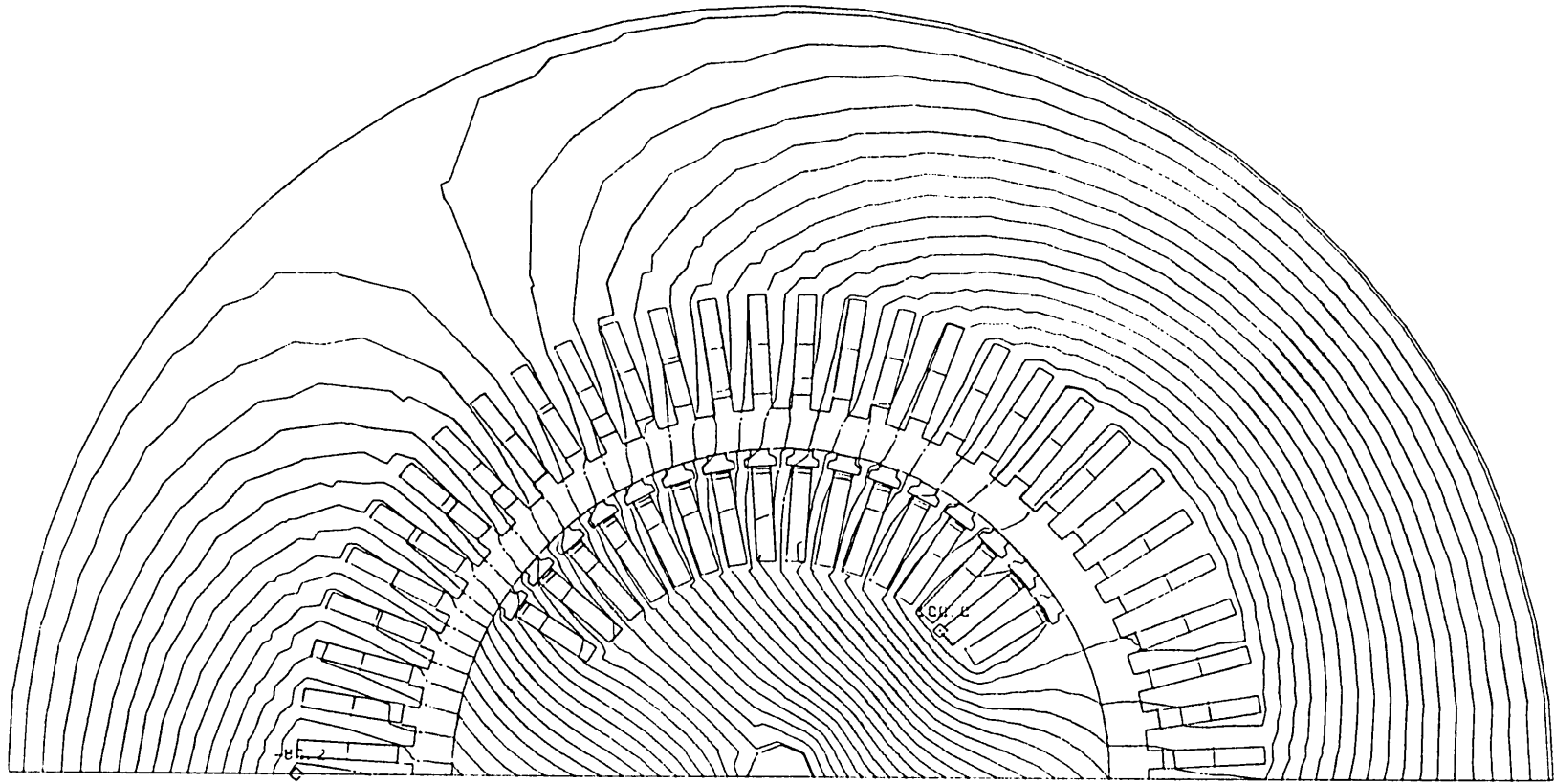


Figure 5.16 Test B initial condition.

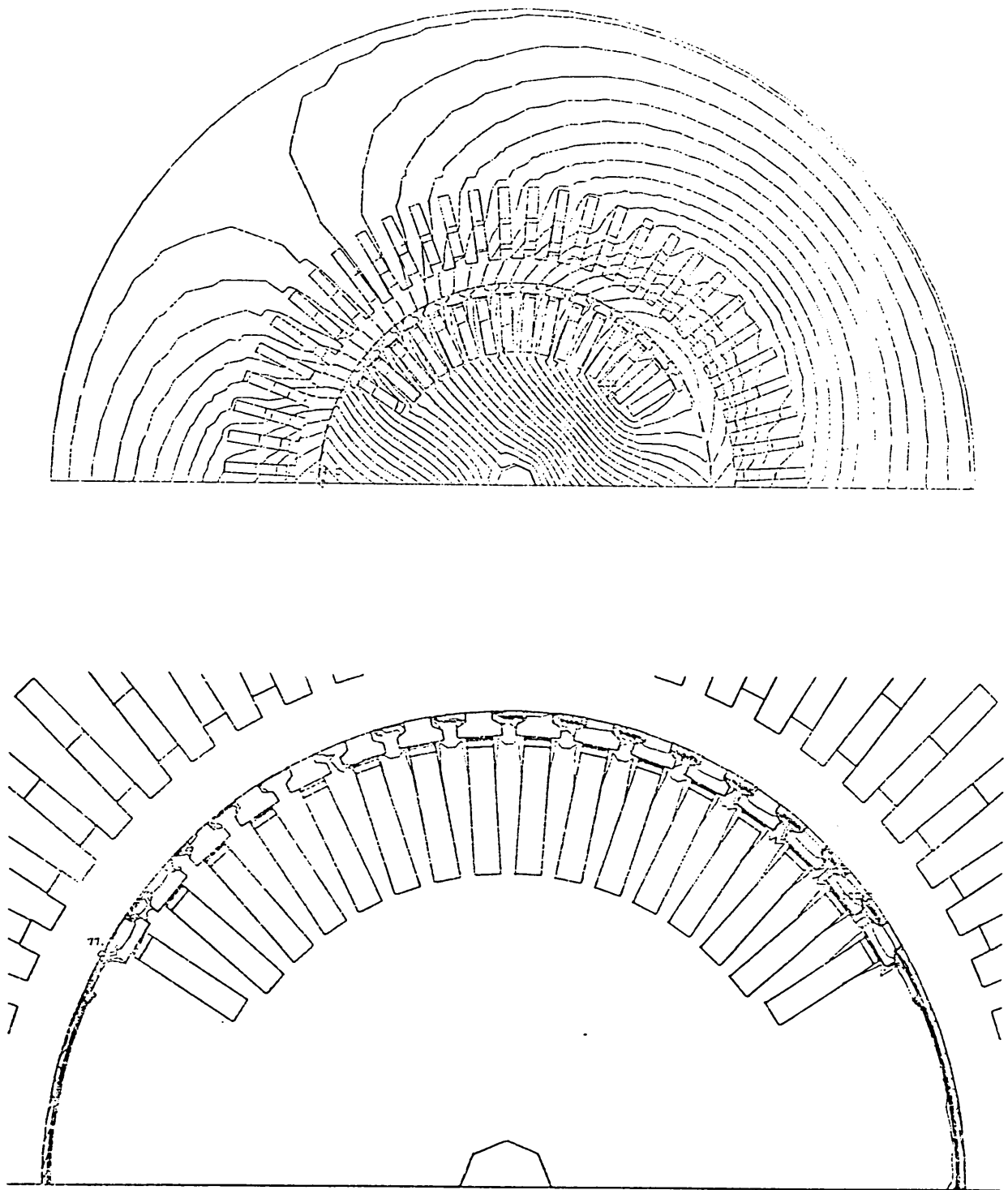


Figure 5.17 time = 0.26 ms current density contours at 5% of $2.00 \times 10^8 \text{ A/m}^2$

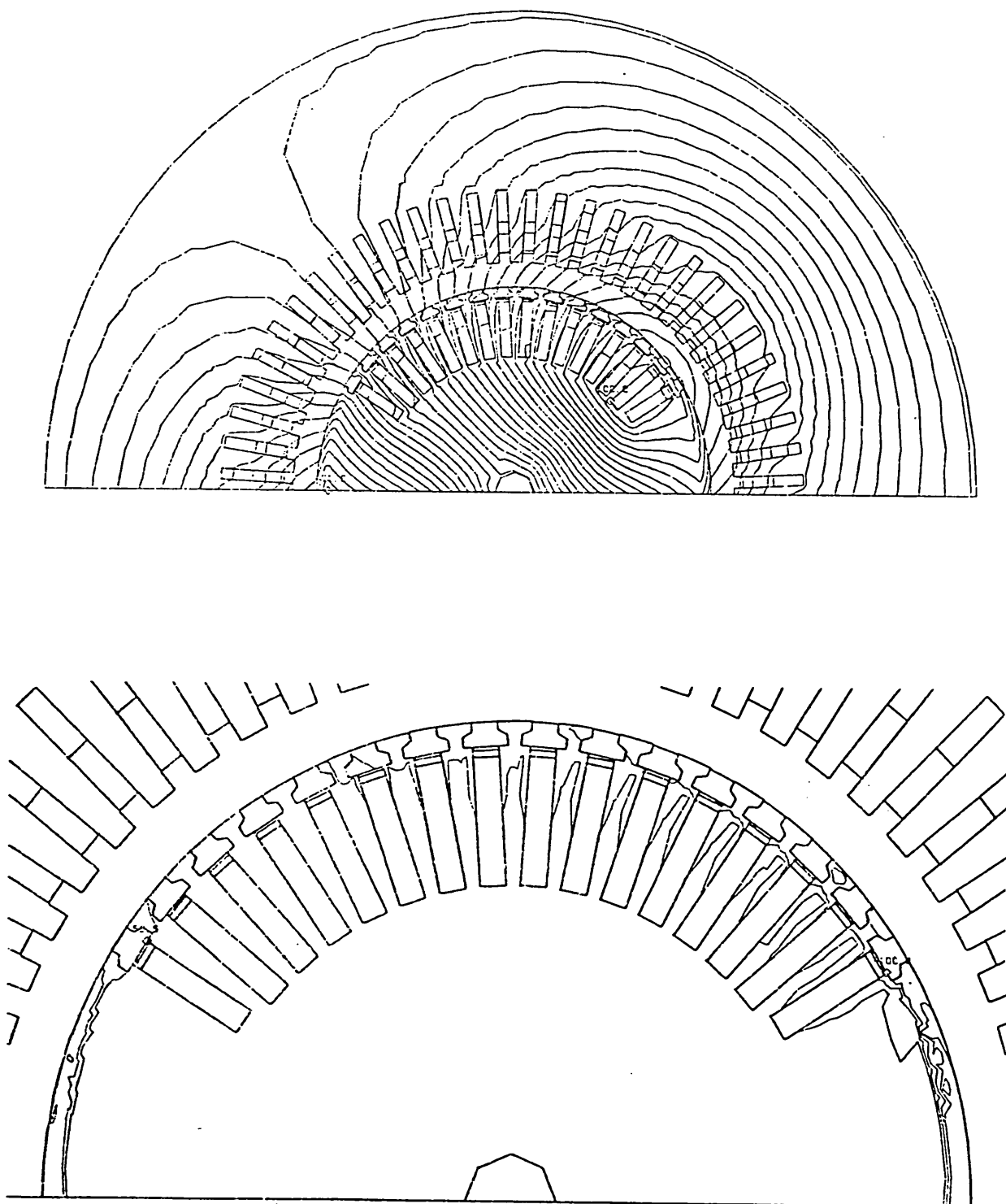


Figure 5.18 time = 2.26 ms current density contours at 5% of $2.92 \times 10^8 \text{ A/m}^2$

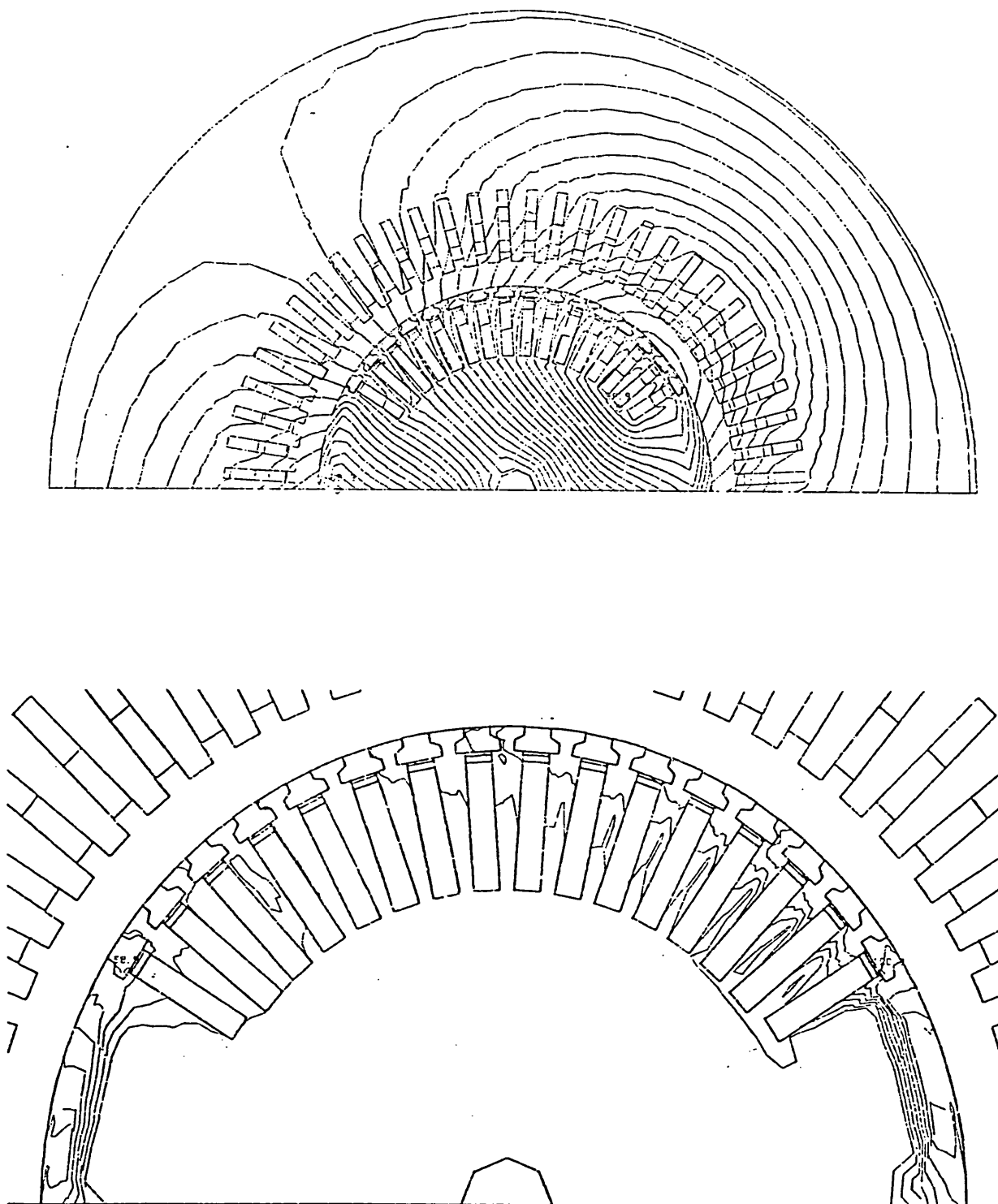


Figure 5.19 time = 10.6 ms current density contours at 2% of $1.40 \times 10^8 \text{ A/m}^2$

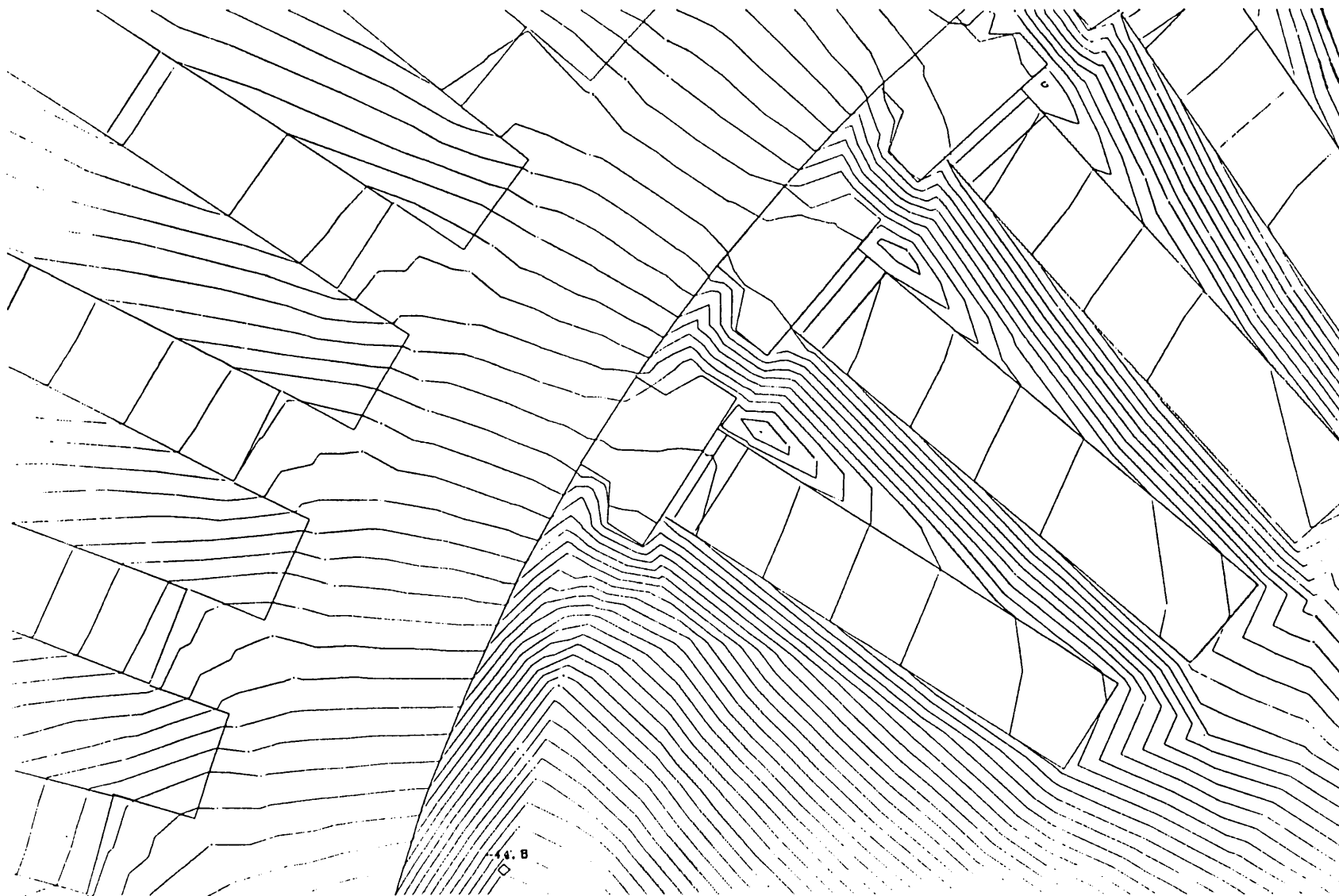


Figure 5.20 time = 10.6 ms detail of flux distribution

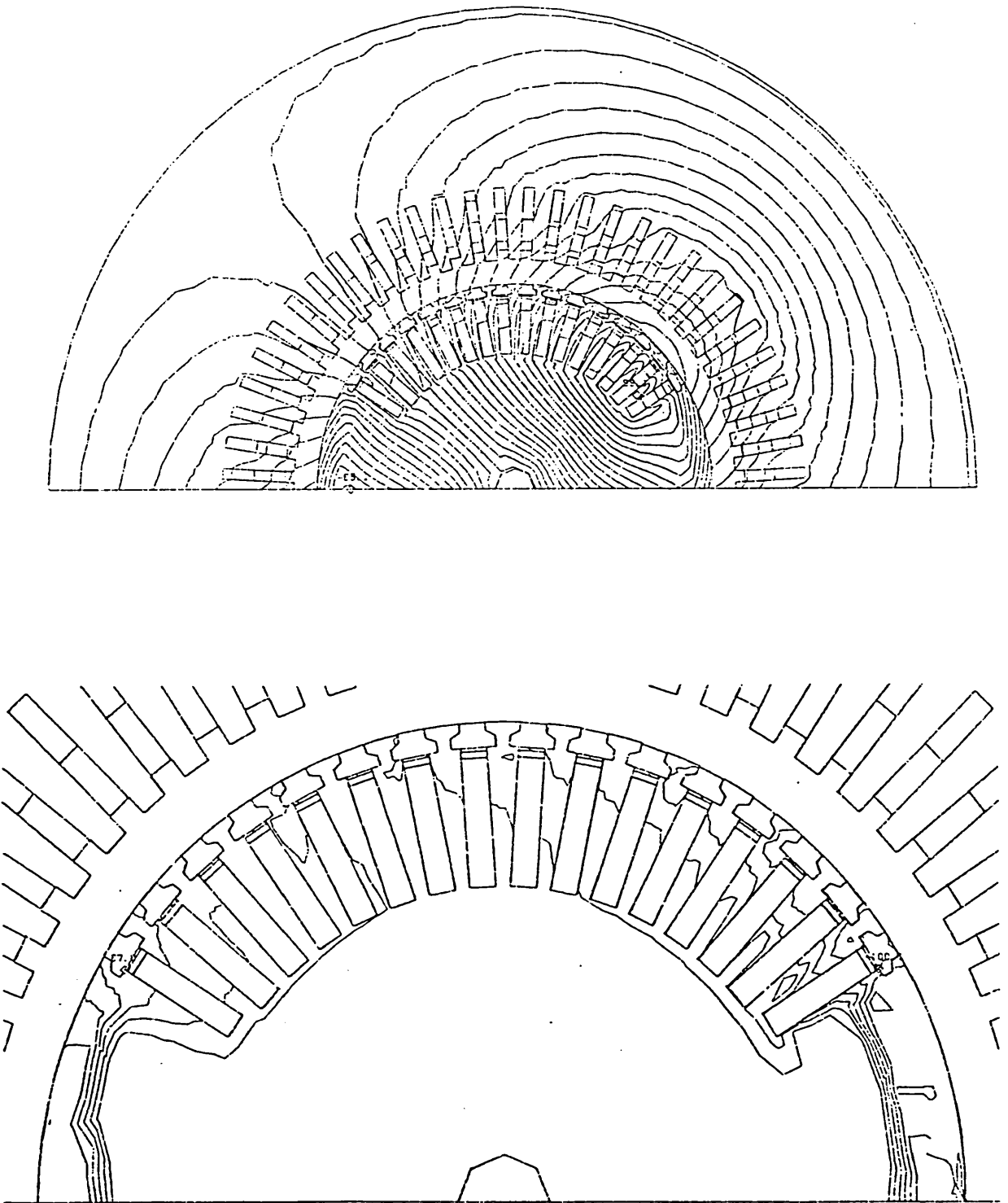


Figure 5.21 time = 20.2 ms current density contours at 2% of $0.97 \times 10^8 \text{ A/m}^2$

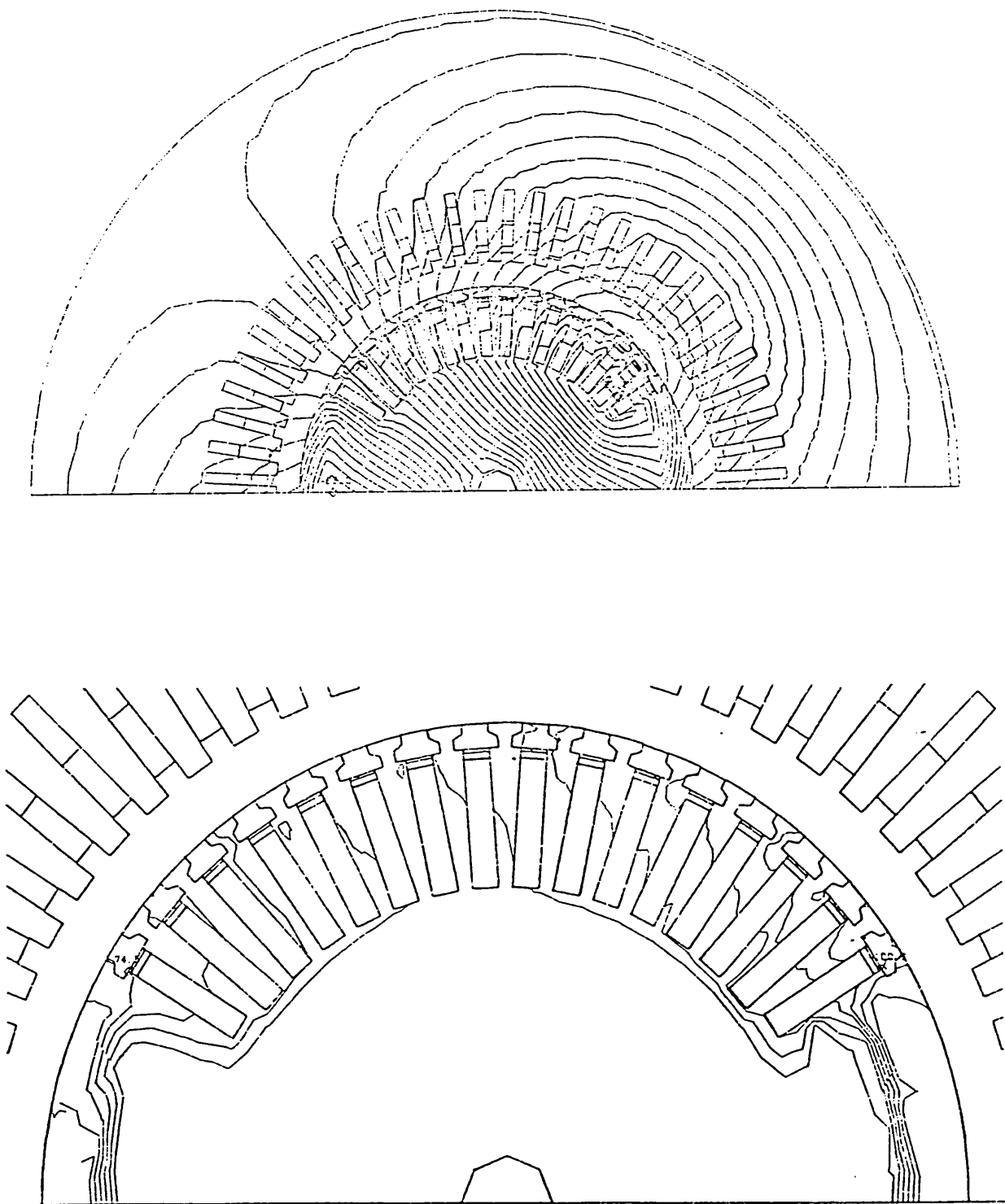


Figure 5.22 time = 30.4 ms current density contours at 2% of $0.70 \times 10^8 \text{ A/m}^2$

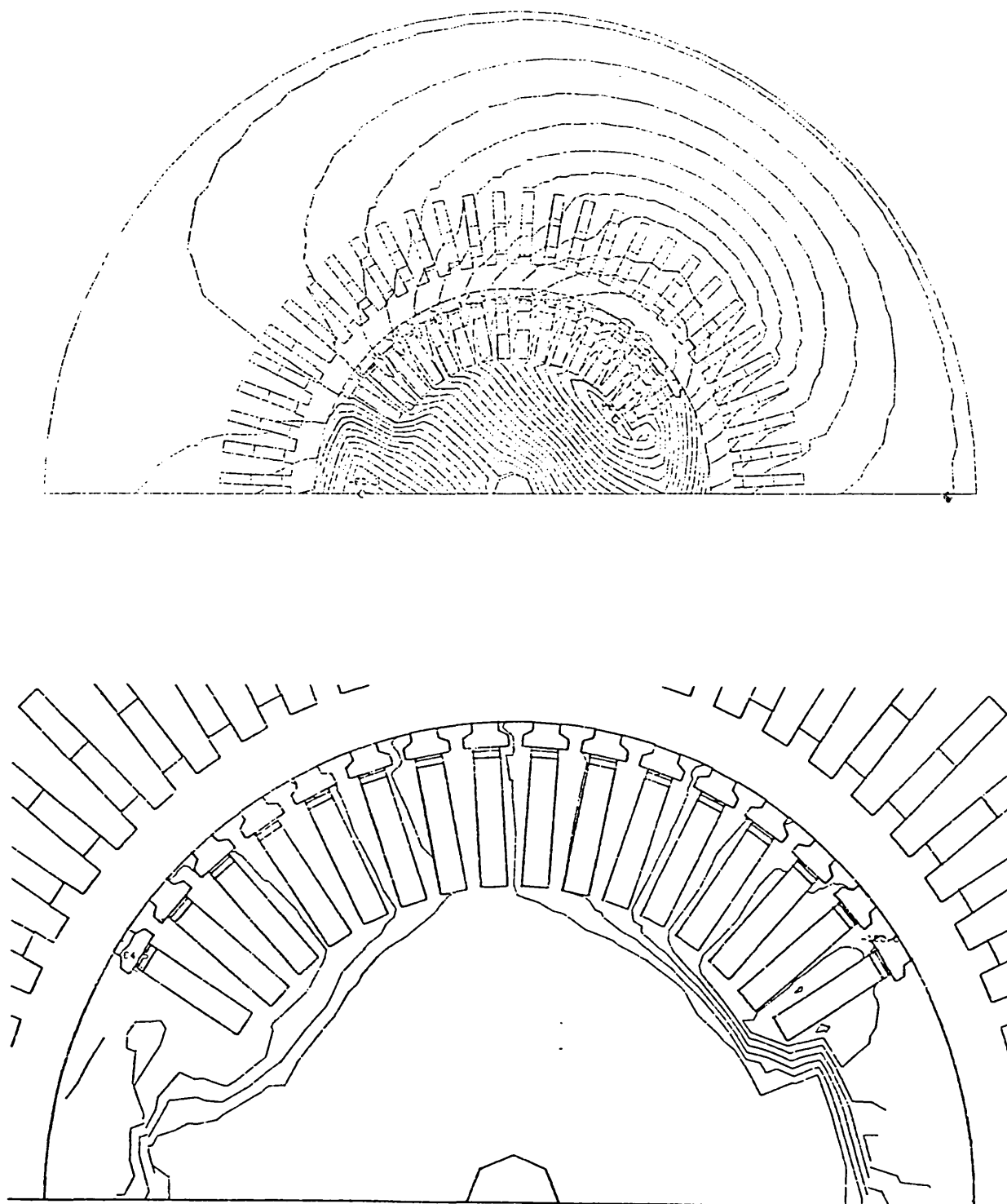


Figure 5.23 time = 139.0 ms - just prior to fault clearance current density contours at 2% of $0.23 \times 10^8 A/m^2$

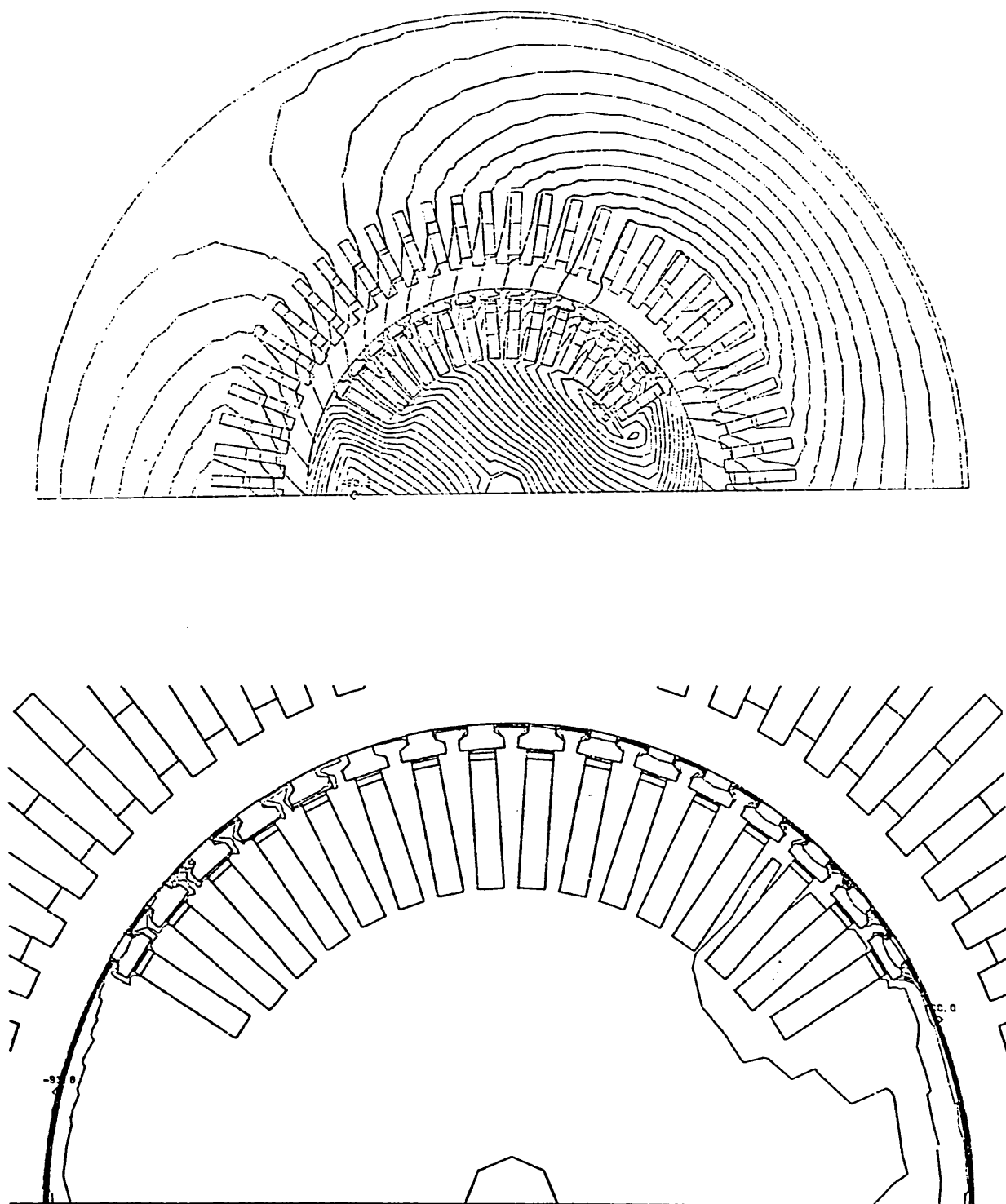


Figure 5.24 time = 139.2 ms - reclosure + 0.2 ms current density contours
at 5% of $2.52 \times 10^8 A/m^2$

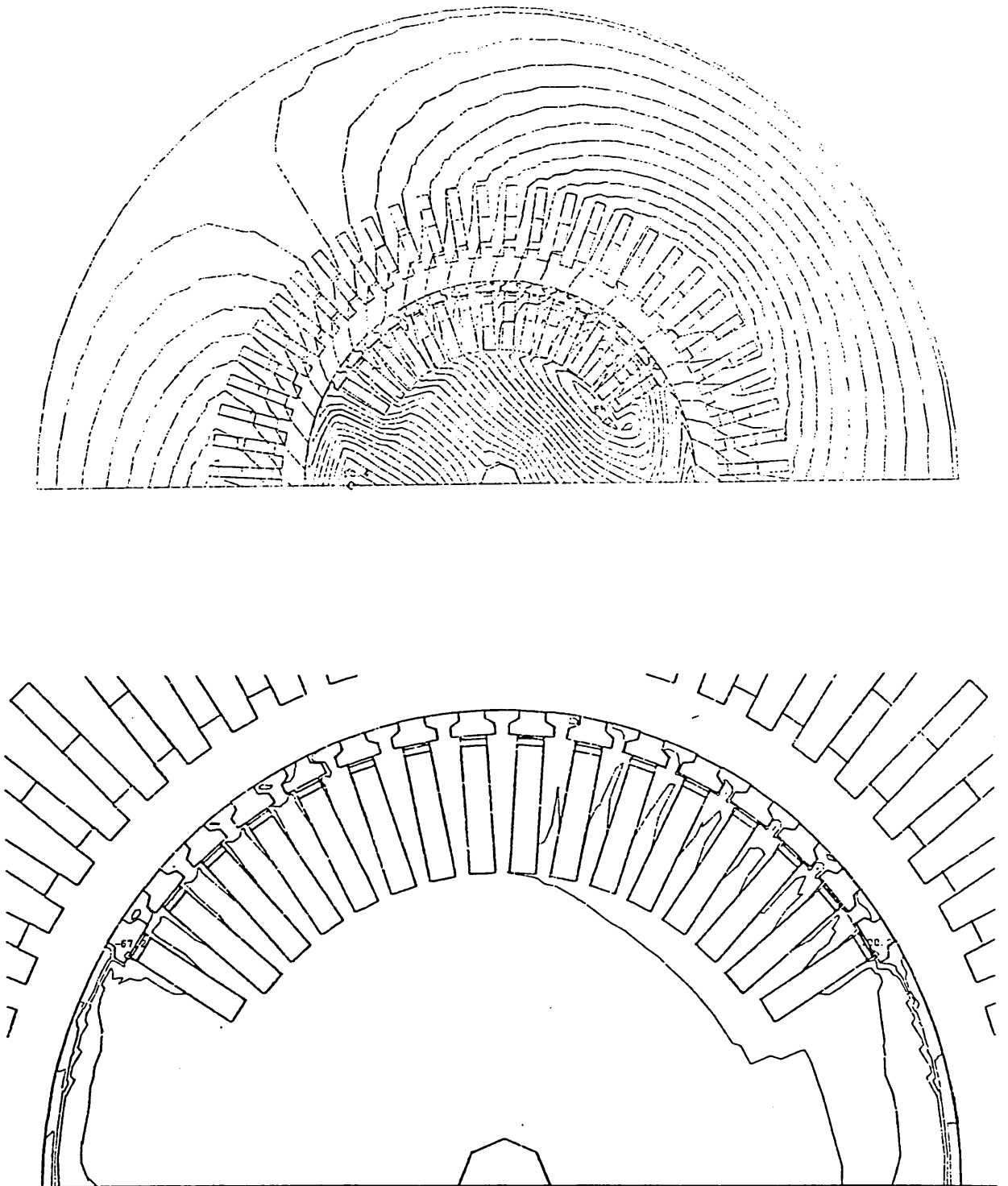


Figure 5.25 time = 141.0 ms - reclosure + 2 ms current density contours
at 5% of $2.17 \times 10^8 \text{ A/m}^2$

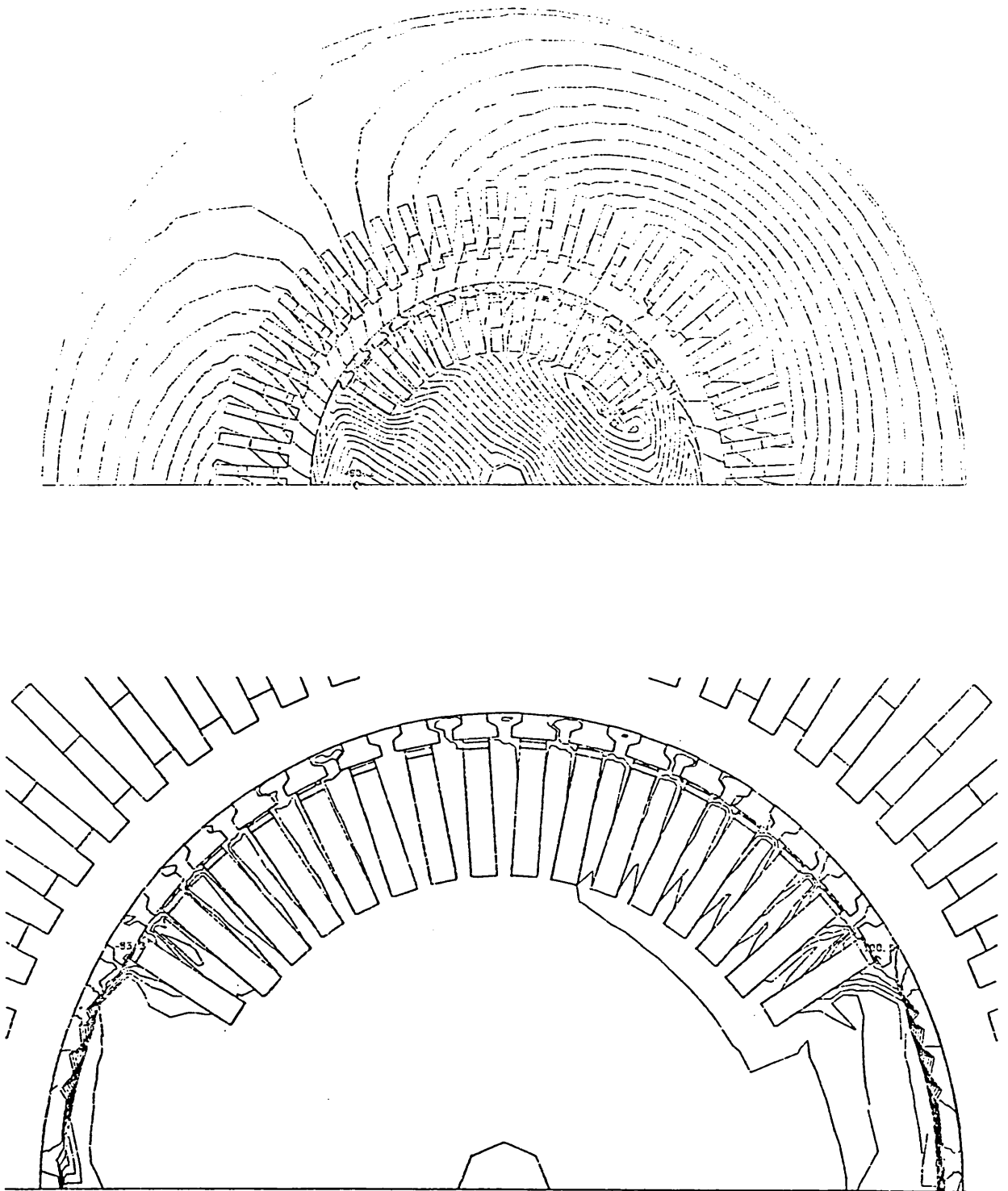


Figure 5.26 time = 149.0 ms - reclosure + 10 ms current density contours
at 2% of $1.00 \times 10^8 \text{ A/m}^2$

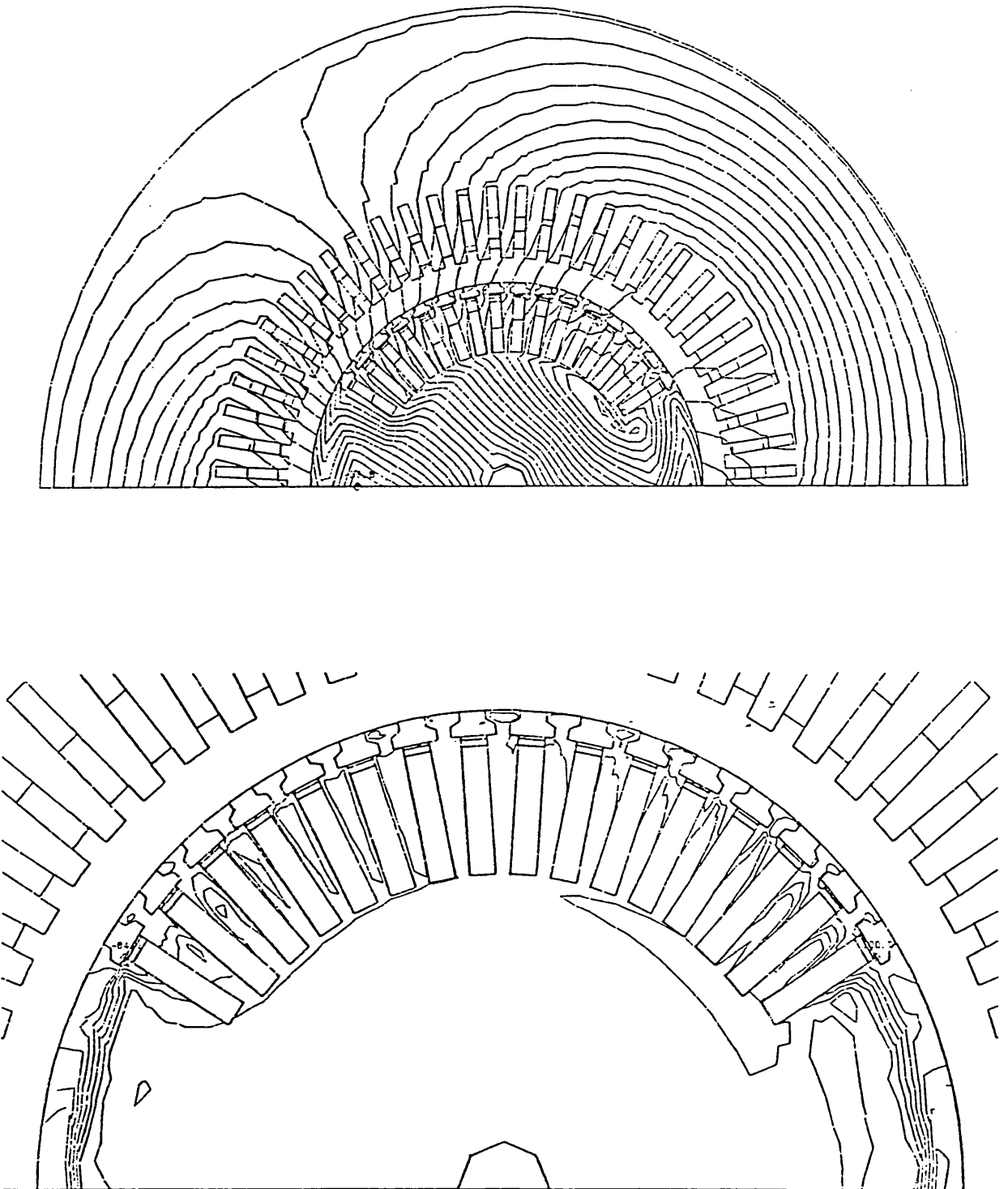


Figure 5.27 time = 159.0 ms current density contours at 2% of $0.60 \times 10^8 \text{ A/m}^2$

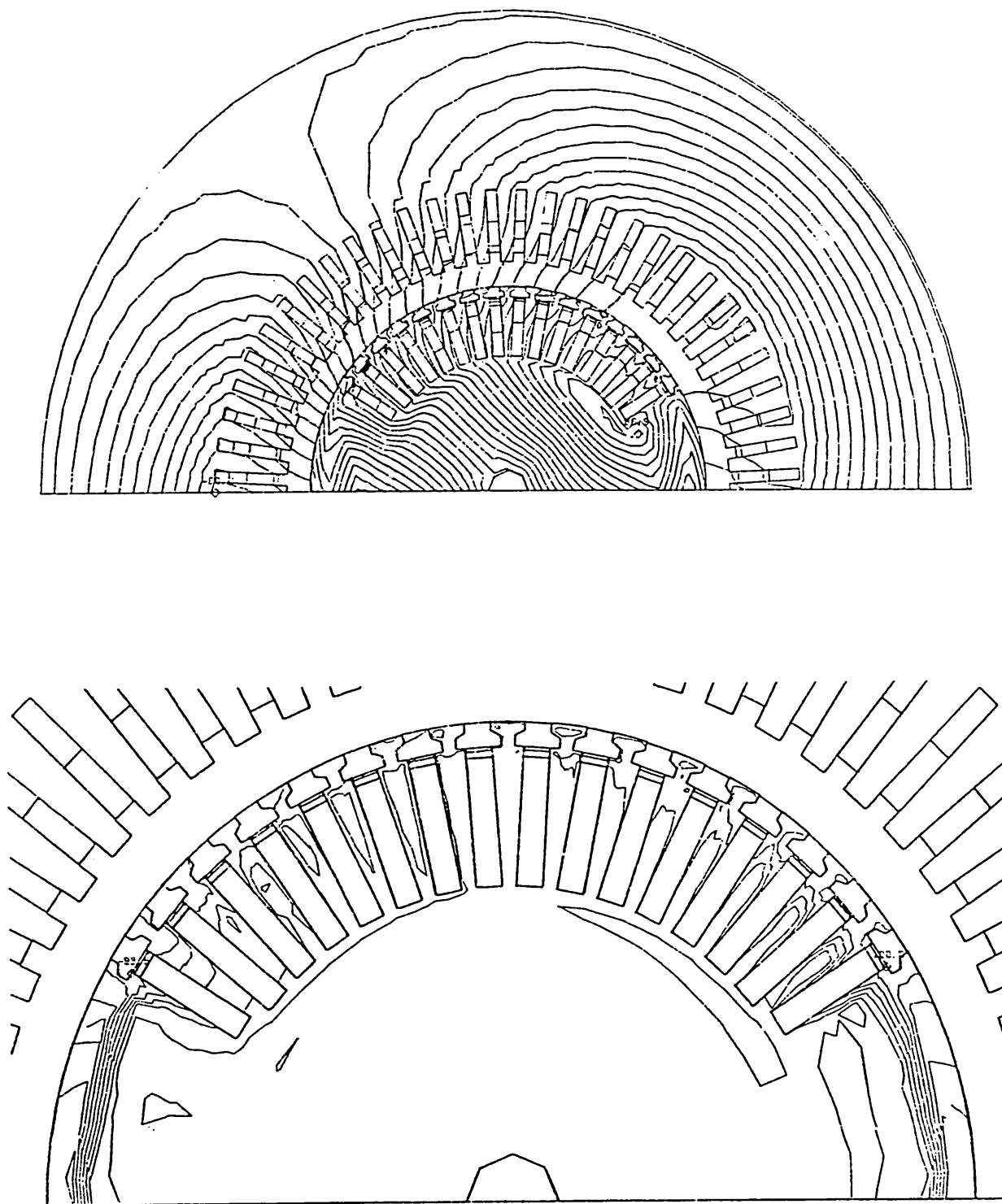


Figure 5.28 time = 169.0 ms current density contours at 2% of $0.42 \times 10^8 \text{ A/m}^2$

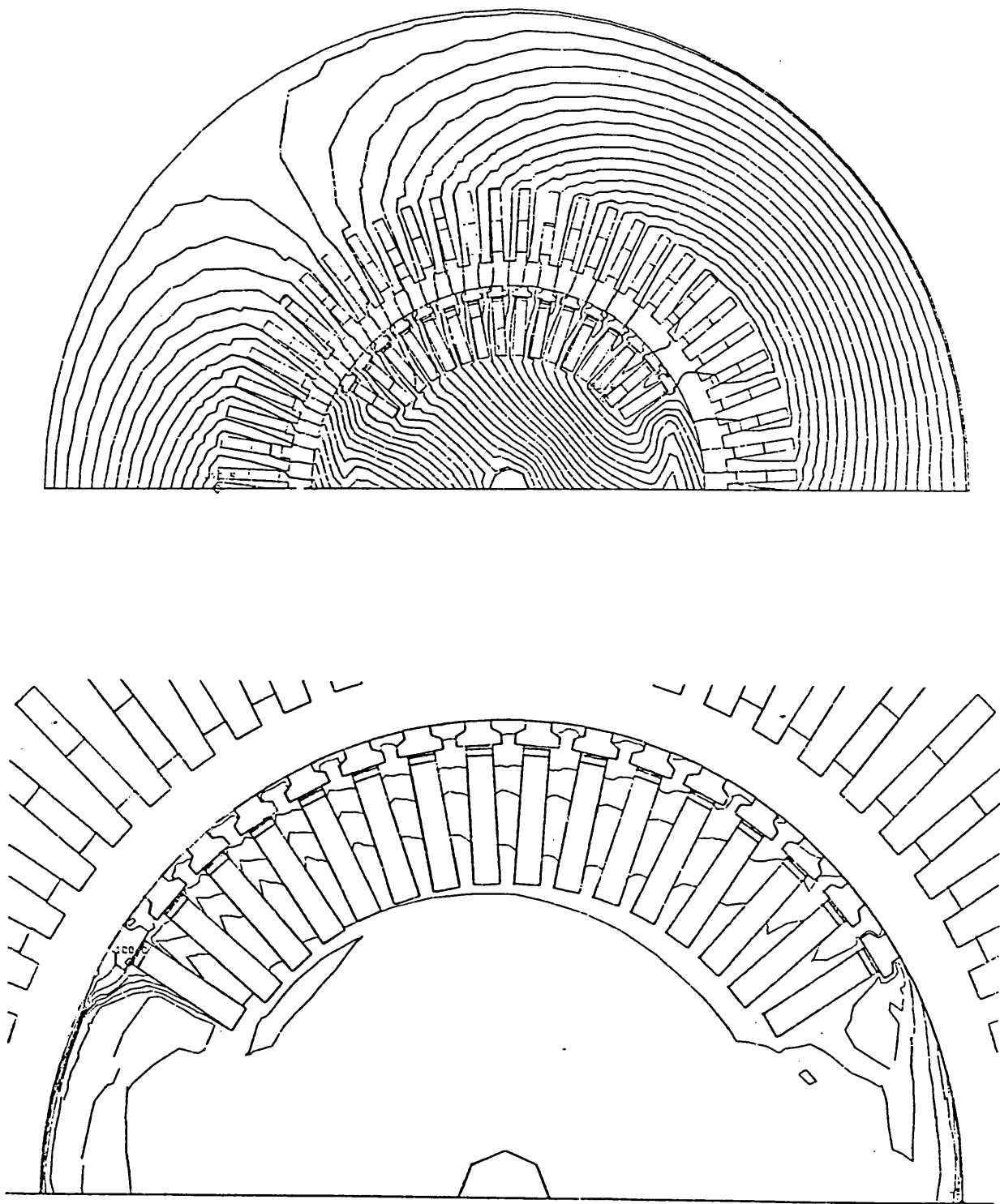


Figure 5.29 time = 600.0 ms current density contours at 2% of $0.14 \times 10^8 \text{ A/m}^2$

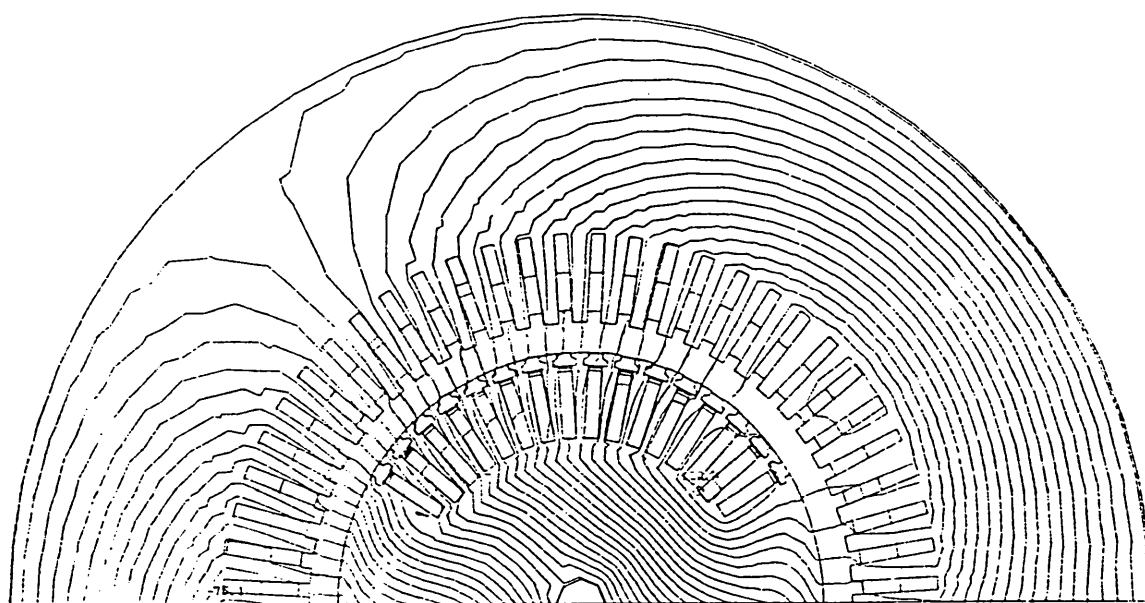


Figure 5.30 time = 3.8 seconds.

lines, but not in the lower conductivity slot wedges. The eddy currents then begin to diffuse deeper into the rotor poles and teeth as the local circulations appearing in the detailed plot of figure 5.20 demonstrate. The figures show the core back flux density falling steadily during the short circuit, while in the rotor body it stays approximately constant, and in the rotor poles it rises slightly.

Just prior to fault clearance, the general level of eddy current activity has fallen by about an order of magnitude, and circulations have begun to appear in the rotor body, the eddy currents having penetrated to the tooth roots and beyond.

As the fault is cleared and the machine is reconnected to the system, a new set of eddy currents are generated in the rotor surface. These flow in the opposite direction to those induced at the start of the short circuit, as is demonstrated by the fact that the flux circulates round them in the opposite direction. The stator flux density is rapidly restored to the pre-fault level, and the overall pattern of flux distribution within the machine now appears similar to that of the initial condition, with the exception of the rotor tooth and pole areas.

This second set of eddy currents gradually diffuse deeper into the rotor, following the first set, and are slowly dissipated. However, the slight flux distortion evident even after 4 seconds (figure 5.30) indicates that there is still some eddy current activity present this far into the transient.

The existence of two sets of eddy currents within the pole face, flowing in opposite directions, is surprising and the explanation of the phenomenon is uncertain. Two contrary possibilities are given below.

- 1) These eddy currents arise as a result of the constraints imposed on the solution by the model, and do not exist in fact. In fact, the two sets of currents would cancel radially, and the flux pattern in the pole area would be far less distorted.

However, the two-dimensional finite element model requires that currents flow only in an axial direction within the machine, and they are thus 'unable' to perform this cancellation.

2) The eddy currents do exist in fact, the existence of adjacent currents of opposite signs being merely the result of a radial space-harmonic distribution of the induced current within the poles. The difference in sign simply reflects the phase difference between the currents at the two points.

Further work will be required to establish the correct explanation of this behaviour, possibly involving a three-dimensional solution at one extreme, which will require substantial additional computational effort; or the analytical analysis of a much simplified problem geometry at the other, which runs the risk of missing the effect altogether.

The problem is only a local one, since the two currents are in sufficiently close proximity for their global effect to be one of cancellation. However, there will be an influence on the machine response through the eddy current loss calculation, and possibly a modification to the local air gap flux density.

5.8.7.2 Current sheet stator.

Figures 5.31 to 5.42 show the flux and eddy current density distributions obtained with the current sheet stator model. They prove to be substantially the same as those of the fully modelled stator, demonstrating how small an effect the stator slotting has on rotor behaviour in machines with a large air gaps.

5.9 PERFORMANCE OF THE PROGRAM.

All calculations were performed as batch jobs on a DEC microVAX II computer (approximately equivalent to a VAX 11/780), under the VMS operating

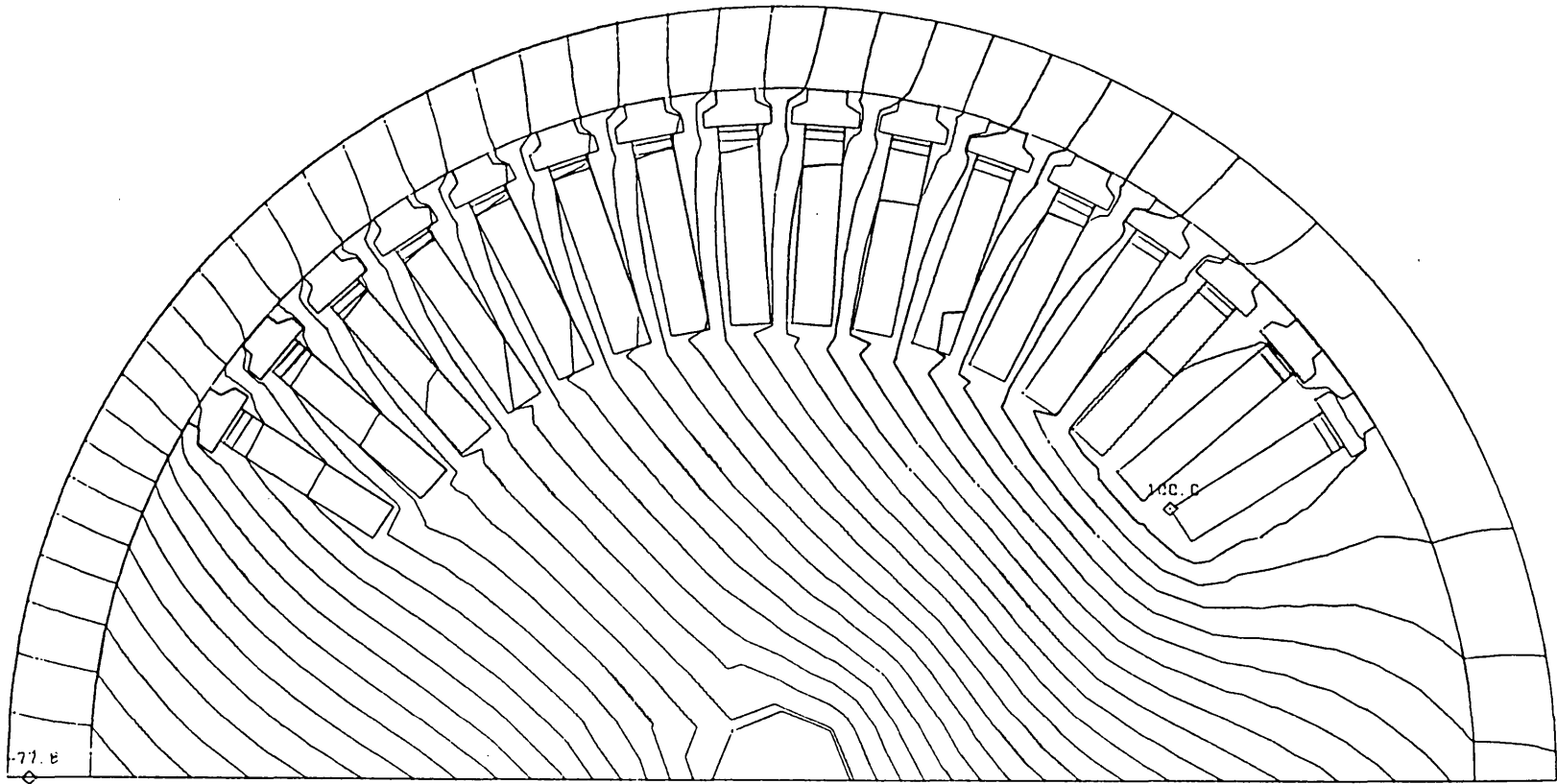


Figure 5.31 Test B initial condition.

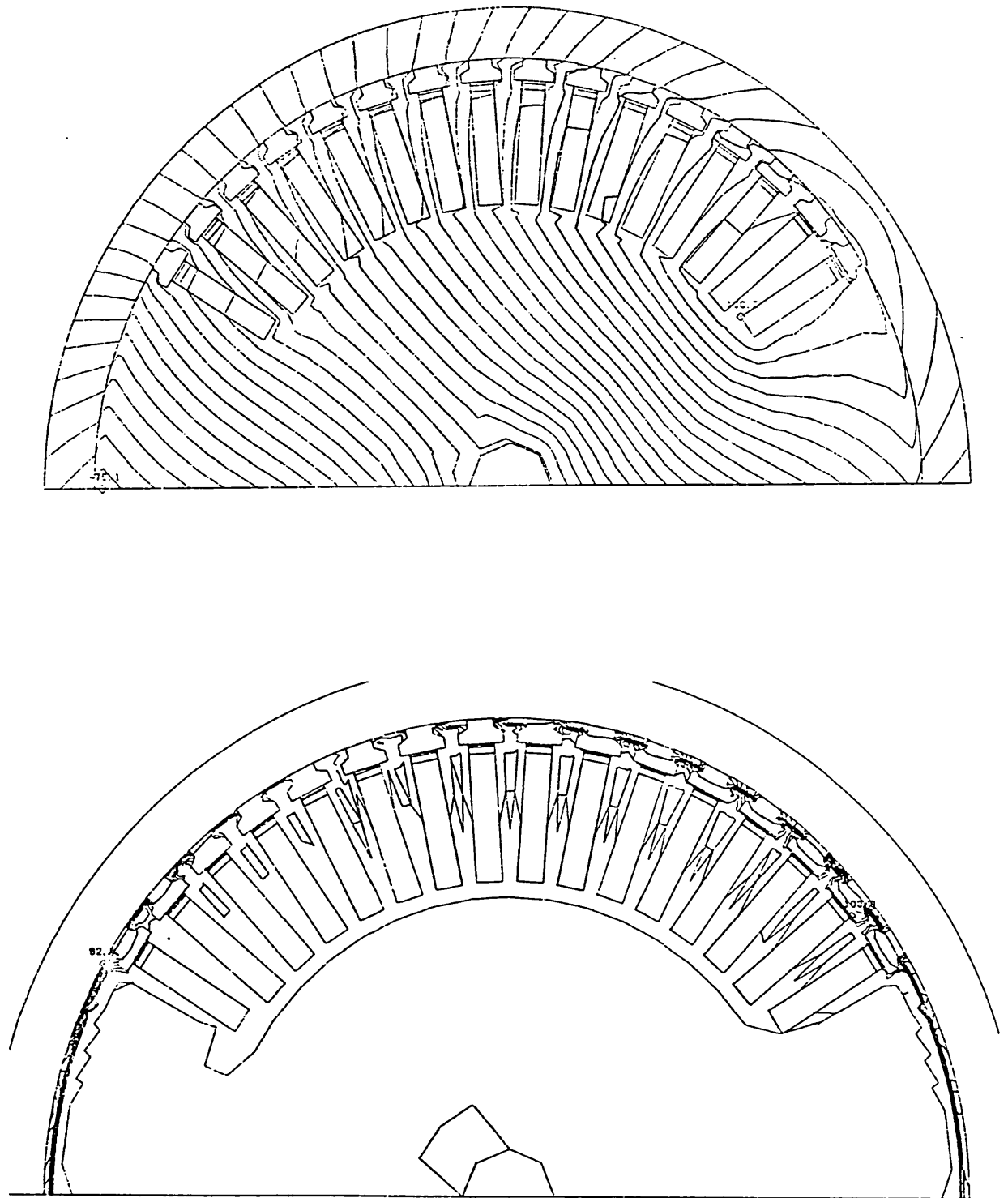


Figure 5.32 time = 0.26 ms current density contours at 5% of $1.91 \times 10^8 \text{ A/m}^2$

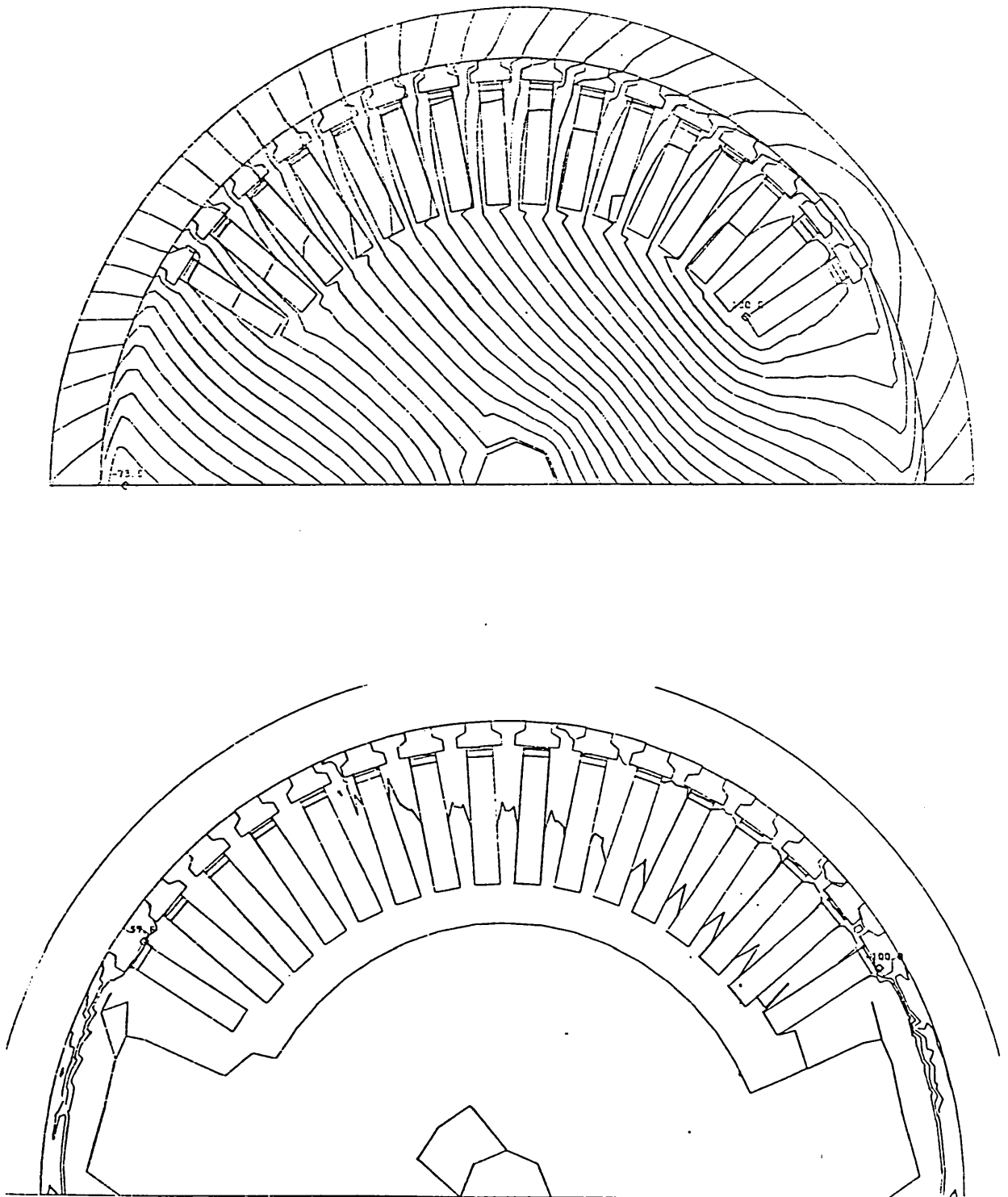


Figure 5.33 time = 2.00 ms current density contours at 5% of $2.84 \times 10^8 A/m^2$

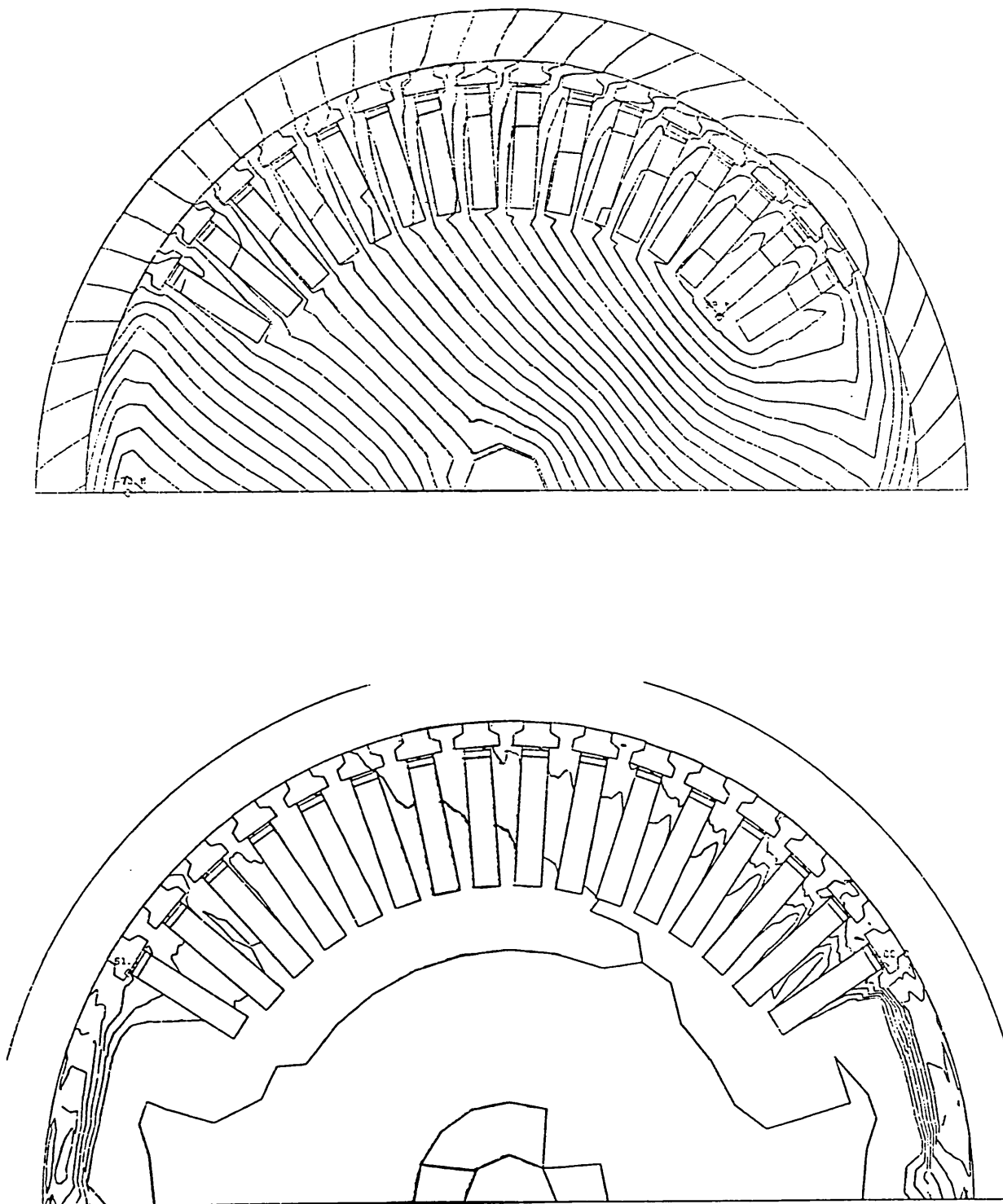


Figure 5.34 time = 11.0 ms current density contours at 2% of $1.34 \times 10^8 \text{ A/m}^2$

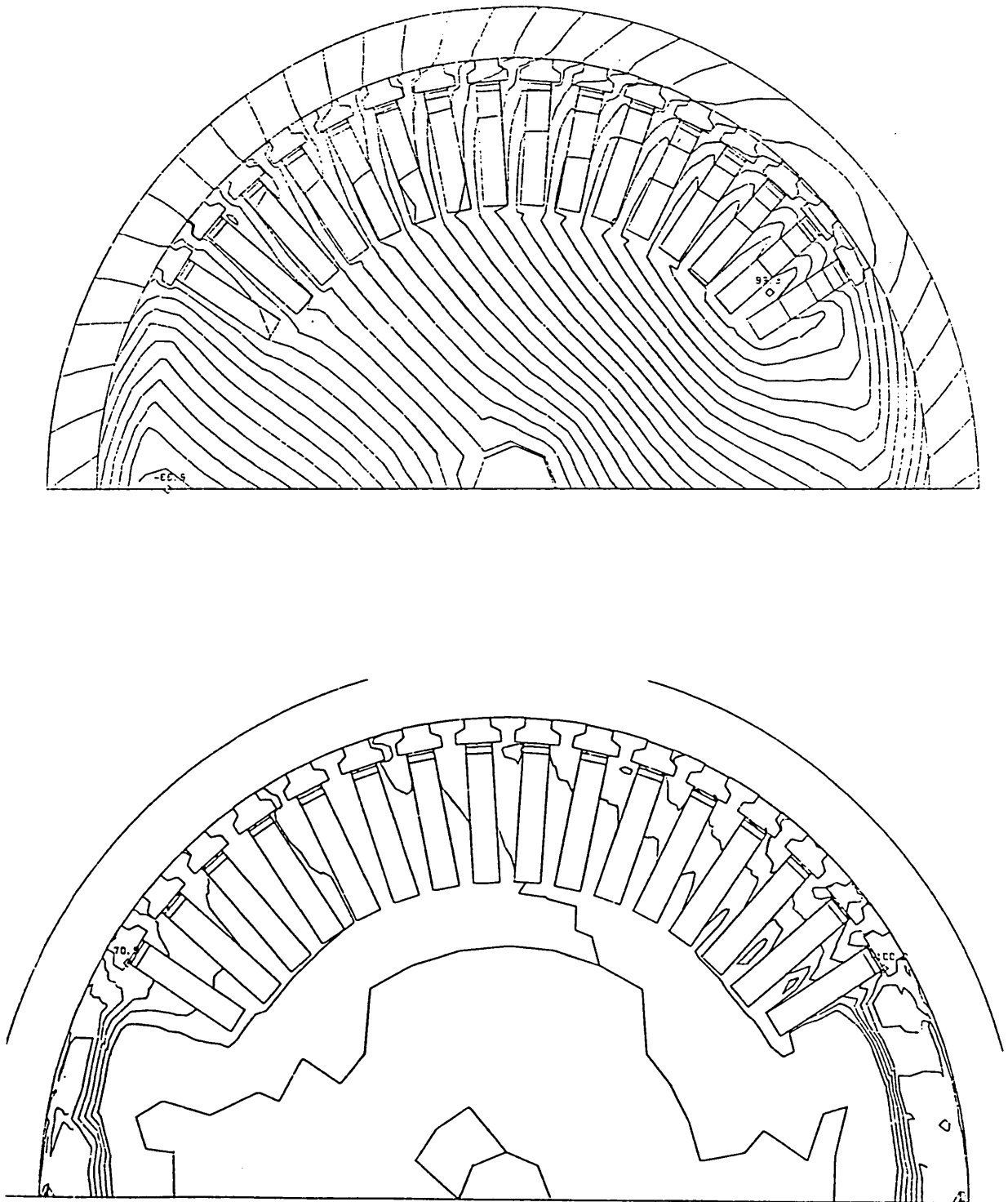


Figure 5.35 time = 21.1 ms current density contours at 2% of $0.90 \times 10^8 \text{ A/m}^2$

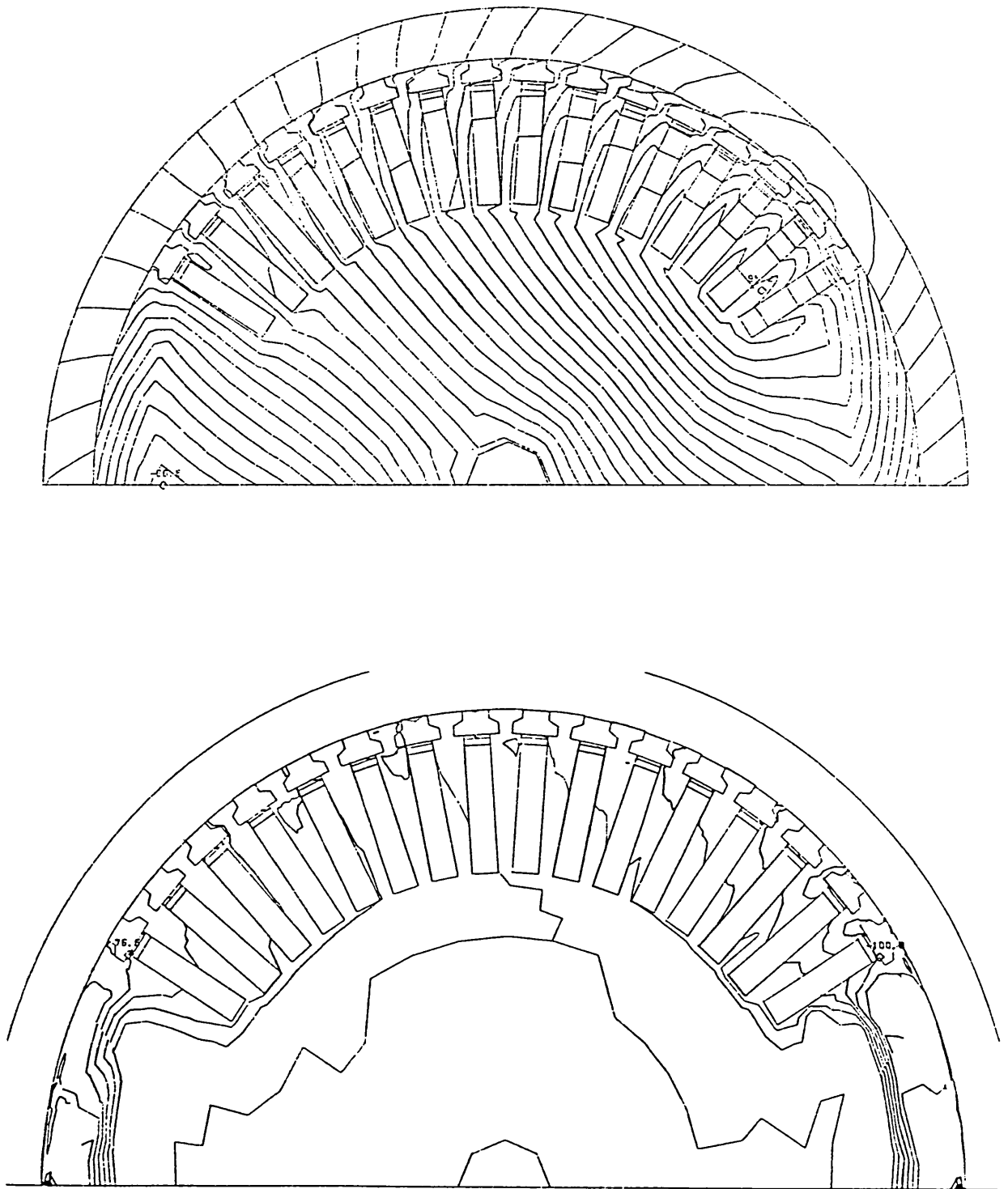


Figure 5.36 time = 30.2 ms current density contours at 2% of $0.69 \times 10^8 \text{ A/m}^2$

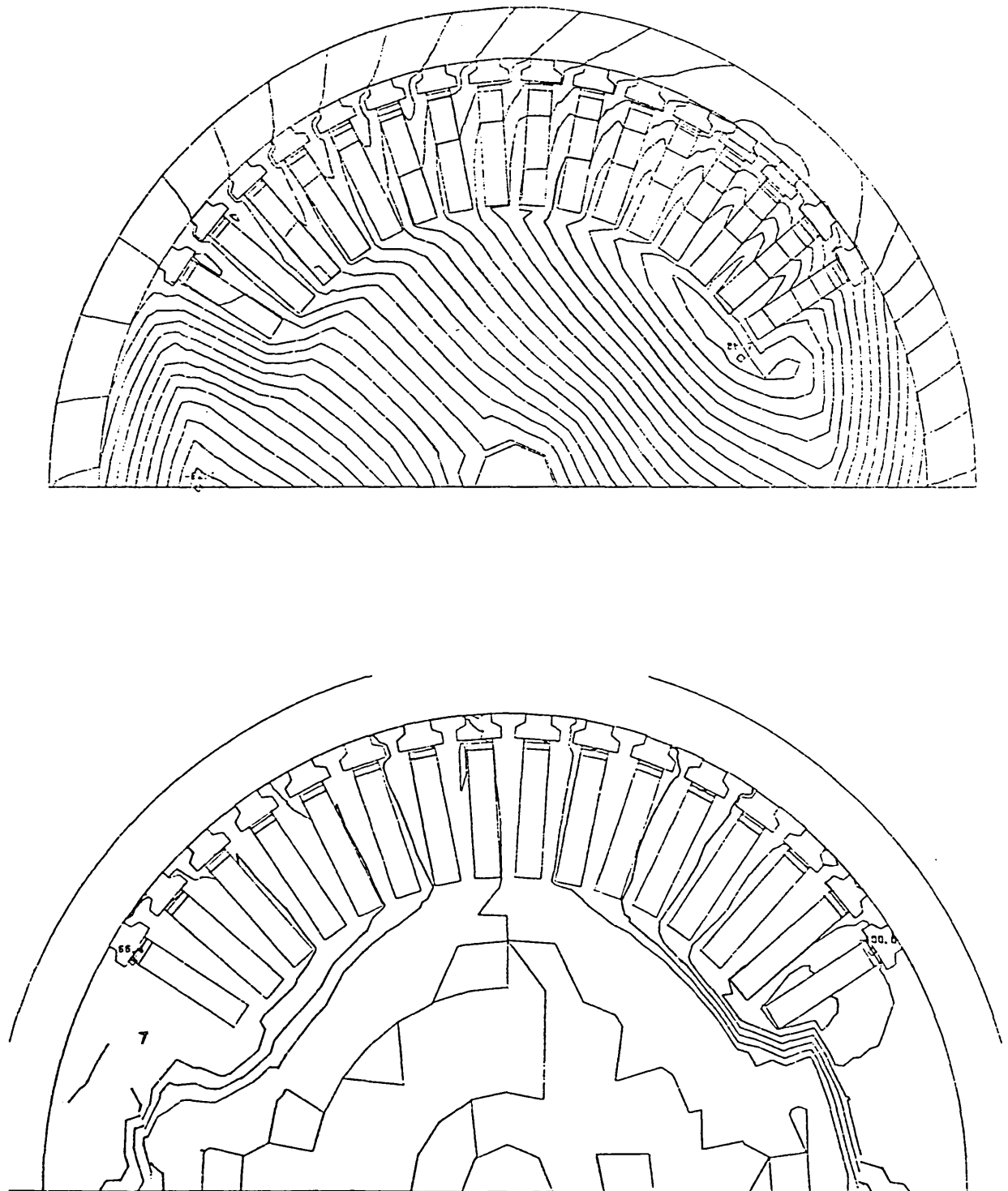


Figure 5.37 time = 139.0 ms - just prior to fault clearance current density contours at 2% of $0.23 \times 10^8 A/m^2$

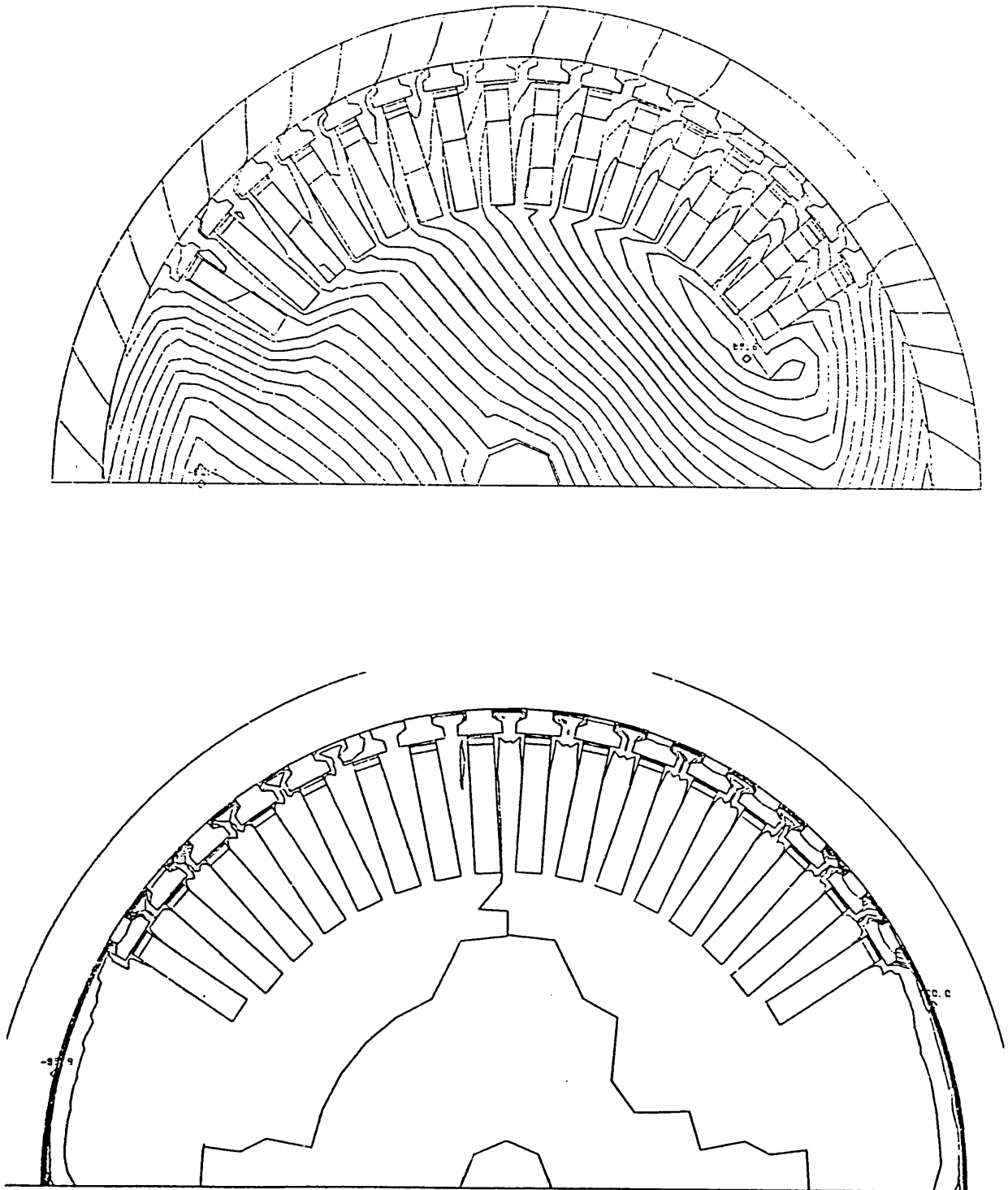


Figure 5.38 time = 139.2 ms - reclosure + 0.2 ms current density contours
at 5% of $2.40 \times 10^8 \text{ A/m}^2$

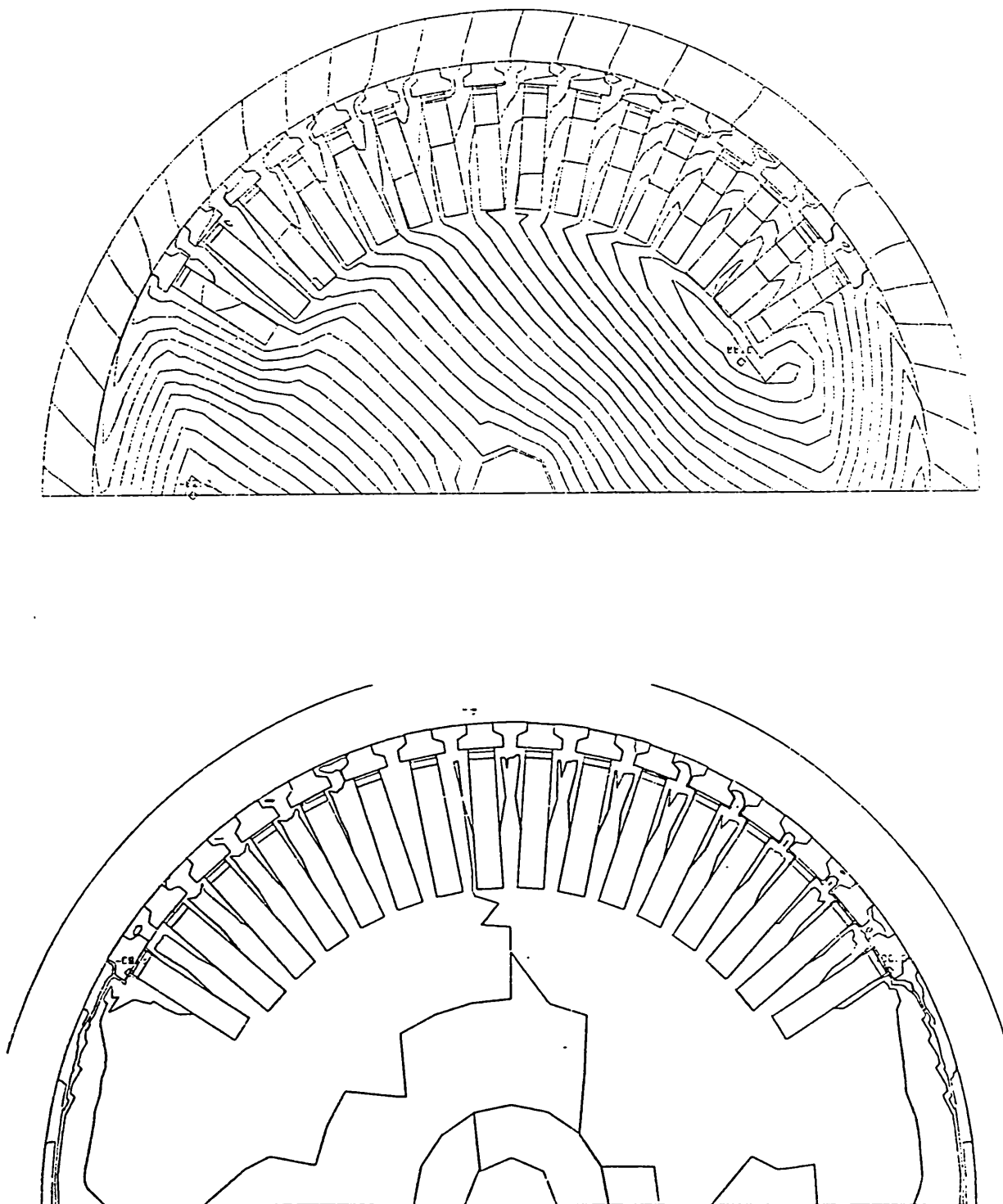


Figure 5.39 time = 141.1 ms - reclosure + 2.1 ms current density contours
at 5% of $2.09 \times 10^8 \text{ A/m}^2$

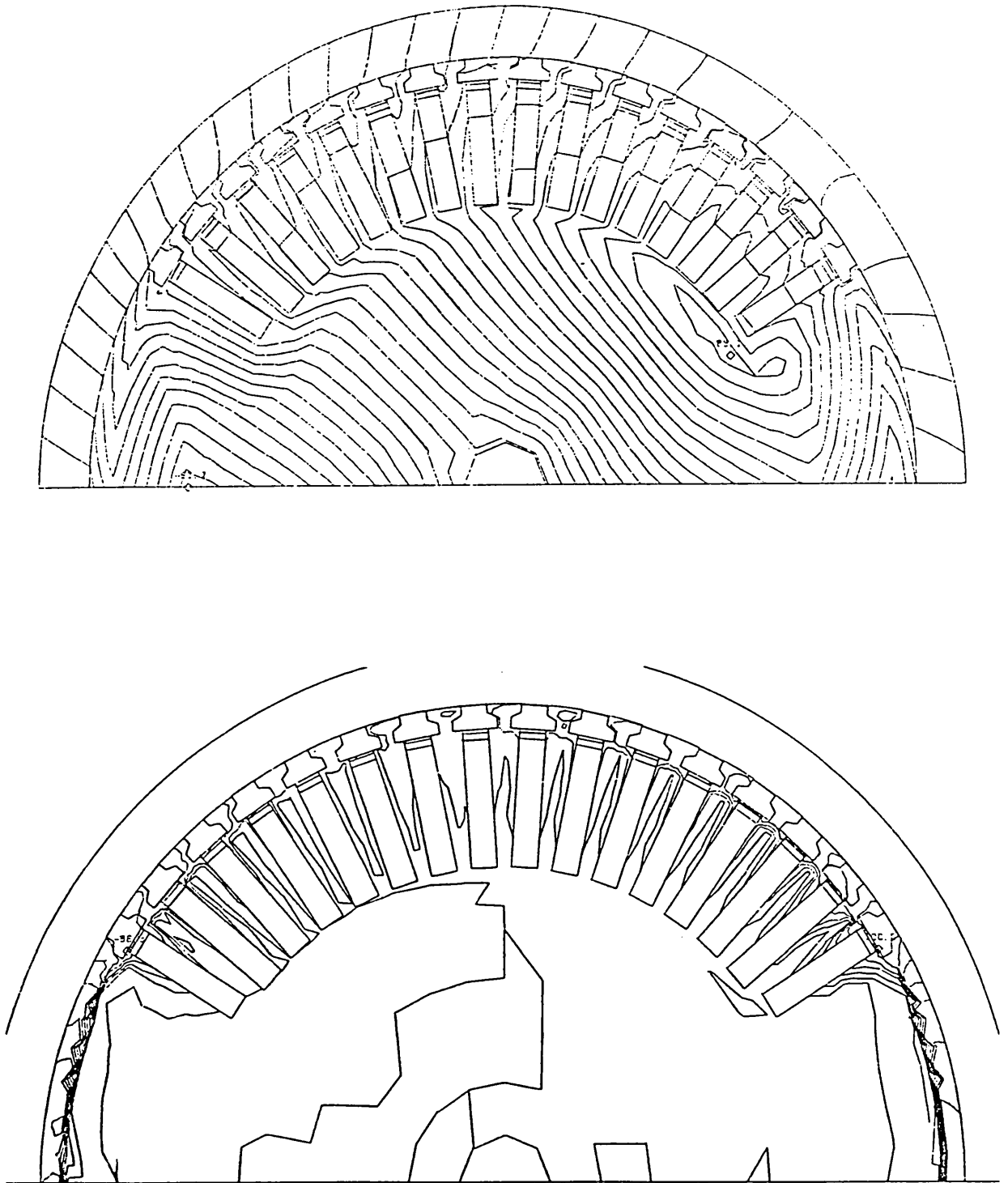


Figure 5.40 time = 149.1 ms - reclosure + 10.1 ms current density contours
at 2% of $0.98 \times 10^8 \text{ A/m}^2$

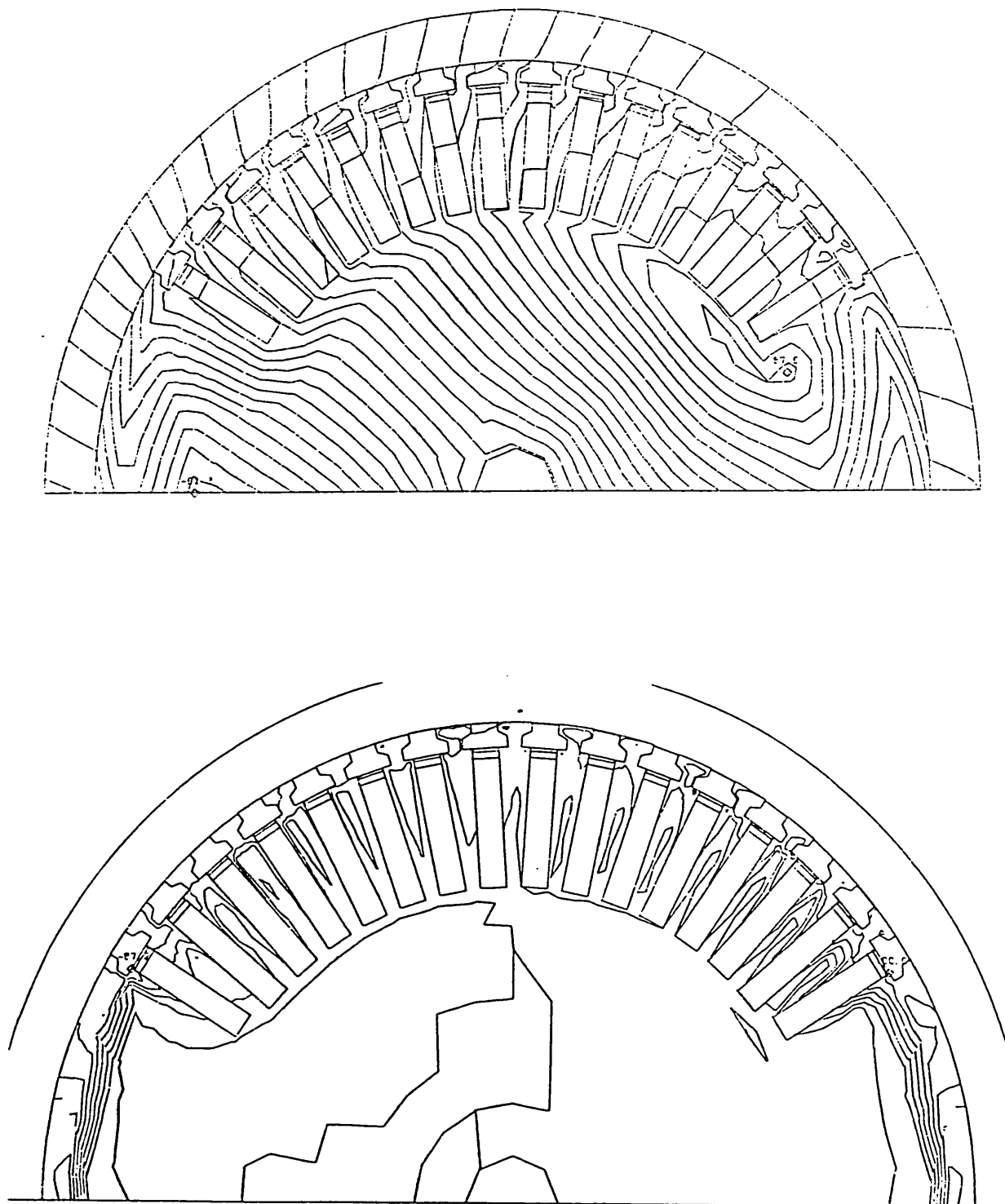


Figure 5.41 time = 160.0 ms current density contours at 2% of $0.56 \times 10^8 A/m^2$

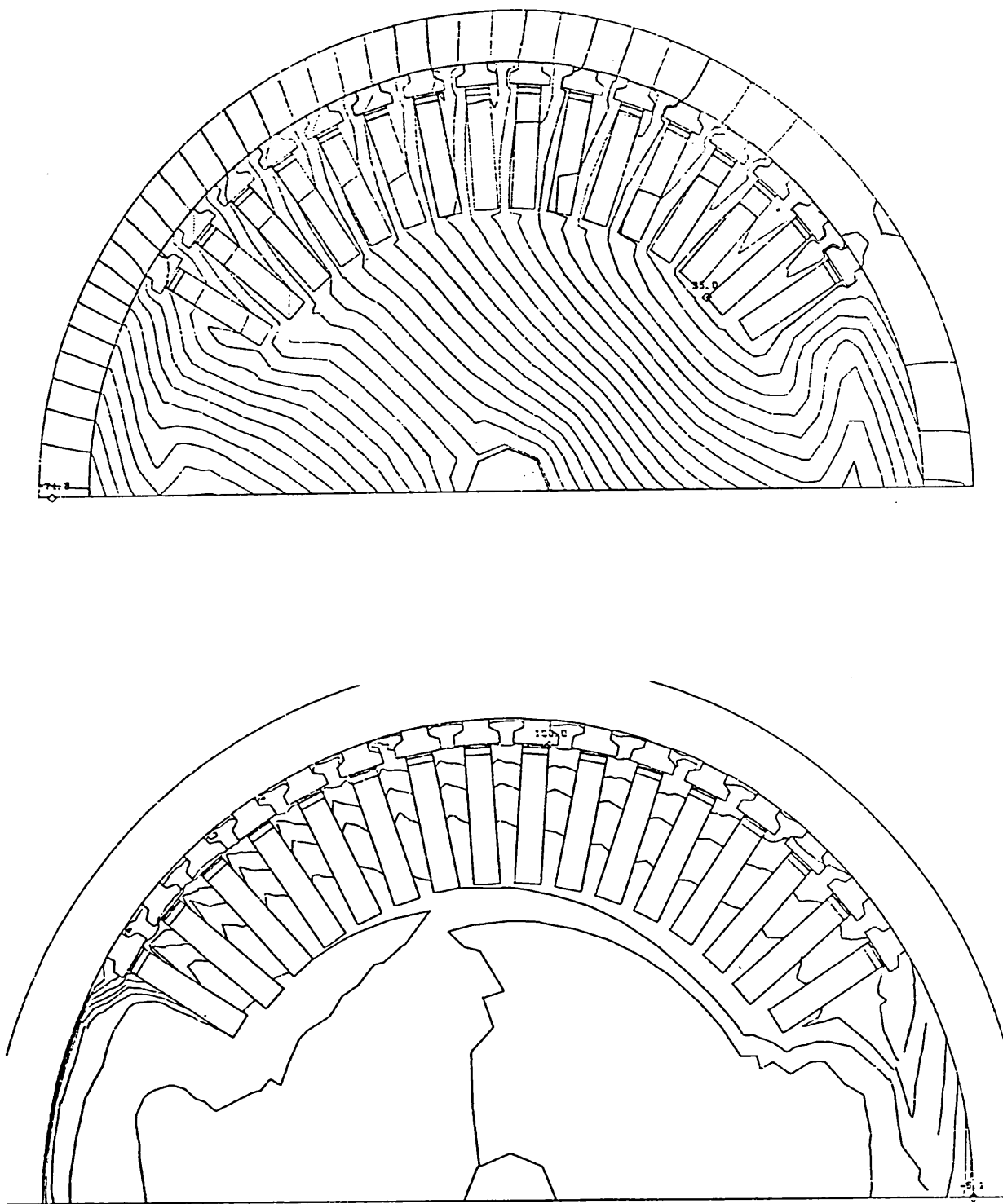


Figure 5.42 time = 600.0 ms current density contours at 2% of $0.13 \times 10^8 \text{ A/m}^2$

system. Comparison of the amount of c.p.u. time required for different jobs cannot be exact, as it depends upon the number of other users on the system. Accordingly, the figures in Table 5.5 are rounded to the nearest 5 c.p.u. minutes.

TABLE 5.5 COMPARISON OF C.P.U. TIME REQUIRED
FOR DIFFERENT CALCULATIONS

CEGB test B	Detailed mesh UM9		Crude mesh UM3		Detailed mesh UM9C	
	Full stator		Full stator		Current sheet stator	
Calculation	Short Reclosure		Short Reclosure		Short Reclosure	
	circuit		circuit		circuit	
	0 -	139 -	0 -	139 -	0 -	139 -
	139ms	600ms	139ms	600ms	139ms	600ms
Initial time	0.02 ms	0.02 ms	0.02 ms	0.02 ms	0.02 ms	0.02 ms
step length						
Final time	0.64 ms	2.56 ms	0.64 ms	5.12 ms	1.28 ms	5.12 ms
step length						
Number of	226	628	225	393	125	191
steps						
c.p.u. time	520 min	945 min	80 min	145 min	140 min	215 min
required						

For the full stator models, the calculation time required is seen to vary approximately as $n^2 - n$ where n is the number of nodes. The current sheet stator model shows an even greater advantage because of the more rapid increase in time step length.

5.10 CONCLUSIONS.

This chapter has described a two-axis model of the stator winding which enables a simplification of the problem formulation by ignoring the stator transformer conductivity matrix term. As a result, the time step length could be lengthened as the transient proceeded, and substantial savings in computational time were obtained.

The formulation leads to the solution of a densely packed, asymmetric matrix, with consequent substantial demands on computing time for each inversion. By the use of the A-average technique and a specially adapted Gaussian elimination scheme, a very efficient solution method was obtained, which required little more computational effort than a sparse, symmetric matrix of the same size.

The effect of neglecting the stator transformer terms on the calculated mechanical behaviour was discussed, and a possible analytical allowance for the neglected term was introduced.

Finding a reliable method of increasing the time step length efficiently while preserving computational accuracy proved difficult. The use of the minimum node time constant alone as an indicator gave patchy results and only a partial solution to this problem was found. Further work is required in this area.

The incorporation of the infinite busbar following reclosure presented some additional problems, as the formulation of the Hessian matrix required for the Newton-Raphson method became very difficult. A compromise was adopted in which the simple Hessian matrix construction was used at the expense of an increase in the number of iterations required per time step and some inaccuracy of solution immediately following reclosure.

The process of substitution of the stator windings by sinusoidally distributed ones was logically extended to a model in which they are reduced to a current sheet and the stator iron is ignored altogether.

This presentation is thought to be the first two-axis finite element analysis of transient conditions where the orientation of the axis of flux within the machine is unknown.

The two-axis model was then used to simulate one of the C.E.G.B. transient tests, and the predicted response compared with the measured one. It was found that the method generally gave good, although somewhat underdamped, results except that the maximum rotor angle predicted was too low. The importance of the stator recovery voltage was discussed with reference to the maximum rotor angle achieved and the timing of subsequent rotor swings. The eddy current power loss and rates of change of energy stored in magnetic fields were found to be not at all well modelled, but had only a minor effect on the machine behaviour. An analytical approximation for the latter was investigated, but gave no better results.

The current sheet stator model proved much faster in computation, as a result of the reduction in problem size and a more rapid increase in time step length, and predicted a higher first swing than the full stator model; although the results were more poorly damped. Calculations with a more refined mesh gave only slightly better results, the most noticeable improvement being in the prediction of rotor movement.

The flux and eddy current plots clearly showed the generation of eddy currents at the rotor surface and in the damper strips at the start of the transient, and their gradual diffusion into the body of the rotor.

When the fault was cleared, eddy currents appeared to be induced in the rotor surface flowing in the opposite direction to those deeper down. It is uncertain whether this observation accords with fact, or whether it arises as a result of the two-dimensional finite element formulation, which constrains currents to flow only in the axial direction.

The current sheet stator mesh gave very similar results to those of the full stator model of the same discretisation. This observation raises the question whether a mesh with a current sheet stator representation and employing the same number of nodes as a fully modelled stator would give superior results in consequence of the finer rotor discretisation achieved, ie. "Is a node better utilised in adding to the rotor discretisation or in modelling the stator ? ". Further work is required to establish guidelines in this area.

CHAPTER SIX

THE PHASE BAND STATOR MODEL

6.1 INTRODUCTION.

Very few machine models have been reported which use a phase band representation of the stator. The method was considered by Minnich et al. [37,38] for predicting machine steady state behaviour, but discarded in favour of the two axis approach because of the multiplicity of solutions required. For many applications the phase band method does prove unnecessarily complicated and time consuming, and the two-axis model provides an acceptable approximation.

Where it is necessary to model unbalanced faults, or both alternating and direct components of the transient response, the two-axis model with the stator transformer conductivity matrix ignored is inadequate. A better approach is to model the stator winding 'as is', with currents assigned directly to phase bands. This will also give the full set of harmonic voltages, rather than the fundamental only as is the case with the two-axis method.

In this chapter, a full solution of the equations of Chapter 2 is presented. A method of allowing for relative motion between rotor and stator is described and the formulation of the stator winding vectors and calculation of terminal voltage and current is outlined. Problems associated with the initial condition calculation and the factors affecting the choice of time step length to be used throughout the calculation are discussed.

The results obtained with this model when simulating the C.E.G.B. Test B are then presented. The method permits a detailed calculation of eddy

current losses and an example design study is performed in which the rotor wedge material is changed to improve performance. Eddy current and flux plots are discussed, and the effects of mesh discretisation on the computational time and the results obtained are illustrated. Various comparisons are then made; of the Maxwell stress and power balance methods of calculating rotor torque, of the two axis and phase band stator model predictions and of the results given by the phase band model when simulating the C.E.G.B. Test C1.

Finally, the chapter discusses the discrepancies between the calculated and measured results, and attempts to offer explanations for them.

6.2 STATOR WINDING REPRESENTATION.

If a phase band solution is to be adopted, some method is required for explicitly incorporating the relative motion between the rotor and stator in the analysis.

Two possible methods of allowing for rotor motion were considered :

- 1) Rotate the rotor portion of the mesh inside the stator portion. A slip plane is defined in the airgap, across which nodal potentials are interpolated. A periodicity condition may be applied to halve the problem size, but post processing of the potential solution is complicated by the use of what is effectively a different mesh at each time step. If tooth ripple effects are to be incorporated, the time step length must be restricted so that the rotor moves only a fraction of one tooth pitch at each step, which will increase the solution time substantially.
- 2) Fix the rotor and stator meshes in one position and move the stator phase bands backwards at synchronous speed. This method, developed by Turner [28], relies on the fact that the air gap is sufficiently large for tooth ripple

effects to be neglected. The technique may result in a stator slot being partially occupied by two different phase bands, but this has not been found to lead to any significant errors. Although now only one mesh is required for the whole problem, the stator winding vectors have become functions of time.

Turner reported a good prediction of machine electromagnetic behaviour when applying the second method to the works sudden short circuit test, so it was decided to use his approach for modelling the stator.

The rotor mechanical equations of Chapter 3 are linked to the electromagnetic solution at this point, since the angle through which the rotor moves in each time step will be determined by the rotor speed.

6.3 STATOR WINDING VECTORS.

In a phase band model, $(\delta A/\delta t)$ is directly proportional to the total stator flux linkage ie. rotational and transformer terms are not separated (although it is possible to do so). In order to assign currents to each winding node, the extent of the individual phase bands at each time instant is calculated, and the nodes that lie within them identified. The total phase current is then distributed to these nodes by the fraction of the total area occupied by that phase that is attributed to each node. Thus the current assigned to node i is :

$$I_i = (A \Delta_i) \frac{I}{n} \quad (6.1)$$

where A is the number of turns per pole per phase

n is the number of stator parallel paths

Δ_i is the fraction of the total winding area attributed to node i

and I is the total phase current

Where the boundary between phase bands falls within a stator slot, the nodes on either side carry a proportion of the current in each winding, and Δ_i is altered accordingly. By this means, a set of winding vectors for each phase, (N_a) , (N_b) and (N_c) are defined, which must, however, be reformed at each time step.

The rotating phase band method can be thought of as equivalent to the application of a rotational voltage of $B\omega$ to the stator conductors. It has the advantage of giving the correct relative rotation of the stator with respect to voltage generation in the rotor.

Equation 6.1 may also be used for determining the flux linking each stator winding. From equation 2.16 the flux linkage with phase a is :

$$\psi_a = pL_{eff}(N_a)^T(A) \quad (6.2)$$

where p is the number of machine poles
and L_{eff} is the machine effective length

Then the phase voltage is :

$$e_a|_{t+\delta t} = pL_{eff} [((N_a)^T(A))_{t+\delta t} - ((N_a)^T(A))_t] / \delta t \quad (6.3)$$

When calculating the phase currents, the stator circuit is incorporated as in figure 6.1 .

Turner demonstrates how the circuit equations derived from figure 6.1 can be used to form conductivity matrices for each phase, which may then be written in the form of three rows and columns for addition to the system matrix using the 'A-average' technique (see Chapter 2.6.8). This gives a symmetric matrix, whose additional terms are related purely to the circuit impedances and winding vectors and which are therefore compatible with the conductivity matrix method.

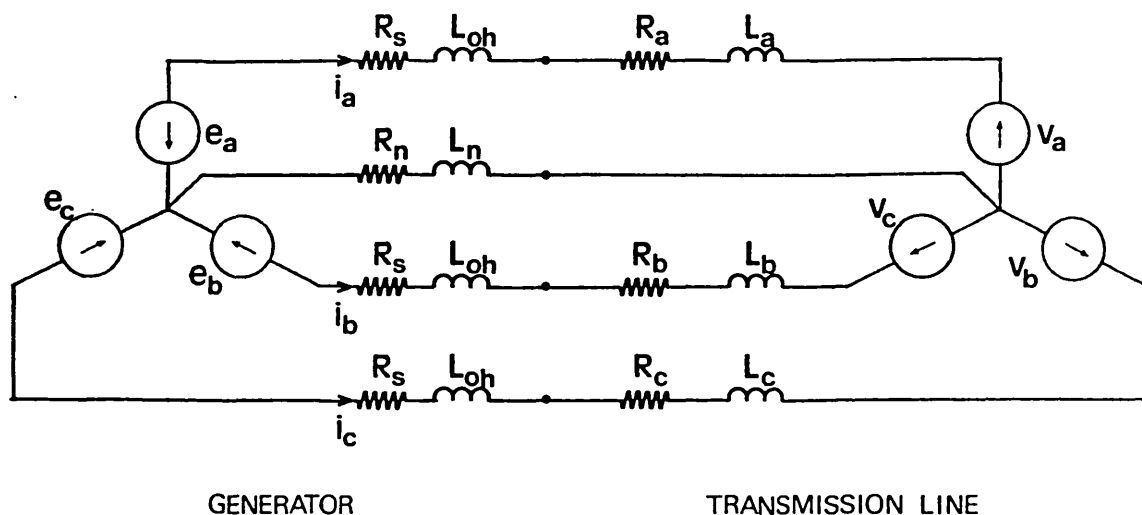


Figure 6.1 Stator circuit arrangement.

The approximations required for incorporating the infinite busbar into the two-axis model of Chapter 5 do not arise here.

6.4 TERMINAL VOLTAGE AND CURRENT.

The single value of 'terminal voltage' may be defined in several ways. In its calculation, all three phase voltages may be used, or one may be deduced from the others on the assumption of balanced operation.

Equation 6.3 gives the machine phase voltages 'at the airgap', ie behind the machine reactance, from which the terminal phase-neutral and line-line voltages may be found. Thus the phase band stator model allows any method of calculation of the terminal voltage to be used. The definition of line voltage used here is the root mean square of the line-line voltages found explicitly from the phase voltages. This is identical to the rms phase voltage in the absence

of harmonics (which the line-line calculation tends to remove). Line current is calculated as the rms phase current.

6.5 INITIAL CONDITION.

The pre-transient initial condition is achieved in a similar manner to that described in Chapter 5, except that the impedance added to the terminals is a series combination of resistance and reactance, rather than a parallel one. Iterating to the correct terminal voltage is not as straightforward, however, since even the steady state must be time stepped to obtain the phase voltages. Two methods may be adopted to speed convergence :

- 1) A good initial estimate of the potential solution is provided by solving the two-axis problem for the same terminal conditions.
- 2) The solid rotor and field winding conductivity matrices are not included in the problem formulation.

Adoption of a phase band stator model enables the fault to be applied at a specific point of the cycle. The time stepping procedure must therefore be stopped at the correct point in the initial condition calculation, if the point on wave is important.

The individual phase voltages contain harmonics, principally the third. The 'steady state' terminal voltage thus contains a harmonic ripple which makes it unsuitable for use as a target for iterative changes to the field current. To solve this problem, a one-cycle, moving average digital filter was applied to the terminal voltage when finding the initial condition, and the filtered voltage used as a basis for field current changes.

The infinite busbar voltage was calculated as described in Chapter 4.4.3.

6.6 TRANSIENT INITIATION.

The transient is started in the manner used for the two-axis method, described in Chapter 5.4, except that values of $(\delta A/\delta t)$ are not zero at $t=0$, but are obtained from the initial condition calculation. It has been found, however, that no significant errors arise if $(\delta A/\delta t) = 0$ is assumed. The second order predictor was found to be less satisfactory than the first order one, possibly because the second order method tended to 'carry through' harmonic terms.

6.7 TIME STEP LENGTH.

The time step length is fundamentally limited by the need to model the alternating voltages and currents accurately. This dictates a maximum step length of the order of 1/100th of a cycle, ie 0.2 ms, to reduce the error in approximating a differential by a difference to a few percent. This restriction means that a very large number of time steps, each of which requires a number of iterations to converge, are required to model a transient that incorporates the machine swing curves - for the 3.8 second C.E.G.B. transient Test B at Uskmouth, 19,000 non-linear time steps are needed. Time step lengths less than 0.2 ms were found to give no significant difference in results.

To capture the first moments of the transient, the initial time step was set at 0.02 ms, and lengthened to 0.2 ms in the three succeeding steps.

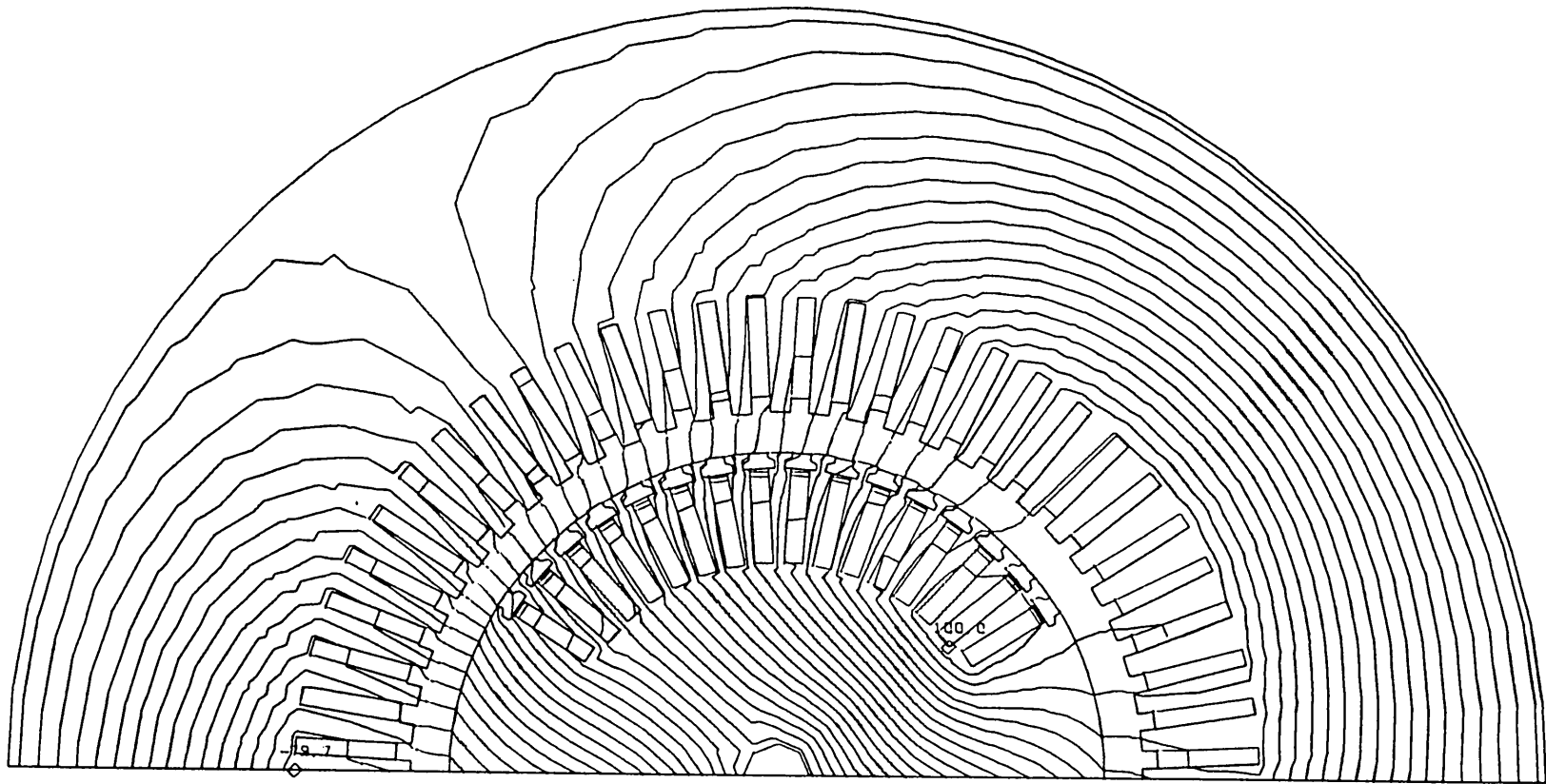


Figure 6.2 Initial condition Test B - flux distribution

USK MOUTH MESH 18 1951 NODES 3810 ELEMENTS.

C.E.G.B. TEST B. INITIAL CONDITION.

LOAD ANGLE = 61.5 DEG.





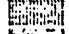
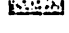

FIELD CURRENT = 854 A.

STATOR PHASE CURRENTS

-310.0 -5819.8 6129.9 AMPS

RED PHASE POINT ON WAVE = 320 DEG.

VARIATION IN
FLUX DENSITY.

<	2.97567E-01
	< 5.95133E-01
	< 8.92700E-01
	< 1.19
	< 1.49
	< 1.79
	< 2.08
	< 2.38

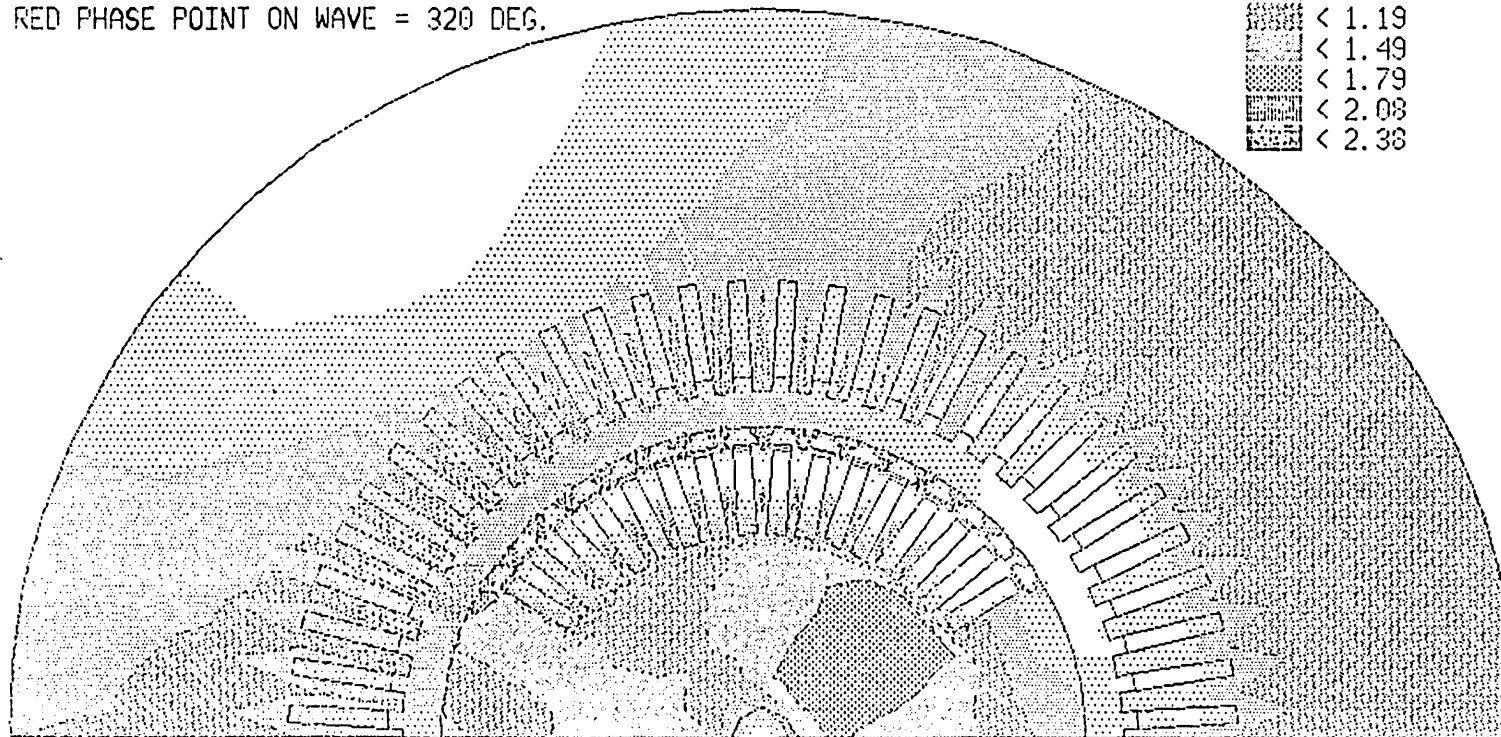


Figure 6.3 Initial condition Test B - flux density distribution

6.8 COMPARISON OF SIMULATED AND MEASURED RESULTS, C.E.G.B. TEST B.

6.8.1 Initial condition

Due to the presence of harmonics in the voltage waveform and the need to time step to a solution, achievement of the desired initial condition can be a time-consuming process if the level of accuracy to which the initial condition terminal values are required is set too high. For the simulations performed, the maximum error level was set at 0.5%, and gave the results in Table 6.1.

TABLE 6.1. INITIAL CONDITIONS - TEST B.

	Crude Mesh UM3	Detailed Mesh UM9	CEGB Test
Line voltage	13.76 kV	13.76 kV	13.80 kV
Line current	4.876 kA	4.883 kA	4.880 kA
Terminal real power	111.2 MW	110.7 MW	111.1 MW
Terminal reactive power	-35.0 MVA _r	-35.7 MVA _r	-35.2 MVA _r
Field current	865 A	854 A	827 A
Load angle	56.0 deg.	58.1 deg.	61.5 deg.

Figures 6.2 and 6.3 show the flux and flux density variation in the machine for the initial condition.

The variable endbell resistivity factor described in Chapter 2.5 was used for all the phase band method calculations.

The results have been digitally filtered where appropriate (see Chapter 4.5.4).

6.8.2 Transient behaviour : time series data.

Figures 6.4 to 6.6 compare the phase band calculation with the C.E.G.B. test results. The 50 Hz oscillations during the transient period, given by the stator transformer conductivity matrix, are clearly seen.

As in Chapter 5, the initial stator recovery voltage is too high, causing more power to be generated, and resulting in less acceleration of the rotor and hence a lower first swing. The rotor swing frequency is correctly predicted, and the damping good, but a little too light.

The filtered results show that the phase band method has overpredicted the line and field currents during the short circuit period, and underpredicted both on fault clearance.

The rotor speed drops at the start of the short circuit, the braking effect of losses being greater than the turbine input. However, this is not large enough to produce a noticeable rotor backswing.

The eddy current power loss and the power flow to stored energy in magnetic fields are shown in figures 6.7 and 6.8. These are very different from the results of the two-axis calculation. Both show a 50 Hz variation; but, while the eddy current loss will always provide a retarding force on the rotor, the power flow to magnetic field storage is bi-directional. The energy storage increases in the first half cycle, as currents rise in linked circuits, and power is taken out of the rotor inertia; but in the second half of the cycle, as currents fall, energy is released, and becomes available to accelerate the rotor. The magnetic circuit stored energy changes may be associated with Shackshaft's 'oscillatory' torque [60], and the eddy current power loss with a 'unidirectional' torque [62,63].

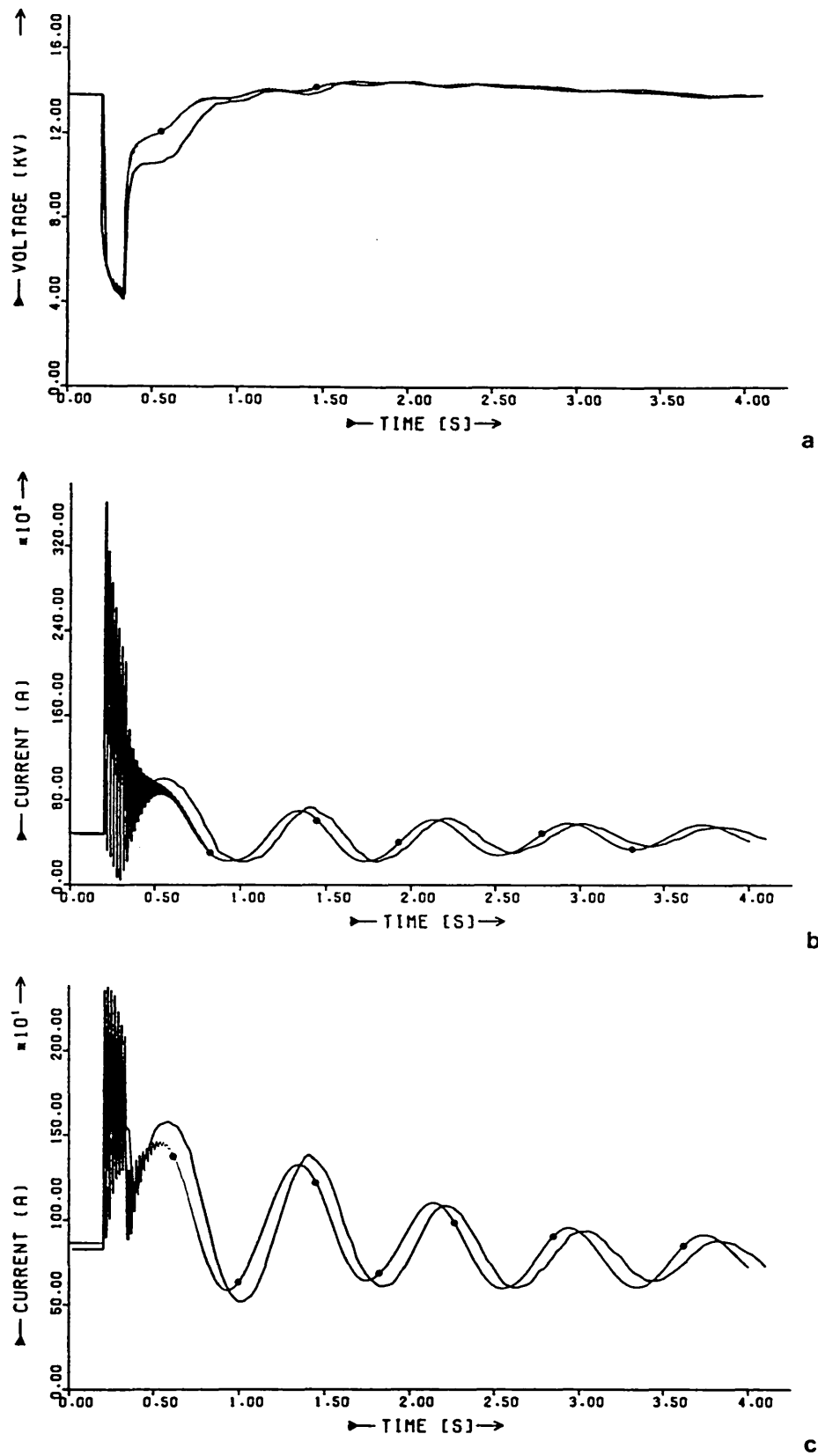
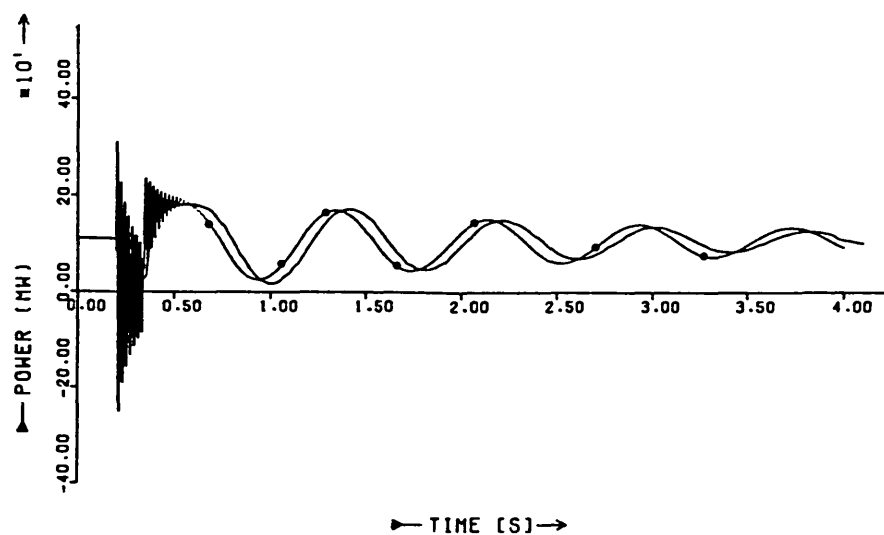


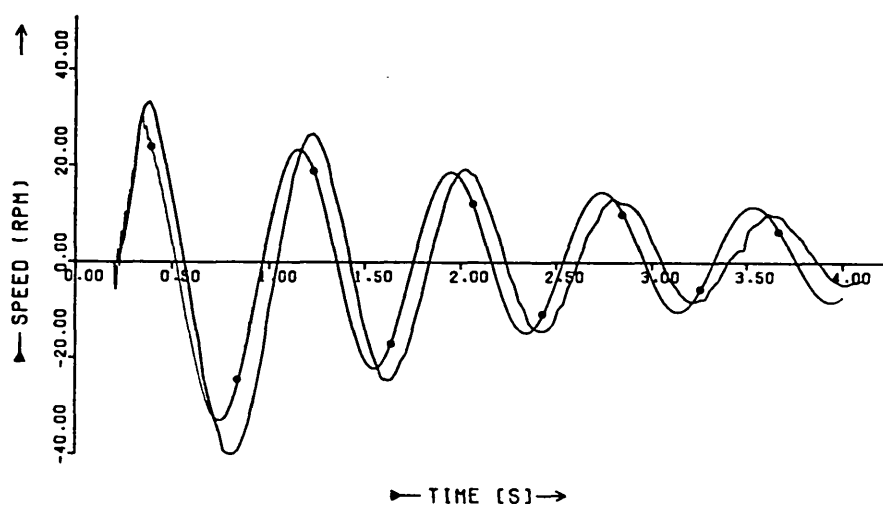
Figure 6.4 Machine response Test B.

— Test results —●— finite element calculation

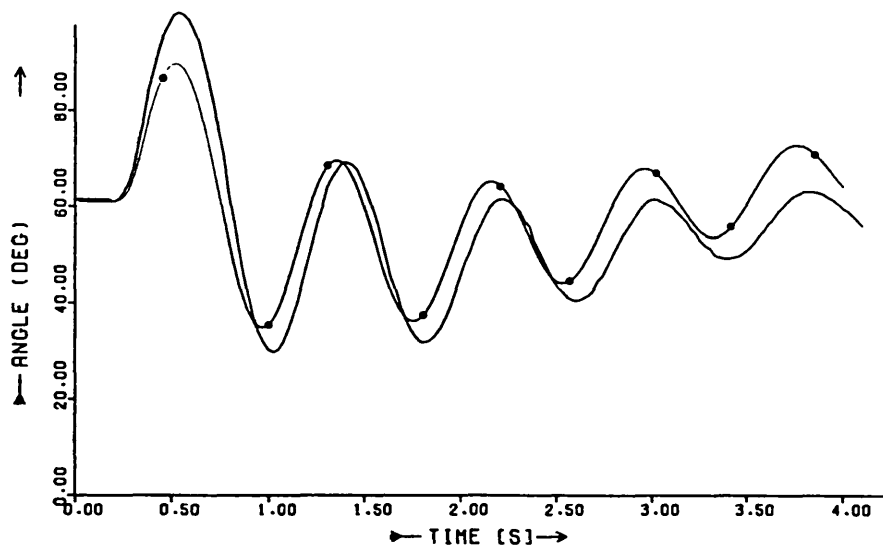
a) line voltage b) line current c) field current



d



e

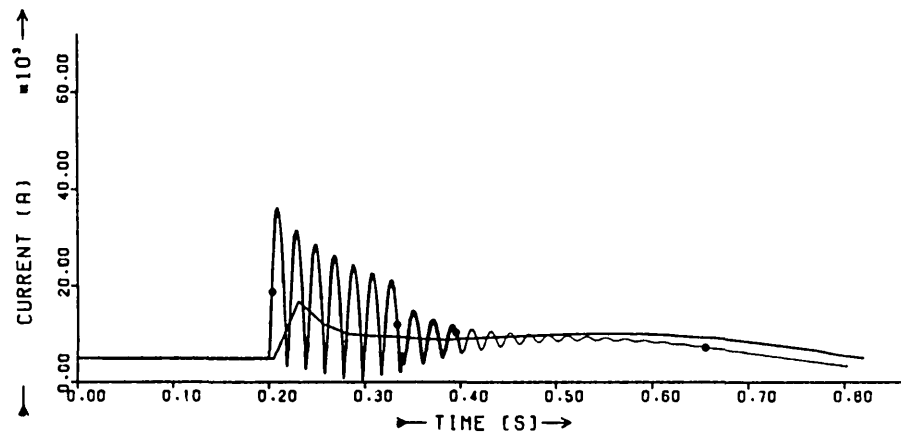


f

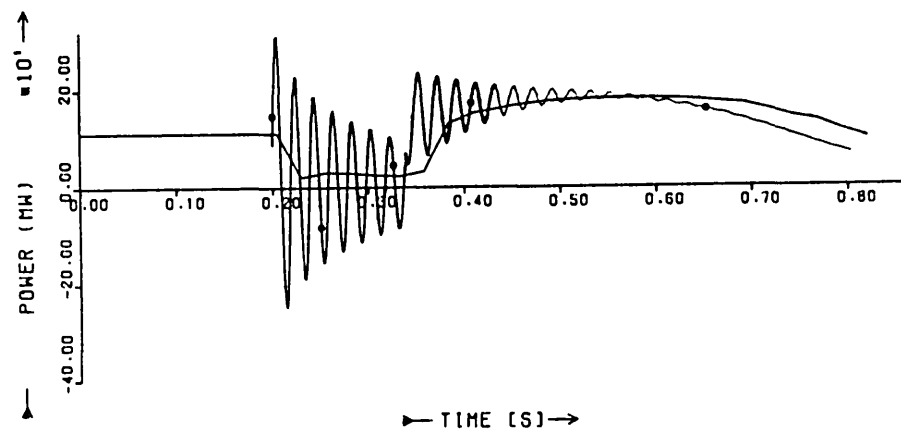
Figure 6.4 Machine response Test B (continued)

— Test results —●— finite element calculation

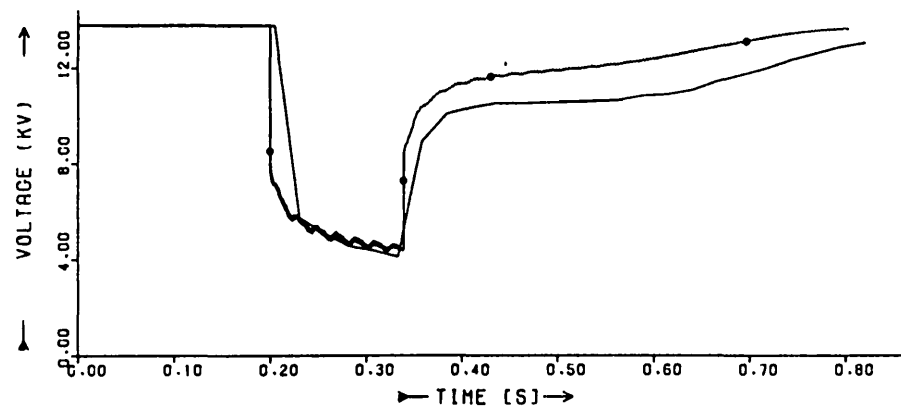
d) electrical power e) speed deviation f) rotor angle



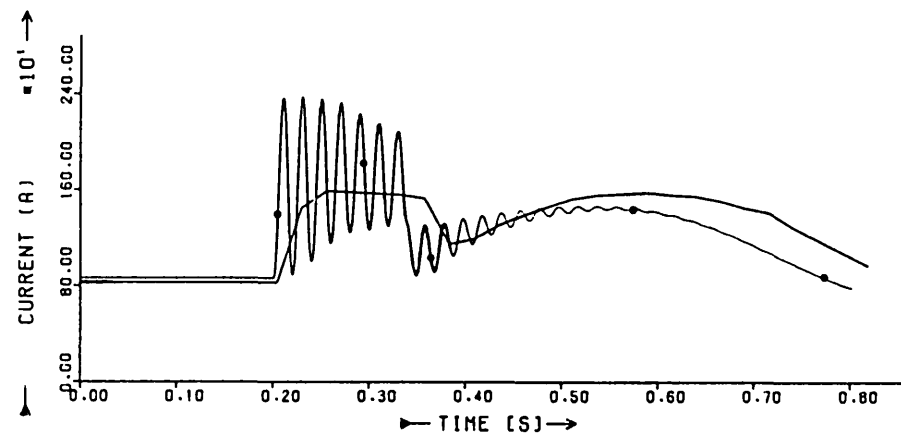
b



d



a

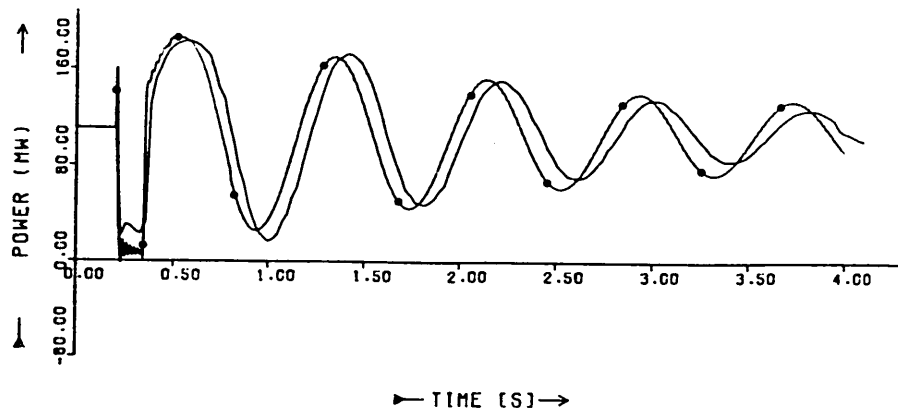


c

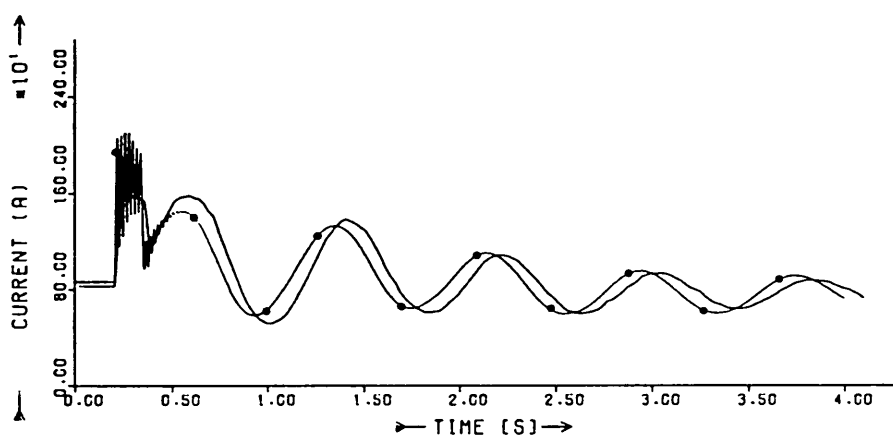
Figure 6.5 Machine response Test B - detail

— Test results —●— finite element calculation

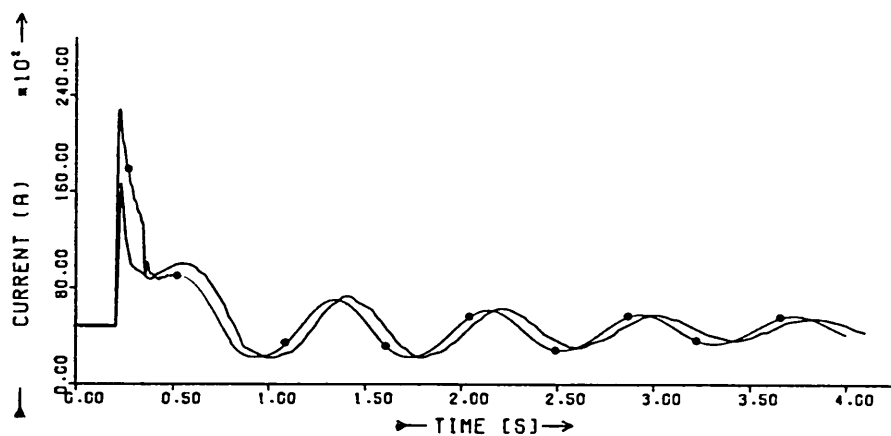
- a) line voltage b) line current
- c) field current d) electrical power



d



c



b

Figure 6.6 Machine response Test B - filtered

— Test results —●— finite element calculation

b) line current c) field current $\frac{13}{25}$ point filter d) electrical power

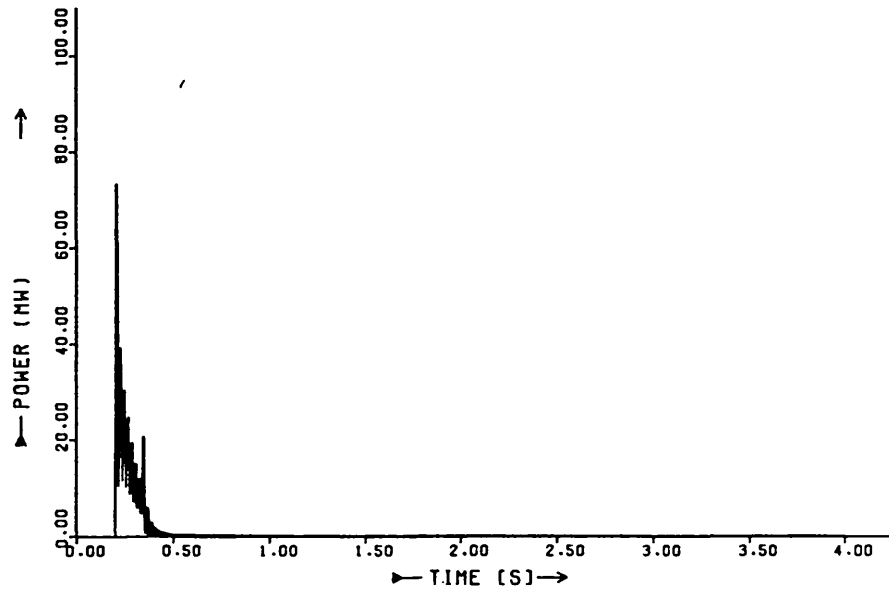


Figure 6.7 Machine response Test B - eddy current power loss

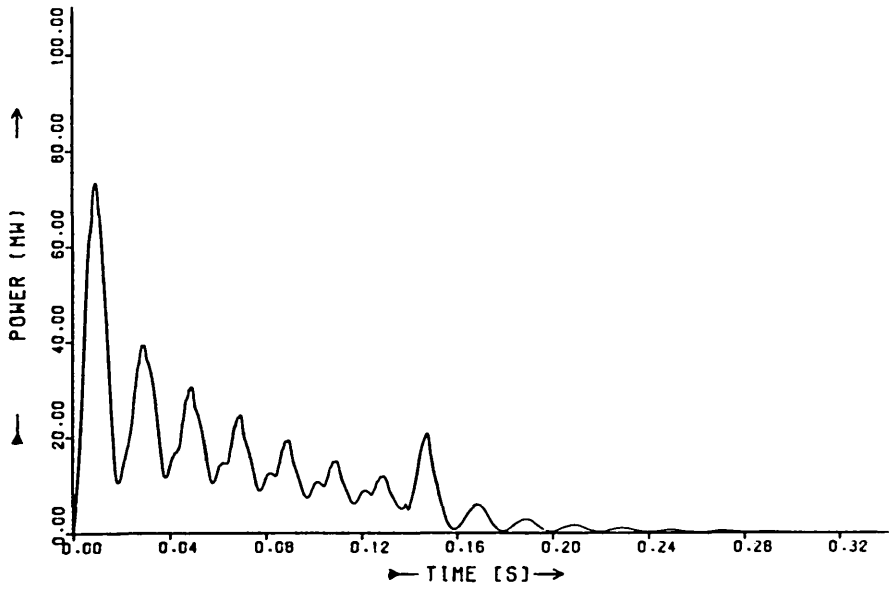


Figure 6.7 Machine response Test B - detail of eddy current power loss

note : no time offset

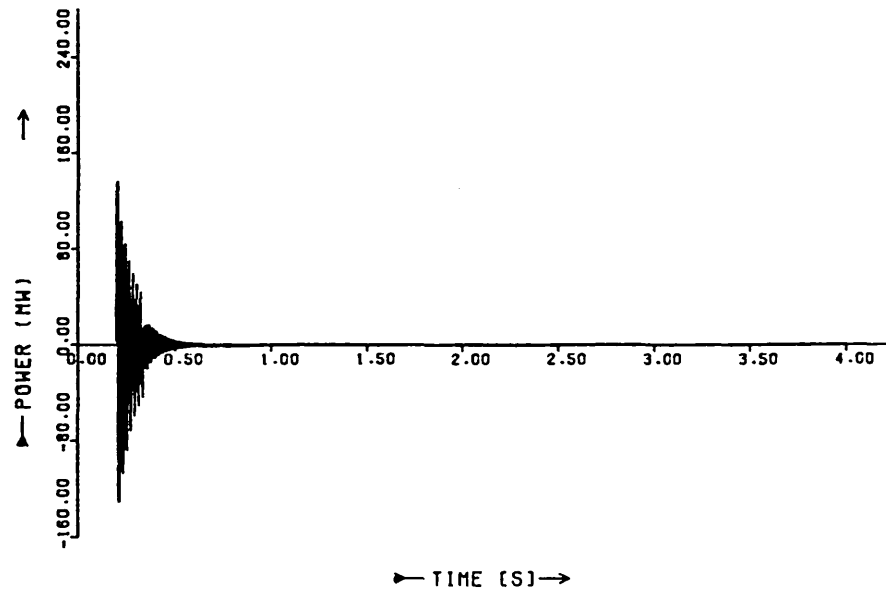


Figure 6.8 Machine response Test B - power flow to magnetic storage

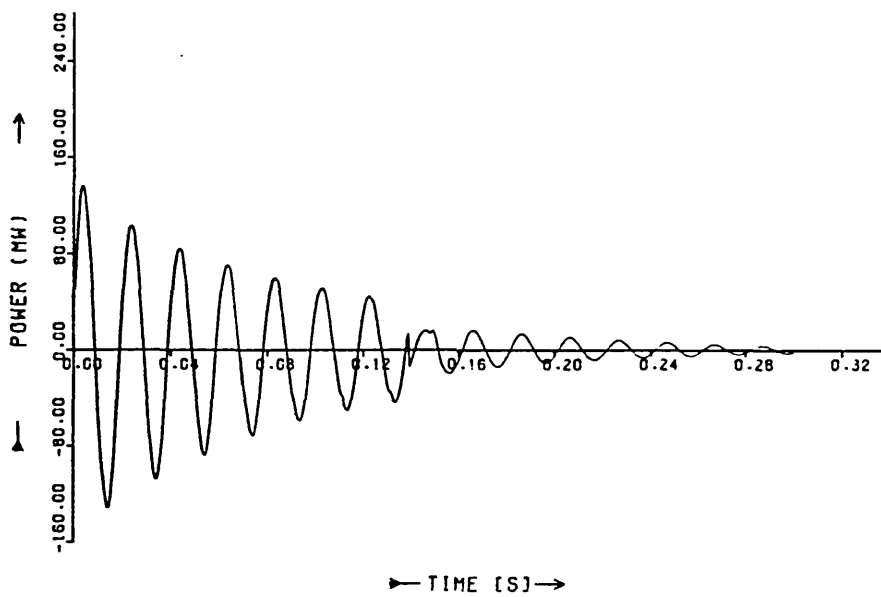


Figure 6.8 Machine response Test B - detail of power flow to magnetic storage

note : no time offset

The individual components of the eddy current power loss, and thus the contributions to damping of the different parts of the rotor, may be simply assessed by defining a separate conductivity matrix for each material or area. The result of this exercise is shown in figure 6.9 , where the losses in the rotor poles, teeth, wedges and copper damping strip are shown. The two-dimensional allowance for the three-dimensional effect of discontinuous wedges, described in Chapter 2.5, means that the division of the total power loss into these separate values is not accurate enough for calculations such as local heating, but do suggest that the damper strip, although carrying a high current density, is too small to make a significant contribution to the overall damping. Design studies featuring simple variations of material would enable a better distribution of power dissipation between rotor poles, teeth and wedges to be found.

As an illustration, figure 6.10 shows the calculation of the short circuit period of Test B repeated with the copper damper strip removed, and aluminium slot wedges substituted for the stainless steel ones originally fitted. As can be seen, although the total eddy current power dissipation is not significantly different, the distribution has been dramatically altered. With the existing design, twice as much power was generated in the rotor teeth as the wedges and damper strips combined. When aluminium alloy wedges are used, the new eddy current pattern results in three times as much power being generated in the wedges as in the rotor teeth. The higher thermal conductivity of aluminium should then allow the whole slotted region of the rotor to run cooler.

6.8.3 Transient behaviour : flux and eddy current plots.

Figures 6.11 to 6.43 show the distribution of flux and eddy currents during the short circuit and reclosure periods.

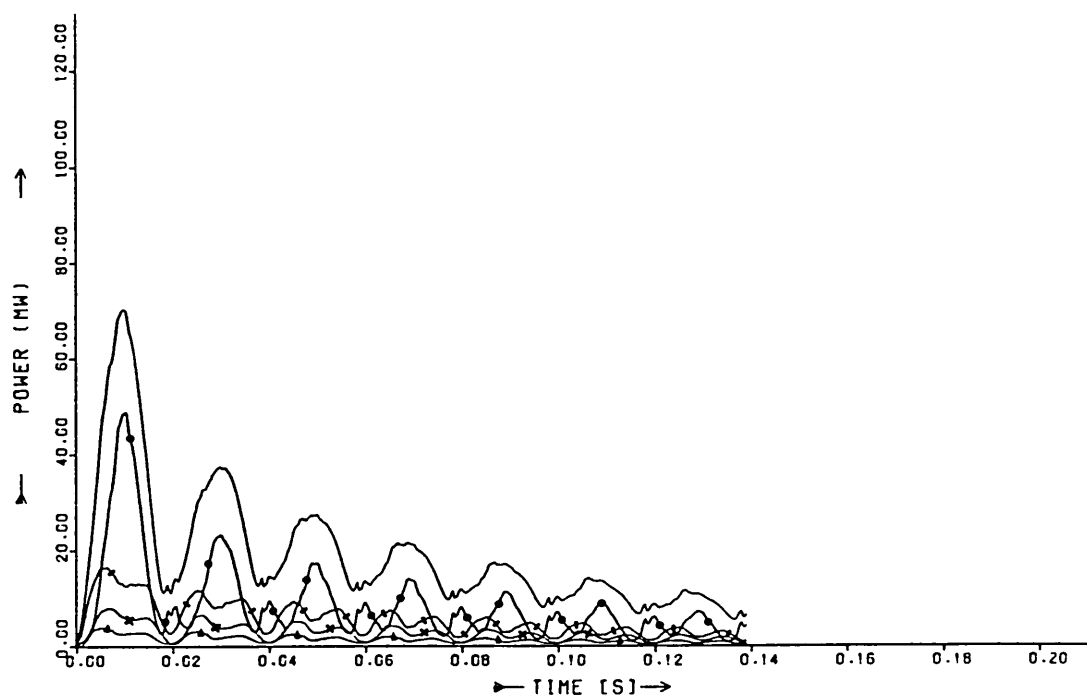


Figure 6.9 Machine response Test B - eddy current power loss components

— total —•— pole —+— teeth —x— dampers —o— wedges

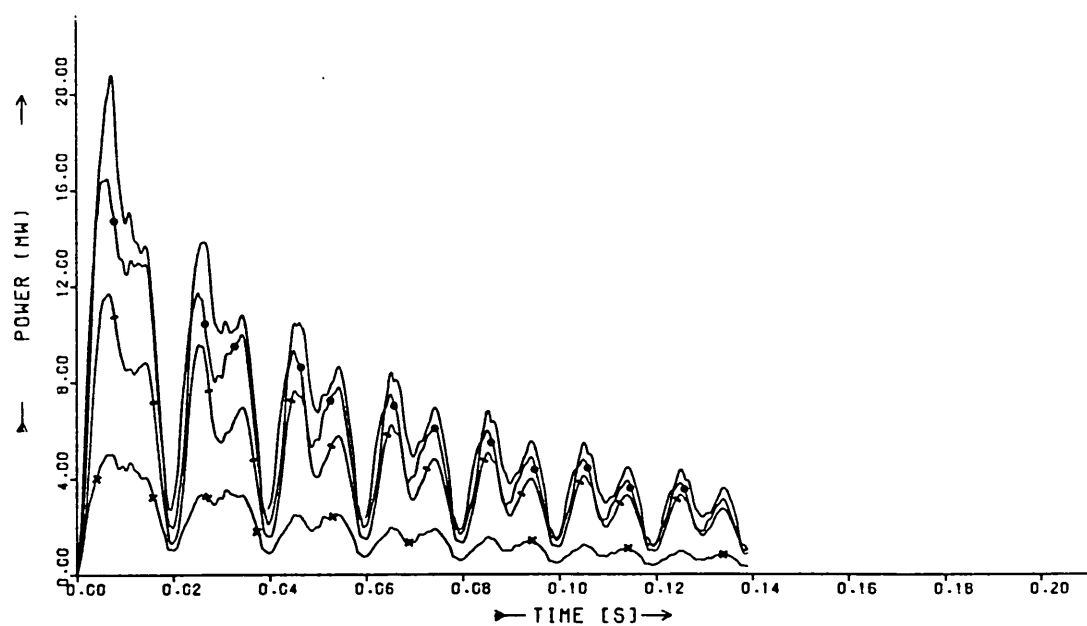


Figure 6.10 Comparison of eddy current power loss components

- machine with wedges as designed and with aluminium wedges

— in aluminium wedge —•— in rotor teeth, stainless steel wedges

—+— in stainless steel wedge and copper damper strip

—x— in teeth, aluminium wedges

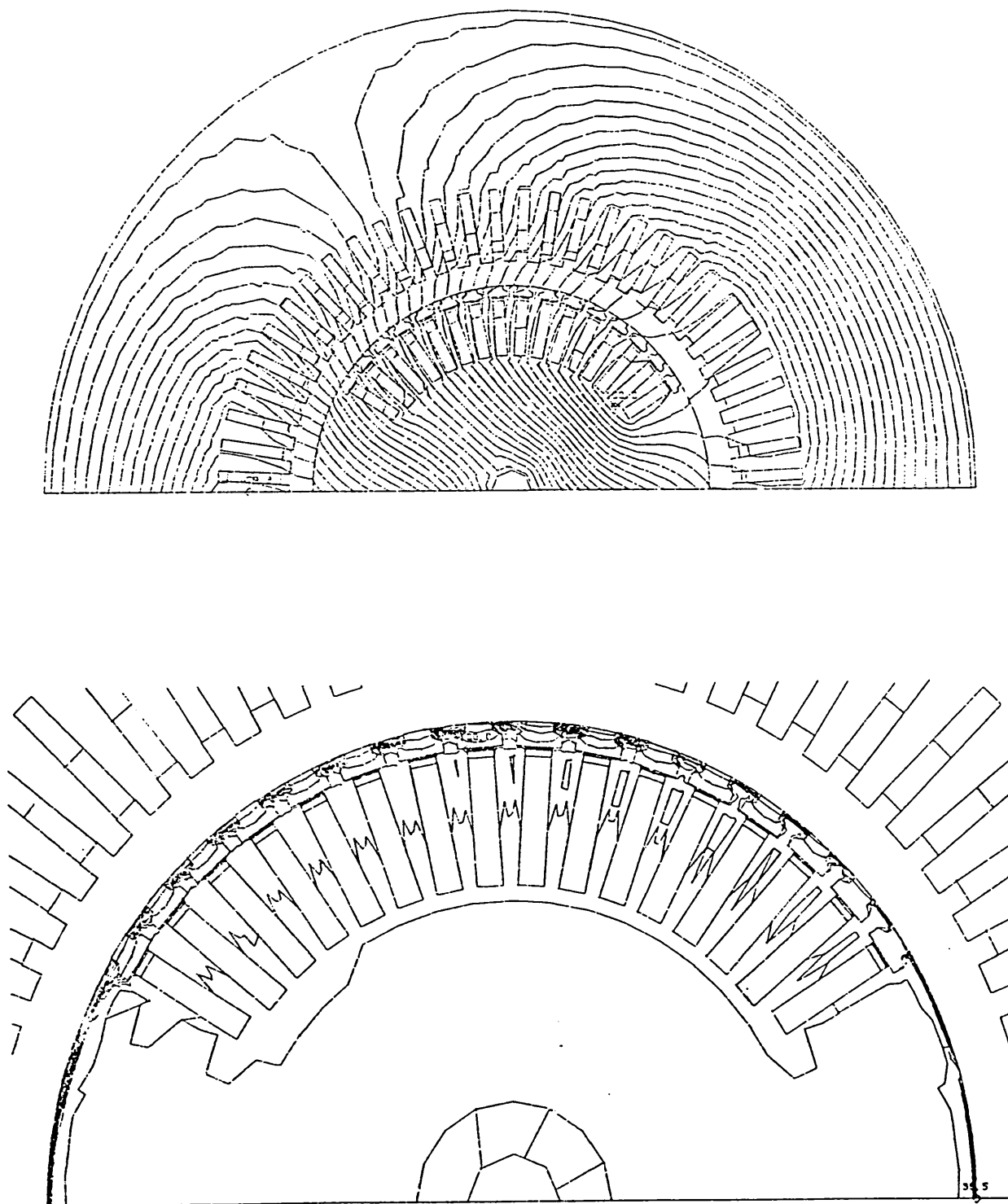


Figure 6.11 time = 1 ms current density contours at 5% of $0.39 \times 10^8 \text{ A/m}^2$

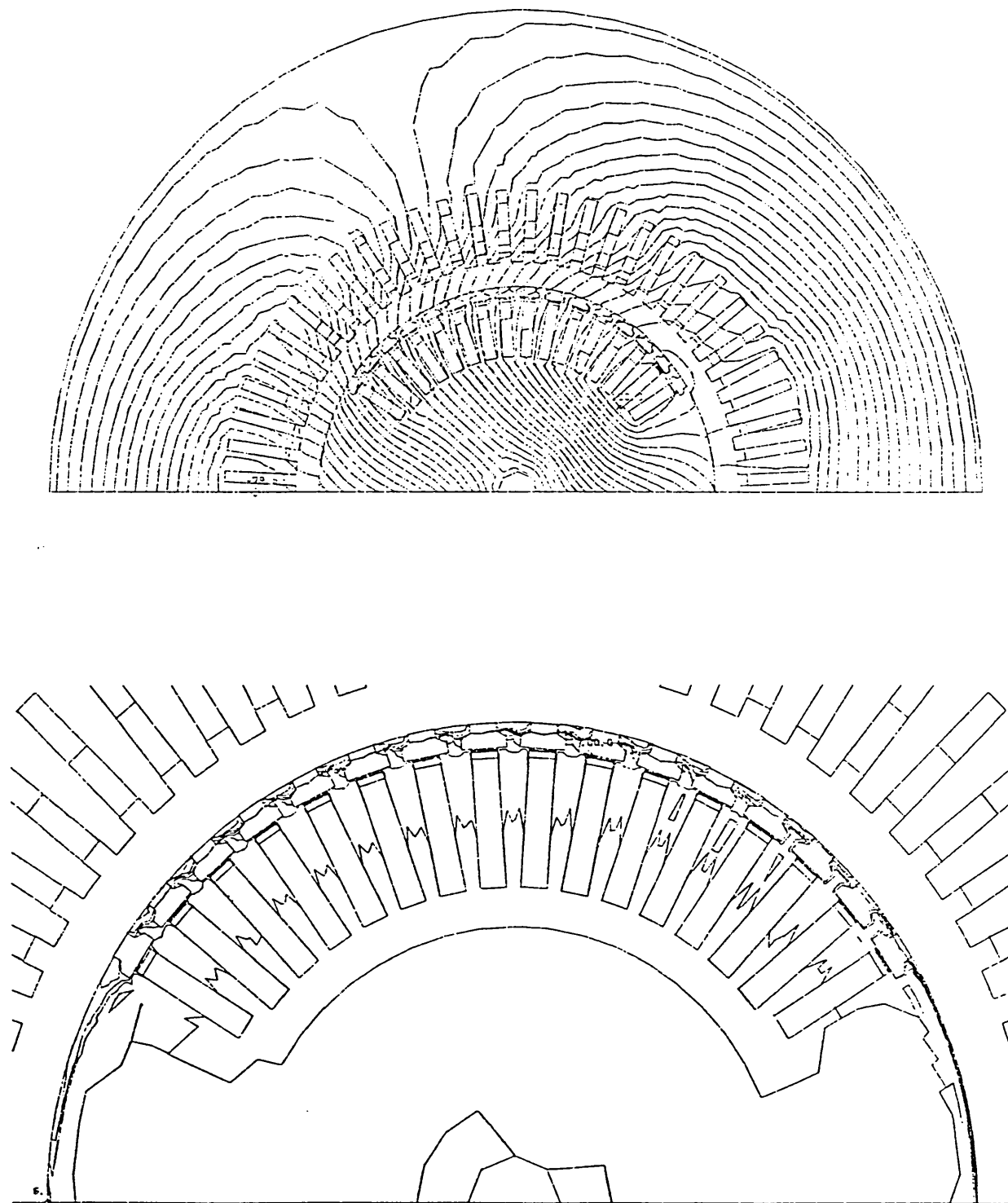


Figure 6.12 time = 2 ms current density contours at 5% of $1.05 \times 10^8 \text{ A/m}^2$

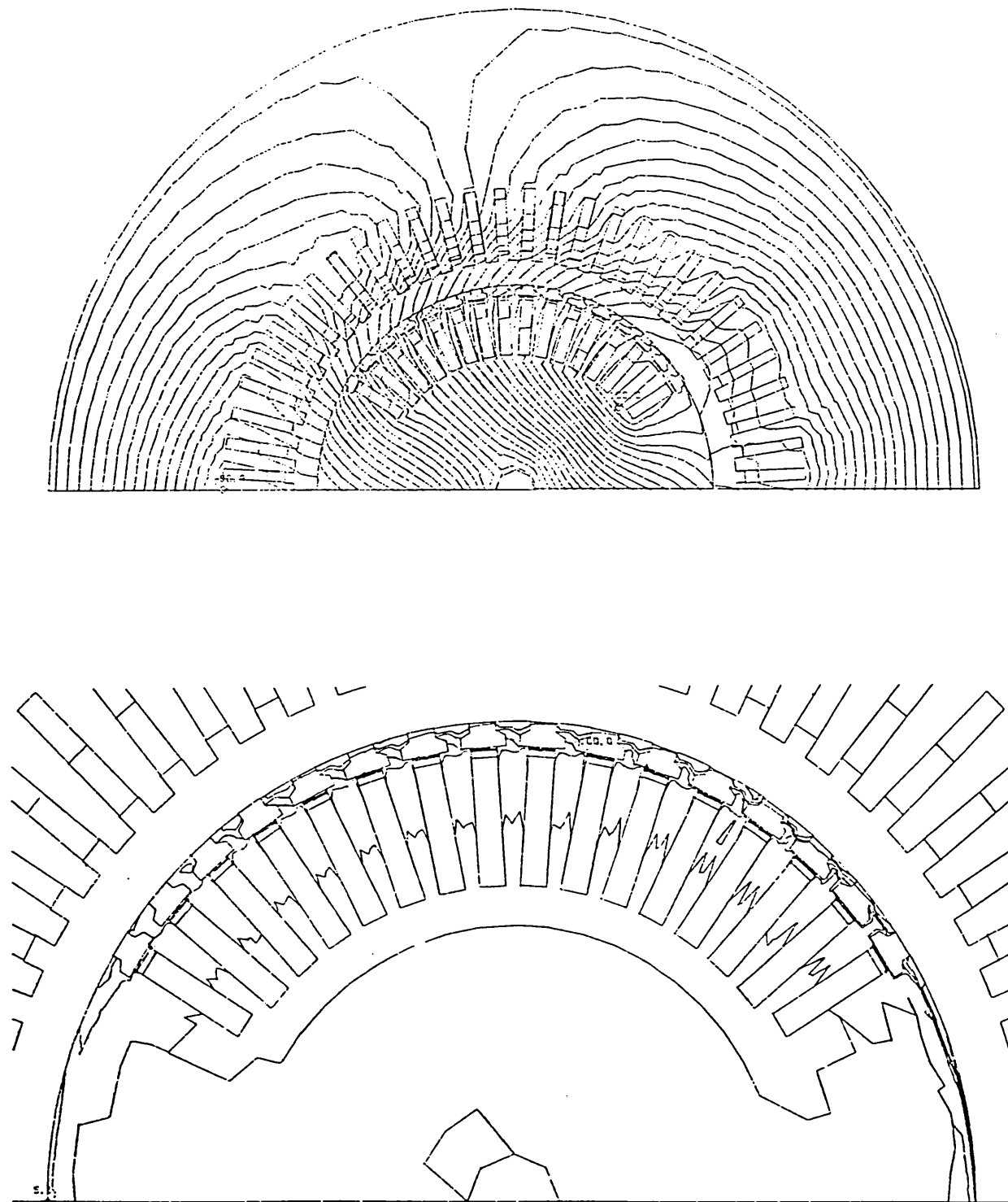


Figure 6.13 time = 3 ms current density contours at 5% of $1.77 \times 10^8 \text{ A/m}^2$

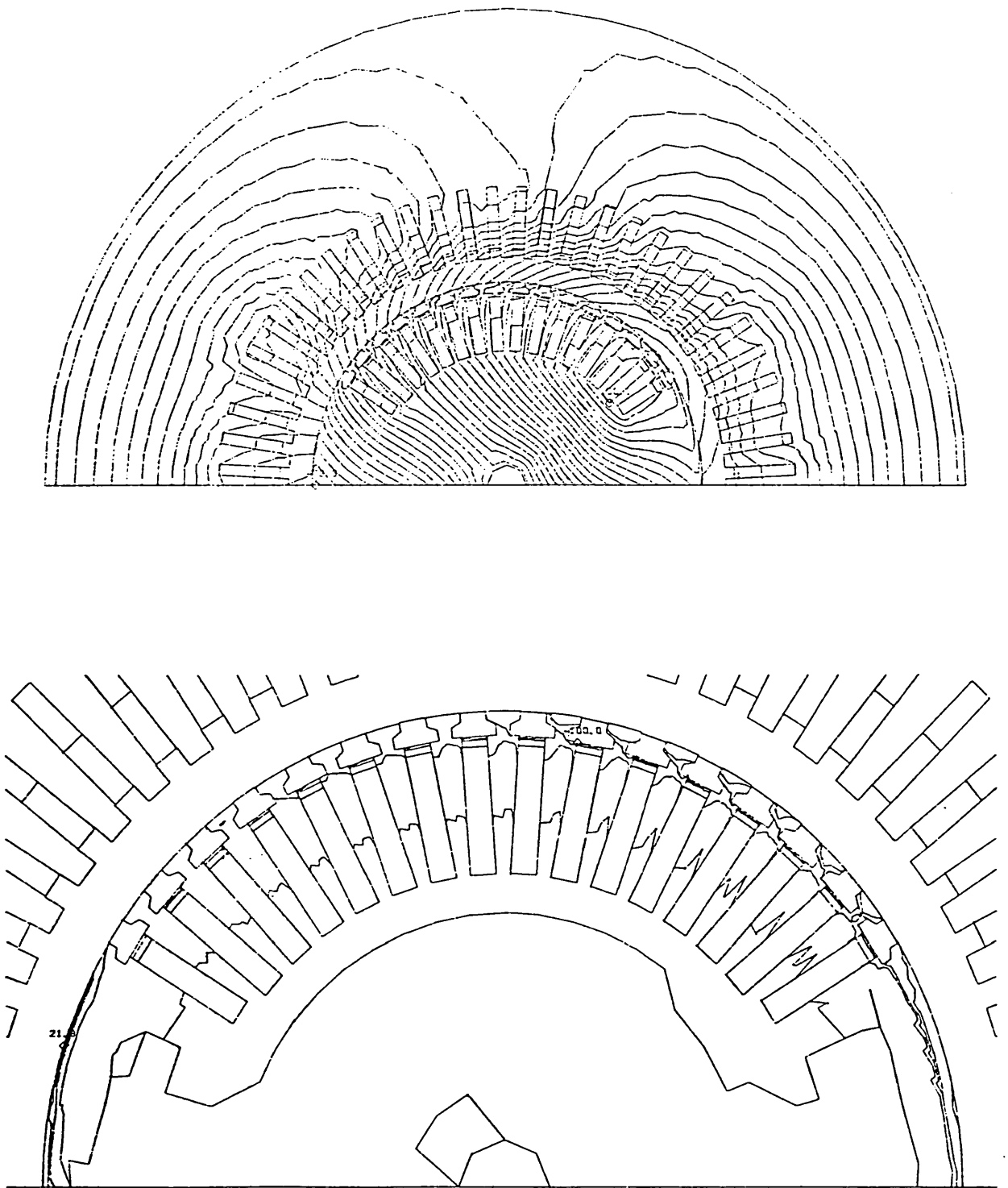


Figure 6.14 time = 5 ms current density contours at 5% of $3.63 \times 10^8 \text{ A/m}^2$

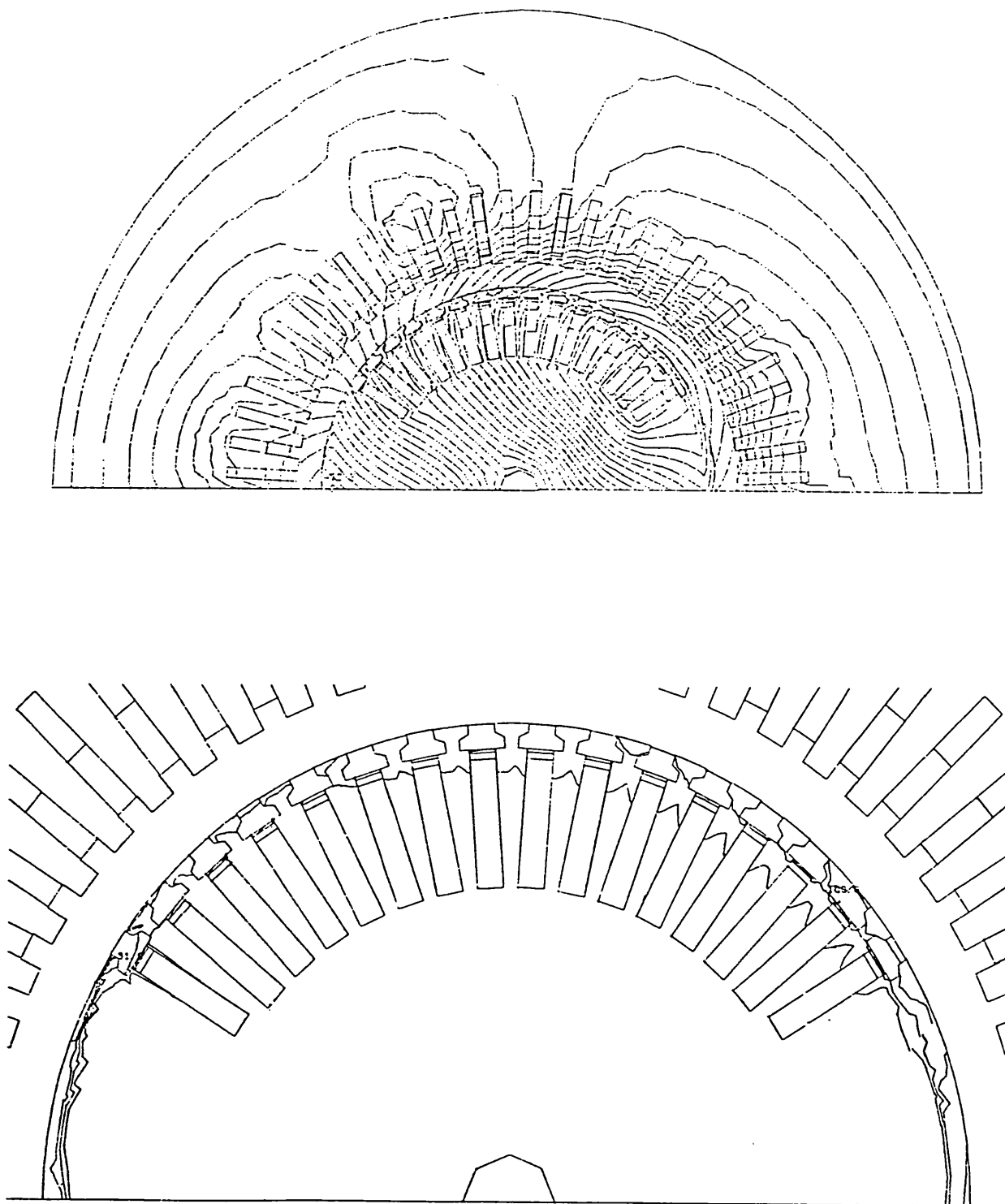


Figure 6.15 time = 7 ms current density contours at 5% of $3.50 \times 10^8 \text{ A/m}^2$

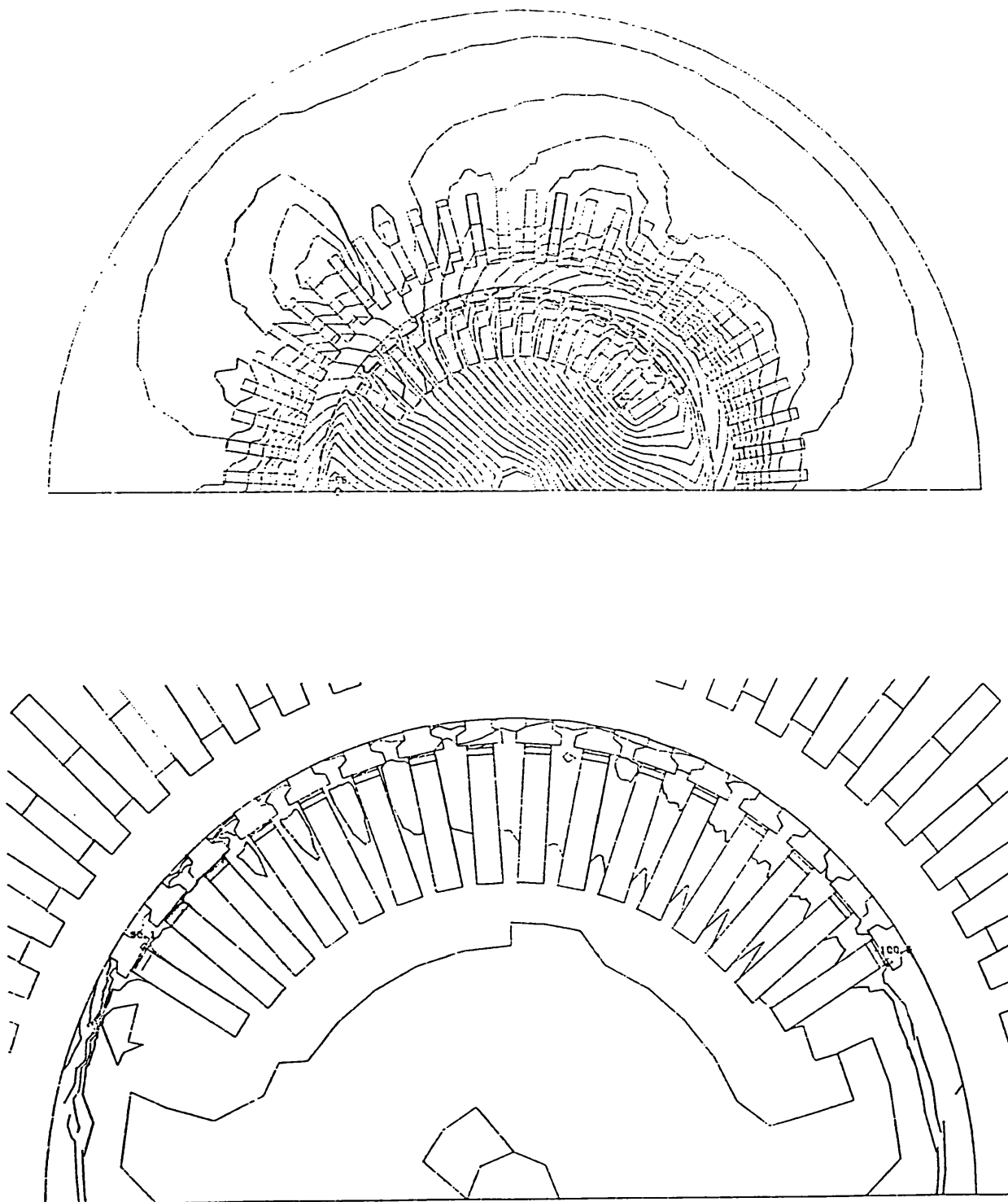


Figure 6.16 time = 10 ms current density contours at 5% of $3.33 \times 10^8 \text{ A/m}^2$

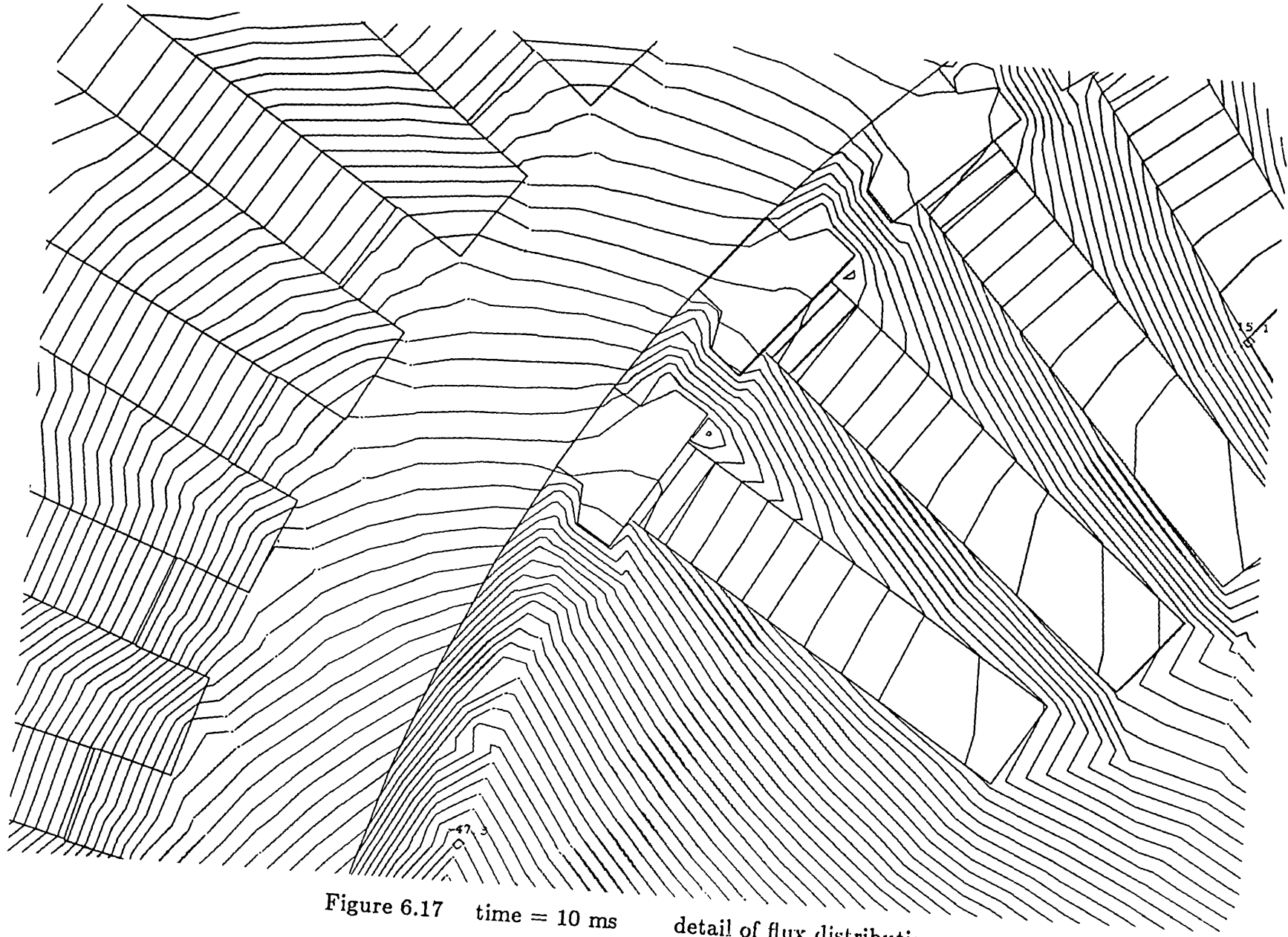


Figure 6.17 time = 10 ms detail of flux distribution

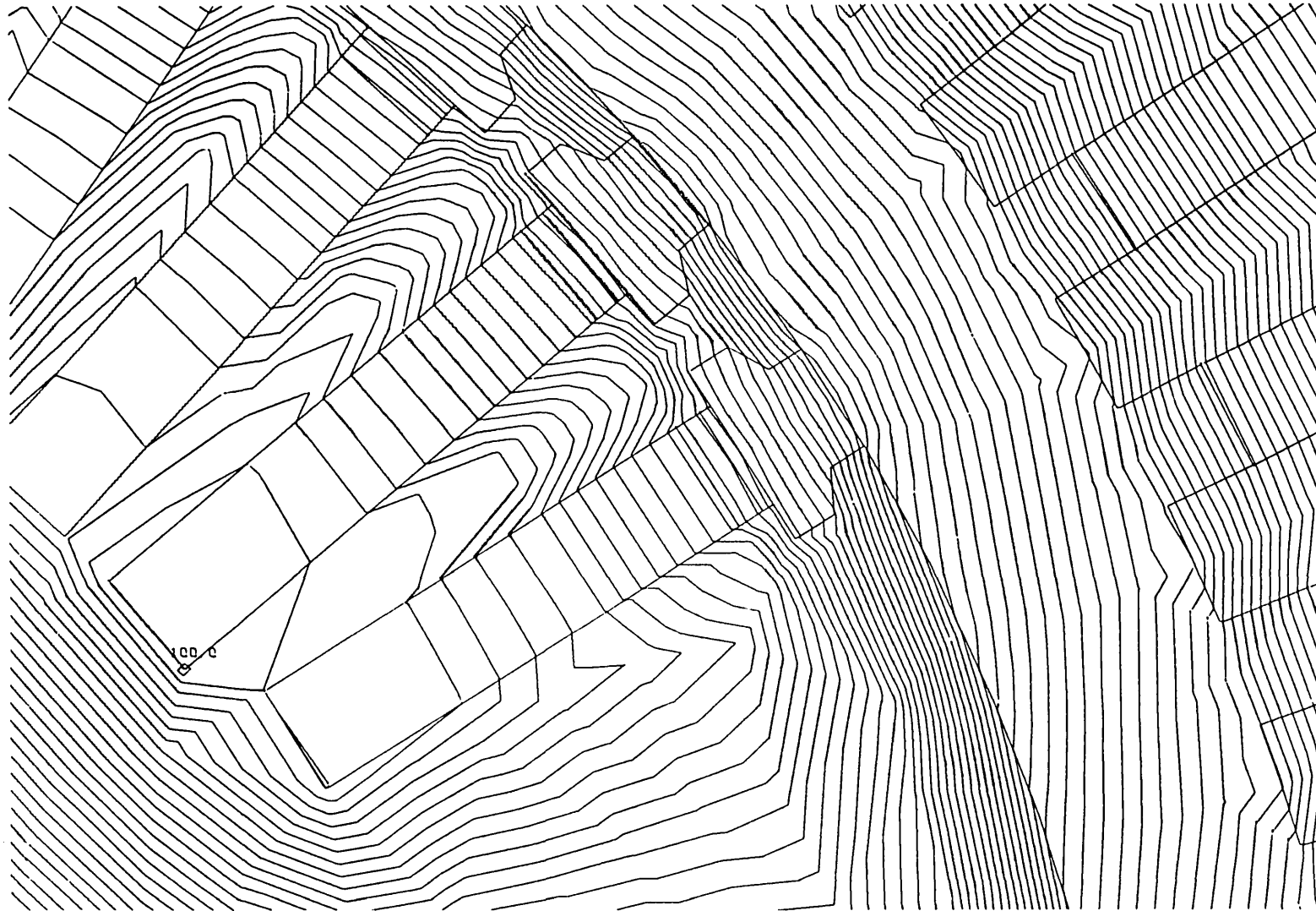


Figure 6.18 time = 10 ms detail of flux distribution

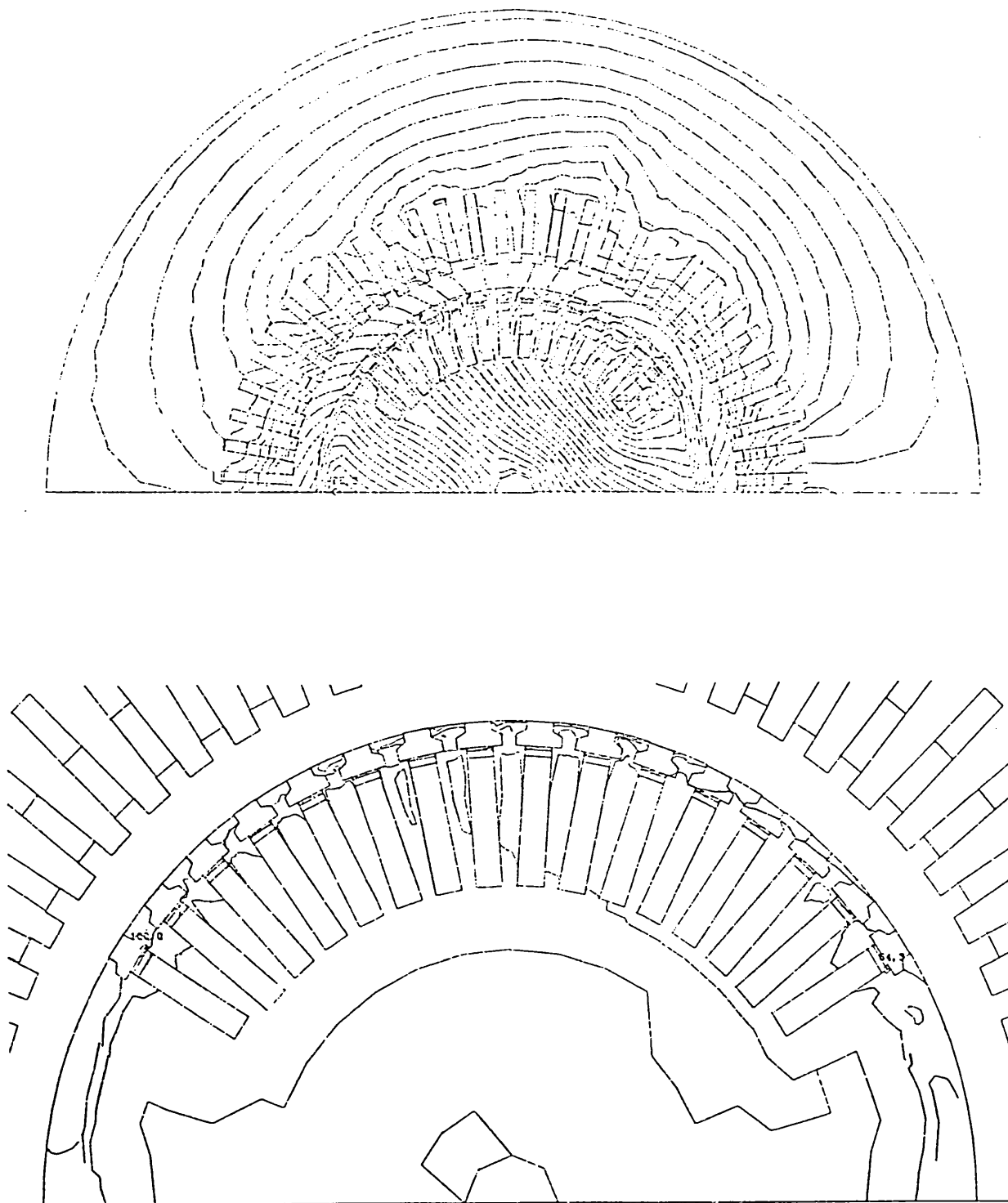


Figure 6.19 time = 13 ms current density contours at 5% of $3.44 \times 10^8 \text{ A/m}^2$

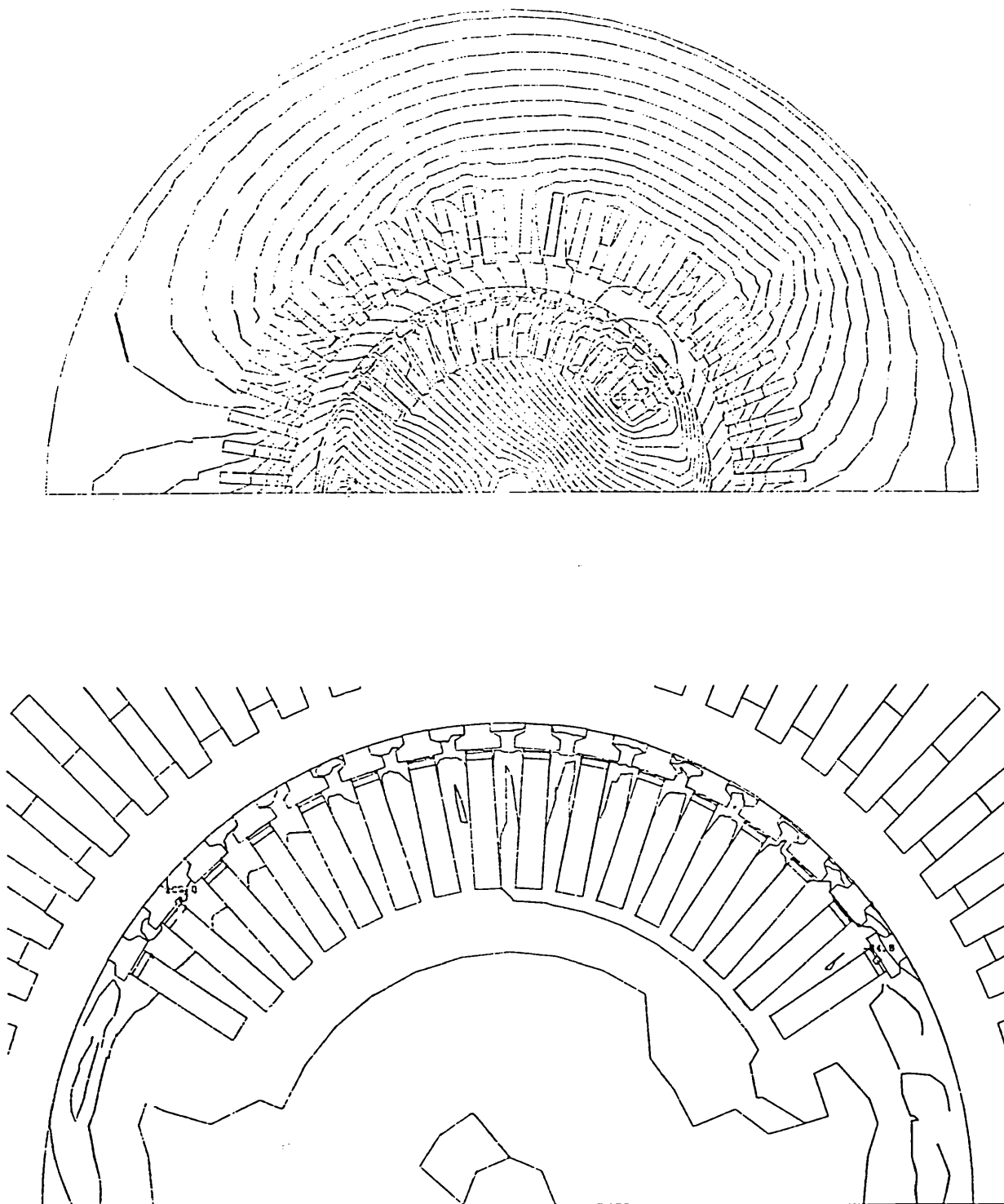


Figure 6.20 time = 15 ms current density contours at 5% of $3.23 \times 10^8 \text{ A/m}^2$

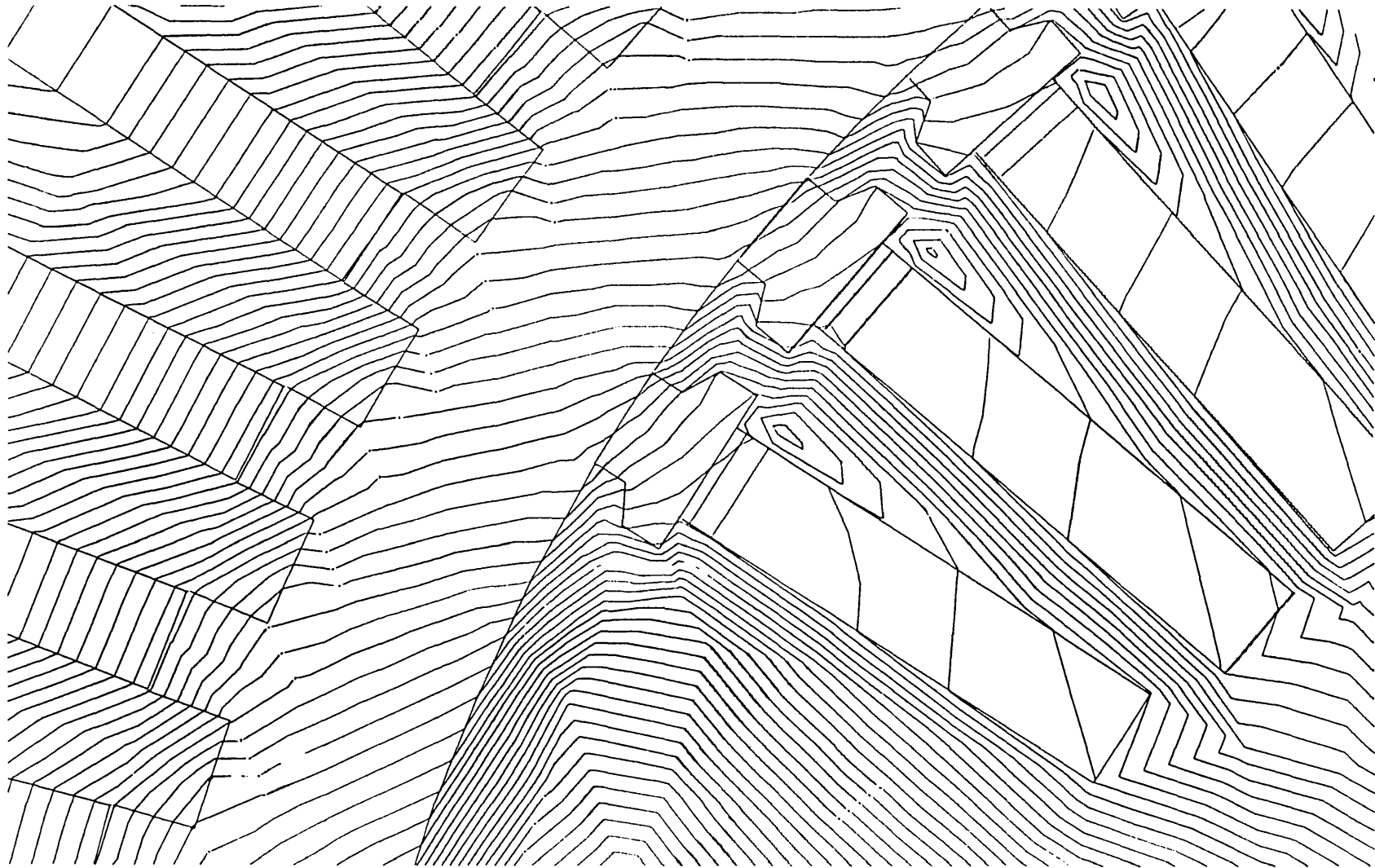


Figure 6.21 time = 15 ms detail of flux distribution

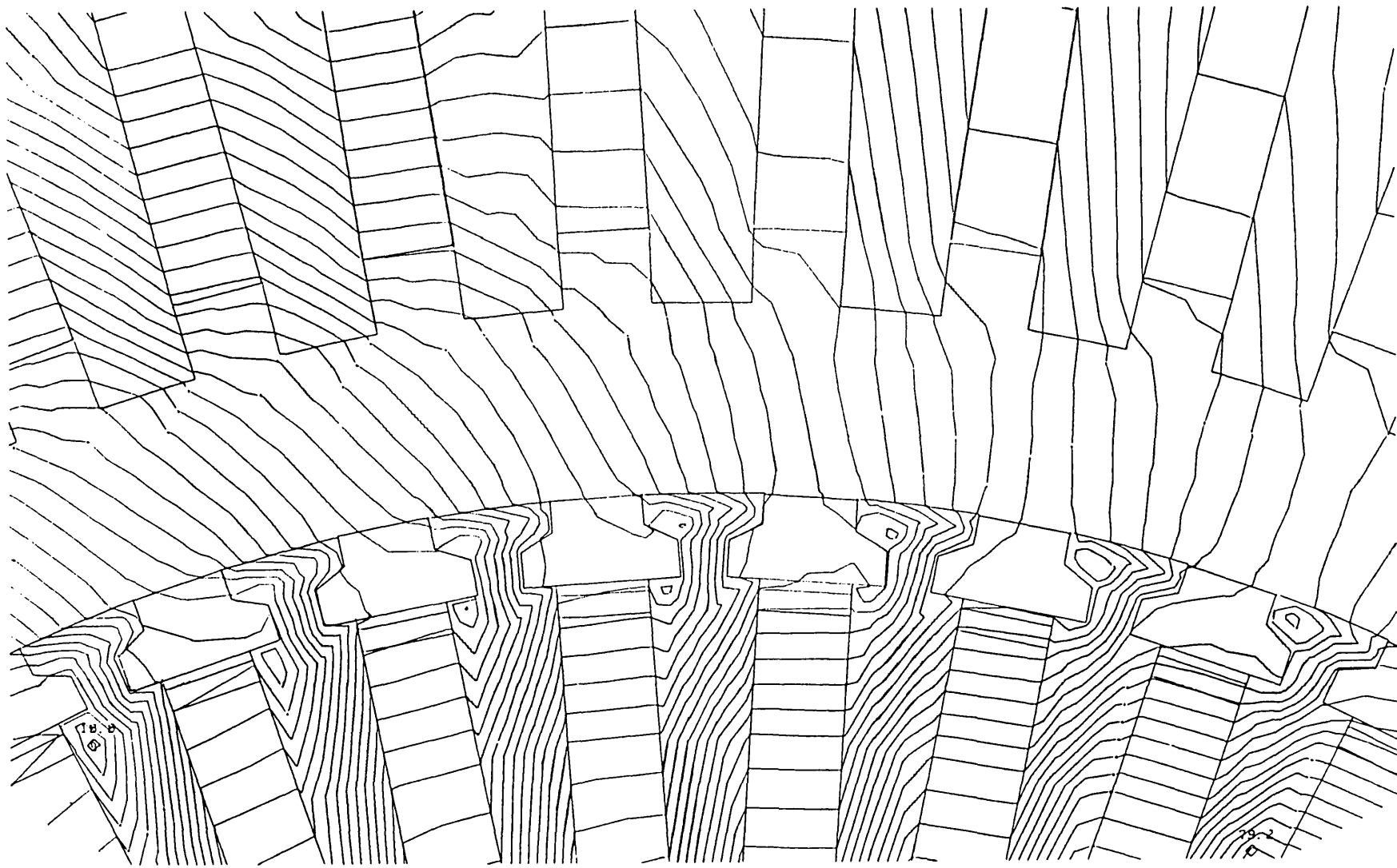


Figure 6.22 time = 15 ms detail of flux distribution

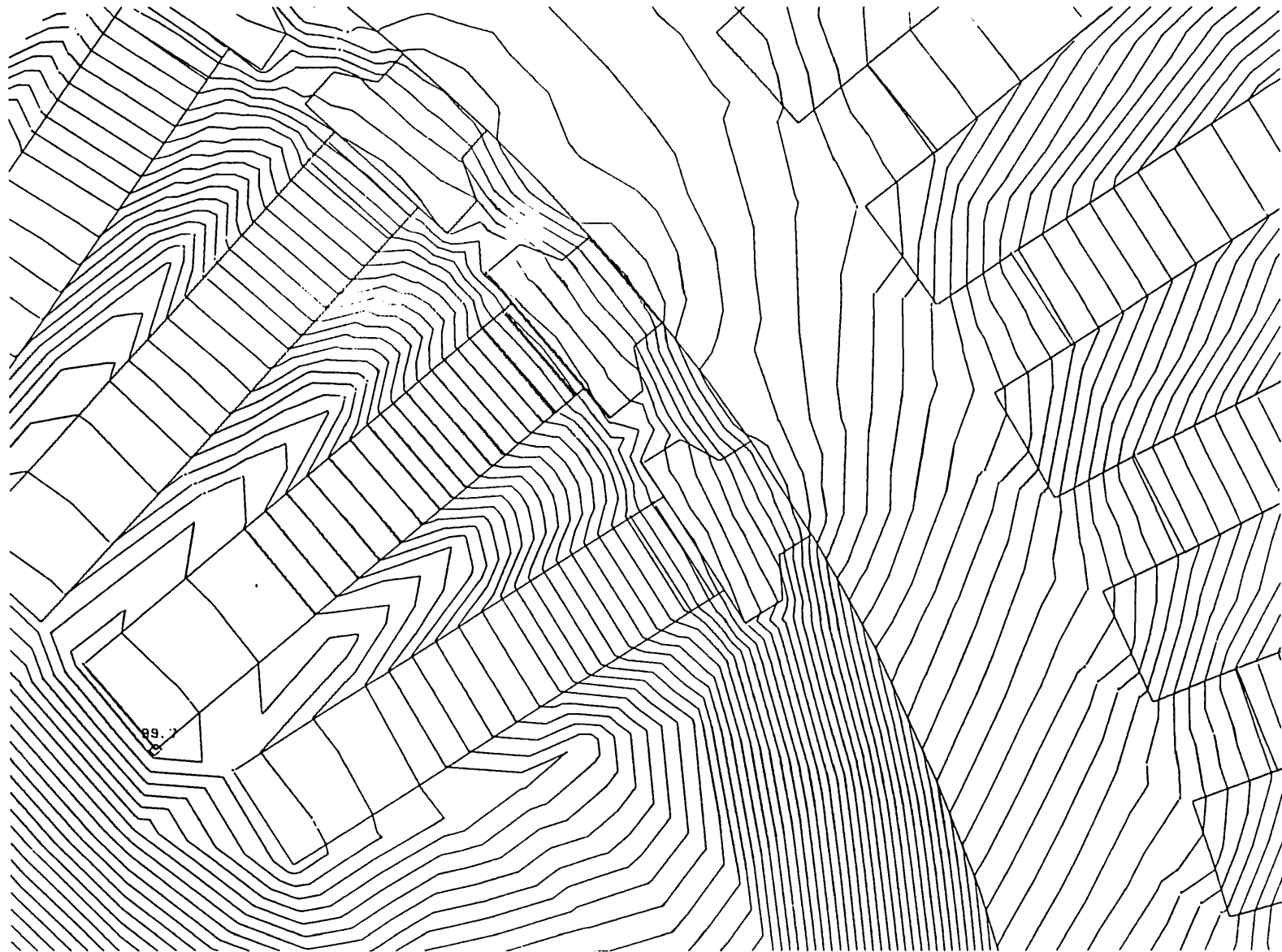


Figure 6.23 time = 15 ms detail of flux distribution

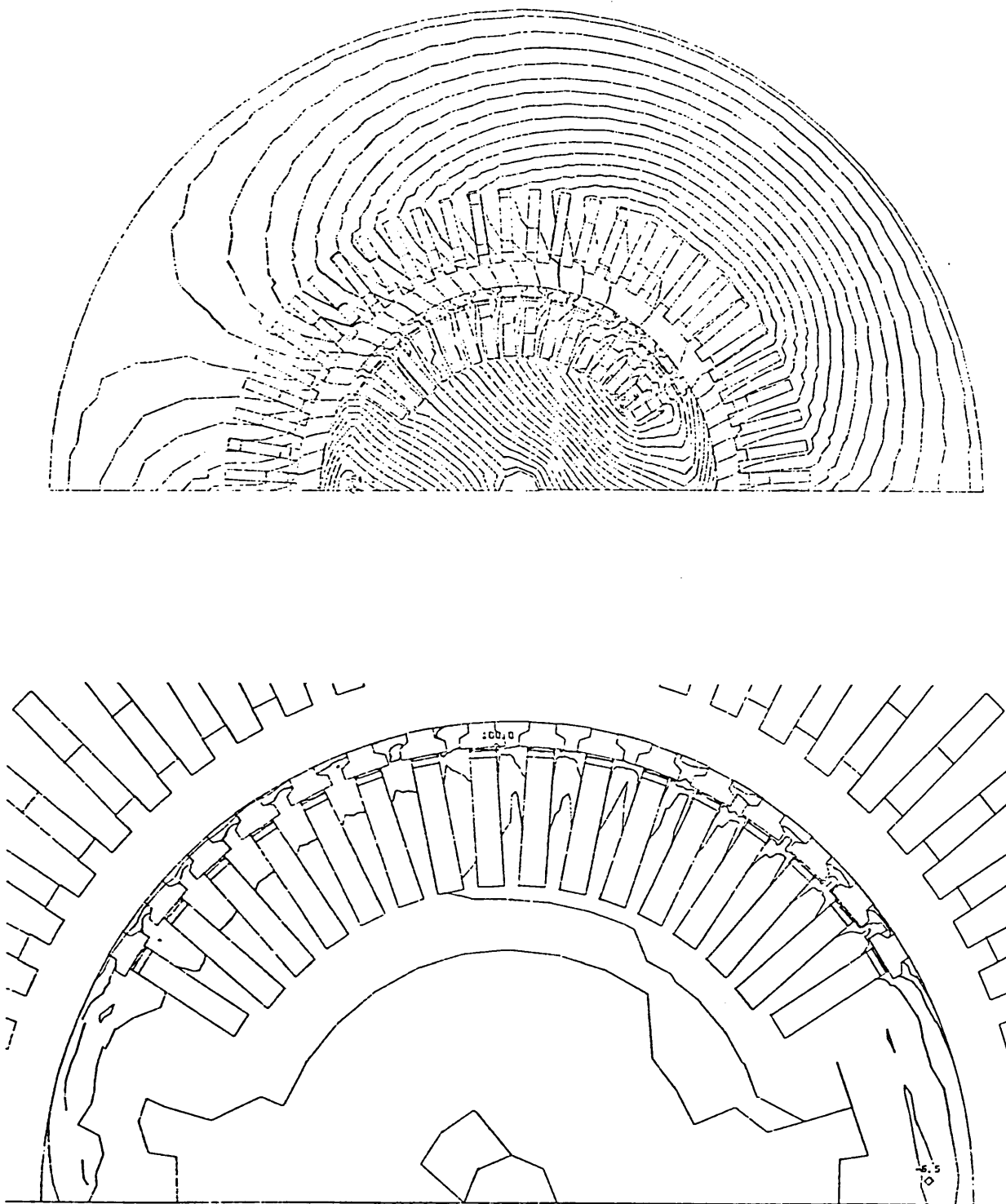


Figure 6.24 time = 17 ms current density contours at 5% of $2.23 \times 10^8 \text{ A/m}^2$

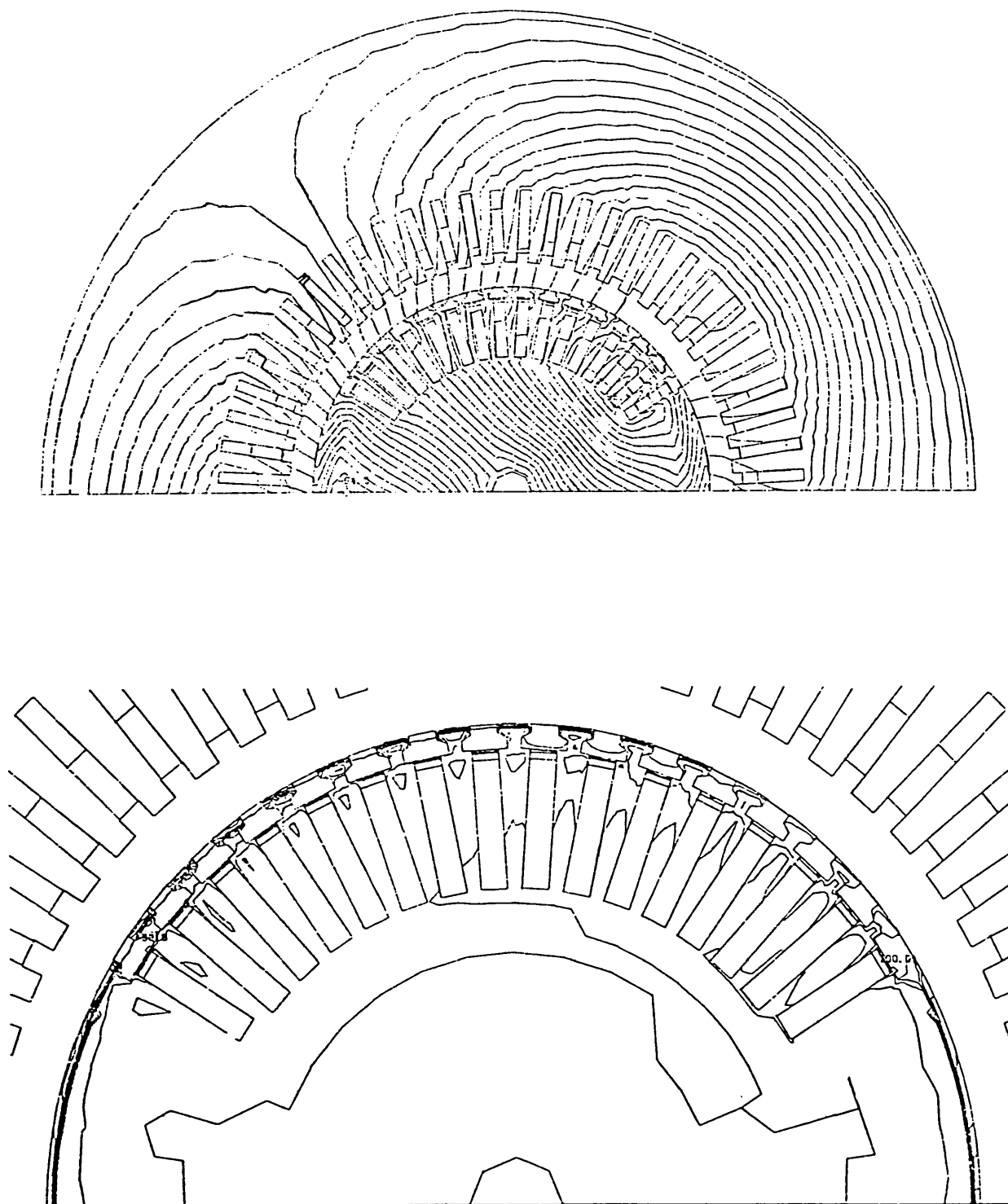


Figure 6.25 time = 20 ms current density contours at 5% of $1.63 \times 10^8 \text{ A/m}^2$

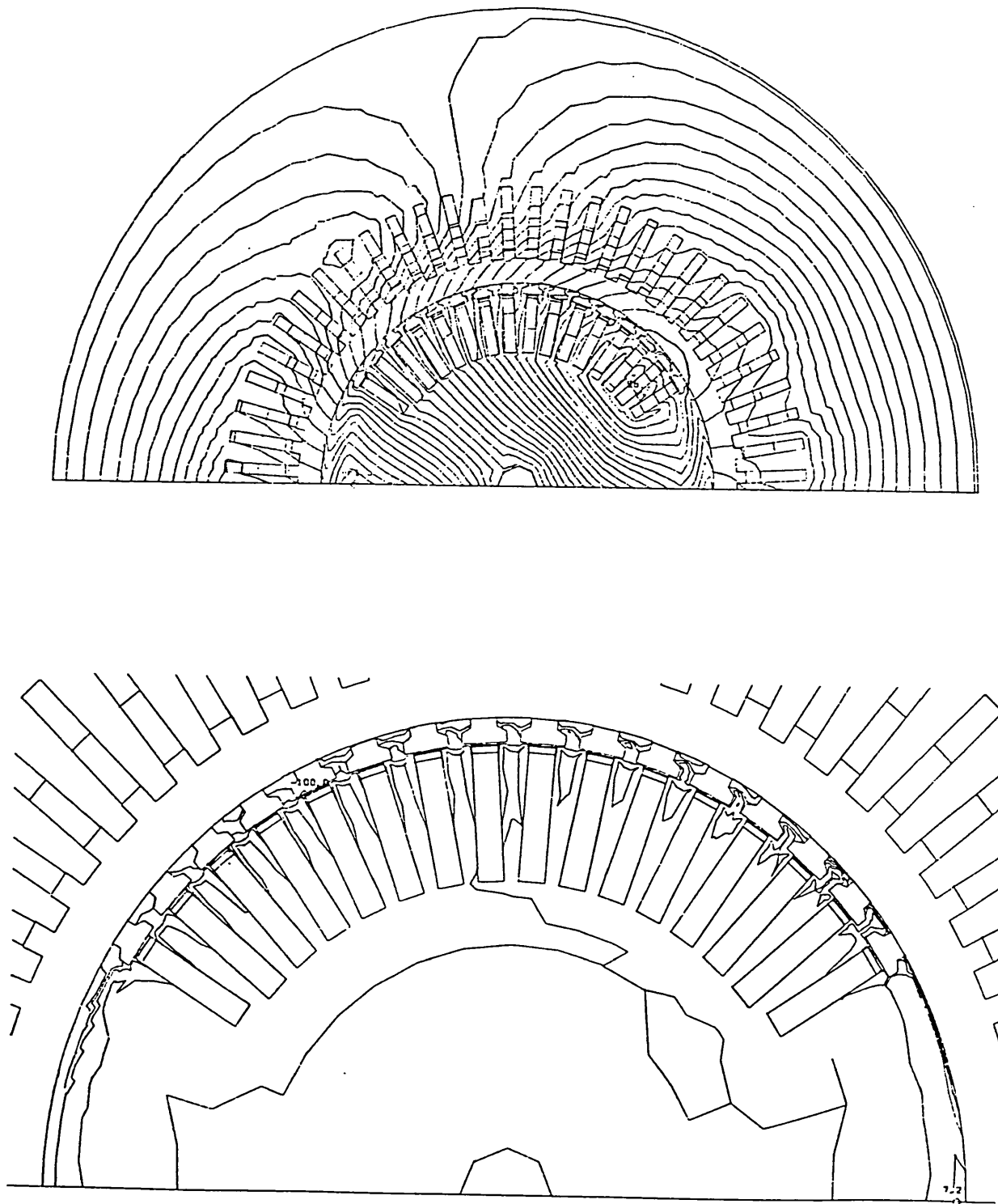


Figure 6.26 time = 23 ms current density contours at 5% of $2.10 \times 10^8 A/m^2$

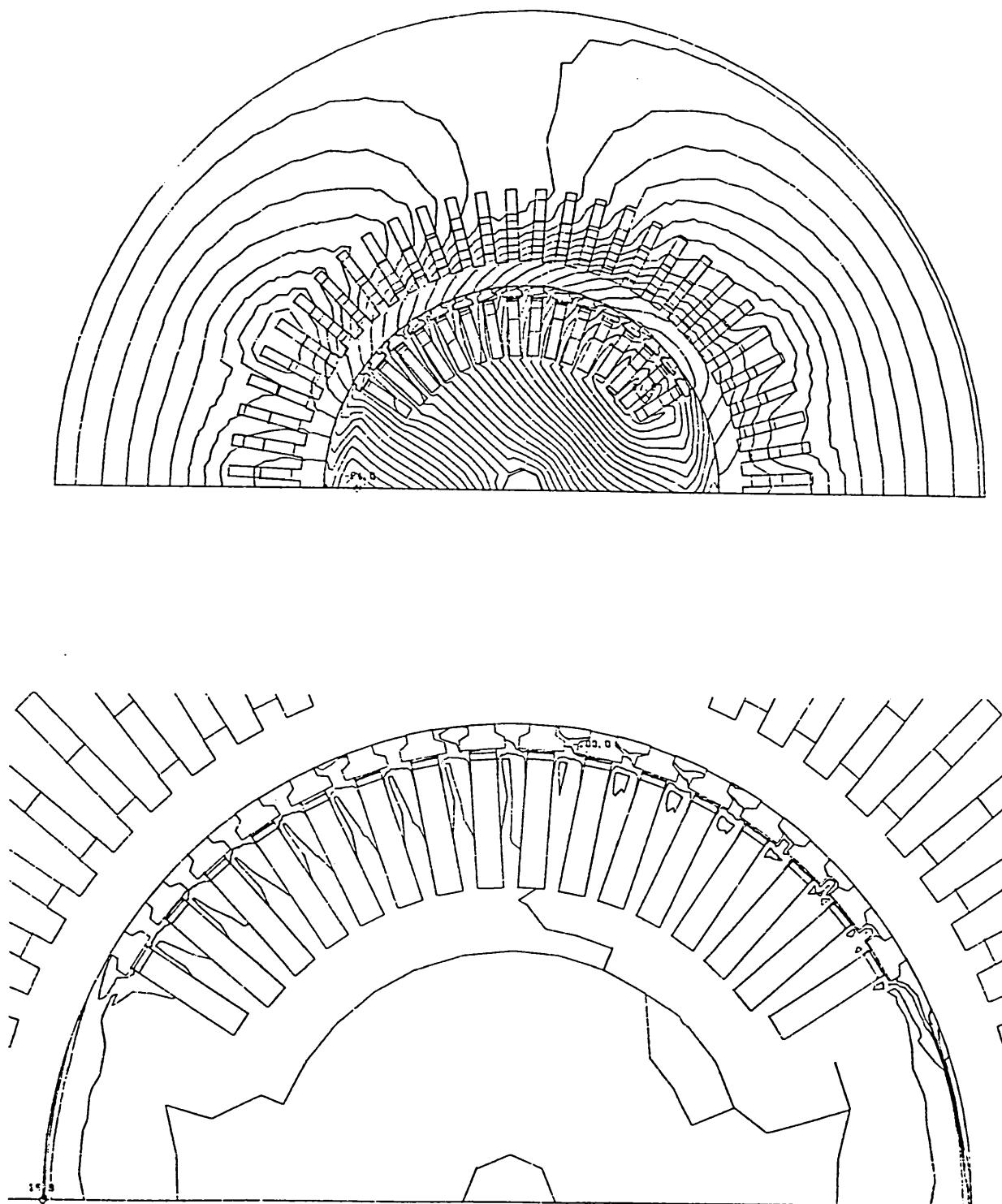


Figure 6.27 time = 25 ms current density contours at 5% of $2.67 \times 10^8 \text{ A/m}^2$

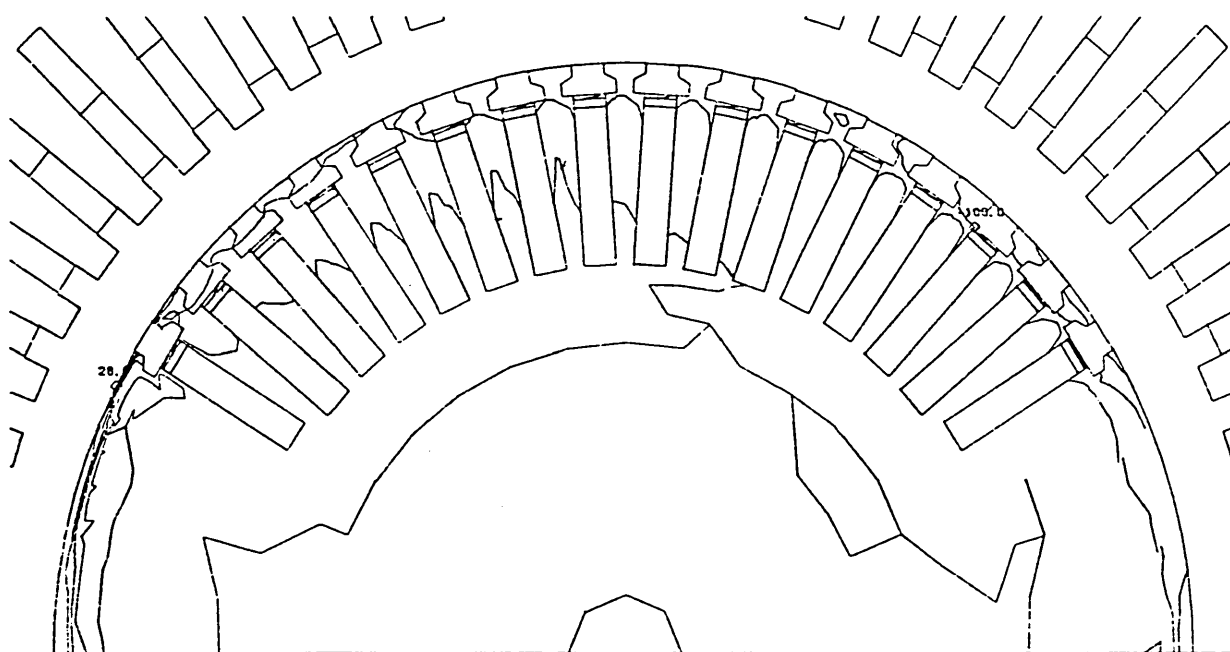
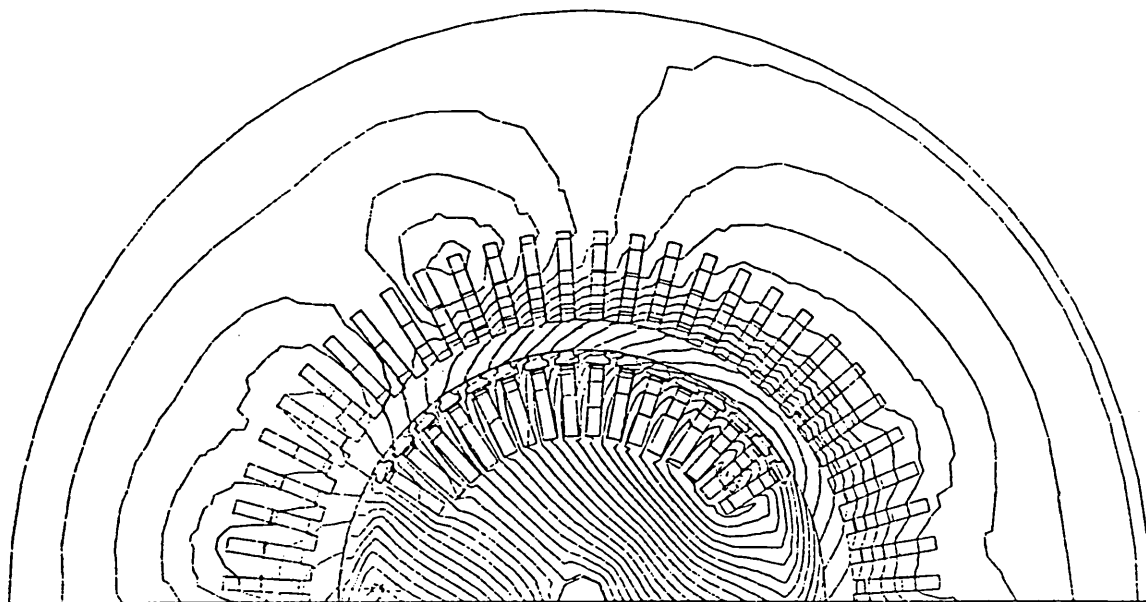


Figure 6.28 time = 27 ms current density contours at 5% of $3.06 \times 10^8 A/m^2$

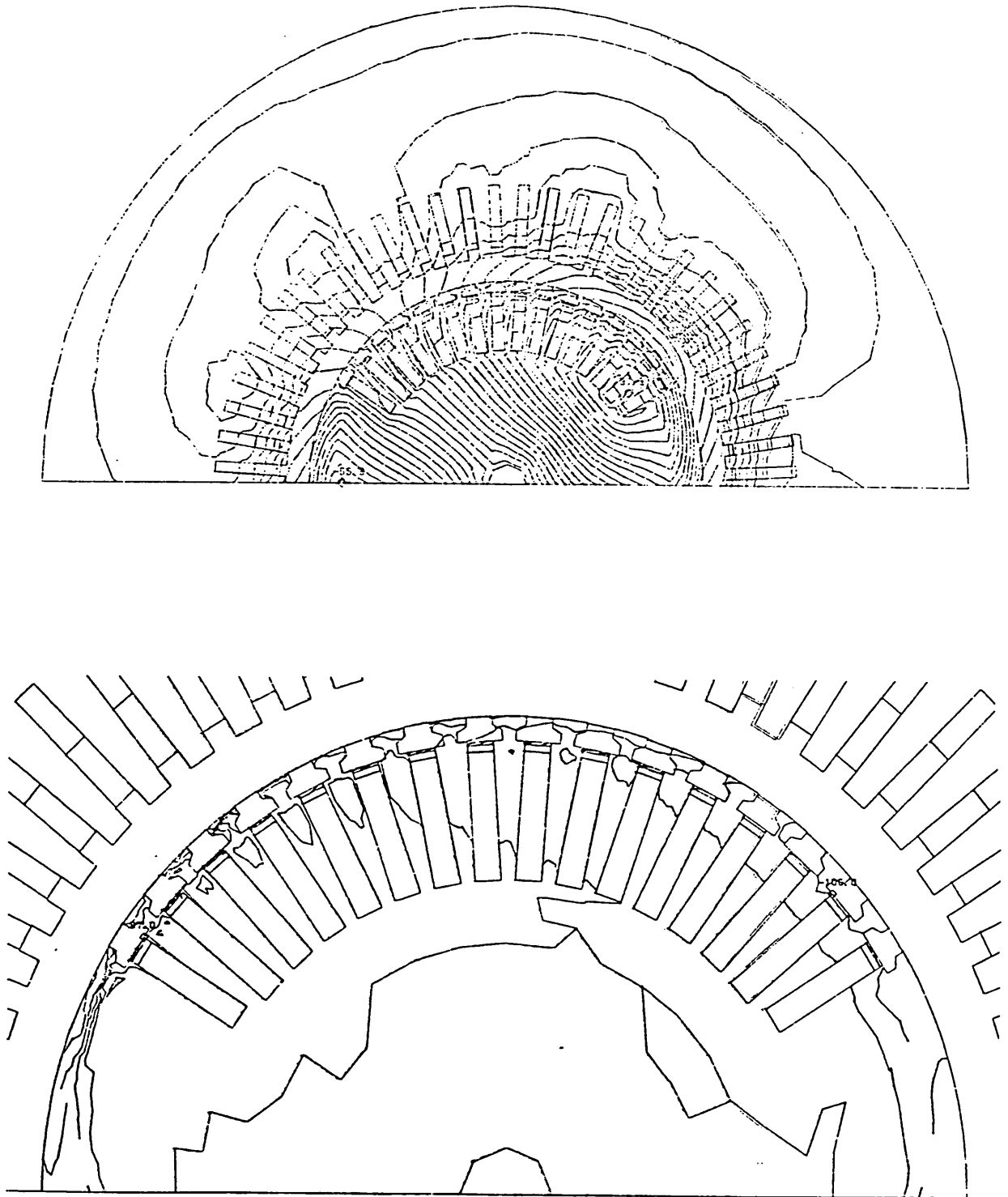


Figure 6.29 time = 30 ms current density contours at 5% of $2.62 \times 10^8 \text{ A/m}^2$

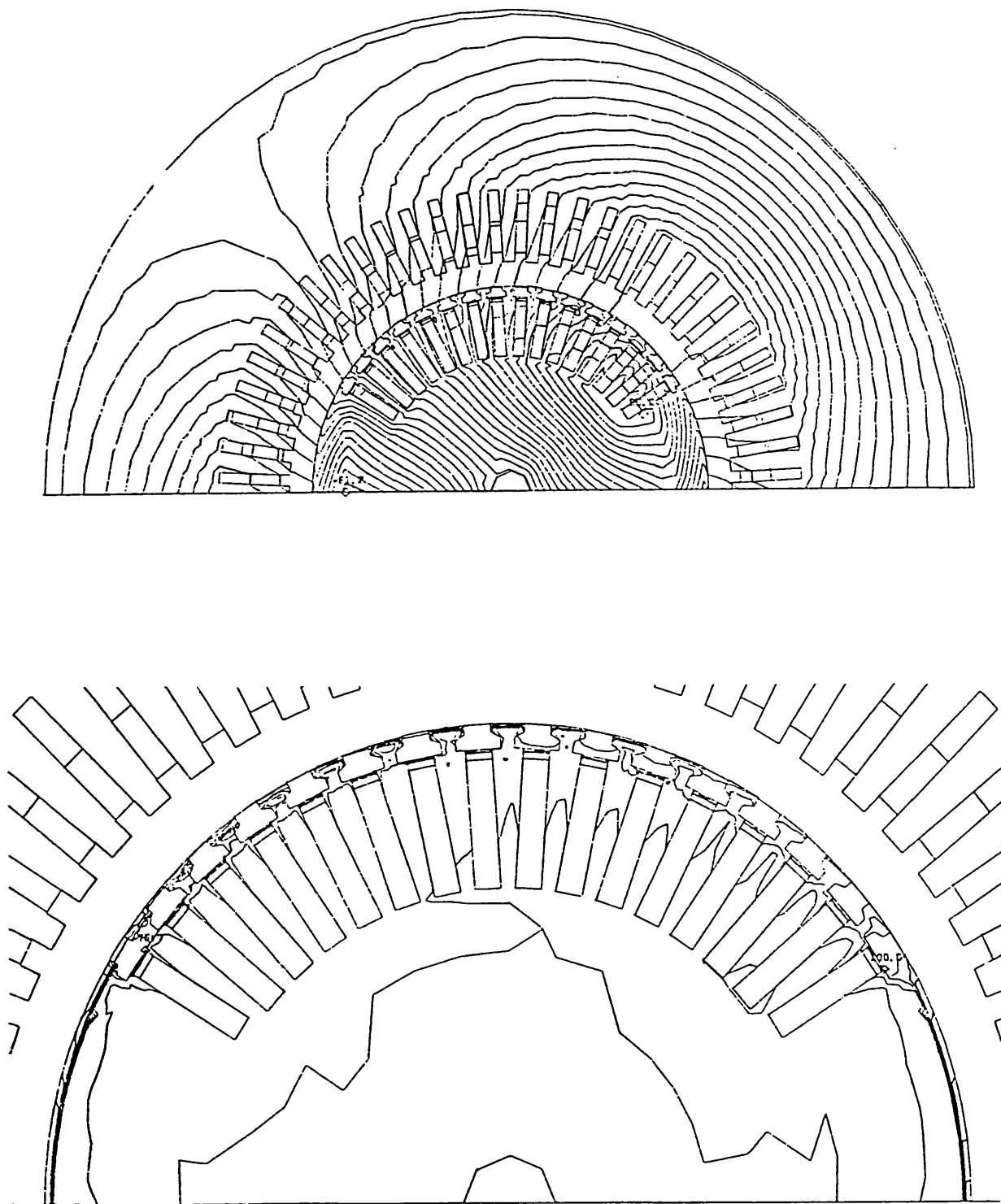


Figure 6.30 time = 40 ms current density contours at 5% of $1.30 \times 10^8 \text{ A/m}^2$

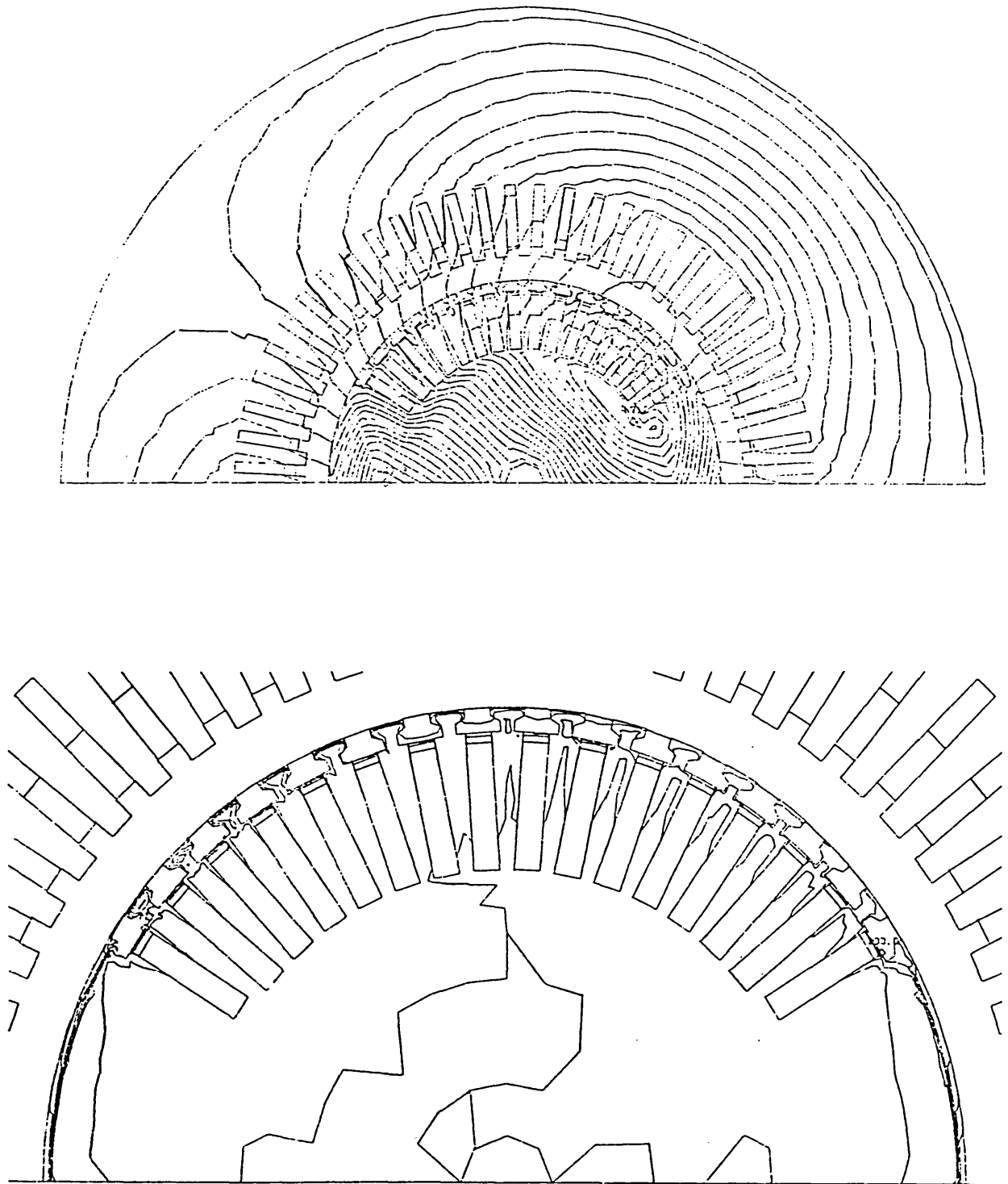


Figure 6.31 time = 139 ms - just prior to fault clearance
current density contours at 5% of $1.07 \times 10^8 \text{ A/m}^2$

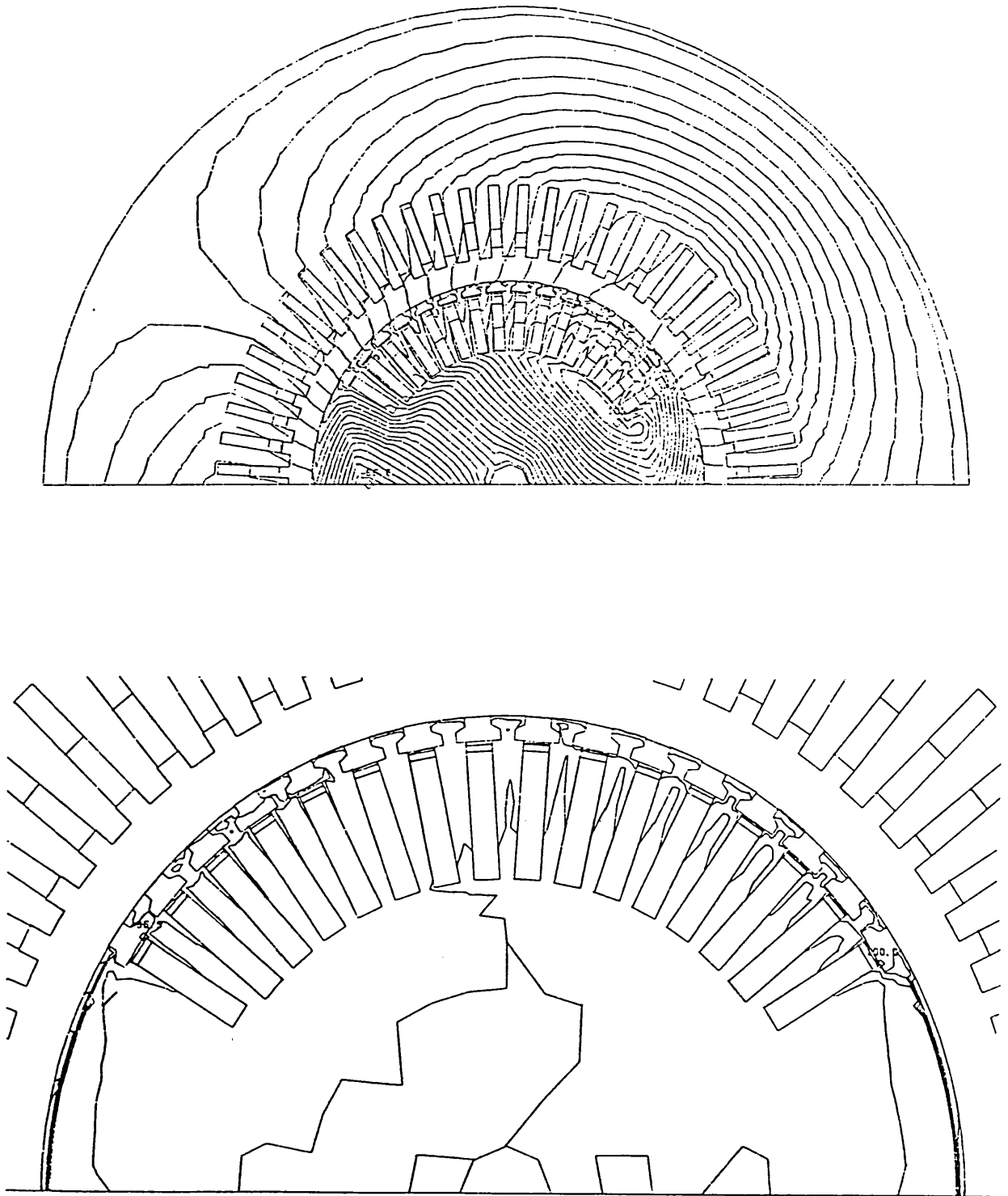


Figure 6.32 time = 140 ms - reclosure + 1 ms current density contours at
5% of $1.07 \times 10^8 \text{ A/m}^2$

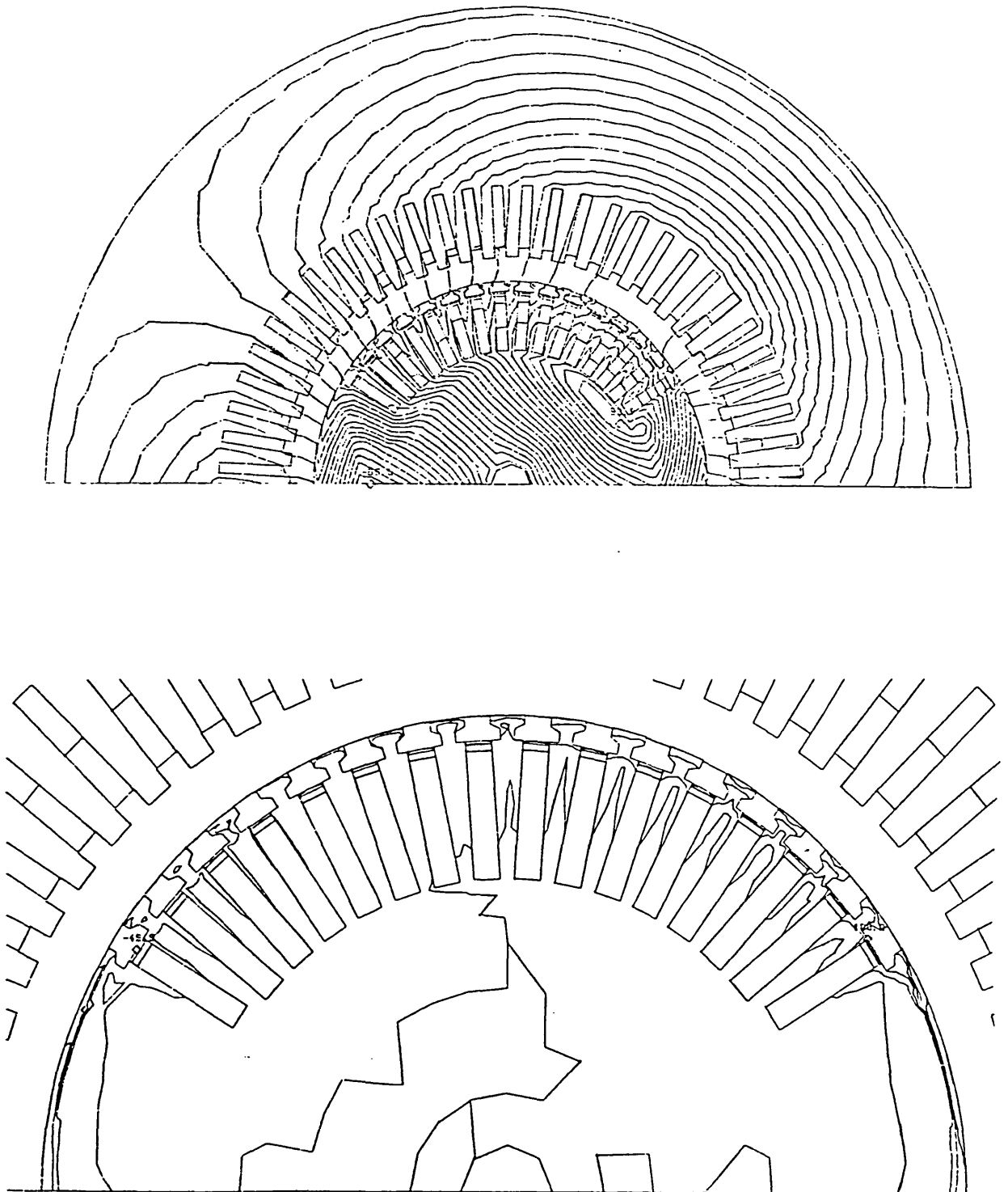


Figure 6.33 time = 141 ms - reclosure + 2 ms current density contours at
5% of $1.25 \times 10^8 \text{ A/m}^2$

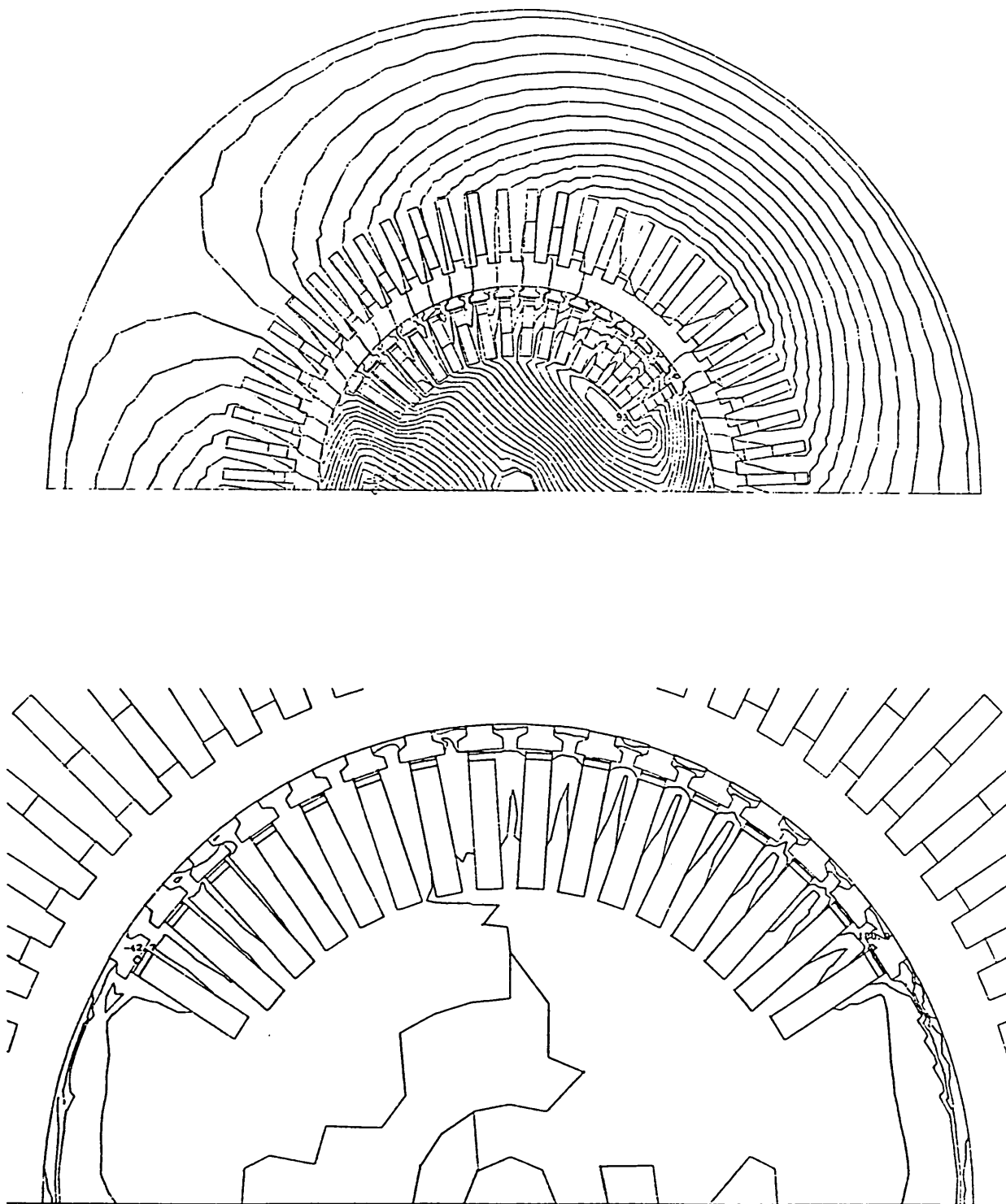


Figure 6.34 time = 142 ms - reclosure + 3 ms current density contours at
5% of $1.34 \times 10^8 \text{ A/m}^2$

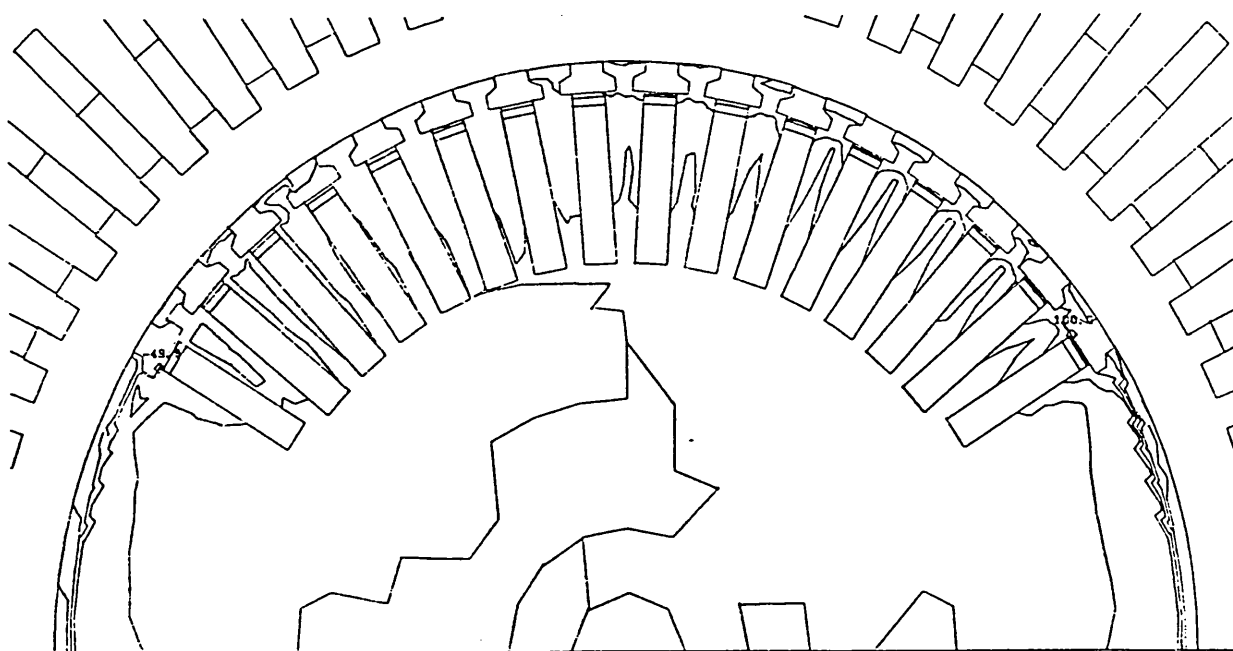
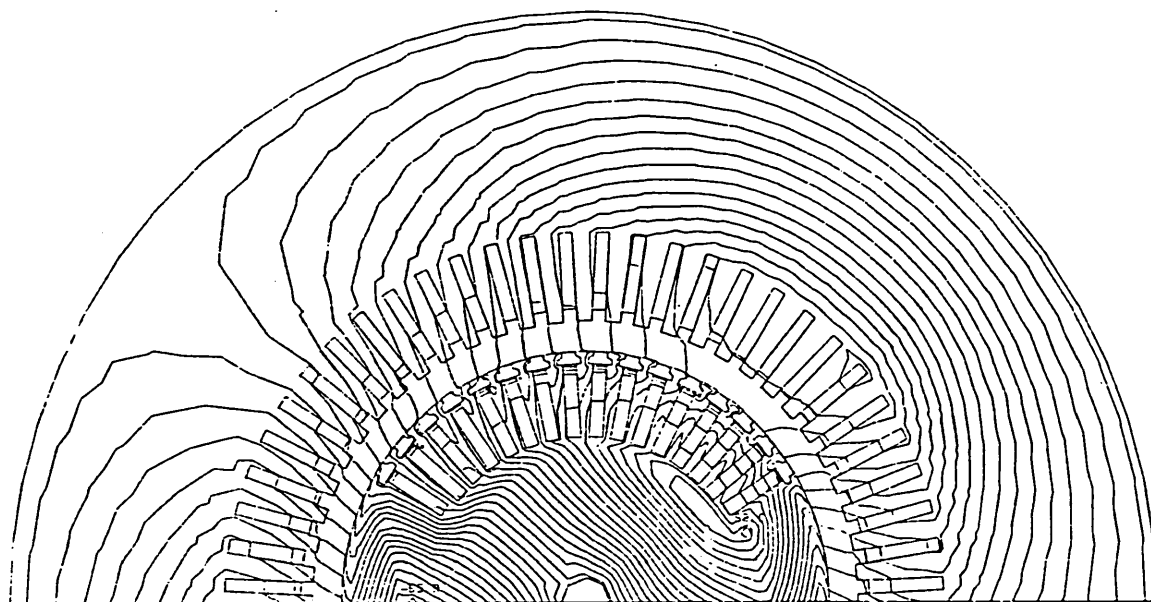


Figure 6.35 time = 144 ms - reclosure + 5 ms current density contours at
5% of $1.51 \times 10^8 A/m^2$

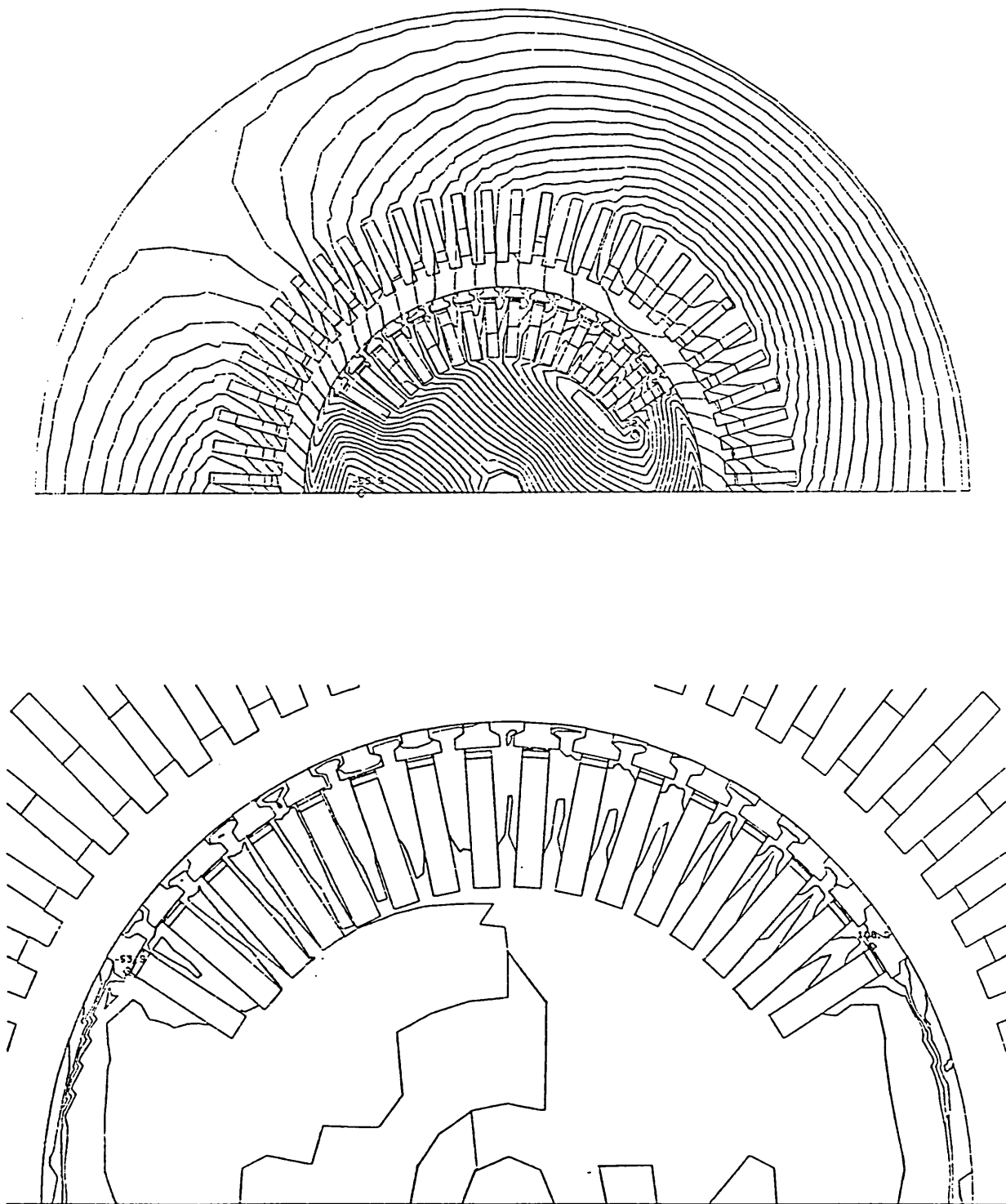


Figure 6.36 time = 146 ms - reclosure + 7 ms current density contours at 5% of $1.57 \times 10^8 A/m^2$

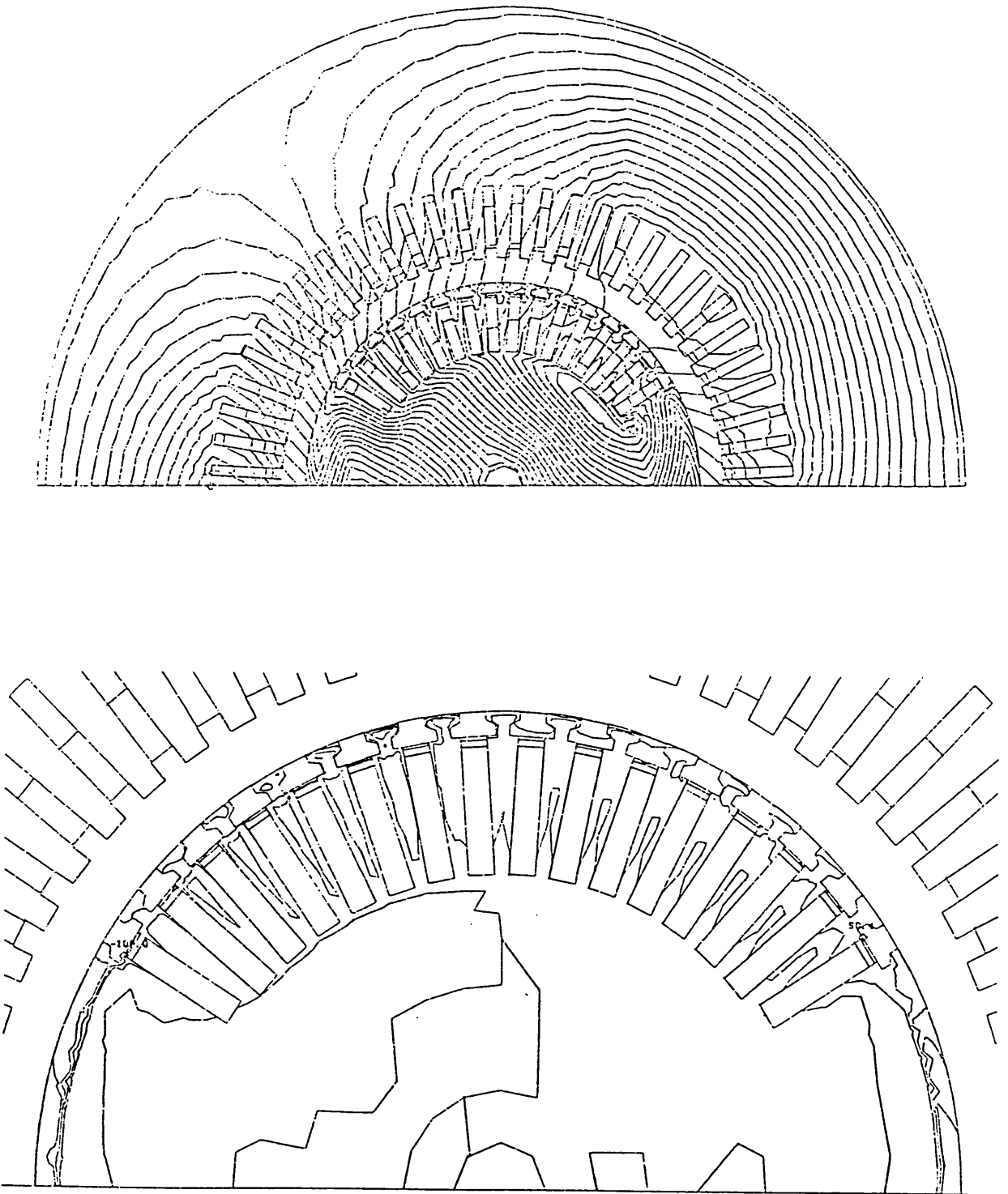


Figure 6.37 time = 149 ms current density contours at 5% of $1.58 \times 10^8 A/m^2$

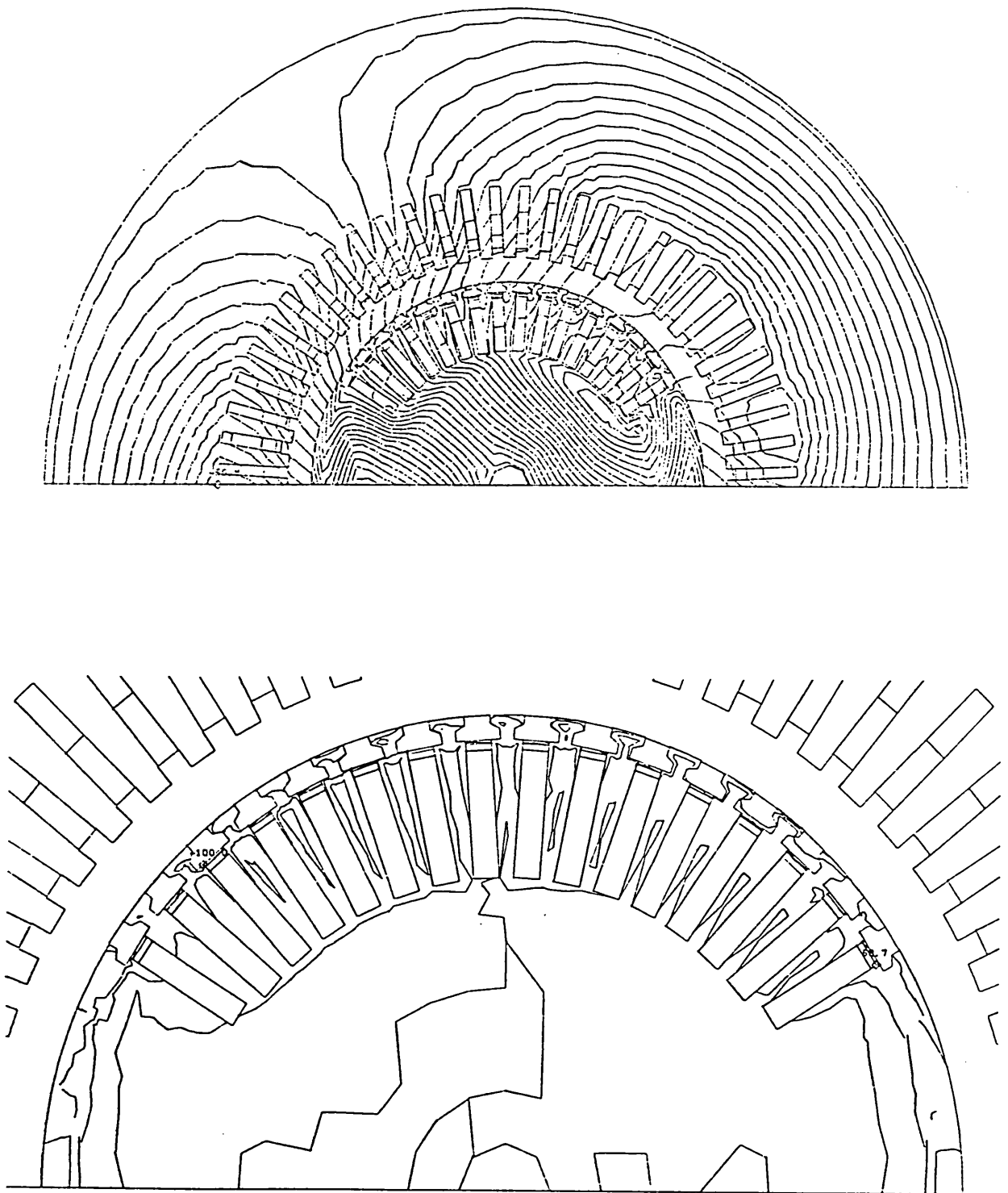


Figure 6.38 time = 152 ms current density contours at 5% of $1.58 \times 10^8 \text{ A/m}^2$

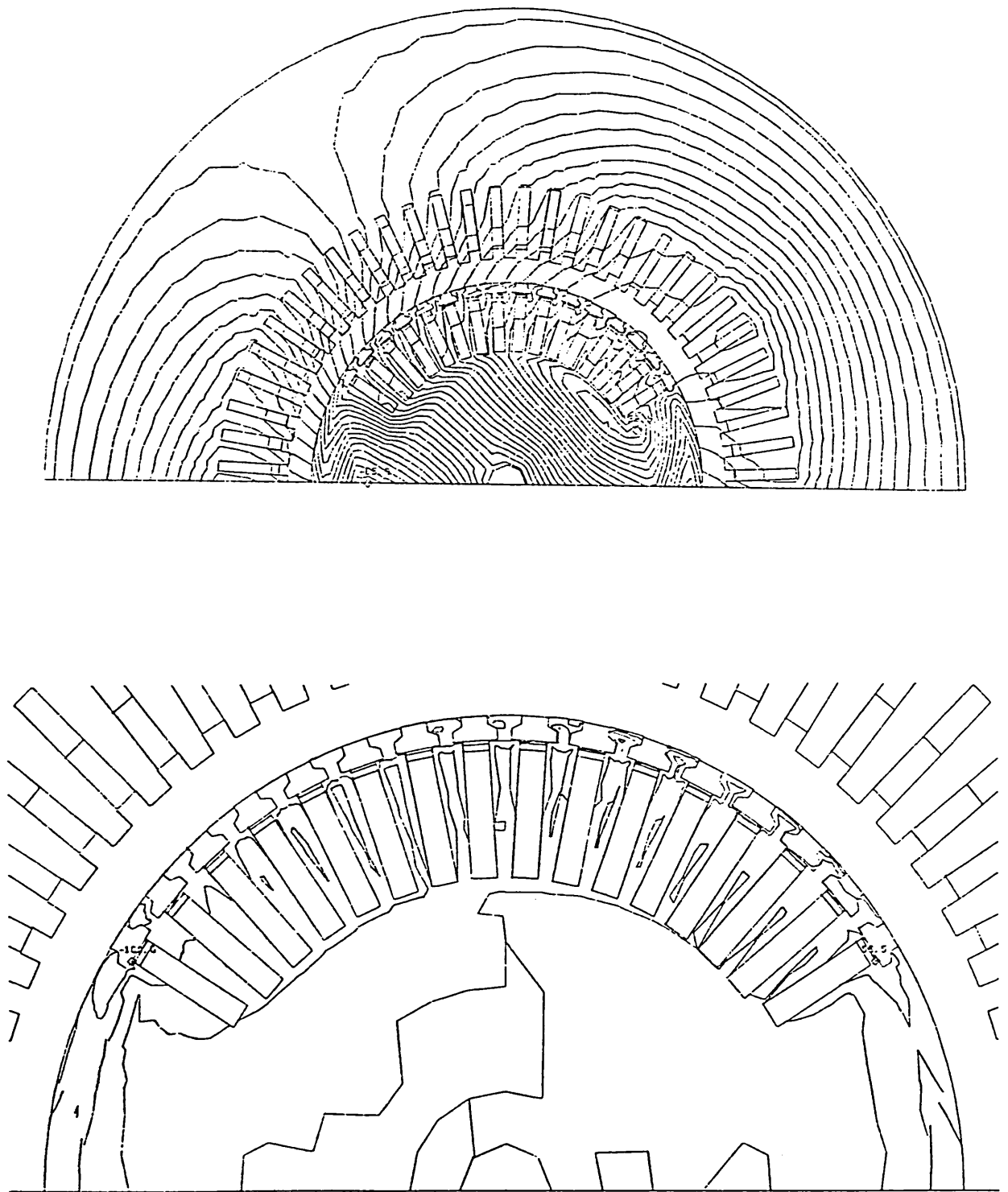


Figure 6.39 time = 154 ms current density contours at 5% of $1.40 \times 10^8 \text{ A/m}^2$

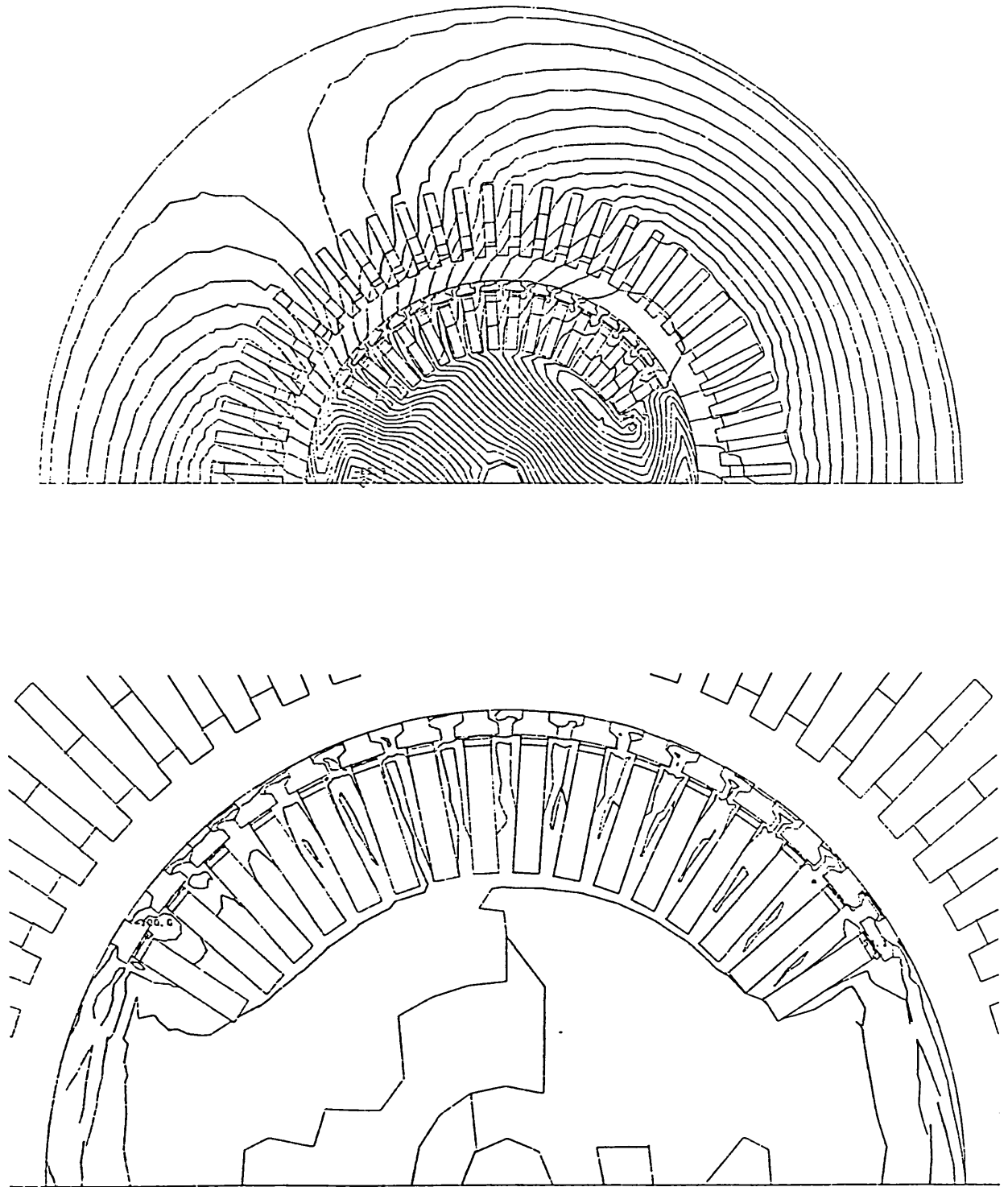


Figure 6.40 time = 156 ms current density contours at 5% of $0.79 \times 10^8 \text{ A/m}^2$

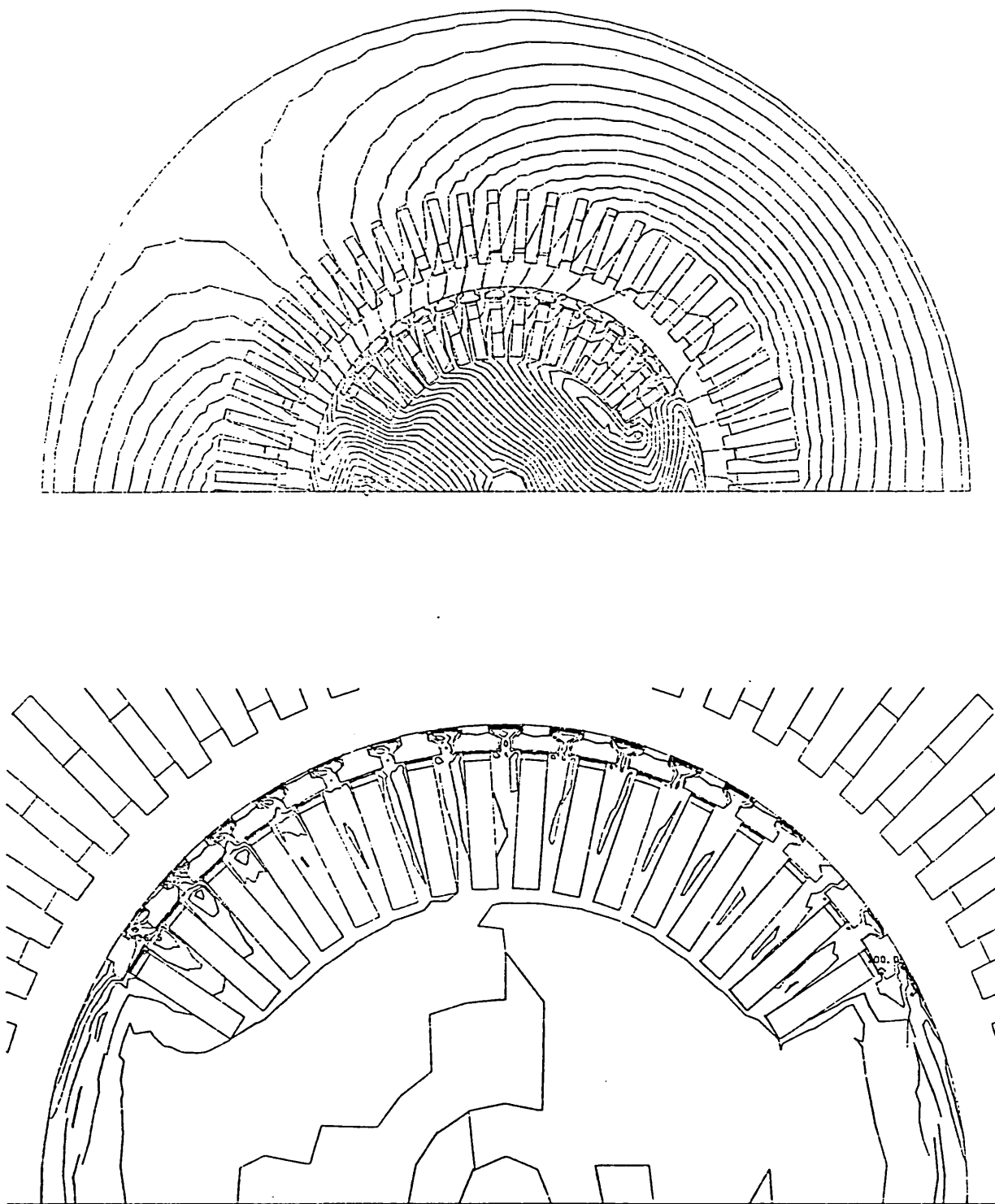


Figure 6.41 time = 159 ms current density contours at 5% of $0.31 \times 10^8 A/m^2$

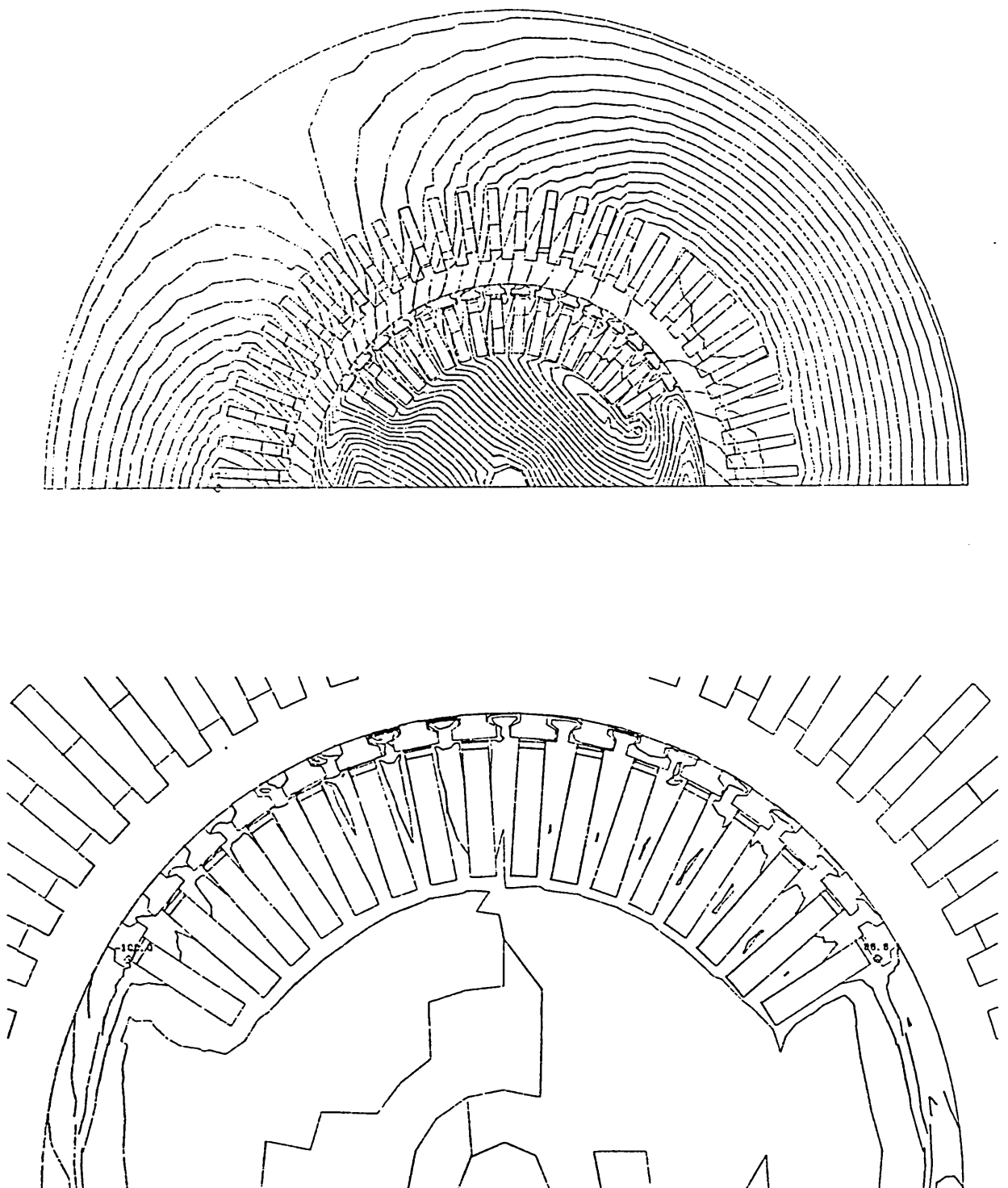


Figure 6.42 time = 169 ms current density contours at 5% of $0.94 \times 10^8 \text{ A/m}^2$

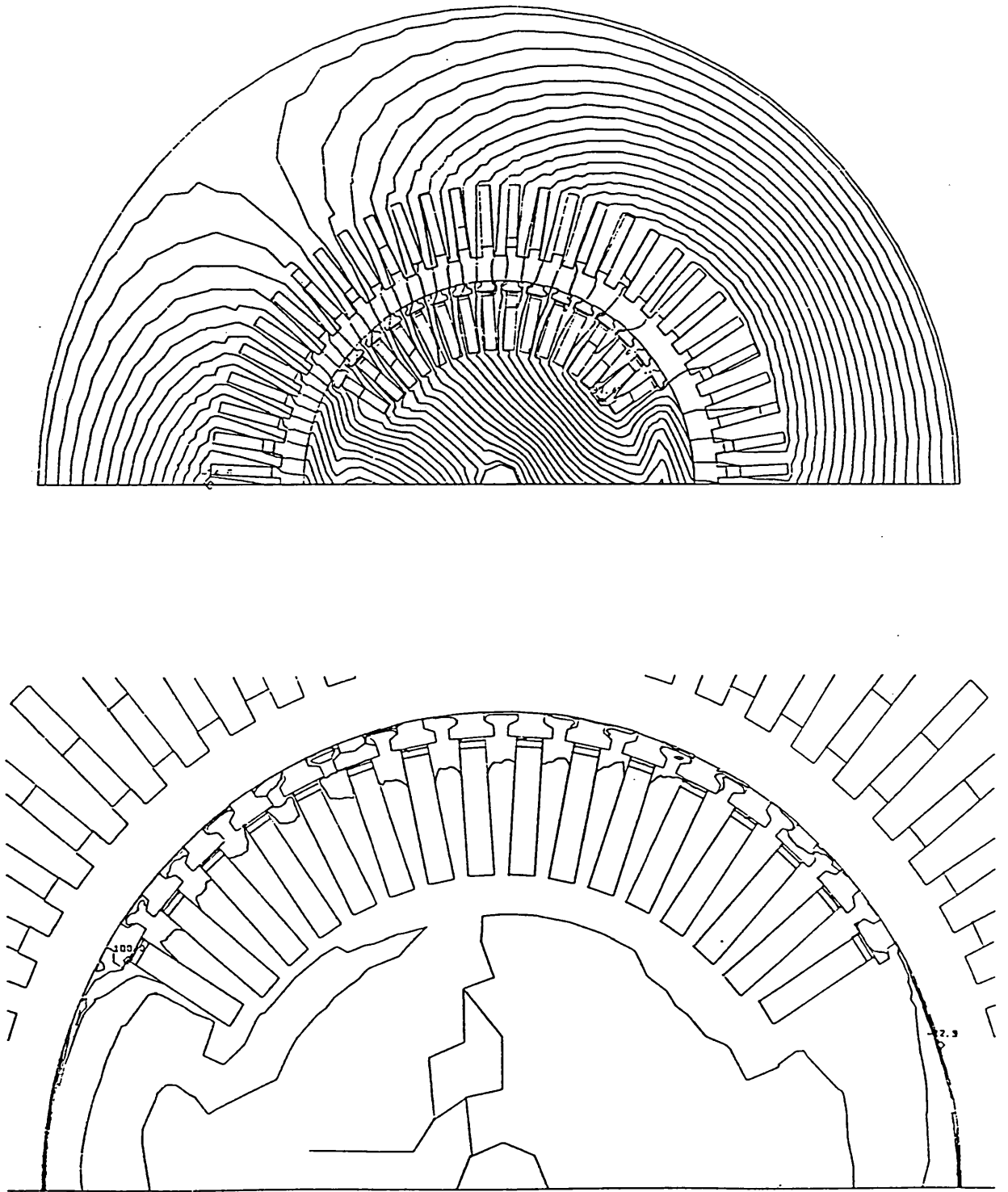


Figure 6.43 time = 600 ms current density contours at 5% of $0.17 \times 10^8 \text{ A/m}^2$

All the flux plots are drawn at 5% contour intervals based on 0.4856 Wb m^{-1} or 0.4199 Wb m^{-1} (the maximum value of A at the start of the short circuit and at the start of fault clearance respectively) as appropriate.

The eddy current density plots are drawn at 5% contour intervals using as a reference the maximum eddy current density at each time step. Closely spaced contour lines represent rapidly changing eddy current density, not high eddy current density, ie. closely spaced contour lines designate the boundary between regions of high and low eddy current activity. See Chapter 5.8.7 for a note regarding discontinuous eddy current contour lines.

The effect of the moving phase band method of modelling the machine rotation may be seen in successive plots where the flux axis rotates clockwise to simulate anticlockwise rotor movement.

At the start of the transient, eddy currents are induced in the copper damper strip and in a very thin layer at the rotor surface. They subsequently diffuse inwards from the surface, distorting the pole and tooth flux patterns.

Comparison of these plots with similar ones in Chapter 5 shows the substantial differences that arise from the inclusion of the stator transformer conductivity matrix. During the first half revolution of the rotor, the stator flux pattern rapidly changes to appear much like that of a sustained short circuit. In the subsequent half revolution, as the rotor returns to the point at which the transient commenced, and the rotor field pattern aligns with that produced by the stationary flux trapped by the stator winding and frozen in the airgap, the machine flux pattern returns to a distribution similar to that of the initial condition. The behaviour is repeated in each revolution.

Examination of the flux plots at each successive complete revolution shows the rate of diffusion of the induced eddy currents into the rotor.

Close inspection of the flux pattern after one revolution (figure 6.25) shows the flux lines immediately under the pole face to be sharply kinked in the opposite direction from those slightly deeper down. This means that eddy currents, flowing in the contrary direction to those initially induced, have been generated at the rotor surface, as the high eddy current density gradient confirms. These new surface currents then begin to diffuse into the rotor (figures 6.26 to 6.28), but are rapidly smoothed out, so that one half revolution later (figure 6.29) they have disappeared. A similar effect is seen at each subsequent complete revolution (figures 6.30 and 6.31).

Eddy currents in the reverse direction are also seen to occur when the fault is cleared and the machine reconnected to the system (figures 6.32 et subs.). In this case, as also found with the two-axis model, the effect is a permanent one and the flux pattern is not smoothed out quickly. It is not known whether this calculated behaviour is correct, or whether it occurs as a result of the constraints imposed by a two-dimensional solution. The matter is discussed more fully in Chapter 5.8.7.

By 600 ms into the transient there is still some eddy current activity circulating flux in the machine poles, but not to any large extent. A small level of eddy current flow will be permanently present as a result of the air gap harmonics.

6.8.4 The effect of discretisation.

The terminal values and mechanical behaviour of the rotor obtained from the detailed mesh UM9 were almost identical to those of the cruder mesh, the differences being significantly smaller than then the same comparison was made with the two-axis approach. Mostly the two sets of results agreed to within a few percent, except for the field current prediction during the short circuit, where the

magnitude of oscillation was about 20% smaller with the more detailed mesh. The difference in maximum rotor angle was 1.0 degree.

Test B	Crude mesh UM3	Detailed mesh UM9	C.E.G.B. Test
Maximum rotor angle change	29.8 deg.	28.8 deg.	39.6 deg.

The eddy current power loss calculated with the two meshes, although similar in form, showed detailed differences, particularly in the distribution of the total between the different parts of the rotor.

6.8.5 Performance of the program.

Comparison of the numerical performance of the model is given in Table 6.2 below. The c.p.u. times given are rounded to the nearest 5 minutes (see Chapter 5.9)

As the transient dies out, so fewer iterations should be required for each time step. The figures above confirm this, the c.p.u. time required per step is less during the reclosure period than during the short circuit.

As with the phase band model, the calculation time varies approximately as $n^2 - n$.

6.8.6 Comparison of Maxwell Stress and Power balance methods.

Figure 6.44 shows a comparison of the Maxwell stress and power balance methods of calculating rotor torque. To provide a more severe torque variation as a basis for comparison, the initial condition of Test B was subjected to a full three phase short circuit placed directly on the machine terminals, rather

TABLE 6.2 COMPARISON OF C.P.U. TIME REQUIRED
FOR DIFFERENT CALCULATIONS

CEGB Test B Calculation	Mesh	UM9	Mesh	UM3
	Short circuit	Reclosure	Short circuit	Reclosure
	0 - 139ms	139 - 600ms	0 - 139ms	139 - 600ms
Number of steps	697	2307	697	2307
c.p.u. time required	1825 min	4140 min	325 min	750 min

than at the transmission line side of the generator transformer. The power balance calculation was performed throughout this transient, and the computed rotor torque is shown in the figure as the solid line. The Maxwell stress was calculated along a contour of integration located at the centre of the air gap using potential solutions generated at 28 points in the transient, these results are plotted as single points. The two calculations are in fairly close agreement; and, given the numerical uncertainties that are a feature of the Maxwell stress calculation (see Chapter 3.3.1), it would be difficult to say which calculation was 'correct' and which 'in error', particularly as they are in exact agreement on the initial condition.

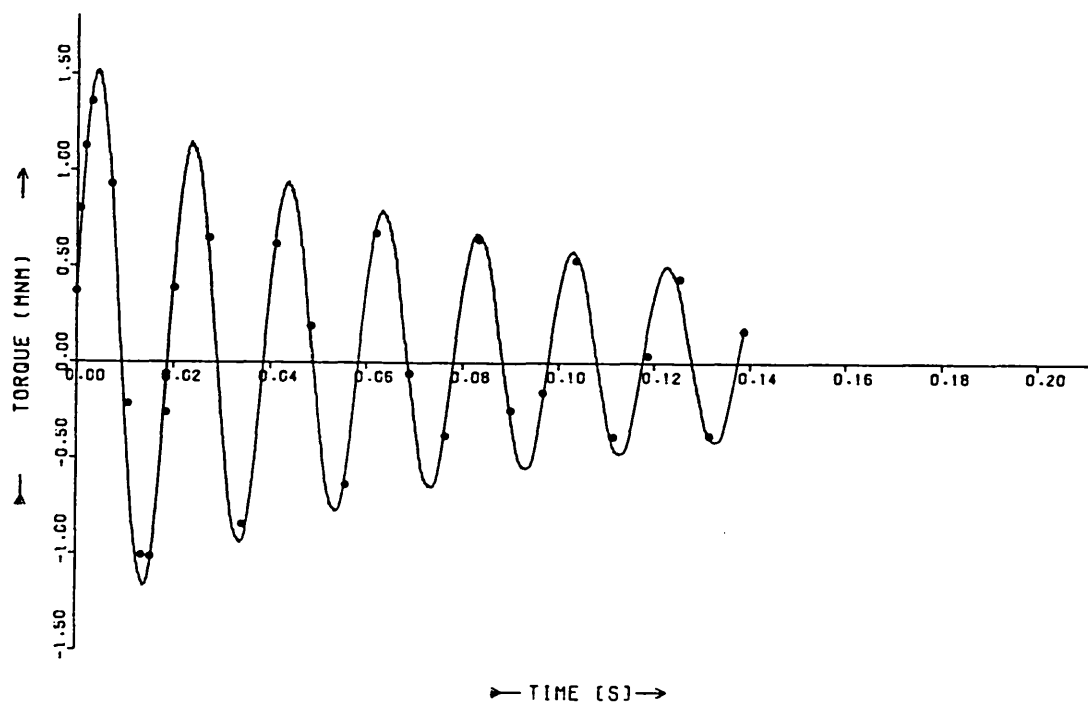


Figure 6.44 Test B - comparison of rotor torque calculation methods

— Power balance • Maxwell stress

6.9 COMPARISON OF TWO-AXIS AND PHASE BAND MODELS, C.E.G.B. TEST B.

Figure 6.45 compares calculations performed with the two-axis and phase band stator models, using the crude mesh UM3. The level of damping of the rotor and terminal values as the rotor swings is much closer to that measured when the phase band model is used, but the first swing prediction is worse. Both these observations may be explained in part as being due to the effects of a higher stator recovery voltage and higher eddy current losses.

Over the time interval 0 - 600 ms, the two-axis method proved to be 4 to 5 times faster computationally than the phase band one. If the comparison were

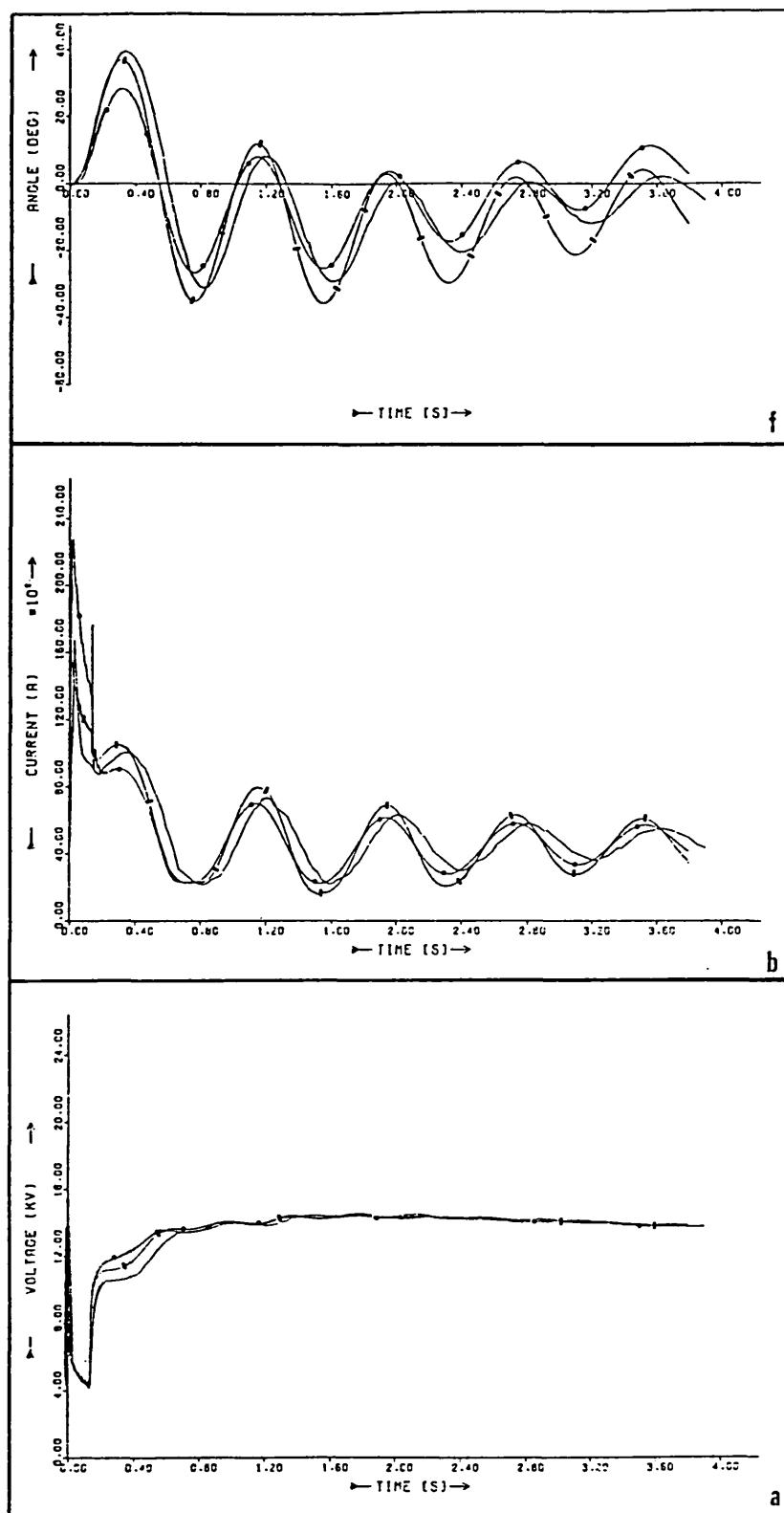


Figure 6.45 Machine response - Test B.

- test results
- finite element phase band (filtered)
- +— finite element two-axis

a) line voltage b) line current f) rotor angle

extended to cover the full 3.8 seconds of the transient, the improvement would be of an order of magnitude.

6.10 COMPARISON OF CALCULATED AND MEASURED RESULTS, C.E.G.B. TEST C1.

For the C.E.G.B. Test C1, the fault period was double that in Test B, and the discrepancy between the calculated and test results becomes significantly greater. Figure 6.46 compares the two up to the point at which the generator was automatically tripped.

During the short circuit period, the line voltage and current predictions are close to the measured values, and the calculated field current is only slightly higher than that measured (which accords with Turner's findings [28]).

On fault clearance, however, the stator voltage is substantially over-predicted, significantly more so than in Test B. As a result, the electrical power output is higher and the net power available to accelerate the rotor is then greatly in error. (The test results show the rotor accelerating in the time period 400 to 600 ms, when the calculation has it decelerating). The consequence is that, whereas the machine actually pole slipped after 475 ms, the calculated time to the first pole slip is 710 ms, and the rotor only slips one pole, instead of two.

With such large differences in the rotor angle, the calculated terminal values cannot be expected to match the measured ones after the reclosure; although they do generally have the same form. In particular, there is a flat portion in the curve of the calculated line and field currents, which does not correspond to any part of the measured curves, but derives from the time period over which the rotor acceleration is small and the rotor angle only slowly changing.

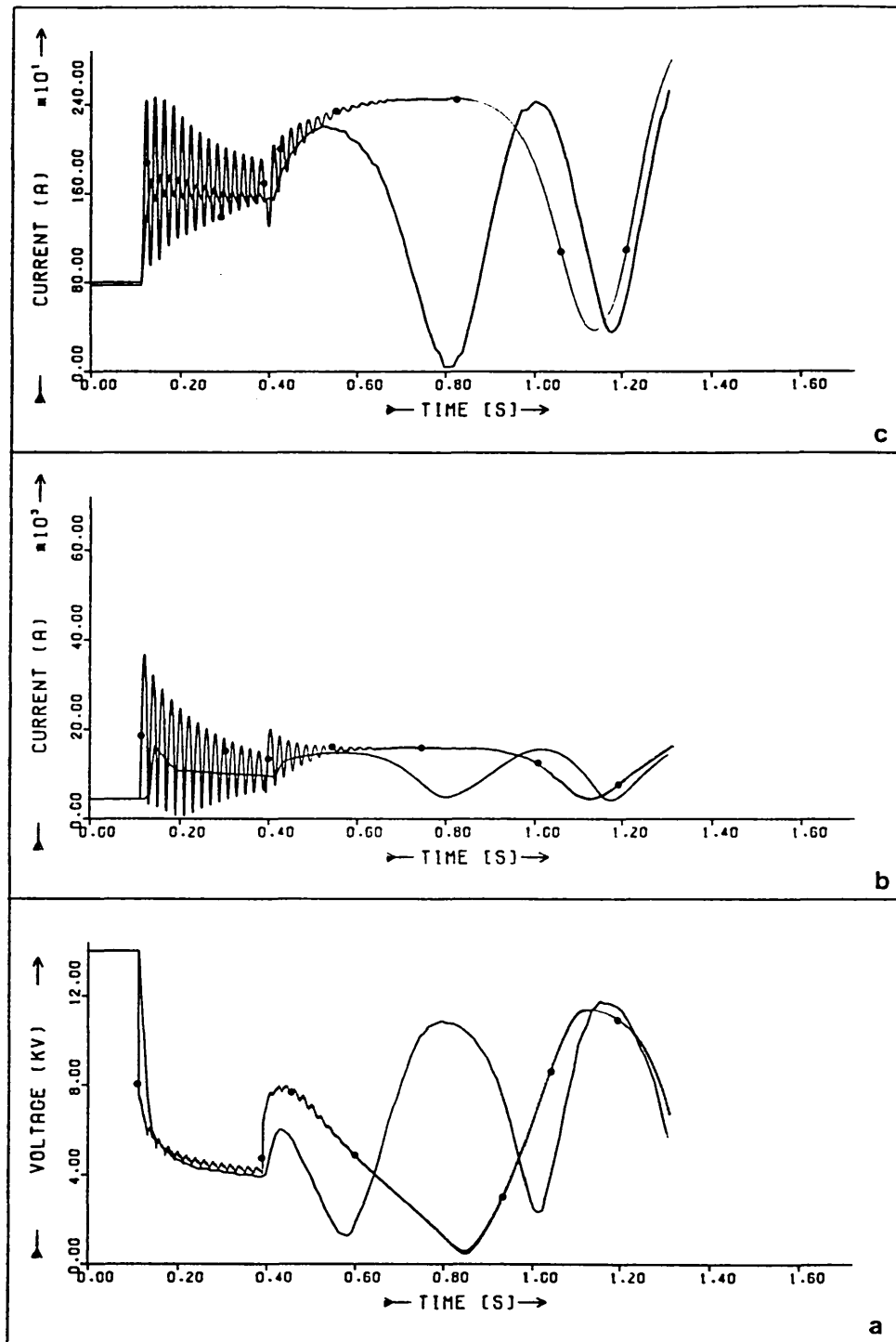


Figure 6.46 Machine response - Test C1

— test results —•— finite element phase band calculation

a) line voltage b) line current c) field current

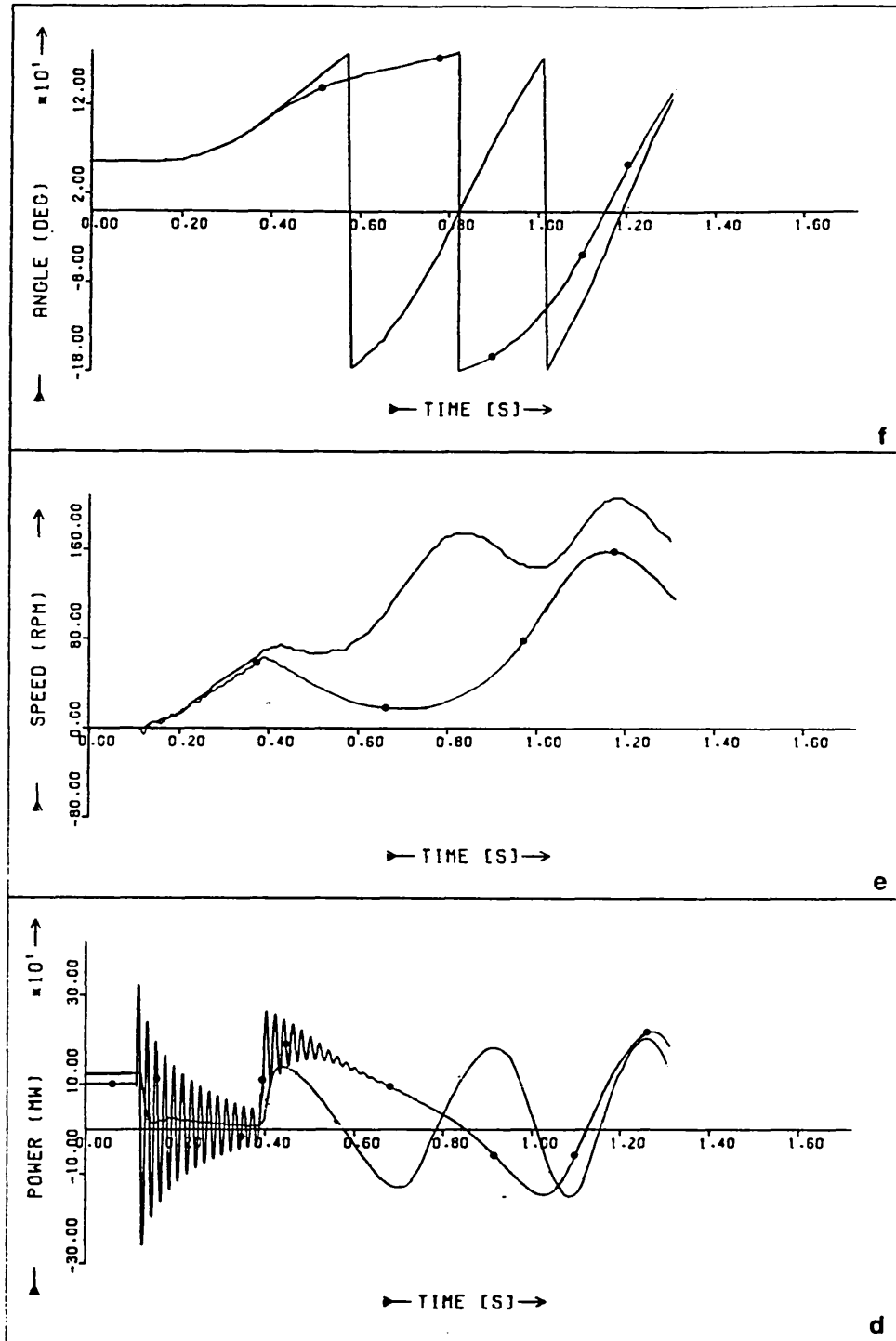


Figure 6.46 Machine response - Test C1 (continued)

— test results —●— finite element phase band calculation

d) electrical power e) speed deviation f) rotor angle

After one second, the test results show the machine pole slipping at a faster rate than calculated. This is surprising, since the interceptor and governor valve operation should have begun to have an effect by this time, even allowing for time constants and entrained steam, but no reduction in the measured rate of pole slipping is evident.

6.11 DISCUSSION OF DISCREPANCIES BETWEEN CALCULATED AND MEASURED RESULTS.

The errors in first swing prediction, particularly with the phase band method, stem from overprediction of the machine stator recovery voltage. To establish the sensitivity of the recovery voltage and the magnitude of the maximum rotor angle change ('first swing') to calculation variables, a number of factors were investigated, using the phase band model and the crude mesh UM3.

- 1) Speed and torque calculation. If the torque calculation is in error, then the calculated rotor position at the point of reclosure will differ from the actual one, and the machine will be operating at a different load angle. To assess the importance of this, a constant speed solution was performed. The result was only a slightly higher recovery voltage.
- 2) Material data. The conductivity data for the rotor materials may be in error, due to uncertainties in composition, in the winding temperature or in the allowances made for effects within the machine length. Two computations were performed to test these effects. A fixed endbell resistivity factor was adopted for each, and the rotor material conductivities doubled in one and halved in the other. The result was a marginal change in the recovery voltage, and a 5% difference in the first swing.

- 3) Point on wave. Although simple machine theory suggests that the point on wave of a three phase fault application is unimportant in the calculation of rotor behaviour, it is possible that the amount of flux frozen in the airgap at the instant of the short circuit is dependent upon the rotor position. Computations at different points on wave confirmed that the effect is not significant.
- 4) Time step length. Halving the time step length to 0.1 ms gave no improvement in results.
- 5) Mesh discretisation. The detailed mesh UM9 gave almost identical results to those of the crude mesh UM3. The level of discretisation of mesh UM9 is similar to that used by previous workers to accurately model other, simpler machine transients, such as the flux decay test [26]. The elements at the rotor surface are of the order of one skin depth thick, which is generally considered to be adequate. It is possible that reducing the element thickness to less than half a skin depth would improve the solution, but, in view of the very long computational time that this would require, this option has not been explored.
- 6) Machine governor and AVR. Although both governor and automatic voltage regulator have long time constants, and thus should not affect the first swing much, it was thought possible that the AVR was keeping the recovery voltage up. A calculation at constant mechanical power and field voltage showed an increase in the first swing prediction by only 1 degree.
- 7) Field circuit resistance. The field circuit resistance is uncertain because of the unknown temperature of the winding, and of the brush contact resistance. Computational studies have shown that the field circuit resistance has a strong effect on the amplitude and damping of the alternating component of field current, but only a small effect on the first swing prediction.

- 8) **Circuit breaker scatter.** For the calculations presented, the fault was applied to all three phases simultaneously, because of the limitations of the delta-star transformer model. The actual timing of the circuit breaker operation shows considerable scatter (Table 4.6), and this could affect the amount of flux trapped by the stator winding at the start of the transient. However, the two-axis model, which cannot allow for circuit breaker scatter, gave better results, which suggests that the effect is not important. In the absence of a better generator transformer model, a partial test of the effects of circuit breaker scatter was made with the Test B initial condition and a scattered application of a fault at the machine terminals, followed by simultaneous clearance, which gave a slightly higher recovery voltage; and a simultaneous fault at the terminals, followed by a scattered clearance to open circuit, which showed no significant difference. On this evidence, circuit breaker scatter does not appear to be an important factor in determining the machine mechanical behaviour.
- 9) **Initial condition.** Although the terminal values and rotor angle found in the calculation for the initial condition agree closely with the C.E.G.B. test results, it is possible that the electromagnetic solution has not converged sufficiently accurately. If this was the case, part of the calculated transient response would be due simply to errors in the field distribution. To test this, a 'transient' calculation was performed in which the fixed terminal impedance of the initial condition was replaced by the transmission line and infinite busbar. A small step response in terminal current and voltage was observed, which showed a tendency to return to the initial condition values with a long time constant. From this, it is deduced that the initial condition calculation is sufficiently accurate for simulating short circuit transient conditions.
- 10) In a first attempt at isolating the problem area, d- and q-axis flux decay tests were simulated. Both the phase band and two-axis stator models were used,

and the calculations were compared with the C.E.G.B. flux decay test results for the Uskmouth machine. Full pole pitch meshes were employed, despite this being unnecessary on account of the additional axis of symmetry that exists in these tests, in order to avoid constraining the solution in a different manner from that used in the general transient case.

The results obtained using the different stator models were almost identical for both d- and q-axis tests, and close to the measured values. A minor discrepancy was seen in the field current prediction, probably due to uncertainty over the resistance of the field circuit and the field winding end leakage reactance.

These calculations indicate that both stator models are capable of simulating the steady collapse of flux linkages within the machine on both axes, and point to the oscillatory component of the general transient response as being the less well modelled. However, Turner's simulation of the works short circuit test [28] (on a different machine design) proved very satisfactory; which may indicate that the problem lies either as a result of the flux axis not being aligned with a machine axis, or in the modelling of the period following the fault clearance and reconnection.

More general reasons for the over-prediction of stator voltage may be :

- i) Too much flux is trapped in the machine by the windings at the start of the transient.
- ii) The flux trapped in the machine does not decay away fast enough.
- iii) There is a sudden loss of flux associated with fault clearance, which has not been incorporated in the model.

The accurate computation of a works short circuit test by Turner [28], would seem to indicate that the amount of flux trapped at the start of the transient is correct.

A higher rate of decay of flux requires greater energy dissipation, which will increase the error in the first swing prediction, unless the fall in the post-clearance electrical power generation more than offsets this. The short circuit line voltage calculation appears to be reasonably accurate, so any greater rate of decay of flux will tend to produce errors during the short circuit period; but the next chapter will reveal that the computed q-axis flux appears to have a longer time constant of decay than occurred in the tests, and this would provide more support of the stator voltage

The source of lost flux could be the circuit breaker arc as the fault is cleared, but this has never been thought to be important in equivalent circuit studies, and should be comparatively small.

The non-linear, transient behaviour of the generator transformer may also be of significance, but again, is not normally incorporated in equivalent circuit studies.

Comparison of finite element predictions with test results for a different machine would be of assistance in pinpointing the source of the discrepancy.

6.12 CONCLUSIONS.

In this chapter, the full solution of the transient equations has been presented. A rotating phase band approach to the modelling of relative motion within the machine was chosen and the formulation of winding vectors and their compact incorporation into the basic finite element method using the A-average technique to give a sparse, symmetric matrix were described.

With a phase band model it is necessary to time step to obtain the required initial condition. This can be a lengthy process, but by removing the rotor and field winding conductivity matrices from the calculation and using an

initial estimate of potentials and field current derived from a two-axis solution, convergence to the solution was speeded up considerably. The terminal current and voltage contain harmonic terms, and it was found necessary to filter the terminal voltage before it could be used as a target parameter for convergence.

A time step length of 0.2 ms was found to provide a good compromise between accuracy and solution time. For other machine designs, a slightly different value may be appropriate to avoid the rotor angle change being a simple fraction of the stator tooth pitch (which could introduce artificial harmonics into the solution)

The results obtained with the model were compared with test data for both coarse and fine mesh discretisations. The outcome was, in general, fairly good, except that the stator voltage on fault clearance was substantially over-predicted, and the maximum rotor angle achieved much reduced as a result. The eddy current power loss within each area of the rotor was considered and the contribution of the copper damper strip to machine damping was shown to be minimal. A numerical study showed the advantages of changing the slot wedge material, and illustrated the application and usefulness of the method as a design tool.

The flux and eddy current plots presented emphasised the difference between the phase band and two-axis models. They show in detail the effect of the flux trapped by the machine windings at the start of the transient and effectively frozen in the airgap. The result is a flux pattern within the machine which alternately resembles that of the sustained short circuit and that of the initial condition, as the rotor flux is opposed to or aligned with the stationary flux pattern.

At each complete revolution, eddy currents flowing in the opposite direction to the main distribution appeared to be induced in the rotor surface, but died away in the subsequent half cycle. On fault clearance, the same effect

was observed, except that the surface eddy currents were permanent and diffused slowly into the rotor.

It is uncertain whether these last observations accord with fact, or whether they arise as a result of the constraint placed upon the problem by the assumption of a two-dimensional solution, where currents can only flow in an axial direction. The problem was more fully discussed in the previous chapter.

Using a more detailed mesh was found to provide few advantages, particularly as the solution took six times as long to compute, and the first swing prediction was worse. A comparison was made between the Maxwell Stress and Power Balance methods of computing rotor torque; the results were in fairly close agreement and neither method could be said to be more accurate on the basis of this comparison.

When the two-axis and phase band models were compared, the former was found to provide a better prediction of the first swing, but worse damping. Since the two-axis method is much faster computationally, on this evidence it would be preferred; but both methods overpredict the stator recovery voltage, and it is likely that, if this were corrected, the phase band method would prove to be more exact, with the two-axis model over-stating the rotor angle because it fails to fully model the machine losses.

The C.E.G.B. Test C1 involved pole slipping. A critical measure of the performance of a simulation is the accuracy with which the onset of pole slipping is calculated. The phase band method proved to be nearly 250 ms out in this, as a result of a substantial error in the prediction of the stator recovery voltage. On this basis, the phase band method is considered to be not yet sufficiently developed to provide a useful predictive technique in power systems analysis.

The last part of the chapter was devoted to a discussion of possible reasons for the discrepancies found. A number of promising ideas were pursued, but most proved unable to provide the explanation sought. Several others could not be fully tested out due to lack of time and the inability of the generator transformer model used to model unbalanced transmission line faults. A few, more general ideas were raised at the end of the chapter, giving an indication of areas where further investigation could be undertaken.

CHAPTER SEVEN

OBTAINING EQUIVALENT CIRCUIT PARAMETERS FROM THE FINITE ELEMENT MODEL

7.1 INTRODUCTION.

There are a variety of ways in which the finite element method has been used to obtain parameters for equivalent circuit machine models. The simplest employ the technique to determine parameter saturation functions [64], more complex methods find the 'steady state' reactances by injecting currents into the machine windings, and examining the voltages induced in others. Typical of these methods is Macdonald et al [65], where the effects of cross-axis saturation are investigated.

Transient machine reactances have also been calculated in a number of ways. The most straightforward use the finite element method to simulate the full machine tests from which parameters are derived, such as sudden short circuit [59], flux decay [26], field decrement [39], operational inductance [66] and frequency response [67,68]. A more complicated method, due to Haydock [14], uses the finite element method to obtain data for a detailed magnetic equivalent circuit model of the machine, which may either be used directly for solving machine transients, or progressively reduced and simplified until the desired equivalent circuit is reached.

This chapter presents a method for determining the damper circuit parameters for an equivalent circuit machine representation directly from the time stepped finite element calculation. The phase band stator model is used for the study because it includes all the components of the machine electromagnetic behaviour.

The equivalent circuit to be used is first introduced, and used to divide the total power flow within the model into three groups. Methods for obtaining d- and q-axis currents and flux linkages directly from the phase band calculation are described, and are used in the determination of the machine's basic reactances.

A technique for calculating the damper circuit impedances, by equating power dissipative terms, is then described, and the variation of the damper circuit parameters over the short circuit period is illustrated.

Finally, in an attempt to explain the unsatisfactory results of this and the previous chapter, the d- and q-axis currents and flux linkages found from the phase band finite element calculation are compared with those obtained from a simple state space solution of the equivalent circuit representation, using damper circuit data derived from the C.E.G.B. Test report.

7.2 THE EQUIVALENT CIRCUIT MODEL.

There are many equivalent circuit models to choose from, but the most widely used are of the two-axis, 5-branch type described by Adkins and Harley [5], whose model has been adopted here along with their per unit convention. The equivalent circuit is illustrated in figure 7.1, and described by equation 7.1, which is taken from reference [5] figure 4.27.

At any instant, the total power associated with the model is :

$$P_{tot} = \frac{1}{2}(u_d i_d + u_q i_q + u_f i_f + R_{kd} i_{kd}^2 + R_{kq} i_{kq}^2) \quad (7.2)$$

Equation 7.2 may be expanded using equation 7.1, and the terms grouped into three types :

- 1) Those associated with power dissipated as resistive loss, of the form :

$$P_1 = \frac{1}{2} R i^2 \quad (7.3a)$$

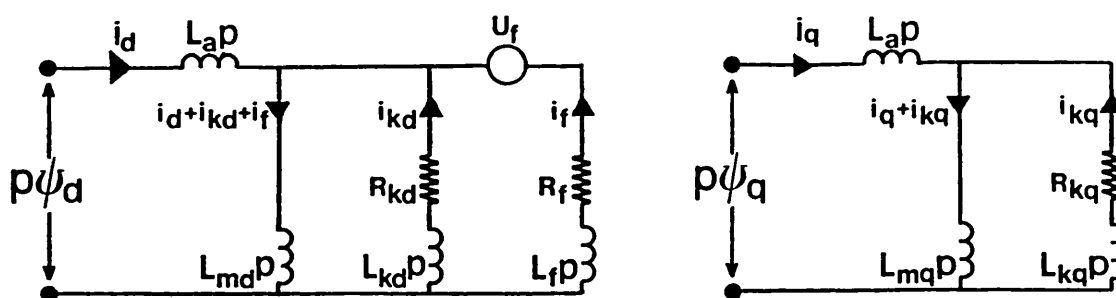


Figure 7.1 Machine equivalent circuit

u_f	$R_f + (L_{md} + L_f)p$	$L_{md}p$	$L_{md}p$			i_f
u_{kd}	$L_{md}p$	$R_{kd} + (L_{md} + L_{kd})p$	$L_{md}p$			i_{kd}
u_d	$L_{md}p$	$L_{md}p$	$R_a + (L_{md} + L_a)p$	$(L_{mq} + L_a)\omega$	$L_{mq}\omega$	i_d
u_q	$-L_{md}\omega$	$-L_{md}\omega$	$-(L_{md} + L_a)\omega$	$R_a + (L_{mq} + L_a)p$	$L_{mq}p$	i_q
u_{kq}				$L_{mq}p$	$R_{kq} + (L_{mq} + L_{kq})p$	i_{kq}

where $u_d = p\psi_d + \omega\psi_q + R_a i_d$

$u_q = -\omega\psi_d + p\psi_q + R_a i_q$

Equations 7.1

- 2) Those associated with changes in the energy stored in the circuit inductances, of the form :

$$P_2 = \frac{1}{2} i L p(i) \quad (7.3b)$$

- 3) The electrical output power :

$$P_3 = \frac{1}{2} \omega_0 (i_d \psi_q - i_q \psi_d) \quad (7.3c)$$

This division is similar to that used in the power balance calculation of Chapter 3.3, and is the basis for the method proposed. Firstly, it is necessary to derive d- and q-axis per unit values from the three phase actual values calculated by the phase band model.

7.3 OBTAINING TWO-AXIS PARAMETERS FROM THE PHASE BAND MODEL.

The d- and q-axis voltages are obtained simply by defining appropriate winding vectors, as described in Chapter 5.1, and using the phase band finite element potential solution at each step to find the flux linking the two-axis windings as per equation 5.5 (see Chapter 5.2.1 for a note regarding multiplying factors of 2/3). The Park transform is used to obtain the d- and q-axis currents from the phase currents at each time step.

7.3.1 Base values.

The base values of power and stator current and voltage are defined straightforwardly as the rated VA, phase current and phase voltage respectively. The base field current is defined from the field current required to give base stator voltage on open circuit, as extrapolated from the air gap line, i_{fo}^a :

$$i_{fb} = \frac{X_{md}^u i_{fo}^a}{\sqrt{2}} \quad (7.4)$$

X_{md}^u is defined from the open and sustained short circuit curves as :

$$X_{md}^u = \frac{i_{fsc}^a}{i_{fo}^a} - X_a \quad (7.5)$$

where i_{fsc}^a is the field current required to give base stator current in a sustained short circuit - in amps

i_{fo}^a is in amps

X_a is the stator leakage reactance in per unit

Both $i_{f_o}^a$ and $i_{f_{sc}}^a$ were found from finite element studies, using the two-axis stator model to avoid the need to time step to the solution. For the calculation of $i_{f_o}^a$ a linear study was performed, ie the permeabilities were fixed at their unsaturated values.

7.3.2 Main axis reactances.

The axis reactances were found from the basic machine reactances using the method of Macdonald et al. [65], with permeabilities appropriate to the machine initial condition. The results are summarised in Table 7.1. The cross axis reactances are all of the order of 5% of the main reactances, which implies that the total flux on each axis cannot easily be directly identified with the currents on that axis.

Turner's studies of machine transients [27], suggest that the saturation levels in a machine stay relatively constant throughout the transient. As an initial approximation, therefore, the axis reactances were considered to be unchanged throughout.

7.3.3 Damper circuit impedance.

If the main machine reactances, flux linkages and the d- and q-axis currents are known, then the damper circuit currents may be calculated as :

$$i_{kd} = \frac{\omega_0 \psi_d - X_d i_d - X_{md} i_f}{X_{md}} \quad (7.6a)$$

$$i_{kq} = \frac{\omega_0 \psi_q - X_q i_q}{X_{mq}} \quad (7.6b)$$

**TABLE 7.1. C.E.G.B. TEST B INITIAL CONDITION.
REACTANCES.**

Field current required for 1 p.u. stator voltage on air gap line	536 A
Field current required for 1 p.u. stator current on short circuit	1006 A
Base field current	669 A
X_{md}^u	1.766 p.u.
X_a	0.111 p.u.
stator endwinding leakage reactance, X_e	0.042 p.u.

Major reactances

$$X_{dd} = \frac{\omega\psi_d}{i_d} \Big|_{i_f, i_q=0} + X_e = 1.785 \text{ p.u.}$$

$$X_{qq} = \frac{\omega\psi_q}{i_q} \Big|_{i_f, i_d=0} + X_e = 1.562 \text{ p.u.}$$

$$X_{df} = \frac{\omega\psi_d}{i_f} \Big|_{i_d, i_q=0} = 1.672 \text{ p.u.}$$

Cross reactances

$$X_{qd} = \frac{\omega\psi_q}{i_d} \Big|_{i_f, i_q=0} = 0.072 \text{ p.u.}$$

$$X_{dq} = \frac{\omega\psi_d}{i_q} \Big|_{i_f, i_d=0} = 0.081 \text{ p.u.}$$

$$X_{qf} = \frac{\omega\psi_q}{i_f} \Big|_{i_d, i_q=0} = -0.078 \text{ p.u.}$$

Axis reactances

$$X_d = \frac{i_d X_{dd} + i_q X_{dq} - i_f X_a}{i_d - i_f} = 1.664 \text{ p.u.}$$

$$X_q = \frac{i_q X_{qq} + i_d X_{qd}}{i_q} = 1.473 \text{ p.u.}$$

Knowing the damper circuit currents, the power dissipated in the rotor circuit resistance :

$$P_k = \frac{1}{2} (i_{kd}^2 R_{kd} + i_{kq}^2 R_{kq}) \quad (7.7)$$

may be equated with the eddy current loss found in the finite element calculation, and the damper resistances found. Some method, however, is required for separating out the d- and q-axis effects in the total P_k .

Once the resistances have been found, the reactances are calculated as :

$$X_{kd} = \frac{-X_{md}(p(i_d) + p(i_f)) - \omega_0 R_{kd} i_{kd}}{p(i_{kd})} - X_{md} \quad (7.8a)$$

$$X_{kq} = \frac{-X_{mq}p(i_q) - \omega_0 R_{kq} i_{kq}}{p(i_{kq})} - X_{mq} \quad (7.8b)$$

7.4 COMPUTATION OF DAMPER CIRCUIT IMPEDANCES.

7.4.1 Resistance.

As a first approximation, the rate of change of R_{kd} and R_{kq} may be assumed small compared with the supply frequency changes in the damper circuit currents. Thus at two close intervals in time, t_1 and t_2 , over which the resistances are assumed constant :

$$\left. \begin{aligned} P_k|_{t_1} &= \frac{1}{2}(i_{kd}^2|_{t_1} R_{kd} + i_{kq}^2|_{t_1} R_{kq}) \\ P_k|_{t_2} &= \frac{1}{2}(i_{kd}^2|_{t_2} R_{kd} + i_{kq}^2|_{t_2} R_{kq}) \end{aligned} \right\} \quad (7.9)$$

and the simultaneous equations may be solved for R_{kd} and R_{kq} .

Figure 7.5 shows the stator axis values obtained from the phase band simulation of Test B, and the computed damper circuit currents. If the damper currents are viewed in conjunction with the pattern of eddy current dissipation that they are required to model, given in figures 6.7 and 6.9, it is evident that the form of the latter is too complex to be modelled well by the sum of two oscillatory terms. If equation 7.9 is applied, the values of resistance obtained will vary wildly from one point to the next, and even become negative. The reason for this behaviour is that the finite element data is being fitted at too many points.

At different points in the cycle, both i_{kd} and i_{kq} are zero. When this occurs, the eddy current power loss must be entirely due to the other current and its associated resistance, which may thus be determined. The resistance so calculated, at one point in each cycle, is assumed to be constant over half a cycle

each side of the point of calculation. The finite element and equivalent circuit solutions are now an exact fit at only two points per cycle but, since the resistances are not changing rapidly, this does not lead to large errors. The overall fit may be improved by making minor adjustments to the resistances so that the areas under the two curves, the energy dissipated, are equal. This may be performed on a cycle-by-cycle basis, or over the whole period modelled. The latter procedure was adopted here, and a 6% correction was found to be needed. Figure 7.2 compares the results, and figure 7.3 shows the values of resistance obtained.

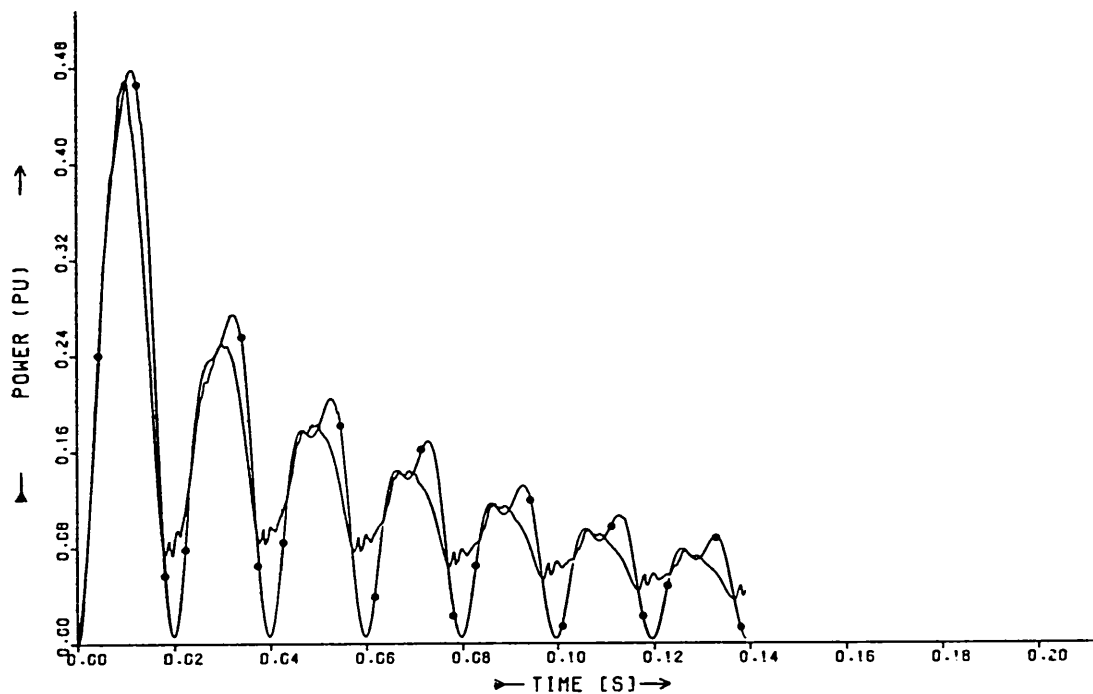


Figure 7.2 Rotor body eddy current power loss

- finite element calculation
- equivalent circuit calculation using resistances of figure 7.3

7.4.2 Reactance.

Having found the damper resistances at specific points, equation 7.8 is applied at the same points to find the reactances. The results are shown in figure 7.4 . Clearly these are incorrect.

Numerical problems have arisen because the calculation of circuit inductance involves finding the difference between two large, similar numbers (in circuit terms, the voltage dropped across the damper inductance, Ldi/dt , is small compared with the drops in the rest of the circuit). Where the behaviour of the finite element solution varies from that given by the simple equivalent circuit model, the magnitudes and rates of change of circuit currents obtained from the finite element method will not be an exact fit to a five branch circuit, and this gives rise to the results of figure 7.4 above.

To examine where the root of the problem lies, it is necessary to solve the transient problem using the equivalent circuit method.

7.5 EQUIVALENT CIRCUIT SOLUTION.

A simple state space method was adopted for the solution of the equivalent circuit model, as described by Adkins and Harley. No AVR or governor action was included, and the mechanical equations assume a single inertia system. The values of X_d and X_q used were those calculated from the finite element initial condition. The other input parameters were obtained from the machine data of Table 4.3 except that, in calculating the q-axis damper values, only the sub-transient q-axis parameters were used, following the recommendation of the C.E.G.B RASM05 documentation [58].

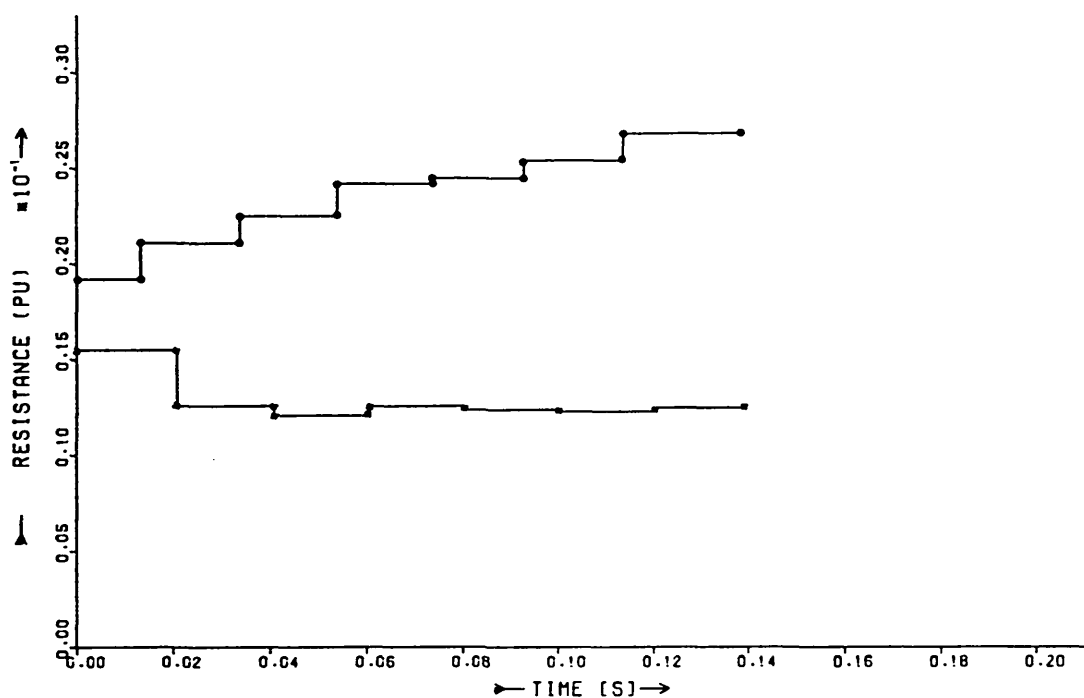


Figure 7.3 Damper circuit resistance calculated from the finite element simulation of Test B. \bullet R_{kd} \blacktriangle R_{kq}

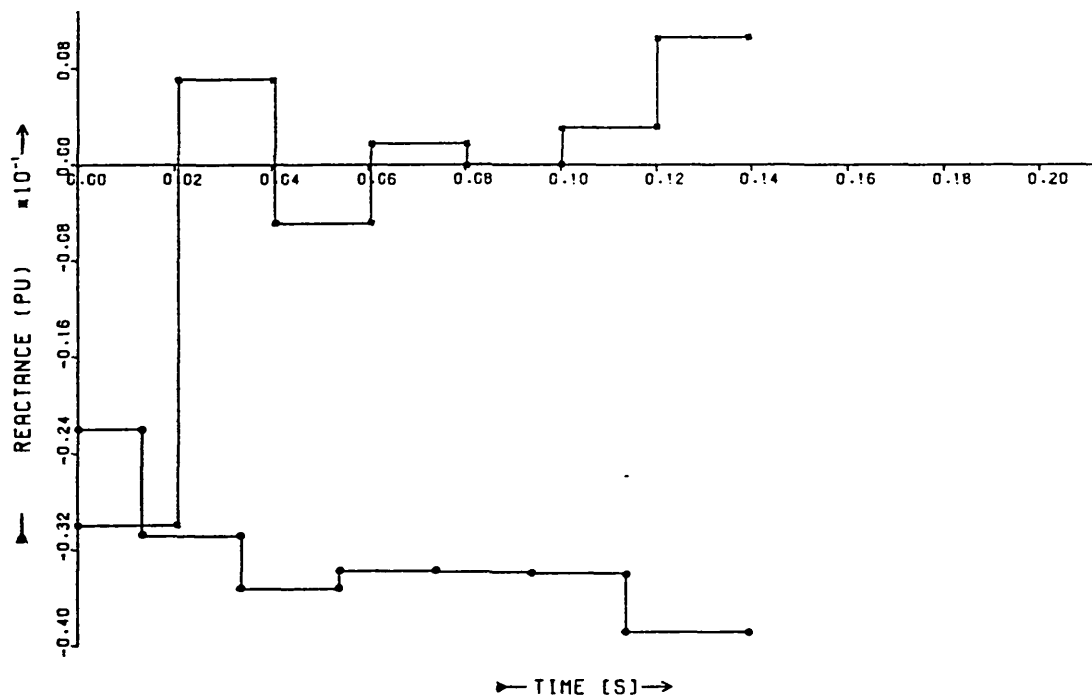


Figure 7.4 Damper circuit reactance calculated from the finite element simulation of Test B. \bullet X_{kd} \blacktriangle X_{kq}

7.5.1 Comparison of finite element and equivalent circuit results.

The equivalent circuit solution provides a better, but still not accurate, first swing prediction (33 degrees) than the finite element phase band one, and shows a similar, but smaller, overprediction of recovery voltage.

In figure 7.5 the axis currents and flux linkages (the latter including the slot leakage component) for both the equivalent circuit and phase band finite element models are compared, during and just after the short circuit period. The most significant feature is the difference in behaviour of the q-axis flux linkage, which shows a much smaller decay in the finite element solution than in the equivalent circuit one. This is partly due to a difference in the magnitude of the step change in flux linkage at the start of the transient, but mainly to the lower rate of decay of the flux as the transient proceeds. As a result, while the equivalent circuit model has the mean q-axis flux linkage falling to zero by the end of the fault period; that in the the finite element model has fallen to only 0.2 p.u.. However, the finite element results show a greater damping of the oscillatory component of the flux linkage, so that the peak flux linkage is almost the same in both models.

The main and damper winding currents on the q-axis also show a lower rate of decay of the direct component, suggesting that the q-axis time constant found using the finite element method is longer than the parameters predict.

The 'holding up' of the q-axis flux in the phase band finite element model may provide the reason for the over-recovery of the stator voltage on fault clearance, but further work is required to establish exactly the reason for the differences between the results obtained with the two models.

One method of approach would be to modify the machine parameters in the equivalent circuit model to provide a good fit firstly to the finite element

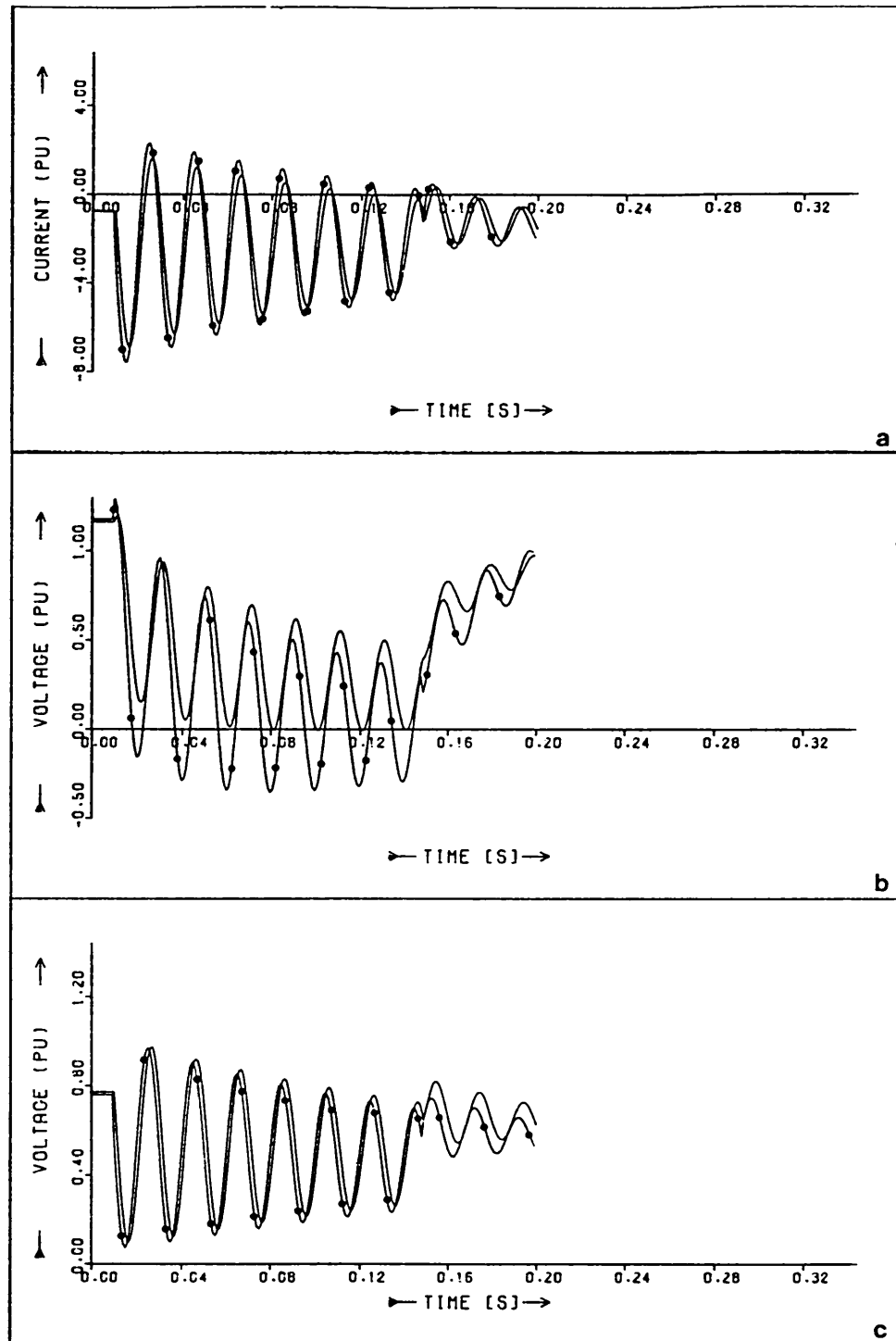


Figure 7.5 d- and q-axis currents and voltages Test B.

— from finite element calculation

—●— from equivalent circuit calculation

a) i_d

b) $\omega_0 \psi_q$

c) $\omega_0 \psi_d$

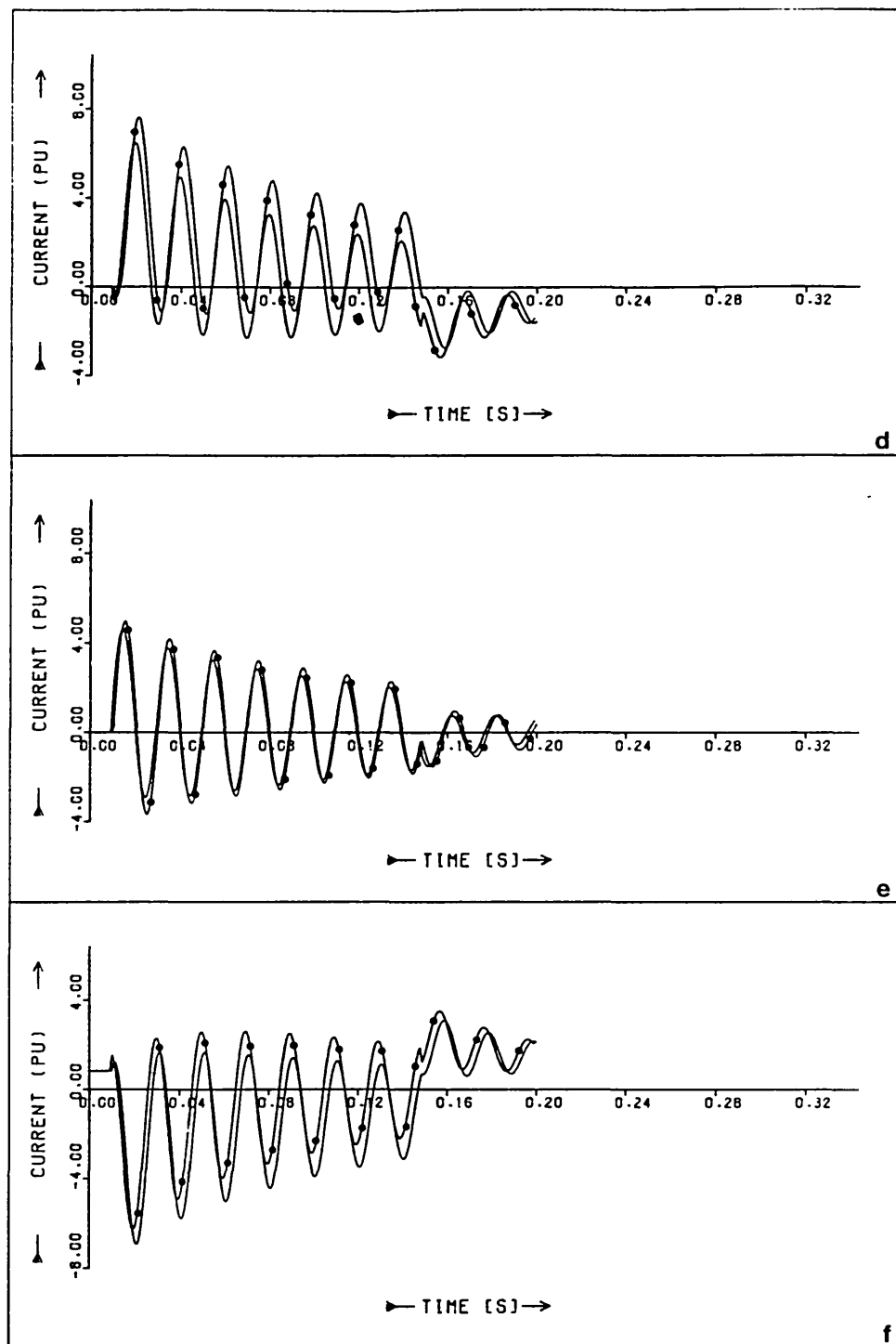


Figure 7.5 d- and q-axis currents and voltages Test B. (continued)

- from finite element calculation
- from equivalent circuit calculation

d) i_{kq}

e) i_{kd}

f) i_q

solution and then to the test results. The difference between the two parameter sets may give an indication of the areas in which to concentrate further investigation.

Another possibility would be to further test the finite element method by constructing a machine model with a non-conducting (laminated) rotor carrying pole face damper bars, thus giving a much better defined damping circuit. Using this model, finite element simulations of flux decay, frequency response or sudden short circuit tests would enable a set of equivalent circuit parameters to be obtained. The finite element and equivalent circuit models could then be used to predict the machine performance under system transient fault conditions, and any discrepancy investigated.

7.6 CONCLUSIONS.

This chapter has presented a method for directly relating the finite element and equivalent circuit machine models in a new manner, through the power dissipative terms. The Adkins and Harley five-branch equivalent circuit and per unit system were adopted.

It was first shown that the equivalent circuit model allowed power flows to be identified and suitably grouped for comparison with the finite element results, and then the basic machine reactances were calculated from the finite element initial condition taking account of cross axis flux, which amounted to approximately 5% of the main axis flux in the case of the C.E.G.B. Test B initial condition.

If the basic reactances are considered to be invariant throughout the transient, then the damper circuit resistance and reactance were shown to be calculable from the eddy current power loss in the rotor, provided that it could be split into d- and q-axis components. This was accomplished by fitting the data at

points in the cycle where one or other damper current was zero, a subsequent small adjustment being made to equalise the energy dissipation in both finite element and equivalent circuit models. The damper circuit resistances were found not to vary significantly over the short circuit period, the d-axis values grew steadily and the q-axis ones were almost constant. The damper circuit reactances, however, varied widely, and even became negative.

In an attempt to explain both why this occurred and the results of the previous chapter, the equivalent circuit model was used to simulate C.E.G.B. Test B, using damper circuit data from the C.E.G.B. test report. This solution proved somewhat more accurate than that provided by the phase band finite element model, and a preliminary investigation of the differences between the d- and q-axis currents and flux linkages obtained from the finite element and equivalent circuit models found that the decay of the quadrature axis flux was more pronounced in the equivalent circuit case.

Suggested further investigations using both finite element and equivalent circuit models were outlined at the end of the chapter.

CHAPTER EIGHT

CONCLUSIONS AND RECOMMENDATIONS FOR FURTHER WORK

8.1 CONCLUSIONS.

This thesis has presented a finite element based method for calculating the general transient performance of a turbine generator. The electromagnetic equations were formulated using the nodal method and the concept of the conductivity matrix; and the mechanical behaviour determined by performing a power balance at each step of the solution to calculate the rotor torque and hence rotor angle.

Two methods of representing the stator winding have been described, the phase band and the two-axis, and the analysis has been extended to incorporate governor, turbine and automatic voltage regulator models and the effect of an infinite busbar in the stator circuit.

The two methods have been used, with limited success, to simulate system transient tests undertaken by the C.E.G.B., and possible reasons for discrepancies have been explored.

Finally, the phase band model has been used as a means of investigating the behaviour of machine parameters during the transient using a technique which directly links the finite element and equivalent circuit solutions.

8.1.1 Problem formulation.

The finite element method may be applied to the solution of the non-linear, transient electromagnetic behaviour of a turbine generator under general fault conditions. The approximations inherent in a two-dimensional calculation may be reduced by means of analytical allowances for effects within the machine length.

In a time stepped non-linear technique, it is important to adopt a problem formulation that allows efficient construction and solution of the equations and minimises the computing time required. The A-average technique has proved important in this respect, and other methods have been adopted both to reduce the computational effort in each time step and to increase the time step length where possible.

The application of a power balance within the machine proved to be a much easier way of calculating the transient torque than the Maxwell stress tensor, and provided a deeper insight into the mechanisms of the transient especially useful in design work. Although the model adopted assumes a single mechanical mode of oscillation of the rotor, there is no fundamental problem in extending the analysis to include all the shaft torsional modes.

The method is not restricted to the simple generator transformer and transmission line models have been used, and more complex representations could be employed, provided that they allow the line current to be calculated from a knowledge of the line voltage.

An 'external' model of the power system at the machine terminals was adopted in preference to one incorporating it in a 'modified machine' representation. This gave a more general method and a more modular construction to an already

complicated computer program and simplified the process of modelling the different stages of the transient. This was also true of the machine control models used, which were 'external' to the central finite element calculation of machine behaviour, as they are in practice.

The level of detail provided by the finite element model gave rise to new problems of interpretation of the results, such as the precise definition of 'terminal voltage' to be used for strict comparison with test results and as an automatic voltage regulator feedback signal. Similarly, if filtering was applied to the measured values it must also be applied to the calculated ones, if predicted and measured values are to be compared.

Some particular problems were encountered when a two-axis stator model was adopted. Principal amongst these was the incorporation of an infinite busbar into the stator circuit. An approximation was found to be necessary to maintain the matrix formulation, at the expense of a slight increase in computational time and loss of accuracy in the period immediately following fault clearance. A second problem arose with the inversion of the asymmetric matrix that resulted. An adaptation of the Gaussian elimination scheme was found to minimise the effect of the asymmetry, and proved to be very effective.

The current sheet stator model provides a logical extension of the two-axis formulation applied to a fully modelled stator. Very little modification to the method was required to accommodate this.

8.1.2 Transient modelling.

Both the two-axis and phase band models proved capable of simulating the behaviour of a turbine generator subjected to a three phase transmission line

short circuit and subsequent reconnection to the system after fault clearance, although neither gave as accurate results as had been anticipated.

On clearance of the fault, the terminal voltage rises suddenly. Both the two-axis and phase band models overpredicted this recovery value, the phase band more severely, and this gave rise to errors in the calculation of generated power and thus machine torque and rotor angle.

When modelling the stable system transient test using the phase band approach, the rotor angle predicted was as much as 10 degrees in 40 less than that measured, and for the pole slipping case, the onset of pole slipping was calculated to be 50% later than was found to occur. The two-axis model gave a much better maximum rotor angle prediction, but it is felt that this may be due to fortuitous cancellation of errors of approximation.

The prediction of terminal current and field current was reasonably accurate once the phase difference associated with the rotor angle calculation error had been allowed for, although comparison of measured and calculated results in the short circuit region is complicated by filtering of the test values. The field current proved to be the most susceptible to different modelling and calculation methods, as would be expected, since the field circuit is more closely coupled with the electromagnetic behaviour of the rotor.

On fault clearance, if the transient is a stable one, the rotor enters a period of damped oscillations, relative to a synchronous reference frame, which produce corresponding variations in the terminal values. The two-axis models gave a rather too lightly damped response, whereas the phase band model, although underestimating the first swing, managed to calculate the subsequent behaviour well. Both models accurately predicted the rotor swing frequency.

The pattern of eddy current power dissipation and of stored energy changes stored in machine fields calculated by the different stator models were, as expected, markedly different. The flux frozen in the airgap at the start of the fault has a dominating effect on this calculation and, accordingly, the two-axis model, which neglects this component, could not be expected to give correct results, although the overall effect of the stored energy calculation was not dissimilar from an analytical approximation for the same effect. The phase band model, on the other hand, clearly demonstrated the existence of both unidirectional (due to resistive losses) and oscillatory (due to stored energy changes) components of the transient rotor torque, and enabled an interesting design study to be carried out in which the effectiveness of the rotor wedges and dampers was assessed and an improvement suggested.

Detailed consideration was given to the behaviour of the machine flux and eddy currents throughout the transient, and the plots produced from the vector potential solution clearly emphasised the difference between the two models, particularly during the short circuit period. The gradual diffusion into the rotor body of eddy currents induced initially at the surface was seen, and the phase band results showed the periodic influence of the stationary air gap flux.

A surprising effect is seen with both models, where eddy currents appear to be induced in the rotor surface that flow in the opposite direction to those deeper inside the rotor body. It is uncertain whether this calculated behaviour is correct, or whether it has arisen as a result of the constraint placed upon the solution by a two-dimensional formulation that only permits an axial flow of current.

Possible reasons for the discrepancies between the measured and calculated results were discussed at length at the end of Chapter 6. Most of the computational tests undertaken in this respect demonstrated the insensitivity of

the overall machine performance to many of the design and test variables. The investigation proved inconclusive, and remains the prime field for further work.

It was generally found that, whichever stator model was adopted, a detailed mesh gave only a minor improvement, mostly in the short circuit period, on the results of a much cruder mesh with only 1/3 the number of nodes. This may not be true for pole slipping behaviour where asynchronous operation is involved, however. Where the principal interest of the calculation lies in the detailed performance of the machine, such as in local heating effects, a fine discretisation will be necessary, but the additional computational time is hardly justified for modelling the general overall transient response.

The two-axis model is significantly faster in computation, for any given transient, on account of its ability to increase the time step length as the transient proceeds, although, as described above, this is done only at the expense of neglecting one component of the transient response. The choice of stator model thus depends upon the detail required, but it may be most profitable to combine the two techniques (for cases where the individual phase voltages and currents are not required) by adopting a phase band model from the start of the transient until there is no further oscillation in terminal values, and then switching to the two-axis representation for modelling the swing curve behaviour.

The two-axis current sheet stator model provided a very useful reduction in problem size, and was found to give results almost as good as the fully modelled stator mesh of the same discretisation in substantially less time. Further work will establish whether a current representation requiring the same computational time as a fully detailed one will provide superior results.

The time step length was observed to increase more rapidly when using a current sheet stator model, which suggests that it might be advantageous to

discard the stator nodes when calculating the minimum node time constant in a full stator model.

8.1.3 Equivalent circuit parameters.

Previous attempts at obtaining a full set of equivalent circuit data from finite element studies have used indirect methods. In Chapter 7 it was shown that the power flow within an equivalent circuit model may be directly equated with that in a finite element representation, and this has been the basis of the method used.

Basic machine reactances were found for the C.E.G.B. Test B initial condition from the finite element solution by the method of injecting currents into windings and calculating the resulting voltages with undisturbed permeabilities. The calculations showed the machine to be carrying approximately 5% cross axis flux.

By obtaining axis currents directly from the finite element calculation the d- and q-axis damper circuit currents may be deduced. Equating the power dissipated in these circuits with the eddy current power loss in the finite element model then enables the damper circuit resistances to be found.

It proved necessary to fit the data at a minimum number of points per cycle to avoid over constraining the results, but the errors that were introduced by calculating each resistance at only one point per cycle were not large. The q-axis resistance was found to be almost constant over the short circuit period, reflecting the large, uniform pole area available for conduction; whereas the d-axis value rose steadily, probably as a result of the smaller cross-sectional area of the rotor teeth at the root than at the tip, where the damper strip and slot wedge are also available for conduction.

An attempt was then made to calculate the corresponding damper circuit inductances using the axis flux linkages derived from the finite element solution and the data already found. Unfortunately, the results were most unreliable, and even unphysical. Partly this was due to numerical problems, but also as a result of attempting to characterise the complex response of the finite element model by a few equivalent circuit parameters. It may be that the errors will become less severe when the other modelling problems described in the previous section are resolved.

8.2 FURTHER WORK.

8.2.1 Unresolved modelling problems.

Chapter 6 has described some attempts made at explaining the discrepancy between the measured and predicted results. Further work in the following areas may assist :

- i) A detailed investigation of the unresolved question of the opposing eddy currents apparently seen in the rotor poles.
- ii) The use of a much finer rotor discretisation, particularly in the damper strip and at the surface of the steel and wedges, where eddy currents are first induced.
- iii) The adoption of a delta/star transformer model that allows for the mutual coupling between phases. This will permit the investigation of the effects of scatter in the operation of the circuit breakers.

- iv) An improved allowance for the effects of the machine overhang and rotor endwinding leakage fields under transient conditions, possibly using three-dimensional magnetostatic end region studies.
- v) An improved allowance for the effects of the rotor endbell on the eddy current generation and dissipation.
- vi) An improved allowance for the effect of the inertia equalising gashes on the eddy current flow in the pole region, possibly involving three-dimensional studies.
- vii) Use of the method to simulate the transient performance of a different machine design for which test data is available.
- viii) Further investigate the differences between the finite element and equivalent circuit models, as described at the end of chapter 7.

8.2.2. Improvements to the existing method.

Various techniques may be investigated to ascertain whether they will improve the speed or accuracy of solution. These include :

- i) Modelling the rotor motion explicitly by moving the rotor mesh round inside the stator mesh, using an airgap slip plane across which the nodal potentials are interpolated.
- ii) Investigating the use of the various conjugate gradient solution methods. For magnetostatic problems, conjugate gradient methods are not normally considered to be an improvement on Gaussian elimination for problems of less than 2000 nodes; but there may be advantages in the transient case where the system matrix changes only slowly from one time step to the next.

- iii) Using higher order elements. The assumption of a higher order (than linear) variation of magnetic vector potential throughout each element complicates problem formulation but reduces the number of nodes required in the model. The net effect may be to enable an overall reduction in the solution time.
- iv) Changing from a phase band to a two-axis model when the oscillatory component of the response has died out. This will then permit the time step length to be increased, so speeding the solution. However, smoothly transferring from one model to the other without introducing an artificial transient due to mismatches in the currents and potentials may not be straightforward.

8.2.3 Developments of the method.

The solution method described in this thesis may be further developed and extended to permit the more accurate solution of more general transient problems. To this end, further work is required to :

- i) Improve the delta/star transformer model to incorporate the mutual coupling between phases. This will permit the inclusion of the effects of scatter in the operation of the circuit breakers and the modelling of the much more common single line, unbalanced faults.
- ii) Include the transient behaviour of the transmission line components.
- iii) Incorporate a multiple inertia model of the turbine generator rotor which will permit the computation of the shaft torsional modes of oscillation.
- iv) Improve on the single-valued allowance for the effects of the machine overhang and rotor endwinding leakage fields under transient conditions, possibly using three-dimensional magnetostatic end region studies.

- v) An improved allowance for the effects of the rotor endbell on the eddy current generation and dissipation.
- vi) An improved allowance for the effect of the inertia equalising gashes on the eddy current flow in the pole region, possibly involving three-dimensional studies.
- vii) Give consideration to the program structure to take advantage of the newly developing parallel processing techniques. This would be particularly applicable for the formulation, inversion and backsubstitution of the system matrix, many of the constituent operations of which are independent one from the other, and may, in principle, be performed simultaneously.

8.2.4 Machine parameters.

In view of the problems experienced with the determination of inductance, the very direct method described for finding damper circuit parameter variations should initially be applied to simpler transients, such as flux decay and works short circuit. This will establish patterns of behaviour of each axis separately, before the more complex case is tackled. Other methods of coupling the two machine models should also be explored.

Ultimately, the work should be directed to provide assistance in the choice of the best set of parameters for any particular transient condition, and possibly to recommend time varying parameters of simple form, which will improve the accuracy of the equivalent circuit solution method.

APPENDIX

**EFFICIENT SOLUTION OF THE ASYMMETRIC MATRIX
RESULTING FROM THE TWO-AXIS STATOR
WINDING CONDUCTIVITY MATRICES**

A.1 Asymmetric matrix formulation.

Equations 5.11 define the four components of the stator current vector. When differentiated with respect to (A) , these give the corresponding conductivity matrices, only two of which are symmetric. Following the A-average technique, the current vectors may also be expressed in terms of average d- and q-axis potentials \bar{D} and \bar{Q} , defined by :

$$\bar{D} = (N_d)^T(A) \quad (A.1a)$$

$$\bar{Q} = (N_q)^T(A) \quad (A.1b)$$

for convenience let

$$G = \frac{p\omega L_{eff}}{R} \quad (A.2a)$$

$$B = \frac{p\omega L_{eff}}{X} \quad (A.2b)$$

then

$$\begin{aligned}
 (I_{dd}) &= i_{dd}(N_d) = G(N_d)(N_q)^T(A) = [\Delta\sigma_{dd}](A) = G(N_d)\bar{Q} \\
 (I_{dq}) &= -i_{dq}(N_q) = -B(N_q)(N_q)^T(A) = [\Delta\sigma_{dq}](A) = -B(N_q)\bar{Q} \\
 (I_{qq}) &= i_{qq}(N_q) = -G(N_q)(N_d)^T(A) = [\Delta\sigma_{qq}](A) = -G(N_q)\bar{D} \\
 (I_{qd}) &= i_{qd}(N_d) = -B(N_d)(N_d)^T(A) = [\Delta\sigma_{qd}](A) = -B(N_d)\bar{D}
 \end{aligned} \quad (A.3)$$

A partially reduced coefficient is the value that would be used to reduce the coefficients of the same row.

Turner [27] has described the functioning of the Jennings method in detail. The significant point here is that the partially reduced terms in any row (up to the leading diagonal) may be found from the fully reduced terms in the corresponding column.

A.3 Application of the Jennings method to the solution of the asymmetric matrix.

The term $-G$ in the bottom right hand corner of equation A.4 is initially replaced by $+G$. The resulting symmetrical matrix is then inverted using the usual Jennings method. The last line of the inversion is then discarded and the correct line $[G(N_d)^T, 0, 0, -G, 0]$ is substituted and re-eliminated. All but the last two terms in this line are the same as before, and need not be recomputed. The partly reduced coefficients needed to reduce the last two terms are also unchanged and available in the last two columns of the solution. There is thus very little additional computation required to re-solve the substituted last row. Adoption of the A-average technique and the modified Jennings method thus leads to a very efficient inversion of the initially asymmetric and densely packed Hessian matrix.

REFERENCES

1. Spooner, E., "Fully slotless turbogenerators", Proc.IEE, 1973, Vol.120, pp 1507-1518.
2. Park, R.H., "Two-reaction theory of synchronous machines", Trans. AIEE., 1929, 48, pp 717-729.
3. Kron, G., "Application of tensors to the analysis of rotating electrical machinery", General Electric Review, 1942.
4. Canay, I.M., "Causes of discrepancies on rotor quantities and exact equivalent diagrams of the synchronous machine", IEEE Trans., 1969, PAS-88, pp 1114-1120.
5. Adkins, B. and Harley, R.G., "The general theory of alternating current machines", 1975, Chapman and Hall, London.
6. Shackshaft, G., "New approach to the determination of synchronous machine parameters from tests", Proc.IEE, 1974, Vol.121, pp 1385-1392.
7. Dandeno, P.L., Kundur, P. and Schulz, R.P., "Recent trends and progress in synchronous machine modelling in the electric utility industry", Proc.IEEE, 1974, 62, pp 941-950.
8. Shackshaft, G. and Neilson, B., "Results of stability tests on an underexcited 120 MW generator", Proc.IEE, 1972, Vol.119, pp 175-188.
9. Shackshaft, G. and Poray, A.T., "Implementation of new approach to determination of synchronous machine parameters from tests", Proc. IEE, 1977, Vol.124, pp 1170-1178.

10. Salvatore, L. and Savino, M., "Experimental determination of synchronous machine parameters", *Proc.IEE*, 1981, Vol.128B, pp 212-218.
11. Diggle, R. and Dineley, J.L., "Generator works testing : sudden short circuit or standstill variable frequency response method", *Proc.IEE*, 1981, Vol.128C, pp 177-182.
12. Binns, K.J. and Smith, J.R., "Prediction of load characteristics of turbogenerators", *Proc.IEE*, 1978, Vol.125, pp 197-202.
13. Smith, J.R., Binns, K.J., Williamson, S. and Buckley, G., "Determination of saturated reactances of turbogenerators", *Proc.IEE*, 1980, Vol.127C, pp 122-128.
14. Haydock, L., "Systematic development of equivalent circuits for synchronous machines", Ph.D. Thesis, 1986, University of London.
15. Demerdash, N.A. and Hamilton, H.B., "A simplified approach to determination of saturated synchronous reactances of large turbogenerators under load", *IEEE Trans.*, 1976, PAS-95, pp 560-566.
16. Zienkiewicz, O.C., "The finite element method", *McGraw Hill*, 1977, 3rd. edition.
17. Silvester, P. and Chari, M.V.K., "Finite element solution of saturable magnetic field problems", *IEEE Trans.*, 1970, PAS-89, pp 1642-1649.
18. Silvester, P. and Konrad, A., "Analysis of transformer leakage phenomena by higher order finite elements", *IEEE Trans.*, 1973, PAS-92, pp 1843-1852.
19. Chari, M.V.K., "Finite element analysis of electrical machines and devices", *IEEE Trans.*, 1980, MAG-16, pp 1014-1019.

20. Chari, M.V.K., Konrad, A., D'Angelo, J. and Palmo, M.A., "Finite element computation of 3-D electrostatic and magnetostatic field problems", IEEE Trans., 1983, MAG-19, pp 2321-2324.
21. Simkin, J. and Trowbridge, C.W., "Application of integral equation methods for the numerical solution of magnetostatic and eddy current problems", Rutherford Laboratory Report, RL-76-041, UK.
22. Simkin, J., "A comparison of integral and differential equation solutions for field problems", IEEE Trans., 1982, MAG-18, pp 401-405.
23. Bossavit, A. and Verite, J.J., "A mixed fem-biem method to solve 3-D eddy current problems", IEEE Trans., 1982, MAG-18, pp 431-435.
24. Salon, S.J., "The hybrid finite element-boundary element method in electromagnetics", IEEE Trans., 1985, MAG-21, pp 1829-1834.
25. IEEE Symposium on synchronous machine modelling for power system studies, IEEE Winter Power Meeting, 1983, 83 THO101-6-PWR.
26. Turner, P.J. and Macdonald, D.C., "Transient electromagnetic analysis of the turbogenerator flux decay test", IEEE Trans., 1982, PAS-101, pp 3193-3200.
27. Turner, P.J., "Finite element electromagnetic analysis of turbine generator performance", Ph.D. Thesis, 1982, University of London.
28. Turner, P.J., "Finite-element simulation of turbine-generator terminal faults and application to machine parameter prediction", IEEE Trans., 1987, EC-2, pp 122-131.
29. Rodger, D., "Finite element method for calculating power frequency three-dimensional electromagnetic field distributions", Proc.IEE, 1983, Vol.130A, pp 233-238.

30. Foggia, A., Sabonnadiere, J.C. and Silvester, P., "Finite element solution of saturated travelling magnetic field problems", *IEEE Trans.*, 1975, PAS-94, pp 866-871.
31. Silvester, P., Cabayan, H.S. and Browne, B.T., "Efficient techniques for finite element analysis of electrical machines", *IEEE Trans.*, 1973, PAS-92, pp 1274-1281.
32. Chari, M.V.K., "Non linear finite element solution of electrical machines under no-load and full-load conditions", *IEEE Trans.*, 1974, MAG-10, pp 686-689.
33. Hanalla, A.Y. and Macdonald, D.C., "A nodal method for the numerical solution of transient field problems in electrical machines", *IEEE Trans.*, 1975, MAG-11, pp 1544-1546.
34. Chari, M.V.K. and Silvester, P., "Analysis of turbo alternator magnetic fields by finite elements", *IEEE Trans.*, 1971, PAS-90, pp 454-464.
35. Chari, M.V.K. and Silvester, P., "Finite element analysis of magnetically saturated d.c. machines", *IEEE Trans.*, 1971, PAS-90, pp 2362-2372.
36. Coulson, M.A., "Magnetic non-linearity", Ph.D. Thesis, 1981, University of Strathclyde.
37. EPRI, "Improvement in accuracy of prediction of electrical machine constants and Generator models for subsynchronous resonance conditions. Volume 2: Application of two-dimensional finite element techniques for synchronous machine modelling", EPRI Report EL-3359, 1984, Vol.2.
38. Berkery, J., Chari, M.V.K., Csendes, Z.J., Minnich, S.H. and Tandon, S.C., "Load characteristics of synchronous generators by the finite element method", *IEEE Trans.*, 1981, PAS-100, pp 1-9.

39. Hanalla, A.Y. and Macdonald, D.C., "Numerical analysis of transient fields by finite elements", Proc.IEE, 1976, Vol.123, pp 863-898.
40. Hestenes, M.R. and Stiefel, E., "Methods of conjugate gradients for linear systems", Na. Bur. Standards J. Res., 1952, 49, pp 409-436.
41. Kershaw, D.S., "The incomplete Choleski-conjugate gradient method for the iterative solution of systems of linear equations", Journal of Computational Physics, 1978, 26, pp 43-65.
42. Jennings, A., "A compact scheme for the solution of symmetric, linear simultaneous equations", Computer Journal, 1966, 9, pp 281-285.
43. Nyamusa, T.A., Demerdash, N.A. and Nehl, T.W., "An accelerated Newton-Raphson technique for finite element analysis of magnetic fields in electrical machines", IEEE Trans., 1986, EC-1, pp 122-129.
44. Aldefeld, B., "Forces in electromagnetic devices", Compumag, 1978, Grenoble.
45. Reichert, K., Freundl, H. and Vogh, W., "The calculation of forces and torques with numerical magnetic field calculation methods", Compumag, 1976, Oxford.
46. Coulomb, J.L., Meunier, G. and Sabonnadiere, J.C., "An original stationary method using local Jacobian derivative for direct finite element computation of electromagnetic force, torque and stiffness", Journal of Magnetism and Magnetic Materials, 1982, 26, pp 337-339.
47. Coulomb, J.L., "A methodology for the determination of global electromechanical quantities from a finite element analysis and its application to the evaluation of magnetic forces, torques and stiffness", IEEE Trans., 1983, MAG-19, pp 2514-2519.

48. IEEE Committee Report, "Dynamic models for steam and hydro turbines in power system studies", IEEE Trans., 1973, PAS-92, pp 1904-1912.
49. IEEE Committee Report, "Excitation system models for power system stability studies", IEEE Trans., 1981, PAS-100, pp 494-509.
50. "IEEE standard criteria and definitions for excitation systems for synchronous machines", IEEE New York, 1972, IEEE Standard 421-1972.
51. McGee, R.W. and Henser, P.B., "Uskmouth system tests 1979. Factual report on pole slipping tests at Uskmouth B power station", C.E.G.B. Report, 1982, TPRD/ST/82/0021R.
52. McGee, R.W. and Henser, P.B., "Results of pole-slipping tests on a 120MW generator at Uskmouth B power station", Proc. 18th. Universities Power Engineering Conference, 1983, pp 9-14.
53. Barber, M.D. and Giannini, M., "Simulation of a synchronous generator connected via a delta-star transformer", Proc.IEE, 1974, 121, pp 1513-1521.
54. Carpenter, C.J., "Magnetic equivalent circuits", Proc.IEE, 1968, 115, pp 1503-1511.
55. Haydock, L. and Macdonald, D.C., "A detailed lumped-parameter method for the study of electrical machines in transient stability studies", Proc. Poly-model 6 Conference, Electromagnetics Modelling, 1983, pp 15-25.
56. Kazmierski, M., Kozlowski, M., Lasocinski, J., Pinkieicz, I. and Turowski, J., "Hot spot identification and overheating preventing when designing a large transformer", Proc. 30th CIGRE, 1984, pp 12.12/1-6.
57. Whitlock, D.K., "RASM05 - revised transient stability program", C.E.G.B. Report, 1972, MS/C/9180.

58. Lewis, E.J., "A revised transient stability program RASM05", C.E.G.B. Report, 1973, PL-ST/27/72.
59. Hanalla, A.Y. and Macdonald, D.C., "Sudden three-phase short circuit characteristics of turbine generators from design data using electromagnetic field calculations", Proc.IEE, 1980, 127c, pp 213-220.
60. Shackshaft, G., "Effect of oscillatory torques on the movement of generator rotors", Proc.IEE, 1970, 117, pp 1964-1974
61. Say, M.G., "Alternating current machines", 5th Edition, 1983, Pitman Publishing Limited, London.
62. Mehta, D.B. and Adkins, B., "Transient torque and load angle of a synchronous generator following several types of system disturbance", Proc.IEE, 1960, 107A, pp 61-74.
63. Concordia, C., "Synchronous machines", 1951, Wiley.
64. Minnich, S.M., Schulz, R.P., Baker, D.H., Sharma, D.K., Farmer, R.G. and Fish, J.H., "Saturation functions for synchronous generators from finite elements.", Proc. IEEE 1987 Winter Power Meeting, paper 87 WM 207-4.
65. Macdonald, D.C., Reece, A.B.J. and Turner, P.J., "Turbine generator steady-state reactances", Proc. IEE, 1985, 132-C, pp 101-108.
66. Dougherty, J.W. and Minnich, S.H., "Operational inductances for turbine generators : test data versus finite element calculations.", Trans. IEEE, 1983, PAS-102, pp 3393-3401.
67. Reece, A.B.J., Khan, G.K.M. and Chant, M.J., "Generator parameter prediction from computer simulation of the standstill variable frequency test.", IEE Int. Conf. on Electrical Machines, 1982.

68. Jack, A.G. and Bedford, T.J., "A study of the frequency response of turbogenerators with special reference to Nanticoke G.S.", IEEE 1986 Summer Power Meeting, paper 86 SM 481-5.